

UNIVERSIDADE FEDERAL DO RIO DE JANEIRO

ESCOLA DE QUÍMICA

Programa de Pós Graduação em Engenharia de Processos Químicos e Bioquímicos

CRISTIANE SÃO BENTO GONZAGA

AUTOMATIZED MONTE-CARLO ANALYSIS OF OFFSHORE
PROCESSING OF CO₂-RICH NATURAL GAS: DESIGN,
ENVIRONMENTAL AND ECONOMIC ASSESSMENTS OF NEW
TECHNOLOGIES

RIO DE JANEIRO

2019

Cristiane São Bento Gonzaga

AUTOMATIZED MONTE-CARLO ANALYSIS OF OFFSHORE PROCESSING OF
CO₂-RICH NATURAL GAS: DESIGN, ENVIRONMENTAL AND ECONOMIC
ASSESSMENTS OF NEW TECHNOLOGIES

Tese de Doutorado apresentada ao
Programa de Pós-Graduação em
Engenharia de Processos Químicos e
Bioquímicos, Escola de Química,
Universidade Federal do Rio de
Janeiro, como parte dos requisitos
necessários à obtenção do título de
Doutora em Ciências.

Orientadores:

Prof. José Luiz de Medeiros, D.Sc.

Prof. Ofélia de Queiroz F Araújo, Ph.D.

Rio de Janeiro

2019

G642a Gonzaga, Cristiane São Bento
Automatized Monte-Carlo Analysis of Offshore Processing of
CO₂-Rich Natural Gas: Design, Environmental and Economic
Assessments of New Technologies / Cristiane São Bento
Gonzaga. – Rio de Janeiro, 2019.
174 f.

Orientadores: José Luiz de Medeiros e Ofélia de Queiroz
Fernandes Araújo.

Tese (doutorado) – Universidade Federal do Rio de Janeiro,
Escola de Química, Programa de Pós Graduação em Engenharia
de Processos Químicos e Bioquímicos, 2019.

1. CO₂-rich natural gas conditioning. 2. Monte Carlo Analysis. 3.
Computer-Aided Engineering. 4. Interoperability. 5. Sustainability. I.
de Medeiros, José Luiz, orient. II. Araújo, Ofélia de Queiroz
Fernandes, coorient. III. Título.

Cristiane São Bento Gonzaga


AUTOMATIZED MONTE-CARLO ANALYSIS OF PROCESSING OF CO₂-RICH
NATURAL GAS: DESIGN, ENVIRONMENTAL AND ECONOMIC ASSESSMENTS
OF NEW TECHNOLOGIES

Tese de Doutorado apresentada ao
Programa de Pós-Graduação em
Engenharia de Processos Químicos e
Bioquímicos, Escola de Química,
Universidade Federal do Rio de
Janeiro, como parte dos requisitos
necessários à obtenção do título de
Doutora em Ciências.


Aprovado em:



Prof. José Luiz de Medeiros, Ds.C., EQ/UFRJ.
(Orientador - Presidente)

Prof. Ofélia de Queiroz Fernandes Araújo, Ph.D., EQ/UFRJ.
(Orientadora)

Prof. Argimiro Resende Secchi, Ds.C., COPPE/UFRJ.

Dr. Wilson Mantovani Grava, Ds.C., PETROBRAS.

Prof. Claudinei de Souza Guimarães, Ds.C., EQ/UFRJ.

Prof. Estevão Freire, Ds.C., EQ/UFRJ.

Rio de Janeiro

2019

AGRADECIMENTOS

Agradeço aos meus orientadores José Luiz de Medeiros e Ofélia de Queiroz Fernandes Araújo pela orientação técnica.

A Siemens A.S., na Noruega, pelo reconhecimento da importância dos meus estudos como aluna de Doutorado.

A minha família e amigos por todo o incentivo ao longo do desenvolvimento desta tese e também pela compreensão nos momentos em que precisei estar ausente e focada.

A meus pais, por sempre estarem ao meu lado, me suportando e acompanhando o meu crescimento profissional, e ao meu namorado Jonas, por todo o suporte e incentivo incondicionais durante a pesquisa.

A Dr. Heriberto Cabezas, Dr. Douglas Yong, Dr. Todd Martin, and Dr. William Barret da US-EPA, por múltiplas explicações e compartilhamento de dados para o algoritmo WAR.

Finalmente, a Deus, por me dar a força de trabalhar nessa pesquisa em paralelo a minha jornada de trabalho.

“All our dreams can come true if we have the courage to pursue them.”

Walt Disney

RESUMO

GONZAGA, Cristiane São Bento. **Análise de Monte-Carlo Automatizada de Processamento Offshore de Gás Natural Rico em CO₂: Avaliação do Dimensionamento e de Performances Ambiental e Econômica de Novas Tecnologias**. Rio de Janeiro, 2019. Tese (Doutorado em Engenharia de Processos Químicos e Bioquímicos) – Escola de Química, Universidade Federal do Rio de Janeiro, Rio de Janeiro, 2019.

A produção *offshore* de petróleo e gás com elevadas concentração de CO₂ e proporção gás-petróleo apresenta o desafio de processamento de grandes volumes de gás rico em CO₂ em plataformas *offshore*. Esse é o caso dos campos de petróleo e gás em águas profundas no polo do Pré-Sal brasileiro que requerem projetos inovadores e pioneiros devido à falta de precedência de projetos em escala comercial, agregando incertezas de projeto às incertezas comuns em operações em águas profundas. Portanto, técnicas para dimensionamento de unidades *offshore* sob fatores probabilísticos são recomendadas a fim de evitar projetos superdimensionados com base no pior cenário ou especificações de produtos não atingidas devido a projetos com margens apertadas, levando a perdas econômico-ambientais. O presente trabalho apresenta uma nova ferramenta de Engenharia auxiliada por computação, *MCAnalysis-HUB*, que consiste em um *framework* de interoperabilidade VB.NET/XML entre o simulador de processos HYSYS e o software MATLAB para avaliar estatisticamente o dimensionamento de projetos e seus desempenhos ambiental e econômico sob incertezas via análise de Monte-Carlo. Em uma primeira aplicação, projetos de plantas offshore para processamento de gás rico em CO₂ por meio de uma Rota-Convencional e de uma nova Rota-Separador-Supersônico são avaliados via análise de Monte-Carlo ao serem submetidos a populações probabilísticas de vazão de gás, concentração de CO₂ e proporção gás-petróleo. A Rota-Separador-Supersônico apresenta maior resiliência a variações de entrada e menor necessidade de alterações no projeto para atender a todas as especificações de processo em pelo menos 75% dos casos amostrados em comparação com a Rota-Convencional. A Rota-Separador-Supersônico também apresenta performance ambiental e econômico superiores à Rota Convencional, além de um consumo médio de energia 15% menor e ajuste do ponto de orvalho de hidrocarbonetos com menor teor médio de CO₂ no condensado. Em uma segunda aplicação, um processamento *offshore* convencional de gás é submetido a vazões de gás probabilísticas e a dois cenários de concentração de CO₂ de modo a avaliar possíveis impactos ambientais por meio do algoritmo *Waste Reduction*. Utilizando Análise de Componentes Principais, a categoria atmosférica foi identificada como a mais relevante em termos ambientais para ambos os cenários. O aumento da concentração de CO₂ no gás prejudica a performance ambiental, enquanto a performance econômica é altamente sensível aos fatores econômicos escolhidos. Os cenários avaliados também estão sujeitos a populações probabilísticas de preços do gás/petróleo e taxa de carbono.

Palavras-chave: Condicionamento de gás natural; Análise de Monte-Carlo; Engenharia auxiliada por computação; Interoperabilidade; Sustentabilidade.

ABSTRACT

GONZAGA, Cristiane São Bento. **Automatized Monte-Carlo Analysis of Offshore Processing of CO₂-Rich Natural Gas: Design, Environmental and Economic Assessments of New Technologies**. Rio de Janeiro, 2019. Thesis (Doctorate in Chemical and Biochemical Processes Engineering) – Escola de Química, Federal University of Rio de Janeiro, Rio de Janeiro, 2019.

Offshore production of oil and gas with high %CO₂ and gas-oil ratio presents the challenge of processing large volumes of CO₂-rich gas on offshore rigs. This is the case of deep-water oil-gas fields in the Brazilian Pre-Salt pole which require innovative and first-of-a-kind designs due to the lack of previous commercial-scale projects, creating uncertainties to the design besides the usual uncertainties of deep-water operations. Therefore, techniques for designing offshore units under stochastic factors are recommended to avoid oversized designs based on worst-case scenarios or underachieved product specifications from tight designs leading to economic-environmental losses. This work presents a novel Computer-Aided Engineering tool, *MCAnalysis-HUB*, a VB.NET/XML interoperability framework between HYSYS process simulator and MATLAB to statistically assess design, environmental and economic performances under uncertainty via Monte-Carlo analysis. In a first application, designs of offshore plants processing CO₂-rich gas via a Conventional-Route and a novel Supersonic-Separator-Route are tested with Monte-Carlo analysis via submission to stochastic populations of gas flow rate, CO₂ content and gas-oil ratio. The Supersonic-Separator-Route presents higher resilience to input overshoots and lower necessity of design changes to accomplish all process specifications in at least 75% of the sampled cases compared to the Conventional-Route. The Supersonic-Separator-Route also shows superior environmental and economic performances relatively to the Conventional-Route in addition to 15% lower average power consumption and hydrocarbons dew-point adjustment with lower average CO₂ content in the condensate. In a second application, a conventional offshore gas processing is submitted to probabilistic gas flow rates and two scenarios of CO₂ content to assess potential environmental impacts via the Waste Reduction algorithm. Using Principal Component Analysis, the atmospheric category was identified as the most relevant for environmental assessment in both scenarios. The increase of gas %CO₂ hinders environmental performance, while economic performance is highly sensitive to the chosen economic factors. Assessed scenarios are also subjected to stochastic populations of gas/oil prices, and carbon tax.

Keywords: CO₂-rich natural gas conditioning; Monte-Carlo analysis; Computer-Aided Engineering; Interoperability; Sustainability.

LIST OF FIGURES

Figure 1. Outlook of primary energy demand. Source: (BP, 2019b), adapted.	7
Figure 2. Pre-Salt layer topology. Source: http://www.petrobras.com.br/pt/nossas-atividades/areas-de-atuacao/exploracao-e-producao-de-petroleo-e-gas/pre-sal , adapted.	8
Figure 3. SS sketch with linear diameter profiles: geometric parameters.	13
Figure 4. MP module sketch.	16
Figure 5. WAR algorithm with plant life cycle (adapted from Young and Cabezas (1999)).	22
Figure 6. WAR algorithm (adapted from Young et al. (2000)).	24
Figure 7. Offshore processing of CO ₂ -rich NG: (a) Conventional-Route (Plant 1); (b) SS-Route (Plant 2); (c) Conventional-Route (Plant 3).	32
Figure 8. Three-phase separator (Conventional-Route and SS-Route).	39
Figure 9. Gas re-recompression from 1st and 2nd oil-gas separators.	39
Figure 10. Conventional-Route NG processing (part I): compression, TEG absorption WDPa, TEG regeneration and JTE HCDPA.	40
Figure 11. SS-Route NG processing (part I): compression and WDPa+HCDPA via SS.	41
Figure 12. Conventional-Route and SS-Route NG processing (part II): MP CO ₂ removal, NG compression and EOR-Fluid.	43
Figure 13. Thermal utility systems: (a) CW/SW; and (b) PHW (Conventional-Route and SS-Route).	44
Figure 14. Elevation profiles with sea-level datum: (a) NG pipeline; (b) EOR-Fluid pipeline (Conventional-Route and SS-Route).	45
Figure 15. SS axial profiles in SS-Route Base-Case: (a) SS silhouette and vapor-fraction vs $x(m)$; (b) $P(\text{bar})$ and Ma vs $x(m)$; (c) $T(K)$ and $c(m/s)$ vs $x(m)$; (d) species %mol condensation vs $x(m)$; (e) Ma_{BS} , final CO ₂ molar fraction and pre-shock vapor-fraction vs Ma^{Shock} for CO ₂ freeze-out design check; and (f) plane $P \times T$ with SS path, feed WDP locus, feed VLE envelope, product VLE envelope and feed CO ₂ freeze-out SVLE border.	50
Figure 16. SS-Route Base-Case: (a) plane $T \times \bar{S}$ with SS path, feed and product VLE envelopes, feed WDP locus and feed CO ₂ SVLE freeze-out boundary; and (b) magnification of (a).	51
Figure 17. Base-Case for $\mu_{U2_1} = 20\%mol$ CO ₂ : NG processing (part I): compression, TEG absorption WDPa, TEG regeneration and JTE HCDPA.	53
Figure 18. Base-Case for $\mu_{U2_1} = 20\%mol$ CO ₂ : NG processing (part II): MP CO ₂ removal, NG compression and EOR-Fluid.	54
Figure 19. Base-Case for $\mu_{U2_2} = 50\%mol$ CO ₂ : NG processing (part I): compression, TEG absorption WDPa, TEG regeneration and JTE HCDPA.	55

Figure 20. Base-Case for $\mu_{U2_2} = 50\%mol$ CO ₂ : NG processing (part II): MP CO ₂ removal, NG compression and EOR-Fluid.	55
Figure 21. Random $0 \leq P \leq 1$ samples generating normal <i>PDF</i> samples via <i>CDF</i> and <i>iCDF</i>	60
Figure 22. MC analysis workflow.	62
Figure 23. <i>MCAnalysis</i> modular architecture.	64
Figure 24. <i>MCAnalysis-HUB</i> modular architecture.	65
Figure 25. Simple-frequency histograms and normal <i>PDFs</i> of input variables: (a) [PU ₁] raw NG flow rate(MMsm ³ /d); (b) [PU ₂] raw NG CO ₂ molar fraction; and (c) [PU ₃] multiphase-feed GOR(sm ³ /m ³).....	70
Figure 26. Conventional-Route Base-Case: simple-frequency histograms and normal <i>PDFs</i> ($\langle X \rangle, S_X^2$): (a) [PS ₁] NG y_{CO_2} ; (b) [PS ₂] NG y_{CH_4} ; (c) [PS ₃] $WDP^{NG} (^{\circ}C)$; (d) [PS ₄] $HCDP^{NG} (^{\circ}C)$; (e) [PS ₅] $P^{NG-Delivery} (bar)$; (g) [PS ₇] $P^{EOR-Delivery} (bar)$; (h) [PS ₈] $HCDP^{MP-Feed} (^{\circ}C)$; and (f) cumulative-frequency histogram and normal <i>CDF</i> ($\langle X \rangle, S_X^2$) of [PS ₆] $WDP^{EOR-Fluid} (^{\circ}C)$	73
Figure 27. Conventional-Route Base-Case: (a) simple-frequency histogram and normal <i>PDF</i> ($\langle X \rangle, S_X^2$) of [PS ₉] $PPCO_2^{MP-Feed}$; and (b) cumulative-frequency histogram and normal <i>CDF</i> ($\langle X \rangle, S_X^2$) of [PS ₁₀] power-consumption.....	74
Figure 28. Re-designed Conventional-Route Base-Case: simple-frequency histograms and normal <i>PDFs</i> ($\langle X \rangle, S_X^2$): (a) [PS ₁] NG y_{CO_2} ; (b) [PS ₂] NG y_{CH_4} ; (c) [PS ₃] $HCDP^{NG} (^{\circ}C)$; (e) [PS ₅] $P^{NG-Delivery} (bar)$; (g) [PS ₇] $P^{EOR-Delivery} (bar)$; (h) [PS ₈] $HCDP^{MP-Feed} (^{\circ}C)$; and (f) cumulative-frequency histogram and normal <i>CDF</i> ($\langle X \rangle, S_X^2$) of [PS ₆] $WDP^{EOR-Fluid} (^{\circ}C)$	76
Figure 29. Re-designed Conventional-Route Base-Case: (a) simple-frequency histogram and normal <i>PDF</i> ($\langle X \rangle, S_X^2$) of [PS ₉] $PPCO_2^{MP-Feed}$; and (b) cumulative-frequency histogram and normal <i>CDF</i> ($\langle X \rangle, S_X^2$) of [PS ₁₀] power-consumption.....	77
Figure 30. SS-Route Base-Case: simple-frequency histograms and normal <i>PDFs</i> ($\langle X \rangle, S_X^2$): (a) [PS ₁] NG y_{CO_2} ; (b) [PS ₂] NG y_{CH_4} ; (c) [PS ₃] WDP^{NG} ; (d) [PS ₄] $HCDP^{NG}$; (e) [PS ₅] $P^{NG-Delivery}$; (f) [PS ₆] $WDP^{EOR-Fluid}$; (g) [PS ₇] $P^{EOR-Delivery}$; and (h) [PS ₈] $HCDP^{MP-Feed}$	80
Figure 31. SS-Route Base-Case cumulative-frequency histograms and normal <i>CDFs</i> ($\langle X \rangle, S_X^2$): (a) [PS ₉] $PPCO_2^{MP-Feed}$; and (b) [PS ₁₀] power-consumption.	81
Figure 32. Re-designed SS-Route Base-Case: simple-frequency histograms and normal <i>PDFs</i> ($\langle X \rangle, S_X^2$): (a) [PS ₁] NG y_{CO_2} ; (b) [PS ₂] NG y_{CH_4} ; (c) [PS ₃] WDP^{NG} ; (d) [PS ₄] $HCDP^{NG}$; (e) [PS ₅] $P^{NG-Delivery}$; (f) [PS ₆] $WDP^{EOR-Fluid}$; (g) [PS ₇] $P^{EOR-Delivery}$; and (h) [PS ₈] $HCDP^{MP-Feed}$	83
Figure 33. Re-designed SS-Route Base-Case cumulative-frequency histograms and normal <i>CDFs</i> ($\langle X \rangle, S_X^2$): (a) [PS ₉] $PPCO_2^{MP-Feed}$; and (b) [PS ₁₀] power-consumption.	84

Figure 34. Re-Designed SS-Route: Conjoint histogram of SS length (L) vs SS throat diameter (D_T).	86
Figure 35. Re-designed Conventional-Route: simple-frequency histograms of main streams and normal $PDFs$: (a) $C3+$ (kgmole/h); and (b) y_{CO_2} of $C3+$; (c) MP-Feed (kgmole/h); (d) EOR-Fluid (kgmole/h); (e) NG (kgmole/h); (f) oil (kgmole/h).	88
Figure 36. Re-designed SS-Route simple-frequency histograms of main streams and normal $PDFs$: (a) $C3+$ (kgmole/h); and (b) y_{CO_2} of $C3+$; (c) MP-Feed (kgmole/h); (d) EOR-Fluid (kgmole/h); (e) NG (kgmole/h); (f) oil (kgmole/h).	89
Figure 37. Simple-frequency histograms and normal $PDFs$ of input variables: (a) $[PU_1]$ raw NG flow rate($MMsm^3/d$); (b) $[PU_2]_1$ raw NG CO_2 molar fraction (Case 20%mol CO_2) ; and (c) $[PU_2]_2$ raw NG CO_2 molar fraction (Case 50%mol CO_2). ...	91
Figure 38. Simple-frequency histograms and normal $PDFs$ of $[PS_1]$ NG y_{CO_2} for (a) Case 20%mol CO_2 ; and (b) Case 50%mol CO_2	92
Figure 39. Simple-frequency histograms and normal $PDFs$ of $[PS_2]$ NG y_{CH_4} for (a) Case 20%mol CO_2 ; and (b) Case 50%mol CO_2	92
Figure 40. Simple-frequency histograms and normal $PDFs$ of $[PS_3]$ $WDP^{NG}(^{\circ}C)$ for (a) Case 20%mol CO_2 ; and (b) Case 50%mol CO_2	92
Figure 41. Simple-frequency histograms and normal $PDFs$ of $[PS_4]$ $HCDP^{NG}(^{\circ}C)$ for (a) Case 20%mol CO_2 ; and (b) Case 50%mol CO_2	92
Figure 42. Simple-frequency histograms and normal $PDFs(<X>, S_X^2)$ of total output PEI (PEI/h) of (a) Conventional-Route; and (b) SS-Route.....	95
Figure 43. Simple-frequency histograms and normal $PDFs(<X>, S_X^2)$ of total output PEI per product mass (PEI/kg) of (a) Conventional-Route; and (b) SS-Route.	96
Figure 44. Simple-frequency histograms and normal $PDFs(<X>, S_X^2)$ of output HTPI (PEI/h) of (a) Case 20%mol CO_2 ; and (b) Case 50%mol CO_2	97
Figure 45. Simple-frequency histograms and normal $PDFs(<X>, S_X^2)$ of output HTPE (PEI/h) of (a) Case 20%mol CO_2 ; and (b) Case 50%mol CO_2	97
Figure 46. Simple-frequency histograms and normal $PDFs(<X>, S_X^2)$ of output ATP (PEI/h) of (a) Case 20%mol CO_2 ; and (b) Case 50%mol CO_2	98
Figure 47. Simple-frequency histograms and normal $PDFs(<X>, S_X^2)$ of output TTP (PEI/h) of (a) Case 20%mol CO_2 ; and (b) Case 50%mol CO_2	98
Figure 48. Simple-frequency histograms and normal $PDFs(<X>, S_X^2)$ of output GWP (PEI/h) of (a) Case 20%mol CO_2 ; and (b) Case 50%mol CO_2	98
Figure 49. Simple-frequency histograms and normal $PDFs(<X>, S_X^2)$ of output ODP (PEI/h) of (a) Case 20%mol CO_2 ; and (b) Case 50%mol CO_2	99
Figure 50. Simple-frequency histograms and normal $PDFs(<X>, S_X^2)$ of output AP (PEI/h) of (a) Case 20%mol CO_2 ; and (b) Case 50%mol CO_2	99

- Figure 51.** Simple-frequency histograms and normal $PDFs(<X>, S_X^2)$ of output PCOP (PEI/h) of (a) Case 20%mol CO₂; and (b) Case 50%mol CO₂.99
- Figure 52.** Simple-frequency histograms and normal $PDFs(<X>, S_X^2)$ of total output PEI (PEI/h) of (a) Case 20%mol CO₂; and (b) Case 50%mol CO₂. 101
- Figure 53.** Simple-frequency histograms and normal $PDFs$ of input variables: (a) [EU₁] NG price; (b) [PU₂] oil price; and (c) [PU₃] carbon pricing. 105
- Figure 54.** Conventional-Route Base-Case: simple-frequency histograms and normal $PDFs(<X>, S_X^2)$: (a) [ES₁] *FCI*; (b) [ES₂] *COM*; (c) [ES₃] Power consumption cost; (d) [ES₄] Carbon tax per power consumption; (e) [ES₅] Carbon tax per outlet waste streams; (f) [ES₆] Carbon tax; (g) [ES₇] Revenue from NG; and (h) [ES₈] Revenue from EOR-Fluid. 106
- Figure 55.** Conventional-Route Base-Case: simple-frequency histograms and normal $PDFs(<X>, S_X^2)$: (a) [ES₉] Revenue; and (b) [ES₁₀] *NPV*. 107
- Figure 56.** SS-Route Base-Case: simple-frequency histograms and normal $PDFs(<X>, S_X^2)$: (a) [ES₁] *FCI*; (b) [ES₂] *COM*; (c) [ES₃] Power consumption cost; (d) [ES₄] Carbon tax per power consumption; (e) [ES₅] Carbon tax per outlet waste streams; (f) [ES₆] Carbon tax; (g) [ES₇] Revenue from NG; and (h) [ES₈] Revenue from EOR-Fluid. 109
- Figure 57.** SS-Route Base-Case: simple-frequency histograms and normal $PDFs(<X>, S_X^2)$: (a) [ES₉] Revenue; and (b) [ES₁₀] *NPV*. 110
- Figure 58.** Simple-frequency histograms and normal $PDFs(<X>, S_X^2)$ of $MLHV^{NG}$ of (a) Conventional-Route; and (b) SS-Route. 113
- Figure 59.** Simple-frequency histograms and normal $PDFs(<X>, S_X^2)$ of NVP without uncertainties in economic inputs of (a) Conventional-Route; and (b) SS-Route. 113
- Figure 60.** Case 20%mol CO₂: simple-frequency histograms and normal $PDFs(<X>, S_X^2)$: (a) [ES₁] *FCI*; (b) [ES₂] *COM*; (c) [ES₃] Power consumption cost; (d) [ES₄] Carbon tax per power consumption; (e) [ES₅] Carbon tax per outlet waste streams; (f) [ES₆] Carbon tax; (g) [ES₇] Revenue from NG; and (h) [ES₈] Revenue from EOR-Fluid. 116
- Figure 61.** Case 20%mol CO₂: simple-frequency histograms and normal $PDFs(<X>, S_X^2)$: (a) [ES₉] Revenue; and (b) [ES₁₀] *NPV*. 117
- Figure 62.** Case 20%mol CO₂: simple-frequency histogram and normal $PDF(<X>, S_X^2)$ of Revenue from NGL. 117
- Figure 63.** Case 50%mol CO₂: simple-frequency histograms and normal $PDFs(<X>, S_X^2)$: (a) [ES₁] *FCI*; (b) [ES₂] *COM*; (c) [ES₃] Power consumption cost; (d) [ES₄] Carbon tax per power consumption; (e) [ES₅] Carbon tax per outlet waste streams; (f) [ES₆] Carbon tax; (g) [ES₇] Revenue from NG; and (h) [ES₈] Revenue from EOR-Fluid. 119

Figure 64. Case 50%mol CO ₂ : simple-frequency histograms and normal PDFs($\langle X \rangle, S_X^2$): (a) [ES ₉] Revenue; and (b) [ES ₁₀] NPV.....	120
Figure 65. Case 20%mol CO ₂ : simple-frequency histograms and normal PDFs($\langle X \rangle, S_X^2$): (a) [ES ₈] Revenue from EOR-Fluid; (b) [ES ₉] Revenue; and (c) [ES ₁₀] NPV.....	123
Figure 66. Case 50%mol CO ₂ : simple-frequency histograms and normal PDFs($\langle X \rangle, S_X^2$): (a) [ES ₈] Revenue from EOR-Fluid; (b) [ES ₉] Revenue; and (c) [ES ₁₀] NPV.....	124

LIST OF TABLES

Table 1. PEI categories and measure of impact associated with PEI category (Barrett et al., 2011).	25
Table 2. Parameters for normal PDFs of input variables (feed variables) for Plants 1 and 2.	34
Table 3. Parameters for normal PDFs of input variables (feed variables) for Plant 3.	34
Table 4. Selected process responses for MC analysis and their specifications	35
Table 5. Constituents of multiphase oil-gas-water feed for Base-Cases	38
Table 6. Straight segments of pipelines (Conventional-Route and SS-Route).....	45
Table 7. SS-Route Base-Case: SS specifications, design, feed and	47
Table 8. Constituents of raw NG feed for Base-Cases considering two CO ₂ content scenarios.....	53
Table 9. Premises for economic assessment.....	57
Table 10. Selected economic responses for MC analysis and their specifications. ..	58
Table 11. Sample statistics $\langle X \rangle, S_X, S_X^2$, parameters μ, σ^2 , statistics standard deviations (SD), statistics standardizations and 95% confidence intervals: $N=1000$ samples of inputs $[PU_1], [PU_2], [PU_3]$ ($\alpha=0.05$).	71
Table 12. MC analysis ($N=1000$) of responses $[PS_1]$ to $[PS_{10}]$ of Conventional-Route Base-Case: approval percentages, statistics ($\langle X \rangle, S_X$) and comparison of simple/cumulative frequency histograms versus normal $PDF/CDF(\langle X \rangle, S_X^2)$	74
Table 13. MC analysis ($N=1000$) of responses $[PS_1]$ to $[PS_{10}]$ of re-designed Conventional-Route Base-Case: approval percentages, statistics ($\langle X \rangle, S_X$) and comparison of simple/cumulative frequency histograms versus normal $PDF/CDF(\langle X \rangle, S_X^2)$	77
Table 14. Original versus re-designed Conventional-Route: changes of approval percentages, statistics ($\langle X \rangle, S_X$) and histograms of responses $[PS_1]$ to $[PS_{10}]$ in MC analysis.....	78
Table 15. MC analysis ($N=1000$) of responses $[PS_1]$ to $[PS_{10}]$ of SS-Route Base-Case: approval percentages, statistics ($\langle X \rangle, S_X$) and comparison of simple/cumulative frequency histograms versus normal $PDF/CDF(\langle X \rangle, S_X^2)$	82
Table 16. MC analysis ($N=1000$) of responses $[PS_1]$ to $[PS_{10}]$ of re-designed SS-Route Base-Case: approval percentages, statistics ($\langle X \rangle, S_X$) and comparison of simple/cumulative frequency histograms versus normal $PDF/CDF(\langle X \rangle, S_X^2)$	84
Table 17. Original versus re-designed SS-Route: changes of approval percentages, statistics ($\langle X \rangle, S_X$) and histograms of responses $[PS_1]$ to $[PS_{10}]$ in MC analysis...	85

Table 18. Debottlenecked Conventional-Route minus debottlenecked SS-Route: differences for responses $[PS_1]$ to $[PS_{10}]$ in terms of: specified samples and statistics ($\langle X \rangle, S_X$).....	87
Table 19. MC analysis ($N=1000$) of responses $[PS_1]$ to $[PS_4]$ of Case 20%mol CO ₂ : approval percentages, statistics ($\langle X \rangle, S_X$) and comparison of simple-frequency histograms versus normal $PDF(\langle X \rangle, S_X^2)$	93
Table 20. MC analysis ($N=1000$) of responses $[PS_1]$ to $[PS_4]$ of Case 50%mol CO ₂ : approval percentages, statistics ($\langle X \rangle, S_X$) and comparison of simple-frequency histograms versus normal $PDF(\langle X \rangle, S_X^2)$	94
Table 21. Environmental responses: simple-frequency histograms versus normal $PDF(\langle X \rangle, S_X^2)$, and debottlenecked Conventional-Route minus debottlenecked SS-Route differences for environmental responses in terms of and statistics ($\langle X \rangle, S_X$).	96
Table 22. Summary of output PEI categories, $\langle X \rangle$ and S_X for Cases 20%mol CO ₂ and 50%mol CO ₂	100
Table 23. Eigenvalues λ_i and variance v_i for each principal component for Case 20%mol CO ₂ and Case 50%mol CO ₂	102
Table 24. \underline{P}_i vector of each principal component: Case 20%mol CO ₂ and Case 50%mol CO ₂	103
Table 25. MC analysis ($N=1000$) of responses $[ES_1]$ to $[ES_{10}]$ of Conventional-Route Base-Case: approval percentages, statistics ($\langle X \rangle, S_X$), comparison of simple-frequency histograms versus normal $PDF(\langle X \rangle, S_X^2)$, and brief analysis.	108
Table 26. MC analysis ($N=1000$) of responses $[ES_1]$ to $[ES_{10}]$ of SS-Route Base-Case: approval percentages, statistics ($\langle X \rangle, S_X$), comparison of simple-frequency histograms versus normal $PDF(\langle X \rangle, S_X^2)$, and brief analysis.	111
Table 27. Debottlenecked Conventional-Route minus debottlenecked SS-Route: differences for responses $[ES_1]$ to $[ES_{10}]$ in terms of: specified samples and statistics ($\langle X \rangle, S_X$).....	112
Table 28. Process and economic stochastic scenarios minus process economic scenario for Conventional-Route: differences for response $[ES_{10}]$ in terms of: specified samples and statistics ($\langle X \rangle, S_X$).....	114
Table 29. MC analysis ($N=1000$) of responses $[ES_1]$ to $[ES_{10}]$ of Case 20%mol CO ₂ : approval percentages, statistics ($\langle X \rangle, S_X$), comparison of simple-frequency histograms versus normal $PDF(\langle X \rangle, S_X^2)$, and brief analysis.	118

Table 30. MC analysis ($N=1000$) of responses $[ES_1]$ to $[ES_{10}]$ of Case 50%mol CO ₂ : approval percentages, statistics ($\langle X \rangle, S_X$), comparison of simple-frequency histograms versus normal $PDF(\langle X \rangle, S_X^2)$, and brief analysis.....	121
Table 31. Debottlenecked Case 20%mol CO ₂ minus debottlenecked Case 50%mol CO ₂ differences for responses $[ES_1]$ to $[ES_{10}]$ in terms of: specified samples and statistics ($\langle X \rangle, S_X$).	122
Table 32. Debottlenecked Case 20%mol CO ₂ minus debottlenecked Case 50%mol CO ₂ differences for responses $[ES_8]$ to $[ES_{10}]$ in terms of: specified samples and statistics ($\langle X \rangle, S_X$).	124

NOMENCLATURE

$A(x)$	Flow section area at x (m^2)
$c(T, P, \underline{Z})$	Sound speed property of multiphase equilibrium fluid at (T, P, \underline{Z}) (m/s)
C_{BM}	Bare module cost
$C_{BM,j}^0$	Bare module cost of piece of equipment j in standard conditions
CDF	Cumulative Distribution Function
CF	Cash flow
C_{GR}	Total module cost of new onshore facility
C_{OL}	Cost of operating labor
COM	Cost of manufacturing
C_P^0	Purchased cost for base conditions
C_{RM}	Cost of raw materials
C_{TM}	Total module cost of existing onshore facility
C_{UT}	Cost of utilities
C_{WT}	Cost of waste treatment
d	Depreciation
D, D_I, D_T, D_O	Diameter and SS internal inlet/throat/outlet diameters (m)
F	Feed flow rate ($kmol/h$)
F_1, F_2, F_3	Cost factors for COM calculation
$F(v_1, v_2)$	Fisher PDF with v_1 and v_2 degrees-of-freedom
F_{BM}	Bare module cost factor
FC_I	Fixed capital investment
i	Discount rate for NPV calculation
I_0	Initial investment
$\dot{I}_{in}^{(cp)}$	Input rate of PEI of chemical process
$\dot{I}_{out}^{(cp)}$	Output rate of PEI of chemical process
$\dot{I}_{in}^{(ep)}$	Input rate of PEI of energy generation process

$\dot{I}_{out}^{(ep)}$	Output rate of PEI of energy generation process
$\dot{I}_{we}^{(cp)}$	PEI output rate with waste energy from chemical process
$\dot{I}_{we}^{(ep)}$	PEI output rate with waste energy from energy generation process
$\dot{I}_{gen}^{(t)}$	PEI generation rate in chemical process and power plant
$iCDF$	CDF inverse
L, L_C, L_D	SS lengths: total, converging and diverging section (m)
L^{Laval}, L^{Shock}	Laval length and SS axial position where $Ma=Ma^{Shock} (=L^{LAVAL})$ (m)
$Ma=v/c$	Mach Number
Ma^{Shock}	Ma just before condensate withdrawal and before shock
Ma_{BS}	Ma just before shock and after condensate withdrawal
Ma_{AS}	Ma just after shock
$\dot{M}_{j,l}$	Mass flow rate of stream j
N	Number of MC samples
n	Number of pieces of main equipment; plant lifetime
nc	Number of components
O	Order
NPV	Net Present Value
$P, PPCO_2$	Absolute pressure (bar) and CO_2 partial-pressure (bar)
PDF	Probability Density Function
$\underline{\underline{P}}_{n \times n}$	Matrix of orthonormal eigenvectors of $\underline{\underline{R}}_X$
$\underline{\underline{P}}_i$	Eigenvector i of $\underline{\underline{R}}_X$
R	Revenue
$REC\%H_2O$	Percent H_2O recovery as SS condensate
$\underline{\underline{R}}_{X \ n \times n}$	Sample variance-covariance matrix of $\underline{\underline{X}}$
\bar{S}	Molar entropy of multiphase fluid ($kJ/mol.K$)
S_X^2, S_X	Sample variance and sample SD
SD	Standard deviation
$\underline{\underline{S}}_i$	Vector of generalized scores S_1, S_2, \dots, S_n from X_1, X_2, \dots, X_n

$(Score)_{ki}$	Impact score of species k in environmental impact category i
$\langle (Score)_k \rangle_i$	Average score of all species in environmental impact category i
T	Absolute temperature (K)
t_v	t -Student PDF with v degrees-of-freedom
t	Taxes for NPV calculation
v	Axial velocity of multiphase fluid (m/s)
x	SS axial position (m)
x_{kj}	Mass fraction of component k in stream j
$\underline{\underline{X}}_{m \times n}$	Matrix of process data with n scalar variables and m samples
$\langle X \rangle$	Sample average
\underline{Z}	Vector ($nc \times 1$) of mol fractions of multiphase fluid

Greek Symbols

α, β	Converging and diverging SS wall angles (deg) with linear diameter profiles
$1-\alpha$	Level of confidence
α_i	Weighting factor for environmental impact category i
λ_i	Eigenvalue i of $\underline{\underline{R}}_X$
$\underline{\lambda}_{n \times 1}$	Column vector of positive eigenvalues of $\underline{\underline{R}}_X$
μ, σ	Normal PDF mean and SD
χ_v^2	Chi-Square PDF with v degrees-of-freedom
$\eta^{EXP}\%, \eta^{CMP}\%$	SS adiabatic expansion/compression efficiencies (%)
ψ	Molar vapor-fraction of multiphase fluid
ψ_{ki}^s	Specific PEI of species k in environmental impact category i

Superscripts

<i>Inlet, Outlet</i>	<i>SS inlet/outlet</i>
<i>Shock</i>	<i>Just before condensate withdrawal and normal shock</i>

Subscripts

<i>AS, BS</i>	Just after shock, just before shock and after condensate withdrawal
---------------	---------------------------------------------------------------------

Abbreviations

AP	Acidification Potential
API	Application Programming Interface
ATP	Aquatic Toxicity Potential
BSW	Basic-Sediment-and-Water
C3+	Propane and Heavier Alkanes
CAE	Computer-Aided Engineering
CAM	Cellulose-Acetate Membrane
CFD	Computational Fluid Dynamics
CW	Cooling-Water
EHS	Environment, Health and Safety
EOR	Enhanced Oil Recovery
GDP	Gross Domestic Product
GWP	Global Warming Potential
GOR	Gas-Oil Ratio
HC	Hydrocarbon
HCDP	Hydrocarbon Dew-Point
HCDPA	Hydrocarbon Dew-Point Adjustment
HTPE	Human Toxicity Per Exposure
HTPI	Human Toxicity Per Ingestion
IRR	Internal Rate of Return
JTE	Joule-Thomson Expansion
LCA	Life Cycle Assessment
LTX	Anti-Hydrate Separator
MC	Monte-Carlo
MMsm ³ /d	Millions of Standard Cubic Meters per Day
MP	Membrane-Permeation
NG	Natural Gas
NGL	Natural Gas Liquids
ODP	Ozone Depletion Potential
PCOP	Photochemical Oxidation Potential
PCA	Principal Component Analysis
PEI	Potential Environmental Impact
PHW	Pressurized-Hot-Water
PR	Peng-Robinson Equation-of-State
SS	Supersonic Separator
SVLE	Solid-Vapor-Liquid Equilibrium
SW	Seawater
TEG	Triethylene Glycol
TTP	Terrestrial Toxicity Potential
VB.net	Visual Basic.NET
VLWE	Vapor-Liquid-Water Equilibrium
VLE	Vapor-Liquid Equilibrium
WAR	Waste Reduction
WDP	Water Dew-Point
WDPA	Water Dew-Point Adjustment
WHRU	Waste-Heat Recovery Unit
XML	eXtensible Markup Language

TABLE OF CONTENTS

1. INTRODUCTION	1
1.1. CONTEXT	1
1.2. GOALS	4
1.3. STRUCTURE OF THIS D.Sc. THESIS.....	5
2. LITERATURE REVIEW	7
2.1. NATURAL GAS CONTEXT	7
2.2. OFFSHORE NATURAL GAS PROCESSING.....	9
2.2.1. Water dew point adjustment (WDPA) and hydrocarbon dew point adjustment (HCDPA) – Conventional technologies.....	9
2.2.2. Water dew point adjustment (WDPA) and hydrocarbon dew point adjustment (HCDPA) – Supersonic separator	10
2.2.3. CO ₂ Removal	13
2.3. PROCESS DESIGN UNDER NON-DETERMINISTIC SCENARIOS.....	18
2.4. MONTE-CARLO ANALYSIS.....	19
2.4.1. Quasi-Monte-Carlo Sampling	21
2.5. ENVIRONMENTAL PERFORMANCE – WAR ALGORITHM	22
2.6. ECONOMIC PERFORMANCE	26
2.7. PRINCIPAL COMPONENT ANALYSIS	28
3. METHODS.....	30
3.1. OFFSHORE PROCESSING OF CO ₂ -RICH NG.....	30
3.2. STOCHASTIC FEED VARIABLES FOR MONTE-CARLO ANALYSIS.....	33
3.3. SELECTED PROCESS RESPONSES	35
3.4. BASE-CASES FOR OFFSHORE PROCESSING OF CO ₂ -RICH NG.....	36
3.4.1. Conventional-Route (Plant 1) and SS-Route (Plant 2) Base-Cases.....	37
3.4.1.1. Supersonic Separator Design: SS-Route Base-Case	46
3.4.2. Conventional-Route (Plant 3) Base-Cases.....	52
3.5. ENVIRONMENTAL AND ECONOMIC PREMISES	56
3.6. INVERSE TRANSFORM MONTE-CARLO SAMPLING	59
3.7. MONTE-CARLO ANALYSIS WORKFLOW	61
3.8. CAE TOOL <i>MCAnalysis</i> -HUB.....	63
4. RESULTS AND DISCUSSIONS: MONTE-CARLO ANALYSIS AND DESIGN OF CO ₂ -RICH NG PROCESSING ROUTES	67
4.1. PROCESS DESIGN ASSESSMENT: CONVENTIONAL-ROUTE versus SS-ROUTE.....	67
4.1.1. Conventional-Route Base-Case	72
4.1.1.1. Re-designed Conventional-Route	75

4.1.2. SS-Route Base-Case	79
4.1.2.1. Re-designed SS-Route	82
4.1.3. Conventional-Route versus SS-Route.....	86
4.2. PROCESS DESIGN ASSESSMENT: CO ₂ CONTENT INCREASE IN NG - CONVENTIONAL-ROUTE	90
4.3. ENVIRONMENTAL ASSESSMENT: CONVENTIONAL-ROUTE versus SS- ROUTE.....	95
4.4. ENVIRONMENTAL ASSESSMENT: CO ₂ CONTENT INCREASE IN NG – CONVENTIONAL-ROUTE	97
4.5. ECONOMIC ASSESSMENT: CONVENTIONAL-ROUTE versus SS-ROUTE 104	
4.5.1. Conventional-Route.....	105
4.5.2. SS-Route.....	108
4.5.3. Conventional-Route versus SS-Route.....	112
4.6. ECONOMIC ASSESSMENT: CO ₂ CONTENT INCREASE IN NG – CONVENTIONAL-ROUTE	115
4.6.1. Case 20%mol CO ₂	115
4.6.2. Case 50%mol CO ₂	118
4.6.3. CO ₂ content increase in NG effects.....	121
5. CONCLUSIONS	125
REFERENCES	130
APPENDIX A – Products of this Thesis: Publications and Registered Software	138
APPENDIX B – CAE tool <i>MCAnalysis</i> -HUB User Manual	147

1. INTRODUCTION

1.1.CONTEXT

Offshore processing of natural gas (NG) is susceptible to many severe uncertainties, such as load conditions (Fleshman et al., 2005), sales-gas price and consumer market, equipment and utilities costs (Arellano-Garcia and Wozny, 2009), meteorological events, and even operational risks of submarine devices and oversea processes. Feed composition and flow rate, temperature and pipeline pressure (Diaz et al., 2002; Mesfin and Shuhaimi, 2010) are critical load conditions as their variation effects propagate throughout the plant, disturbing operating conditions and also compromising the attainment of product specifications (Getu et al., 2015).

Multiple deep-water oil-gas fields in Brazilian Pre-Salt pole present additional technology challenges due to elevated gas-oil ratio (GOR) and high CO₂ content, as huge gas flow rates cannot simply be flared (as commonly and freely done 40 years ago) for environmental reasons. In other words, such CO₂-rich raw NG at high flow rates must be processed and exported (or even re-injected), and the huge CO₂ inventory adequately separated and handled.

Large-scale processing of CO₂-rich NG on the topside of offshore rigs aims at increasing NG heating value (Peters et al., 2011), avoiding occupying gas pipeline capacity with inert (e.g., CO₂) and providing a safe destination for CO₂ separated from NG as re-injection fluid for Enhanced Oil Recovery (EOR). Such gas processing must ensure water dew-point adjustment (WDPA) via dehydration, hydrocarbon dew-point adjustment (HCDPA) via removal of propane and heavier hydrocarbons (C₃+) (if applicable), efficient CO₂ removal and huge machinery for dispatching treated gas through pipeline to onshore facilities and for dispatching high-pressure CO₂ to EOR (Araújo et al., 2017). Hence, offshore CO₂-rich NG processing requires innovative topside technologies, usually with first-of-a-kind (FOAK) designs, which brings uncertainties into discussion derived from the lack of previous similar commercial-scale projects to allow moving along the technology upgrade curve.

However, uncertainties can significantly affect safety, reliability and economic decisions of the process (Duong et al., 2016), and overestimation of operational parameters caused by worst-case assumptions of uncertain process parameters is a classic practice in the industry (Arellano-Garcia and Wozny, 2009) with deleterious consequences in several expensive steps of offshore NG processing, such as compression and subsea pipelines. Overdesign of process equipment, besides leading to feasible plants with profitability drastically reduced (Li et al., 2004), has a direct impact on the stringent limited availability of footprint and weight on offshore topsides.

Another relevant uncertainty concerns the impact of the CO₂ re-injection in the reservoir for EOR. Although EOR increases the efficiency of oil recovery and provides a safe destination for the large volume of CO₂ removed from the NG, it results in a long-term increase of CO₂ content in raw NG. In fact, up to 60% of the re-injected CO₂ can be retained in the reservoir (Gozalpour et al., 2005), meaning that 40% (or more) stay in the gas phase, rising its CO₂ content, and leading to incremental costs and risks throughout the lifetime of offshore NG processing.

Such huge uncertainties demand the use of decision techniques under the influence of stochastic factors for safely and tightly designing offshore units of CO₂-rich NG processing. Associated with advances in Computer-Aided Engineering (CAE), the Monte-Carlo (MC) method is a powerful technique for decision under non-deterministic scenarios. Monte-Carlo analysis can estimate the probability of success of process designs to accomplish all specifications or targets within a defined stochastic scenario of interest. Monte-Carlo analysis generates samples of target process responses under stochastic scenarios randomly sampled according to the probability density function (*PDF*) of certain non-deterministic factors influencing such responses (Dzobo et al., 2012).

In addition, the process industry is moving towards the design of innovative and more sustainable processes that show improvements in both economic and environmental factors (Tula et al., 2017). Corporations worldwide are realizing that sustainability makes good business sense and is fundamental to their survival and growth (Bakshi, 2003). Especially, concerns about the impacts of Oil and Gas exploitation on the

wellbeing of the environment and society have led to increasing pressures for the O&G industry to move towards more sustainable processes (Wan Ahmad et al., 2016).

For designing more sustainable processes, besides multiple metrics (Sikdar, 2003), ad hoc criteria (Araújo et al., 2015) and tools for quantifying sustainability, statistics algorithms for evaluating performance metrics and for supporting decision making have been developed (Sikdar et al., 2016). In the procedure of achieving superior environmental performance, several alternative process flowsheets are generated by combining multiple unit operations, rendering performance assessment of alternatives cumbersome. Therefore, it is beneficial the use of computer-aided engineering (CAE) methods to evaluate all possible alternatives for defining the most sustainable option (Tula et al., 2017).

In this context, a novel CAE tool, *MCAnalysis-HUB*, is presented in this work. *MCAnalysis-HUB* integrates process simulator HYSYS (AspenTech Inc.) and MATLAB (The Mathworks Inc.) to generate automatized Monte-Carlo analysis based on collecting process responses after submitting process flowsheet to samples of stochastic input variables with known *PDF*. *MCAnalysis-HUB* is designed as an interoperability framework with following capabilities: (i) management of sampling of stochastic input variables with hundreds or thousands of elements; (ii) submission of input samples to a process model represented by a HYSYS flowsheet with all pertinent streams and unit operations; (iii) gathering the generated data of output variables (responses) to check attainment of specifications; and (iv) generation of stochastic diagnostics and graphic reports to estimate the success probability of the design in accomplishing specifications. Based on such success probability, the designer can evaluate if the design is approved or if further changes are required to raise such probability.

Considering the result of multiple MC samples of the process responses, *MCAnalysis-HUB* also integrates the Waste Reduction (WAR) algorithm (Cabezas et al., 1999) to produce Potential Environmental Impacts (PEIs) as statistics indicators for assessing environmental performance under non-deterministic scenarios of process conditions. Statistics indicators for assessing economic performances are

also generated by *MCAnalysis-HUB* under both process and economic stochastic scenarios using the methodology of Turton *et al.* (2009) for onshore facilities adapted to offshore context and new technologies. Based on the statistics PEIs generated by *MCAnalysis-HUB*, Principal Component Analysis (PCA) can be used to identify the most relevant ones (Roffel and Betlem, 2006).

1.2. GOALS

This D.Sc. Thesis aims at assessing design, environmental and economic performances of new technologies of offshore processing of CO₂-rich NG via automatized Monte-Carlo analysis using novel CAE tool *MCAnalysis-HUB*. Therefore, this work has the following goals:

1. Introduce a new design concept for offshore processing of CO₂-rich NG under uncertainties via Monte-Carlo analysis conducted by *MCAnalysis-HUB*, to lead to more sustainable NG processing by avoiding oversized, excessive power consumption, pollutants emissions, and/or unachieved specifications.
2. Design sustainable offshore rigs, which comprise very risky systems operating at very special conditions in terms of safety concerns and exposition to hazards, for processing of CO₂-rich NG under influence of stochastic factors to accomplish given success probability of product specifications, operational constraints, and economic specifications. Based on such success probability, critical aspects of the projects can be achieved:
 - Minimize offshore rig footprint and weight by avoiding oversized process design;
 - Minimize environmental/economic impacts by avoiding losses of products with unachieved specifications,
 - Minimize CO₂ emissions by minimizing power consumption;
 - Minimize investment and operational costs;
 - Evaluate if the process design is sustainably viable or not, and adjust process design to achieve satisfactory sustainability indicators.

3. Assess and compare design, environmental and economic performances of processing of CO₂-rich NG under non-deterministic scenario of feed and economic variables according to two processing routes, Conventional-Route and Supersonic-Separator-Route (SS-Route), to fulfill all design and economic specifications in at least 75% of sampled cases.
4. Evaluate, via Monte-Carlo analysis, supersonic separator performance for treating CO₂-rich raw NG aiming at WDPA+HCDPA in offshore rigs with stochastic input variables. This procedure was never tried before and can unveil possible weaknesses or, on the contrary, resilience of SS units for treating CO₂-rich raw NG under uncertainties.
5. Evaluate design, environmental and economic impacts of the increase of CO₂ content in raw NG, considering a Conventional-Route submitted to two scenarios of CO₂ content, with focus on the environmental performance behavior in relation to stochastic feed variables, and on the identification of the most relevant PEIs to the scenarios.
6. Develop a novel, reliable, robust and flexible CAE tool, *MCAnalysis-HUB*, in HUB architecture, to automatize MC analysis of multiple systems and build several different scenarios of sustainability assessment.

1.3. STRUCTURE OF THIS D.Sc. THESIS

This D.Sc. Thesis contains 4 chapters, including the present introduction chapter, which presents the context/motivation, the goals, and the structure of the Thesis.

Chapter 2 presents a literature review on NG context and offshore processing, Monte-Carlo analysis, environmental and economic performances and PCA.

Chapter 3 details the methods used for process simulation of offshore processing of CO₂-rich NG, describing stochastic feed variables and process responses, as well as the design of the process simulations assessed in the Thesis; environmental and

economic premises; Inverse Transform Method for generating *PDFs* of input stochastic variables; the proposed Monte-Carlo approach for plant design; and the architecture of CAE tool *MCAAnalysis-HUB*.

The results of process design, environmental and economic assessments via Monte-Carlo analysis of the designs of offshore processing of CO₂-rich NG evaluated in the Thesis are detailed in Chapter 4. This chapter is divided by sub-topics of process design assessment, environmental assessment and economic assessment of targeted designs of CO₂-rich NG processing: Conventional-Route versus SS-Route; and CO₂ content increase in Conventional-Route.

Chapter 5 presents the conclusions of this Thesis.

2. LITERATURE REVIEW

2.1. NATURAL GAS CONTEXT

Energy demand of natural gas, the cleanest of the fossil fuels, has been increasing worldwide and shall continue to increase over the years to similar magnitude as oil demand (BP, 2019a,b), as Figure 1 shows.

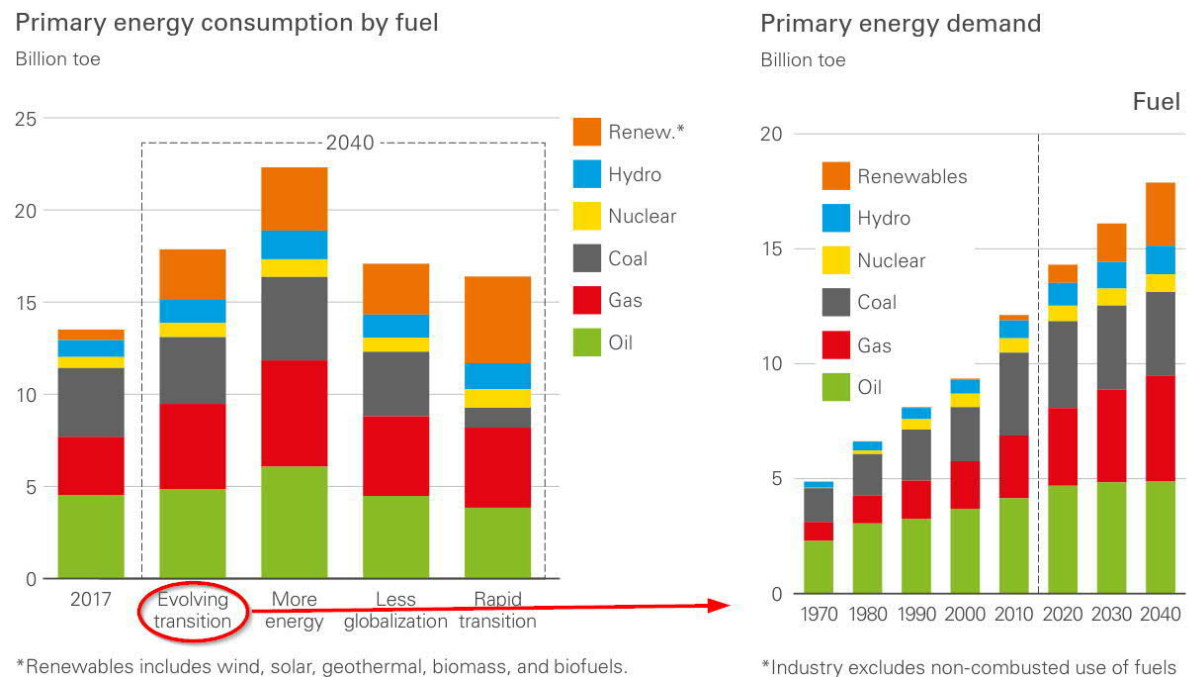


Figure 1. Outlook of primary energy demand. Source: (BP, 2019b), adapted.

In all the scenarios considered on the BP Energy Outlook (2019b), world gross domestic product (GDP), representing the total monetary value of all final goods and services produced, more than doubles by 2040 driven by increasing prosperity in fast-growing developing economies. In the 'Evolving transition' scenario, this improvement in living standards causes energy demand to increase by around a third over the Outlook, driven by India, China and other countries in Asia which together account for two-thirds of the increase. Around 80% of the world's population today live in countries where average energy consumption is less than 100 GJ per head. In the 'Evolving transition' scenario, this proportion is still around two-thirds even by 2040. In the scenario 'More energy', this share is reduced to one-third by 2040, requiring around 25% more energy by 2040. The scenario 'Less globalization' scenario considers a case in which trade disputes increase and have a persistent impact on the energy system, as international trade has an important influence on the

global energy system: it underpins economic growth and allows countries to diversify their sources of energy. In the 'Rapid transition' scenario, the growth of renewables is even quicker, with the share increasing from 1% to 10% in just 15 years. Such rapid growth would be literally off-the-charts relative to anything seen in history. Much of the Outlook is described with reference to the 'Evolving transition' scenario, but that does not imply that the probability of this scenario is higher than the others.

In Brazil, the Pre-Salt pole is among the most important discoveries of oil and natural gas in the last years. It is located in an area of approximately 149,000 square kilometers in the territorial sea between the states of Santa Catarina and Espírito Santo. The total depth (distance between the surface of the sea and the oil reservoirs below the salt layer) can reach 7,000 meters. The reserves are composed of large accumulations of light oil, which has excellent quality and a high commercial value. As the oil in several Pre-Salt basins presents high GOR and high CO₂ content in the associated gas, offshore processing of CO₂-rich NG requires especial attention due to technology challenges of FOAK designs. The topology of the Pre-Salt layer is depicted on Figure 2.

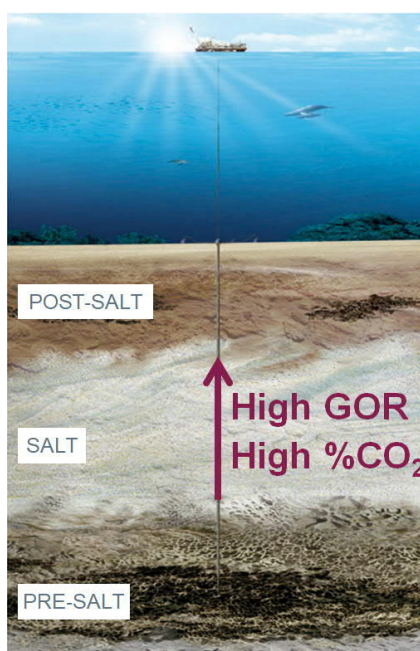


Figure 2. Pre-Salt layer topology. Source: <http://www.petrobras.com.br/pt/nossas-atividades/areas-de-atuacao/exploracao-e-producao-de-petroleo-e-gas/pre-sal>, adapted.

2.2. OFFSHORE NATURAL GAS PROCESSING

2.2.1. Water dew point adjustment (WDPA) and hydrocarbon dew point adjustment (HCDPA) – Conventional technologies

WDPA is achieved by gas dehydration, and this is a fundamental operation in NG process to avoid the generation of hydrocarbons (HCs) hydrates, which occurs at high pressures and temperatures under 15°C, common conditions in subsea offshore pipelines. Such hydrates can precipitate as solids similar to ice, which can deposit in the pipelines as snow and re-freeze, reducing the ducts diameter and causing load loss, capacity reduction, shut-downs or even violating limits of operational safety (Sant'Anna et al., 2005). Netusil and Dittl (2011) compared three methods for NG dehydration which are commonly applied in industry.

- **TEG absorption:** Wet NG is dehydrated via direct contact with lean TEG in a glycol contactor with countercurrent flows. During the contact, TEG is enriched by water (rich TEG). Rich TEG is heated to be regenerated (lean TEG) and recycled to the contactor.
- **Solid desiccant adsorption:** Water is removed from wet NG by a solid desiccant on a molecular sieve, silica gel or alumina. The amount of adsorbed water molecules increases with pressure and decreases with temperature. As adsorption dehydration columns always work periodically, they shall work with parallel beds to ensure operational continuity. Usually, one bed dries the gas while the other is being regenerated by reverse contact with preheated dehydrated gas.
- **Condensation:** NG is cooled by pressure drop for water condensation and removal from NG stream. Natural gas liquids (NGLs) and condensed higher HCs can also be recovered from NG by cooling for simultaneous WDPA by dehydration and HCDPA by NGL recovery. NG can be advantageously cooled by JTE, which describes how the temperature of a gas changes with pressure drop under constant enthalpy in a valve. NG expansion under constant enthalpy makes the average distance between molecules increase, leading to increase of potential energy associated to Van der Waals forces. During the

expansion, there is no heat exchange or work creation, therefore, according to the 1st Law of Thermodynamics, the increase of potential energy leads to a decrease in kinetic energy and thus decrease of NG temperature. Netusil and Dittl (2011) concluded that this process is more suitable to NGL recovery for achieving HCDPA.

According to Bahadori and Vuthaluru (2009), NG dehydration via TEG absorption for achieving WDP is the most economically favorable option under standard conditions, despite its heat consumption for TEG regeneration. In the Conventional-Route selected for this work, WDP is done via TEG dehydration and HCDPA is accomplished via JTE (Gonzaga et al., 2017a; Gonzaga et al., 2019a;b;c;d).

2.2.2. Water dew point adjustment (WDP) and hydrocarbon dew point adjustment (HCDPA) – Supersonic separator

Supersonic separator (SS) is a new technology for some steps of onshore processing of raw NG – e.g., HCDPA (Machado et al., 2012) – and offshore processing of raw CO₂-rich NG – e.g., WDP, HCDPA and CO₂ removal (Arinelli et al., 2017).

SS comprises a Laval nozzle (L^{LAVAL}) followed by an ending diffuser (L^{Diff}) as sketched in Figure 3 for linear diameter profiles. The Laval comprehends the converging section (L_C), the throat and the Laval diverging section (L_D - L^{Diff}). In the converging section, there are static vanes impelling the fluid to swirl, while at the Laval end there are side collectors to catch liquid droplets under centrifugal motion. The ending diffuser (L^{Diff}) is a continuation of the Laval diverging section (Figure 3) after the liquid collector. Throughout SS, the flow is described by the Mach Number, $Ma=v/c$, where v and c respectively represent axial flow velocity and the sound speed property. Flow is subsonic ($Ma<1$) in the Laval converging section and accelerates to become sonic ($Ma=1$) at the Laval throat; then further accelerates to supersonic ($Ma>1$) in the Laval diverging section, causing great temperature and pressure drops. Due to high rate of enthalpy conversion into kinetic energy, water and C3+ change to low-enthalpy liquid mists, and the flow becomes two-phase (gas and liquid C3+; or gas and super-cooled water) or three-phase (gas, liquid C3+ and super-cooled water). At this point, c is a multiphase sound speed property which must be predicted

adequately for correct Ma determination as shown in (de Medeiros et al., 2017) and in the Chapter 5 of (de Medeiros et al., 2019).

Supersonic flow is metastable for outlet pressure (P^{Outlet}) higher than the supersonic pressure (P); and this instability grows as $P^{Outlet}-P$ increases as the fluid expands supersonically. Therefore, at some point the supersonic flow experiences the normal shock irreversible adiabatic transition becoming a stable subsonic flow at higher pressure, temperature and entropy, while conserving mass, momentum and energy flow rates. For successful SS operation, liquid must be collected before the shock front (Figure 3), otherwise separation is lost by re-vaporization across the shock. The after-shock flow is subsonic with $Ma_{AS} < 1$ (Ma just after shock) and performs a subsonic compression through the ending diffuser (L^{Diff}) recovering pressure and temperature up to (P^{Outlet}, T^{Outlet}) at SS outlet. Even in the case of isentropic expansion/compression SS steps, some head-loss must occur because normal shock is eminently irreversible and a strong entropy creator, forcing the discharge pressure (P^{Outlet}) to be lesser than inlet pressure ($P^{Inlet}-P^{Outlet} > 0$). The SS head-loss increases (and the minimal SS temperature decreases) with the maximum attained (multiphase) supersonic Ma just before condensate withdrawal. This value is called Ma^{Shock} and is a SS specification, indirectly specifying P^{Outlet} . After condensate removal, Ma falls at constant section normally attaining a lower supersonic Ma when not too intense condensation occurs as in regular WDPA+HCDPA (Arinelli et al., 2017). This value is referred as Ma_{BS} (Ma just before shock and after condensate withdrawal), so that in general $Ma_{AS} < 1 < Ma_{BS} < Ma^{Shock}$. It must be noted that the three points on the SS axis with subscripts “ BS ”, “ AS ” and superscript “ $Shock$ ” are virtually the same in space (Figure 3) as liquid ejection is assumed instantaneous and the immediate shock front has extremely narrow thickness (Arinelli et al., 2017).

Two main SS research lines dominate the literature: (i) thermodynamic frameworks (Arinelli et al., 2017; de Medeiros et al., 2019; Teixeira et al., 2018; Brigadão et al., 2019); and (ii) computational fluid dynamic (CFD) approaches (Wen et al., 2012; Yang et al., 2014). As pointed out in Arinelli et al. (2017), CFD approaches for SS simulation have some issues as CFD cannot handle multicomponent vapor-liquid equilibrium (VLE) or vapor-liquid-water equilibrium (VLWE) transitions, neither the multiphase sound speed (c), all essential aspects for SS modeling with feeds that

generate condensate such as high-pressure raw NG. Other CFD limitations are: (i) multiphase c is not correctly determined as phase-behavior is ignored; (ii) too cold pre-shock temperatures result from neglecting condensation, implying entropy destruction and violation of the 2nd Law of Thermodynamics; and (iii) pressure, temperature and Mach profiles cross normal shock (a sudden discontinuous front) following inclined linear patterns accompanied by oscillating anomalies upstream/downstream the front. On the other hand, thermodynamic SS approaches model VLE and VLWE compressible flows and multiphase c , and satisfy the 2nd Law everywhere, but the hypothesis of thermodynamic equilibrium is not likely to be fulfilled in the real SS during a few milliseconds of SS lapse (i.e., a kinetic limitation). Nonetheless, thermodynamic SS approaches are more adequate for raw NG feeds because SS performance is represented in the thermodynamic limit strictly satisfying the 2nd Law, while common CFD approaches for SS with raw NG violate the 2nd Law as unrealistic too cold pre-shock temperature results meaning adiabatic entropy destruction.

In this work, SS is simulated in HYSYS via two Unit Operation Extensions SS-UOE (Arinelli et al., 2017) and PEC-UOE (de Medeiros et al., 2017). SS-UOE is a rigorous thermodynamic SS model for multiphase compressible flow adopting rigorous phase-splitting and using any Equation-of-State available in HYSYS palette such as the Peng-Robinson (PR-EOS). SS-UOE designs SS matching sonic throat flow, and executing supersonic expansion, condensate withdrawal, shock transition and diffuser compression. Consequently, SS-UOE calculations demand accurate Ma determination along SS flow path. For this finality, PEC-UOE is used for correct determination of the (multi) phase-equilibrium c also using any available HYSYS Equation-of-State.

SS-UOE models SS as a converging-diverging nozzle with linear diameter profiles (Figure 3), but any diameter profile with/without cylindrical sections can also be installed. SS-UOE design specifications comprise: (i) feed data (temperature, pressure, flow rate and composition); (ii) number of parallel SS's; (iii) SS inlet/outlet diameters (D_I , D_O); (iv) SS converging/diverging angles (α , β); (v) adiabatic expansion/compression efficiencies ($\eta^{EXP\%}$, $\eta^{CMP\%}$); and (vi) Ma^{Shock} . SS-UOE retrieves feed data from HYSYS flowsheet, designs SS determining throat diameter

(D_T), converging length (L_C), total length (L) and SS head-loss, and installs the corresponding streams of lean gas and condensate products back to HYSYS flowsheet. The modeling algorithm and thermodynamic correctness of SS-UOE were proved in previous work (Arinelli et al., 2017; Brigadão et al., 2019). For instance, SS-UOE algorithm and its validation, using data from (Yang et al., 2014), can be found in Brigadão et al. (2019), where SS was used in a new air purification system, and in Arinelli et al. (2019), which studied SS for processing CO₂-rich NG at supercritical conditions.

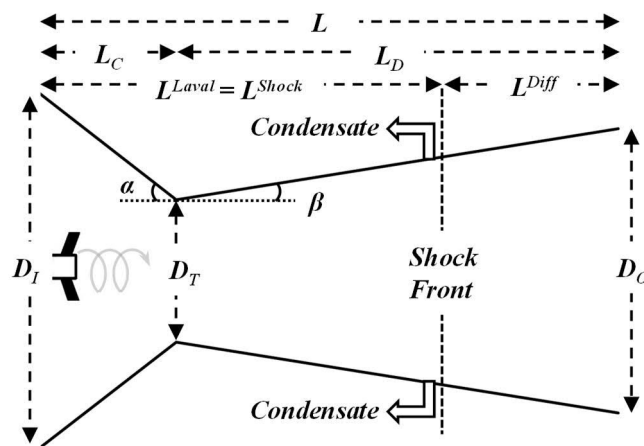


Figure 3. SS sketch with linear diameter profiles: geometric parameters.

2.2.3. CO₂ Removal

As there has been increasing demand for the use of NG a more efficient and cleaner fuel, CO₂ removal is an important operation to remove such pollutant which also decreases NG heating value, occupies gas pipeline as inert, and can create corrosive acids or acid solutions with water, leading to potential damage to pipelines and equipment. The level of CO₂ in the atmosphere has increased by a third since the beginning of the industrial age and CO₂ emissions currently contributes to about 73 of the potential for global warming (Grossmann, 2004). Yeo et al. (2012) compared conventional processes and MP for CO₂ removal from NG.

Conventional processes:

- **Chemical absorption:** Chemical absorption for CO₂ capture is based on exothermic reaction of a sorbent with CO₂ present in the gas stream at low temperature. The reaction is then reversed in so called regeneration at higher temperature and low pressure. Loading capacity is limited by the amount of the active component in the solution. When saturation level is reached, only a minor loading can be achieved by physical absorption in the solution. Chemical solvents bind strongly to CO₂, which is effective even at low partial pressures, however, the regeneration of the rich solvent is high energy demanding. In the case of low CO₂ content in NG and high purity CO₂ of the product, chemical solvents are mostly used. Two groups of chemicals commonly applied to CO₂ removal are amines and potassium carbonate.
 - **Alkanolamine sweetening:** Monoethanolamine, diethanolamine, triethanolamine, diisopropanolamine, methyldiethanolamine, and diglycolamine are examples of the family of organic compounds that can be used in aqueous solutions ($\approx 30\%w/w$) for CO₂ capture. Among these amines, monoethanolamine is most widely used as it is more selective to CO₂, higher thermo stability for regeneration and lower regeneration enthalpy than other amines. Aqueous solution is needed to keep the solvent selective only to acid gases, helping to keep HCs in gas phase. CO₂ loading capacity is limited to amine conversion ratio (amine + water + CO₂ \rightarrow amine carbonate + heat), and such loading is hardly over 1 mol CO₂/1 mol amine. Amine regeneration is also required via reverse reaction. Such technique has wide commercial use and can be considered one of the most mature technology for CO₂ removal from NG, however, it has several drawbacks such as low CO₂ loading capacity, high equipment corrosion, high energy consumption during solvent regeneration, amine degradation, high solution circulation rate and solution degradation.
 - **Hot-Carbonate Absorption:** This is a chemical conversion process that removes CO₂ from NG via reaction at high temperature with

carbonates aqueous solution (most commonly potassium carbonate (K_2CO_3)) generating bicarbonates ($K_2CO_3 + CO_2 + \text{water} \rightarrow 2KHCO_3$). Solvent is selective to acid gases, not reacting with other NG components. CO_2 loading capacity is limited to carbonate conversion rate.

- **Physical absorption:** Physical uses solvents that do not react with CO_2 and loading capacity is directly proportional to the partial pressure of the component to be removed. CO_2 solubility within the solvents depends both on the partial pressure and the temperature of the feed NG where it favors the higher CO_2 partial pressure and lower temperature. This method has the advantages of that regeneration of the rich solvent requires is not high energy demanding and that CO_2 loading capacity is not limited by reaction stoichiometry. However, physical solvents have a weaker affinity towards acid gas, which means that the lean solvent does not rapidly absorb acid gases and HCs are also absorbed, leading to NG losses. In that matter, to mitigate HCs absorption, such processes make use of oxygenated compounds, such as methanol, propylene carbonate and polyglycols, being Rectisol and Selexol the most common ones.
- **Physical-chemical absorption:** This process uses a combination of amine and other organic physical solvents, which can usually accept a higher loading than an aqueous amine solution, thereby reducing solvent rates. Solfinol is the most common process.
- **Adsorption:** Adsorption is the enrichment of gaseous or dissolved solvents on the boundary surface of a solid. These surfaces have so called active sites which can bind foreign molecules. The most common processes are: molecular sieve adsorbents (zeolites, aluminum-phosphate) and activated carbon.

Chemical absorption has been proven to be a well-accepted technology in NG processing industry. However, this process requires a particularly expensive absorber tower: large, thick walled and heavy vessels. Besides, large amounts of absorbent fluid must be used and high maintenance is needed to keep absorber

stripper units in good condition. On the other hand, adsorption is not an attractive approach for CO₂ removal in industrial treatment due to both CO₂ capacity and low selectivity of available adsorbents. Besides, conventional CO₂ adsorption in natural gas processing has been proven to be costly, low efficiency, requires pre-treatment, and produces large amounts of waste water. Other drawbacks of conventional processes used for CO₂ removal generally include energy demanding, high equipment costs, expensive solvents, and extreme complexity of the processes. In addition, negative environmental impacts may result due to volatile solvents of these processes undergoing degradation and loss during operation (Yeo et al., 2012).

Membrane permeation:

In MP, CO₂ is removed from NG due to the membrane selectivity to CO₂ compared to other NG components, which are retained in the high-pressure side of MP module (Figure 4) in the retentate stream, while CO₂ permeates through the membrane as the low-pressure permeate stream. The preferred membranes used for CO₂ removal from NG in NG offshore processing plants are cellulose-acetate membranes (CAM) produced as hollow-fiber (ex.: Cynara from Schlumberger) or flat sheets packaged as spiral-wound modules (ex.: Separex from UOP) (Baker and Lokhandwala, 2008).

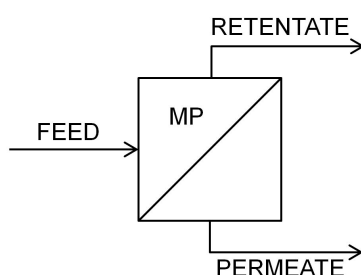


Figure 4. MP module sketch.

Given the scenario of conventional technologies, CO₂ removal from NG via MP has becoming a promising approach due to advantages such as (i) operational simplicity and high reliability; (ii) low capital and operating cost; (iii) environmentally friendly; (iv) good weight and space efficiency; (v) reduced energy consumption, low maintenance required, energy efficient and clean process; (vi) requires simple and inexpensive filtration; and (vii) the process is continuous and does not require regeneration unlike absorption and adsorption processes (Yeo et al., 2012).

However, MP also has some drawbacks, such as (i) binomial selectivity and processing capacity cannot be fulfilled simultaneously; i.e. MP units are selective to CO₂ and operate with low permeation capacity or they operate at high permeation capacity with low selectivity to CO₂ (losses of methane in the permeate), (ii) indirect compression power to pressurize low pressure CO₂-rich permeate for EOR, (iii) degradation of MP material to continue exposure to C₃+ condensed in MP, high pressure and CO₂ solubilization, which leads to swelling and plasticization (Hao et al., 2008), limiting MP lifespan. Therefore, in some conditions of NG flow rate and CO₂ content, alkanolamine sweetening or a combination of MP and alkanolamine sweetening are the most efficient processes for CO₂ removal from NG.

In the Conventional-Route and in the MP-Route selected for this work (Gonzaga et al., 2017a; Gonzaga et al., 2019a;b;c;d), MP is preferred due to its capability of processing CO₂-rich feeds with low footprint and operational costs, while offering modularity (Reis et al., 2017), a key attribute for offshore operation under uncertainties that allows plant adaptation for feed fluctuations, despite the low-pressure CO₂-rich permeate, which demands compression to high-pressure for EOR utilization in the reservoir via subsea pipelines.

2.3. PROCESS DESIGN UNDER NON-DETERMINISTIC SCENARIOS

Current literature of NG offshore processing normally focuses on process design under constant feed conditions and often the impacts of non-deterministic scenarios are neglected. However, as huge feed uncertainties affect NG processing (especially when NG processing comprises high CO₂ content and elevated GOR), techniques for process design under non-determinist scenarios are necessary.

In this matter, a common practice in the industry is to overestimate operational parameters based on worst-case assumptions of uncertain process input variables (Arellano-Garcia and Wozny, 2009). Such practice usually leads to oversized design of not only costly process equipment, but equipment which also presents high operation risks with immediate impacts to personnel and to the environment in case of incidents/accidents, as compressors and subsea pipelines. This leads to feasible plants with profitability drastically reduced (Li et al., 2004), besides direct impact on the stringent limited availability of footprint and weight on offshore topsides, and increase of environment, health and safety (EHS) risks of the plant.

Another usual practice is to accomplish process design based on average values, which often leads to undersized plants, leading to the production of unachieved products. This approach also hinders both economic and environmental performances of the plant.

On the other hand, techniques for process design under non-deterministic scenarios, as Monte-Carlo analysis, can provide a tighter process design considering stochastic distributions of process input variables and estimating the approval percentage for process output variables to accomplish mandatory specifications and targets. Such techniques avoid the usual practice of addressing best/average/worst case scenarios and lead to more sustainable designs for NG offshore processing.

2.4. MONTE-CARLO ANALYSIS

Monte-Carlo analysis is appropriate for studying real systems under non-deterministic scenarios, especially when analytical solutions are complex or impossible to be solved due to non-deterministic components not known a priori (Dzobo et al., 2012) or also for real data analysis without resorting to approximations based on average values (Taut et al., 2000). Monte-Carlo analysis approaches the problem solution by stochastic sampling of input variables of the system obeying known *PDF* instead of solving the numeric-mathematical problem directly. Therefore, Monte-Carlo techniques can be used to solve any mathematical problem or complex model demanding excessive analytical solution effort. Based on the Central Limit Theorem, Monte-Carlo analysis reproduces the stochastic behavior of a non-deterministic system at the limit of infinite sampling. For this statement to be valid, sampling must be random and the number of samples must be high enough to represent the system variability, a condition known as ergodicity (Ratick and Schwarz, 2009).

Hastings (1970) pointed out that Monte-Carlo solutions could be more efficient than conventional numeric methods; in spite of the usually high computational effort required for Monte-Carlo applications (Grossmann et al., 2015). In oil and gas engineering Monte-Carlo analysis was used by Eckstein et al. (2000) in turbulent mixing, by Lagache et al. (2004) for predicting thermodynamic properties of NG at high-pressure, by Tang et al. (2015) in oil/gas drilling, and by Jain et al. (2003) in porous-medium flow. Albrecht (2013) used Monte-Carlo Markov Chain to estimate reaction parameters under uncertainty, while Dehghani et al. (2017) used Monte-Carlo molecular simulation to investigate structural-transport properties of polyether block amide-MFI zeolite membranes for CO₂/CH₄/N₂ separation. In connection with exploration and production of shale-gas, Perez and Devegowda (2017) and posteriorly Zhang et al. (2018) carried out Grand Canonical Monte-Carlo simulations to study methane adsorption in the organic matrix of shales. In the context of NG transmission pipelines, Yu et al. (2018) applied Monte-Carlo reliability analysis under effects of underground gas storages, while Yu et al. (2019) considered the reliability analysis under market uncertainties. Zhang et al. (2019) used Monte-Carlo analysis for design/operation optimization of NG distribution pipelines under market uncertainties, while Tan et al. (2017) applied it to planning of carbon management

networks. Regarding health/safety/environment risk assessments, Monte-Carlo analysis was used by Arunraj et al. (2013) in benzene extraction, by Lonati and Zanoni (2013) in mercury emissions, by Habib et al. (2014) regarding radioactivity in Libyan oil fields, and by Olaru et al. (2014) for environmental risks. Monte-Carlo is also used in cancer studies regarding uncertainties on cancer causes and treatments. In this context, Monte-Carlo was used by Yeh et al. (2014) to modulate radiation therapy doses for nasopharyngeal cancer and by Guimarães et al. (2014) for liver cancer treatment via microspheres with beta-emitting radioisotopes. Lastly, Monte-Carlo was used by Andronov (2005) in probability distributions of Boolean functions.

In Monte-Carlo analysis of processes, the objective is to assess the performance of given dependent variables of interest (output variables or responses) according to the behavior of stochastic independent variables with influence over them (input variables). The procedure creates samplings of input variables by generating pseudo-random numbers converted to random samples obeying input variables *PDFs*. When a high number of random samples of input variables is used to calculate the correspondent samples of output variables, the stochastic behavior of the output variables can be approximated as frequency histograms that asymptotically converge to the respective *PDFs*. Such graphical reconstitution can be used for understanding the system behavior and thus can shed some light for sizing (design) decisions. Although the Monte-Carlo concept is simple, its operationalization requires high number of process simulations and numerical methods. The Inverse-Transform Method, described by Jacques (1998) and used by Eckstein et al. (2000) and Arunraj et al. (2013), was selected in this work for generation of pseudo-random populations of stochastic input variables.

2.4.1. Quasi-Monte-Carlo Sampling

The Quasi-MC (Quasi-Monte-Carlo) is an alternative sampling method for certain contexts where conventional MC sampling is used, such as numerical multi-dimensional integrations. Differently from MC sampling, low-discrepancy sequences – e.g., Halton and Sobol sequences – also called sub-random or quasi-random sequences are used in Quasi-MC (Caflisch, 1998), which is presented in opposition to the regular MC sampling applications based on pseudo-random sequences. Both MC and Quasi-MC samplings can be used in multi-dimensional integrations where common numerical methods – e.g., Newton-Cotes formulas – encounter some difficulties. The advantage of Quasi-MC over regular MC has to do with the faster rate of convergence of the former ($O(1/N)$) relatively to the latter ($O(1/\sqrt{N})$), where N is the number of samples. Nevertheless, Quasi-MC has some shortcomings relatively to MC (Lemieux, 2009), such as: (i) superiority of Quasi-MC over MC only appears for high N and not too high dimensionality (number of stochastic input variables); (ii) upper bounds of Quasi-MC error sometimes cannot be found for highly non-linear responses – e.g. output variables with multi-modal behavior; (iii) regular MC sampling is easy to implement and to automatize even for non-linear complex systems as in offshore processing of CO₂-rich NG; and (iv) the high non-linear behavior of some output variables may entail multi-modal responses for unimodal inputs (e.g., normal input variables) – as confirmed in multiple figures of Sec. 4 of this work – with the consequence that the superior performance of Quasi-MC is held back by such patterns, whereas MC sampling is quite resilient in such cases.

In spite of the apparent superiority of Quasi-MC over MC, the present work uses regular MC sampling. The reason arises from the discussion in the previous paragraph and also from the much easier and robust implementation of MC sampling in *MCAnalysis-HUB*, added to the fact that the number of HYSYS flowsheet simulations is not too high for statistical convergence of output variables populations measured in terms of sample mean ($\langle X \rangle$) and sample variance (S_X^2).

2.5. ENVIRONMENTAL PERFORMANCE – WAR ALGORITHM

Several methodologies for characterizing the environmental impact of products and processes are available in the literature, such as Life Cycle Assessment (LCA) and WAR algorithm, both well-established techniques to include environmental considerations into process design (Sepiacci et al., 2017). The LCA methodology assesses the environmental performance of a product or process thorough its life cycle: from the primary resources to recycling or safe disposal (Clift, 2006). However, this methodology requires a large amount of information and few data are publicly available due to legal or intellectual property concern (Jiménez-González et al., 2000). The WAR algorithm considers only the product manufacturing step (Young and Cabezas, 1999), as Figure 5 shows. WAR is selected to be used in this work due to its simplicity when compared to LCA. It is worth noting that WAR, contrarily to LCA, is restricted to *gate-to-gate* analysis (Figure 5).

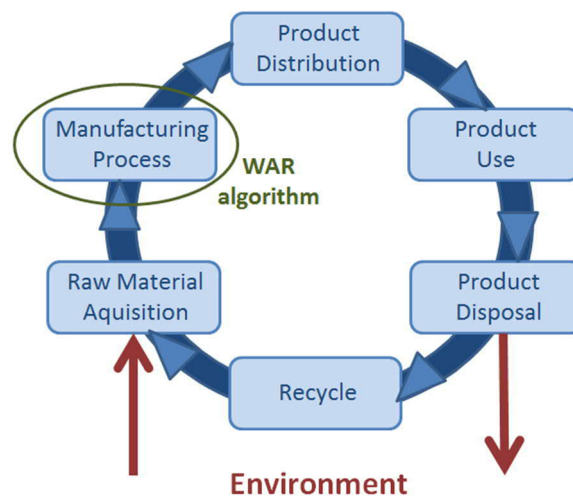


Figure 5. WAR algorithm with plant life cycle (adapted from Young and Cabezas (1999)).

Another reason why WAR algorithm is selected for this work is the incorporation of pollution prevent techniques into process design (Young et al., 2000) as evaluating just the amount of produced waste/power consumption with metrics such as absolute waste production/power consumption, or waste production/power consumption per product mass may not be enough if the environmental impact of the waste streams are not taken into consideration on the evaluation. One process design may release more waste, but another design may release less waste which is more pollutant than

the first process, depending on the components present in each waste. Besides, Barret et al. (2011) and Sepiacchi et al. (2017) presented several applications of the WAR algorithm in the engineering context, such as: optimization of chemical manufacture and recovery, design of eco-efficient biodiesel processes, modeling of industrial utility systems, evaluation of environmental impact of cumene production, assessment of acetic acid recovery from waste mixture, determination of the effect of different gasoline additives, design of separation processes with fugitive emissions, optimization of reactor design, minimization of the impact of a utility plant, design of refrigerant mixtures, optimization of a distillation unit, comparison of ethanol production from sugar cane and corn, and analysis of different schemes for producing n-butyl acetate.

WAR was proposed by (Cabezas et al., 1999) as a general theory for the flow and generation of potential environmental impacts (PEIs) through a chemical process and is used to quantify its environmental performance. By definition, PEI is the unrealized average effect or impact that the emission of mass and energy would cause to the environment, being essentially a probability function associated to a potential effect. A PEI conservation equation based on an accounting of the flow of PEI in/out of the product manufacturer and energy generation (Young and Cabezas, 1999) is introduced by WAR in Eq. (1) for steady state balance, where $\dot{I}_{in}^{(cp)}$ and $\dot{I}_{out}^{(cp)}$ are the input and output rates of PEI of the chemical process, $\dot{I}_{in}^{(ep)}$ and $\dot{I}_{out}^{(ep)}$ are the input and output rates of PEI of the energy generation process, $\dot{I}_{we}^{(cp)}$ and $\dot{I}_{we}^{(ep)}$ are the output of PEI associated with the waste energy lost from the chemical and energy generation processes and $\dot{I}_{gen}^{(t)}$ represents the creation or consumption of PEI by chemical reactions inside the chemical process and the power plant. Figure 6 illustrates Eq. (1).

$$\dot{I}_{in}^{(cp)} + \dot{I}_{in}^{(ep)} - \dot{I}_{out}^{(cp)} - \dot{I}_{out}^{(ep)} - \dot{I}_{we}^{(cp)} - \dot{I}_{we}^{(ep)} + \dot{I}_{gen}^{(t)} = 0 \quad (1)$$

PEI is calculated by a unified score obtained by the weighted sum of eight environmental impact categories, listed in Table 1, and a specific PEI for each impact

category is associated to the components of the process streams as shown in Eq. (2), where l is an indicator for input or output, α_i is the weighting factor for environmental impact category i , $\dot{M}_{j,l}$ is the mass flow of stream j , x_{kj} is the mass fraction of component k in stream j and ψ_{ki}^s is the specific PEI of component k associated with environmental impact category i . The measures for calculating each ψ_{ki}^s are also listed in Table 1. The calculation of ψ_{ki}^s is given by Eq. (3) where $(Score)_k$ represents the impact score of component k correlated with environmental category i and $\langle (Score)_k \rangle_i$ represent the average impact score of all components in category i . This normalization of the component impact eliminates unnecessary bias within the category. The specific correlations among each category score and its corresponding measure of impact are described in (Young and Cabezas, 1999).

$$\dot{I}_l = \sum_i^{EnvCats} \alpha_i \sum_j^{Streams} \dot{M}_{j,l} \sum_k^{Comps} x_{kj} \psi_{ki}^s \quad (2)$$

$$\psi_{ki}^s = \frac{(Score)_{ki}}{\langle (Score)_k \rangle_i} \quad (3)$$

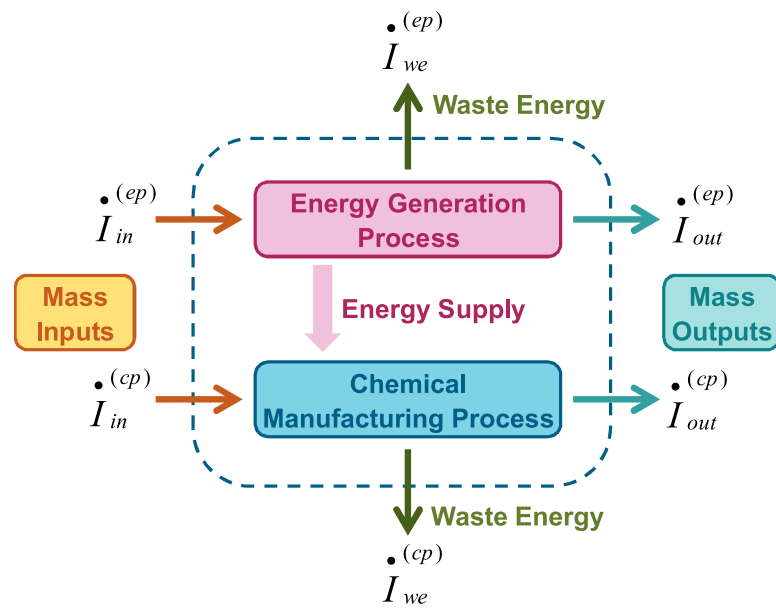


Figure 6. WAR algorithm (adapted from Young et al. (2000)).

Table 1. PEI categories and measure of impact associated with PEI category (Barrett et al., 2011).

General PEI category	PEI category	Measure of impact of PEI category
<i>Human toxicity</i>	<i>Ingestion (HTPI)</i>	<i>LD₅₀</i>
	<i>Inhalation/dermal (HTPE)</i>	<i>OSHA PEL</i>
<i>Ecological toxicity</i>	<i>Aquatic toxicity (ATP)</i>	<i>Fathead Minnow LC₅₀</i>
	<i>Terrestrial toxicity (TTP)</i>	<i>LD₅₀</i>
<i>Global atmospheric impacts</i>	<i>Global warming potential (GWP)</i>	<i>GWP</i>
	<i>Ozone depletion potential (ODP)</i>	<i>ODP</i>
<i>Regional atmospheric impacts</i>	<i>Acidification potential (AP)</i>	<i>AP</i>
	<i>Photochemical oxidation potential (PCOP)</i>	<i>PCOP</i>

2.6. ECONOMIC PERFORMANCE

Equipment sizing, based on heuristics rules (Machado et al., 2012; Araújo et al., 2017), is the first step to estimate fixed costs associated to the plant.

The methodology proposed by Turton et al. (2009) is used in this work. The fixed cost of investment (FCI) to build a new facility is calculated via Eqs. (4) to (6), using bare module equipment cost to quantify the cost of a new onshore facility.

Bare module cost of every piece of equipment is calculated as the sum of its direct and indirect costs via Eq. (4), where C_{BM} represents bare module equipment cost: direct and indirect costs, C_p^0 represents purchased cost for base conditions: cheapest material (usually carbon steel) and operating at ambient pressure, and F_{BM} represents bare module cost factor.

$$C_{BM} = C_p^0 F_{BM} \quad (4)$$

Total module cost C_{TM} of an existing facility is calculated via Eq. (5) to consider contingent cost and fees of, respectively, 15% and 3% of C_{BM} , where C_{TM} = total module cost, C_{BM} = equipment bare module cost and i = number of pieces of main equipment.

$$C_{TM} = \sum_{i=1}^n C_{TM,i} = 1,18 \sum_{i=1}^n C_{BM,i} \quad (5)$$

To calculate the cost of a completely new facility C_{GR} , in which construction starts on essentially undeveloped land (grass field), the value of the modules in base conditions $C_{BM,i}^0$ shall be increased in 50% to consider costs for site development, auxiliary buildings, and off-sites and utilities, via Eq. (6).

$$C_{GR} = C_{TM} + 0,5 \sum_{i=1}^n C_{BM,i}^0 \quad (6)$$

As C_{GR} corresponds to the cost of a new onshore facility, such cost shall be adjusted to offshore context via Eq. (7) (Araújo et al., 2017).

$$FCI = C_{GR_Offshore} = 2 * C_{GR_Onshore} \quad (7)$$

The cost of manufacturing (COM) for operating a facility is calculated via Eq. (8), where C_{OL} = cost of operating labor; C_{RM} = cost of raw materials, C_{WT} = cost of waste treatment and C_{UT} = cost of utilities. $F_1=0.18$, $F_2=2.76$, $F_3=1.21$ are cost factors.

$$COM = F_1 * FCI + F_2 * C_{OL} + F_3 (C_{RM} + C_{WT} + C_{UT}) \quad (8)$$

Economic viability can be achieved by positive Net Present Value (NPV), calculated from the cumulative discounted cash flow (CF) over plant lifetime (n). CF is calculated via Eq. (9) and NPV via Eq. (10), where R = Revenue, d = depreciation, t = taxes (45%), i = discount rate (10%) and I_0 = initial investment.

$$CF = (R - COM - d) * (1 - t) + d \quad (9)$$

$$NPV = \sum_{t=1}^n \frac{CF_t}{(1+i)^t} - I_0 \quad (10)$$

Considering Eqs. (8) to (10), (i) C_{OL} can be influenced by uncertainties on economic input variables, as cost of labor, working hours; (ii) C_{RM} by uncertainties on both process and economic input variables, as flow, composition, price and demand of raw materials; (iii) C_{WT} by uncertainties on both process and economic input variables, as waste effluents flow and composition, and cost for waste effluent treatment; (iv) C_{UT} by uncertainties on both process and economic input variables, as utilities flow and price; (v) R by uncertainties on both process and economic input variables, as products flow, price and demand, power consumption, and carbon tax; (vi) FCI by uncertainties on both process and economic input variables, as plant capacity varies due to raw materials flow and composition, products specifications, and equipment prices.

2.7. PRINCIPAL COMPONENT ANALYSIS

PCA consists in re-organizing data sets (e.g. data from process plants), which often exhibit correlated patterns, in order to find a set of new uncorrelated variables as linear combination of the original ones. The new variables are assigned to fractions of the variance in the original data in decreasing order (Roffel and Betlem, 2006). The original data set is organized as a matrix $\underline{\underline{X}}_{m \times n}$, where the scalar variables of the problem correspond to the columns and their samples correspond to the rows, meaning that each vector of sampled data $\underline{X}_i_{m \times 1}$ for variable X_i corresponds to a column of the matrix $\underline{\underline{X}}$, as illustrated by Eq. (11). Each vector \underline{X}_i originates a sample scalar mean $\langle X_i \rangle$ given by Eq. (12). Such sample means are gathered in the vector of means $\langle \underline{X} \rangle$ as shown in Eq. (13) (Gonzaga et al., 2019a). $\underline{U}_{m \times 1}$ is a compatible vector of ones.

$$\begin{array}{c}
 X_1 \ X_2 \ \dots \ X_n \\
 \downarrow \ \downarrow \ \dots \ \downarrow \\
 \underline{\underline{X}} = \begin{bmatrix} x_{11} & x_{12} & \dots & x_{1n} \\ x_{21} & x_{22} & \dots & x_{2n} \\ \dots & \dots & \dots & \dots \\ x_{m1} & x_{m2} & \dots & x_{mn} \end{bmatrix} = [\underline{X}_1 \ \underline{X}_2 \ \dots \ \underline{X}_n]; \ \underline{X}_1 = \begin{bmatrix} x_{11} \\ x_{21} \\ \dots \\ x_{m1} \end{bmatrix}; \ \underline{X}_2 = \begin{bmatrix} x_{21} \\ x_{22} \\ \dots \\ x_{m2} \end{bmatrix}; \ \underline{X}_n = \begin{bmatrix} x_{1n} \\ x_{2n} \\ \dots \\ x_{mn} \end{bmatrix}
 \end{array} \tag{11}$$

$$\langle X_i \rangle = \underline{U}^T \underline{X}_i / m \tag{12}$$

$$\langle \underline{X} \rangle = [\langle X_1 \rangle \ \dots \ \langle X_n \rangle]^T \tag{13}$$

PCA factorizes the matrix of sample variance-covariance $\underline{\underline{R}}_{X_{n \times n}}$ – symmetric and positive definite – obtained by Eq. (14). The n eigenvalues of $\underline{\underline{R}}_{X_{n \times n}}$ are calculated and expressed as a column vector of positive eigenvalues $\underline{\lambda}$ sorted in decreasing order, while the respective orthogonal normalized n eigenvectors ($n \times 1$) are stored as columns of matrix $\underline{\underline{P}}$ as illustrated in Eq. (15).

$$\underline{\underline{R}}_X = \frac{(\underline{X} - \underline{U} \cdot \langle \underline{X} \rangle^T)^T (\underline{X} - \underline{U} \cdot \langle \underline{X} \rangle^T)}{m - 1} \quad (14)$$

$$\underline{\lambda} = \begin{bmatrix} \lambda_1 \\ \vdots \\ \lambda_n \end{bmatrix}, \quad \underline{\underline{P}} = [\underline{P}_1 \quad \cdots \quad \underline{P}_n] \quad (15)$$

Matrix $\underline{\underline{P}}$ contains the directions capable of describing the variability of original data \underline{X} by decreasing relevance, meaning that \underline{X} data show more variability over the direction defined by the first column of $\underline{\underline{P}}$. This is the 1st principal direction for describing the statistical behaviour of \underline{X} . The second column of $\underline{\underline{P}}$ is the 2nd principal direction and so on. A matrix of generalized scores $\underline{\underline{S}}_{m \times n}$ is obtained by projecting \underline{X} over the directions (columns) of $\underline{\underline{P}}$ after subtracting the respective sample means $\langle X_i \rangle$ as Eq. (16) shows, where \underline{P}_i is the principal direction i of $\underline{\underline{P}}$ and \underline{S}_i contains $m \times 1$ samples of the generalized score S_i . The generalized scores are the new scalar variables S_1, S_2, \dots, S_n candidates to substitute the original variables X_1, X_2, \dots, X_n with the advantage of having the variability condensed to its maximum and decreasing along the elements of the set. Usually, the first elements represent most of the variability of the original set. The percentage of the variance associated to the general score S_i is calculated considering its contribution over the total variance of the sample as shown in Eq. (17).

$$\underline{S}_i = (\underline{X} - \underline{U} \cdot \langle \underline{X} \rangle^T) \underline{P}_i \quad (16)$$

$$v_i(\%) = 100 \frac{\lambda_i}{\sum_i \lambda_i} \quad (17)$$

3. METHODS

3.1. OFFSHORE PROCESSING OF CO₂-RICH NG

Two alternatives of offshore processing of CO₂-rich NG are considered: (i) the Conventional-Route (TEG+JTE+MP) – Plant 1; and (ii) the SS-Route (SS+MP) – Plant 2. Plant 1 and Plant 2 are designed to compare design, environmental and economic performances of the novel SS-Route versus the Conventional-Route. A “light” version the Conventional-Route is considered – Plant 3 – to assess effects of CO₂ content increase in NG in design, environmental and economic performances.

Plant 3 is the first design of the Conventional-Route (Gonzaga,2014), which was later improved into Plant 1. The reason why Plant 3, and not Plant 1, is used in this Thesis for assessments of the effects of CO₂ increase in NG is due to products generated by Plant 3 (Gonzaga et al., 2017; 2019a;b). Plants 1 and 2 also generated products (Gonzaga et al., 2019c;d) focused on assessing the Conventional-Route versus the SS-Route.

Processes for Plants 1 and 2 start with three-phase oil-water-gas separation of the incoming multiphase feed from the field. Oil is stabilized via multiple depressurizing degassing stages (Nguyen and de Oliveira Júnior, 2018), while the arising gas is compressed for WDPA+HCDPA at high-pressure. In the Conventional-Route, WDPA is done via TEG dehydration, the most economically favorable option under standard conditions (Bahadori and Vuthaluru, 2009), despite its heat consumption for TEG regeneration. WDPA is the first step of gas processing to avoid downstream gas-hydrates in deep-water pipelines (Kamal et al., 2016).

After WDPA, HCDPA is accomplished in the Conventional-Route via JTE for C₃+ removal avoiding condensate in MP step potentially damaging membranes (Hao et al., 2008). In the SS-Route, SS's execute WDPA+HCDPA simultaneously, normally implying less power-consumption than JTE (Arinelli et al., 2017). From this point onwards, both routes follow to CO₂ removal via MP. MP is preferred due to its capability of processing CO₂-rich feeds with low footprint and operational costs, while offering modularity (Reis et al., 2017), a key attribute for offshore operation under

uncertainties that allows plant adaptation for feed fluctuations. A MP disadvantage is the low-pressure CO₂-rich permeate, which demands compression to high-pressure for EOR utilization in the reservoir via subsea pipelines. This provides a safe CO₂ destination and aggregates value by increasing oil production. Final NG also demands compression for exportation via subsea pipelines. Production water treatment is of less operational significance and is not considered (Gonzaga et al., 2019c;d).

Process for Plant 3 is the same as described for Plant 1, except that it starts with the gas leaving the three-phase oil-water-gas separator (Gonzaga et al., 2017; 2019a;b).

Figure 7 sketches Conventional-Route (Plants 1 and 3) and SS-Route (Plant 2) block diagrams for offshore processing of CO₂-rich NG. NG and EOR-Fluid subsea pipelines for Plants 1 and 2 are detailed posteriorly. Plant 3 does not consider subsea pipelines.

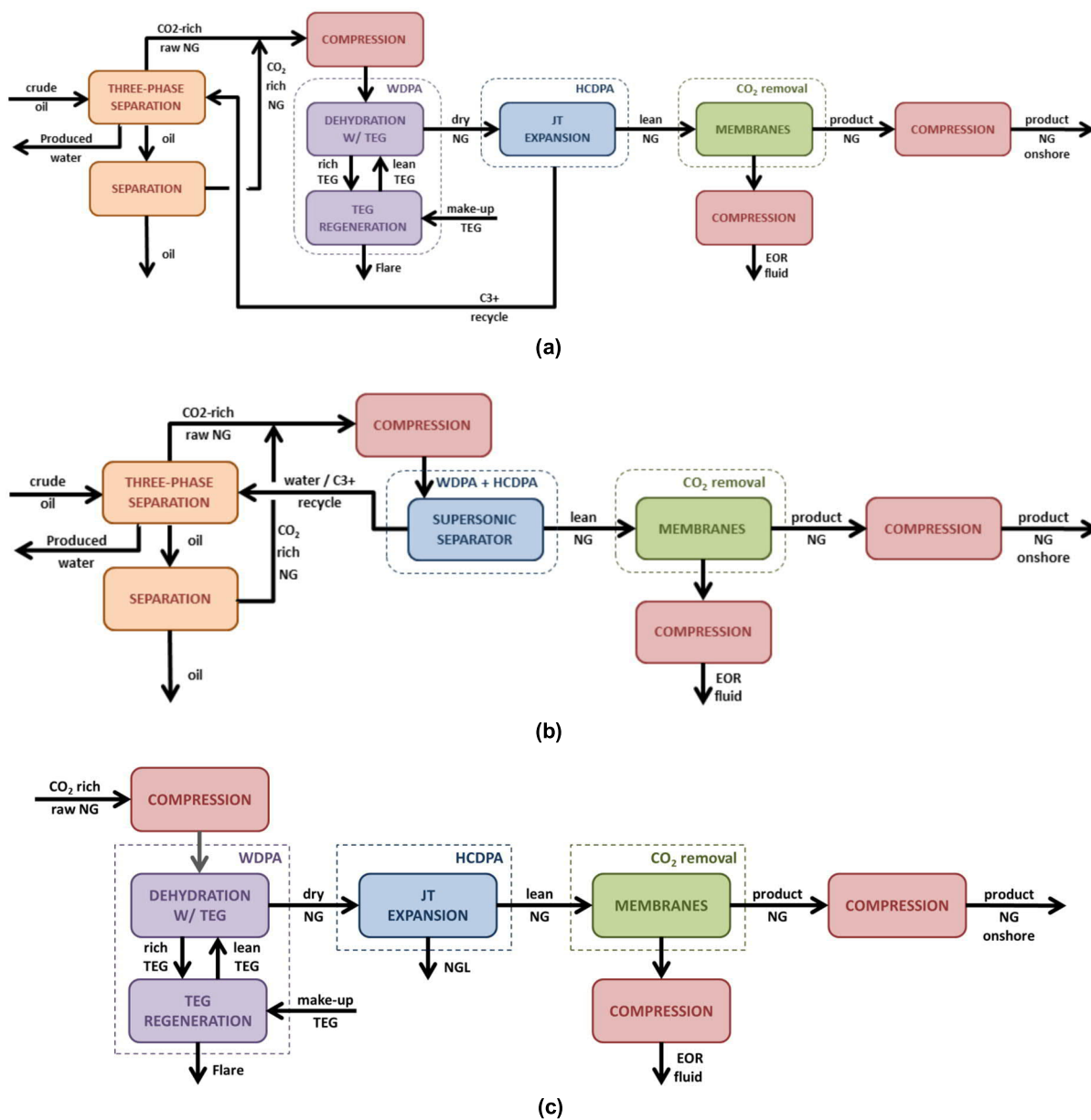


Figure 7. Offshore processing of CO₂-rich NG: (a) Conventional-Route (Plant 1); (b) SS-Route (Plant 2); (c) Conventional-Route (Plant 3).

3.2. STOCHASTIC FEED VARIABLES FOR MONTE-CARLO ANALYSIS

Load uncertainties represent critical factors for safety and reliability of deep-water offshore rigs. Thus, the multiphase (oil-gas-water) feed for Plants 1 and 2 is defined by combining three selected independent stochastic inputs: $[PU_1]$ dry CO_2 -rich NG flow rate (MMsm^3/d), $[PU_2]$ dry CO_2 -rich NG CO_2 molar fraction and $[PU_3]$ multiphase feed GOR (sm^3/m^3). Such variables are normally subjected to uncertainties, exhibiting severe fluctuations along the field life and impacting process responses in great magnitude. As CO_2 is the main separation target, $[PU_1]$ and $[PU_2]$ drastically affect specification attainment as both influence the CO_2 inventory to be captured and disposed, while $[PU_3]$ ties oil processing to gas processing also highly impacting the offshore rig. Moreover, $[PU_1]$, $[PU_2]$ and $[PU_3]$ severely impact power-consumption and compressor investment, both critical bottlenecks of offshore rigs.

Non-correlated continuous random behaviors are assumed to $[PU_1]$ to $[PU_3]$ via normal *PDFs*. Normal *PDFs* are chosen from their relevance in physical, biological and financial unimodal phenomena. Eq. (18) represents the normal *PDF* of variable X with parameters μ (mean) and σ^2 (variance). Characteristic fingerprints of normal *PDFs* encompass unimodality, symmetry and infinite domain. Unimodality and symmetry are common in nature thanks to the Central Limit Theorem, which states that the normal behavior of a given macroscopic nature variable results from myriads of small contributing independent factors following arbitrary *PDFs* (Jacques, 1998). Thus, only the normal unboundedness seems to be problematic. Despite real disturbances cannot reach infinite amplitudes (i.e., they are typically bounded), normal *PDFs* with their infinite tails can still represent real stochastic phenomena since 99.73% and 99.99% probability domains correspond, respectively, to the finite intervals $[\mu-3\sigma, \mu+3\sigma]$ and $[\mu-4\sigma, \mu+4\sigma]$. This implies that $O(10^4)$ outcomes must be sampled to find a single one outside the $[\mu-4\sigma, \mu+4\sigma]$ range, while Monte-Carlo analysis is usually applied sampling from 500 to 3000 individuals for ergodicity (Hastings, 1970). That is, there is no practical risk of unbounded amplitudes when working with numerical normal *PDFs*. Another more subtle reason for assigning normal *PDFs* to stochastic inputs has to do with the traceability of normal signals through the process. In this regard, if output variables follow similar normal patterns, this indicates linear cause-effect relationships entailing process elasticity and

resilience; conversely, in case of non-normal output behavior (e.g. multimodal or stone-wall behaviors), very non-linear causality relationships must dominate the process to the detriment of its resilience. Therefore, assigning normal *PDFs* to input variables, besides being a natural choice for nature phenomena, allows identifying where there is strong non-linearity in process responses. Table 2 shows the chosen parameters for normal *PDFs* of input variables for Plants 1 and 2.

$$PDF(X, \mu, \sigma) = \frac{1}{\sqrt{2\pi\sigma^2}} \exp\left(-\frac{(X-\mu)^2}{2\sigma^2}\right), \quad -\infty < X < \infty \quad (18)$$

Table 2. Parameters for normal *PDFs* of input variables (feed variables) for Plants 1 and 2.

Input Variable	Description	Mean (μ)	St. Deviation (σ)	99.99% probability interval
[PU ₁]	Dry CO ₂ -rich NG flow rate	6.0 MMsm ³ /d	0.9 MMsm ³ /d	PU ₁ ∈ [2.4MMsm ³ /d, 9.6MMsm ³ /d]
[PU ₂]	Dry CO ₂ -rich NG CO ₂ molar fraction	0.45	0.03	PU ₂ ∈ [0.33, 0.57]
[PU ₃]	Multiphase feed GOR	450 sm ³ /m ³	30 sm ³ /m ³	PU ₃ ∈ [330sm ³ /m ³ , 570sm ³ /m ³]

As Plant 3 starts with raw NG leaving the three-phase oil-water-gas separator, input variables [PU₁] dry CO₂-rich NG flow rate (MMsm³/d) and [PU₂] dry CO₂-rich NG CO₂ molar fraction are considered (Table 3). In addition, two scenarios of [PU₂] are considered.

Table 3. Parameters for normal *PDFs* of input variables (feed variables) for Plant 3.

Input Variable	Description	Mean (μ)	St. Deviation (σ)	99.99% probability interval
[PU ₁]	Dry CO ₂ -rich NG flow rate	6.0 MMsm ³ /d	1 MMsm ³ /d	PU ₁ ∈ [2.0MMsm ³ /d, 10.0MMsm ³ /d]
[PU ₂] ₁	Dry CO ₂ -rich NG CO ₂ molar fraction	0.20	0.03	PU _{2_1} ∈ [0.08, 0.32]
[PU ₂] ₂	Dry CO ₂ -rich NG CO ₂ molar fraction	0.50	0.03	PU _{2_2} ∈ [0.38, 0.62]

The values from Table 2 and Table 3 are based on average values of Pre-Salt offshore rigs (Araújo et al., 2017).

3.3. SELECTED PROCESS RESPONSES

Process specifications for Monte-Carlo analysis correspond to operational constraints, and NG and EOR-Fluid specifications. Table 4 shows the selected output variables and their respective specifications for Plants 1 and 2. Plant 3, as a “light” version, considers only process specifications $[PS_1]$ to $[PS_4]$.

Table 4. Selected process responses for MC analysis and their specifications
($DP \equiv$ Dew-Point, $y \equiv$ molar fraction in NG product)

Output Variable	Description	Specification	Comment
$[PS_1]$	NG CO ₂ content: $S_1 = y_{CO_2}$	$y_{CO_2} \leq 0.03$	NG sales spec.
$[PS_2]$	NG CH ₄ content: $S_2 = y_{CH_4}$	$y_{CH_4} \geq 0.85$	NG sales spec.
$[PS_3]$	NG water DP: $S_3 = WDP^{NG}$	$WDP^{NG} \leq -45^\circ\text{C}@1\text{atm}$	NG pipeline spec.
$[PS_4]$	NG hydrocarbon DP: $S_4 = HCDP^{NG}$	$HCDP^{NG} \leq 0^\circ\text{C}@45\text{bar}$	NG sales spec.
$[PS_5]$	NG onshore delivery pressure: $S_5 = p^{NG-Delivery}$	$p^{NG-Delivery} \geq 70 \text{ bar}$	NG pipeline spec.
$[PS_6]$	EOR-Fluid Water DP: $S_6 = WDP^{EOR-Fluid}$	$WDP^{EOR-Fluid} \leq -45^\circ\text{C}@1\text{atm}$	EOR pipeline spec.
$[PS_7]$	Reservoir delivery pressure: $S_7 = p^{EOR-Delivery}$	$p^{EOR-Delivery} \geq 650 \text{ bar}$	EOR pipeline spec.
$[PS_8]$	MP-Feed hydrocarbon DP: $S_8 = HCDP^{MP-Feed}$	$HCDP^{MP-Feed} \leq -10^\circ\text{C}@45\text{bar}$	MP constraint*
$[PS_9]$	MP CO ₂ partial-pressure: $S_9 = PPCO_2^{MP-Feed}$	$PPCO_2^{MP-Feed} \leq 30 \text{ bar}$	MP constraint*
$[PS_{10}]$	Plant power-consumption: $S_{10} = \text{Power}$	$\text{Power} \leq 84 \text{ MW}$	Power constraint [#]

*To avoid membrane damage (Shahid and Nijmeijer, 2014). [#]Plant powered by 3x28MW gas-fired turboshafts (Araújo et al., 2017).

3.4. BASE-CASES FOR OFFSHORE PROCESSING OF CO₂-RICH NG

Base-Cases for CO₂-rich NG processing via Conventional-Route (Plant 1) and SS-Route (Plant) 2 are designed via HYSYS 8.8 considering the average values of process input variables [PU_1] to [PU_3] for compliance of output variables [PS_1] to [PS_{10}] to specifications in Table 4. Base-Cases for the “light” Conventional-Route (Plant 3) are designed via HYSYS 8.8 considering the average values of process input variables [PU_1] and [PU_2] (2 scenarios) for compliance of output variables [PS_1] to [PS_4] to specifications in Table 4.

Such designs also passed convergence tests for all combinations of extreme values of input variables. Peng-Robinson Equation-of-State (PR-EOS) was selected for the overall flowsheet in both routes due to its reasonable applicability in multicomponent CO₂-rich NG systems, despite some new EOS's in the literature – such as the modified RK-EOS (Rostamian and Lotfollahi, 2019) – which can represent well pure supercritical CO₂ density, but are not generally available for mixtures. HYSYS Glycol-Package is used only in TEG absorption/regeneration of Conventional-Route.

All processes and units are solved in the thermodynamic limit (i.e., assuming equilibrium in all streams). This is a consistent approach because the selected thermodynamic modeling (e.g., PR-EOS) is acceptable for CO₂-rich NG streams at high-pressure. Therefore, the results generated in this work would be valid under the equilibrium assumption. This corresponds to a useful limiting case, because, if the process cannot accomplish targets in the thermodynamic limit, surely it does not work at real conditions (a rejected design in the thermodynamic limit does not work at real conditions). Therefore, validation of the simulated results is unnecessary if the EOS's are appropriate and if the equilibrium hypothesis is acceptable.

It is important to highlight that not all equipment is fixed by Base-Case design values (average values of process input variables) and presents flexible design dependent on the sampling values of process input variables. Fixed design equipment is MPs, absorption and regeneration columns, JTE valve and pipelines, while flexible design equipment is SS, compressors, heat exchangers, pumps and vessels. In order to ensure fixed design of all equipment, the implementation of control loops are needed.

3.4.1. Conventional-Route (Plant 1) and SS-Route (Plant 2) Base-Cases

This section describes the process design of Base-Cases for the Conventional-Route – Plant 1 – and for the SS-Route – Plant 2 – starting start with three-phase oil-water-gas separation of the incoming multiphase feed from the field (Figure 7a,b).

To stipulate values of $[PU_1]$ CO₂-rich NG flow rate, $[PU_2]$ CO₂ mole fraction in CO₂-rich NG and $[PU_3]$ GOR for designing the Base-Cases, mean values μ_{PU1} , μ_{PU2} and μ_{PU3} (Table 2) define the CO₂-rich NG, dry oil, and water streams to be mixed for generating the multiphase feed of a typical offshore oil-gas rig. To do this, oil flow rate (m^3/d) is given by μ_{PU1}/μ_{PU3} and water flow rate (m^3/d) is calculated from oil flow rate (m^3/d) considering 22% of Basic-Sediment-and-Water ($BSW=0.22=Water/(Water+Oil)$) as an arbitrary value compatible with Brazilian offshore production. BSW influences investment costs related to the three-phase separator as water flow affects its design volume. The entire CO₂ content comes from the dry CO₂-rich NG. Table 5 shows compositions and flow rates of dry CO₂-rich NG, dry oil and water for reconstitution of the multiphase feed for designing Base-Cases of Conventional-Route and SS-Route.

To design the Base-Cases of Conventional-Route (Plant 1) and SS-Route (Plant 2), the multiphase oil feed from Table 5 enters the three-phase separator at $T=40^\circ C$ and $P=20$ bar, generating raw oil, raw gas and water streams (Figure 8). For oil stabilization, oil from the three-phase separator is pre-heated to $T=90^\circ C$ with pressurized-hot-water (PHW, $T=200^\circ C$) and gas is stripped in two downstream oil-gas separators after respective oil expansions from $P=20$ bar to $P=5.5$ bar and from $P=5.5$ bar to $P=2.5$ bar. The stabilized oil comes from the second separator and is cooled down to $T=35^\circ C$ with cooling-water (CW, $T=30^\circ C$). The stripped gases from both separators are re-compressed to $P=20$ bar. After each re-compression stage, gas is cooled down to $T=40^\circ C$ in an intercooler with CW ($T=30^\circ C$). Water-C3+ condensates from knock-out vessels are pumped back to the three-phase separator. Re-compressed gases are added to the raw gas from the three-phase separator for processing (Figure 9).

Table 5. Constituents of multiphase oil-gas-water feed for Base-Cases
(GOR=450*sm³/m³, Water/(Water+Oil)=BSW=0.22).

Feed Phase	Dry CO₂-rich NG	Oil	Water
Flow Rate	<i>6 MMsm³/d *</i>	<i>13333.3 m³/d</i>	<i>3760.8 m³/d</i>
Molar Fractions			
CO ₂	<i>0.4500*</i>	-	-
CH ₄	<i>0.5050</i>	-	-
C ₂ H ₆	<i>0.0250</i>	-	-
C ₃ H ₈	<i>0.0150</i>	-	-
iC ₄ H ₁₀	<i>0.0020</i>	-	-
nC ₄ H ₁₀	<i>0.0010</i>	-	-
iC ₅ H ₁₂	-	<i>0.0100</i>	-
nC ₅ H ₁₂	-	<i>0.0200</i>	-
C ₆ H ₁₄	-	<i>0.0300</i>	-
C ₇ H ₁₆	-	<i>0.0500</i>	-
C ₈ H ₁₈	-	<i>0.0800</i>	-
C ₉ H ₂₀	-	<i>0.0890</i>	-
C ₁₀ H ₂₂	-	<i>0.0650</i>	-
C ₁₁ H ₂₄	-	<i>0.0531</i>	-
C ₁₂ H ₂₆	-	<i>0.0483</i>	-
C ₁₃ H ₂₈	-	<i>0.0476</i>	-
C ₁₄ H ₃₀	-	<i>0.0400</i>	-
C ₁₅ H ₃₂	-	<i>0.0379</i>	-
C ₁₆ H ₃₄	-	<i>0.0290</i>	-
C ₁₇ H ₃₆	-	<i>0.0241</i>	-
C ₁₈ H ₃₈	-	<i>0.0255</i>	-
C ₁₉ H ₄₀	-	<i>0.0241</i>	-
C ₂₀₊	-	<i>0.3264</i>	-
N ₂	<i>0.002</i>	-	-
H ₂ O	-	-	<i>1.000</i>

*Mean values from Table 2.

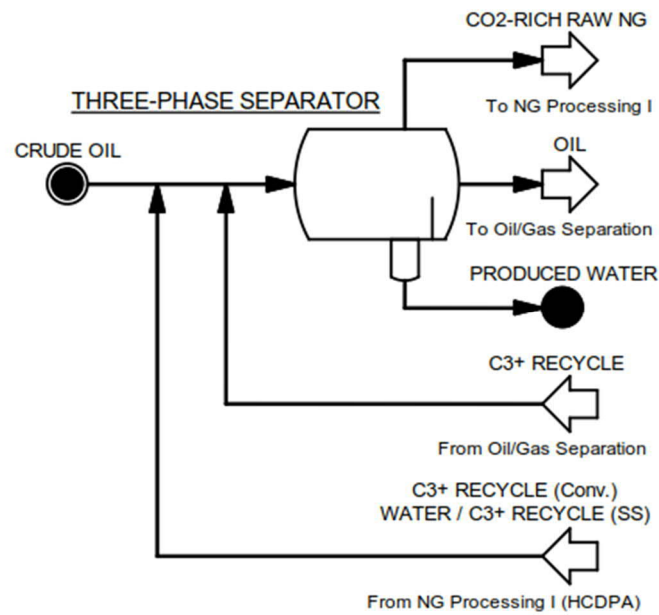


Figure 8. Three-phase separator (Conventional-Route and SS-Route).

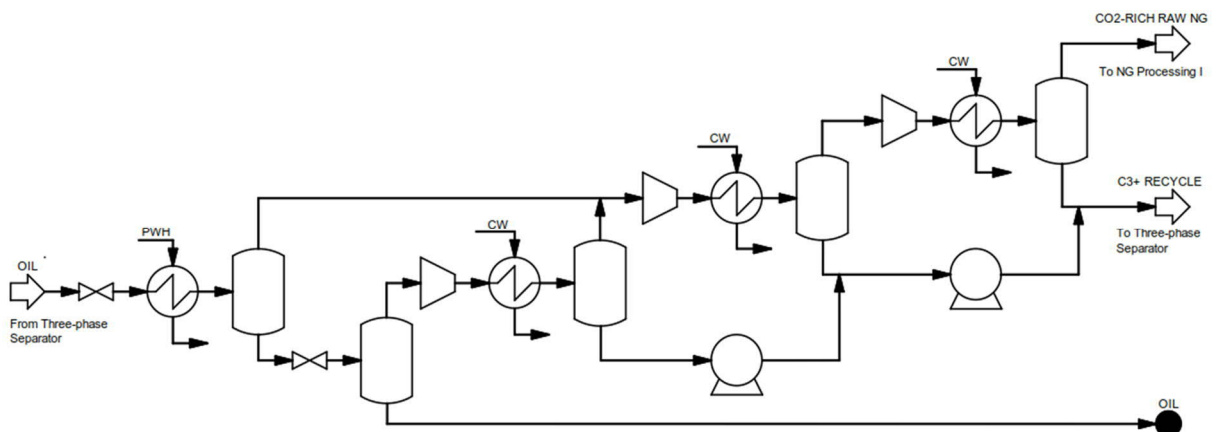


Figure 9. Gas re-recompression from 1st and 2nd oil-gas separators (Conventional-Route and SS-Route).

In the Conventional-Route, gas processing (Figure 10) starts with two-staged intercooled compression (2.14 stage compression-ratio) for TEG dehydration in a four-staged absorption column at $P=90$ bar and $T=40^{\circ}\text{C}$. Water-saturated CO_2 -rich raw NG is admitted at the absorber bottom with lean TEG (99.3%w/w) fed at the top. Dry gas leaves at the top and rich TEG as bottoms. Dry gas goes to JTE unit where it is cooled down to $T=12^{\circ}\text{C}$ with cold gas ($T=-18.3^{\circ}\text{C}$) from JTE and expanded to $P=45.5$ bar for extracting liquid C_3+ at $T=-18.3^{\circ}\text{C}$. C_3+ is heated and expanded, returning to the three-phase separator at $P=20$ bar. The JTE lean gas is heated to

$T=50^{\circ}\text{C}$ for CO_2 removal in the membrane-permeation (MP) unit. At this point in the Conventional-Route Base-Case, lean gas already attains specifications of three output variables (Table 4) $PS_3=WDP^{NG}=-62.5^{\circ}\text{C}@1\text{atm}$ ($\text{PPM}_{\text{Water}}=13.5\text{ppm}$), $PS_8=HCDP^{MP\text{-Feed}}=-18.3^{\circ}\text{C}@45.5\text{bar}$ and $PS_9=PPCO_2^{MP\text{-Feed}}=20.2\text{ bar}$. Rich TEG is expanded to $P=1.5\text{ bar}$, pre-heated to $T=140^{\circ}\text{C}$, and feeds the top of the two-staged TEG regeneration column, which operates injecting dry stripping-gas in the reboiler. Lean TEG (99.3%w/w) leaves the regenerator bottom, is cooled and pumped back to the absorber after make-up (Figure 10).

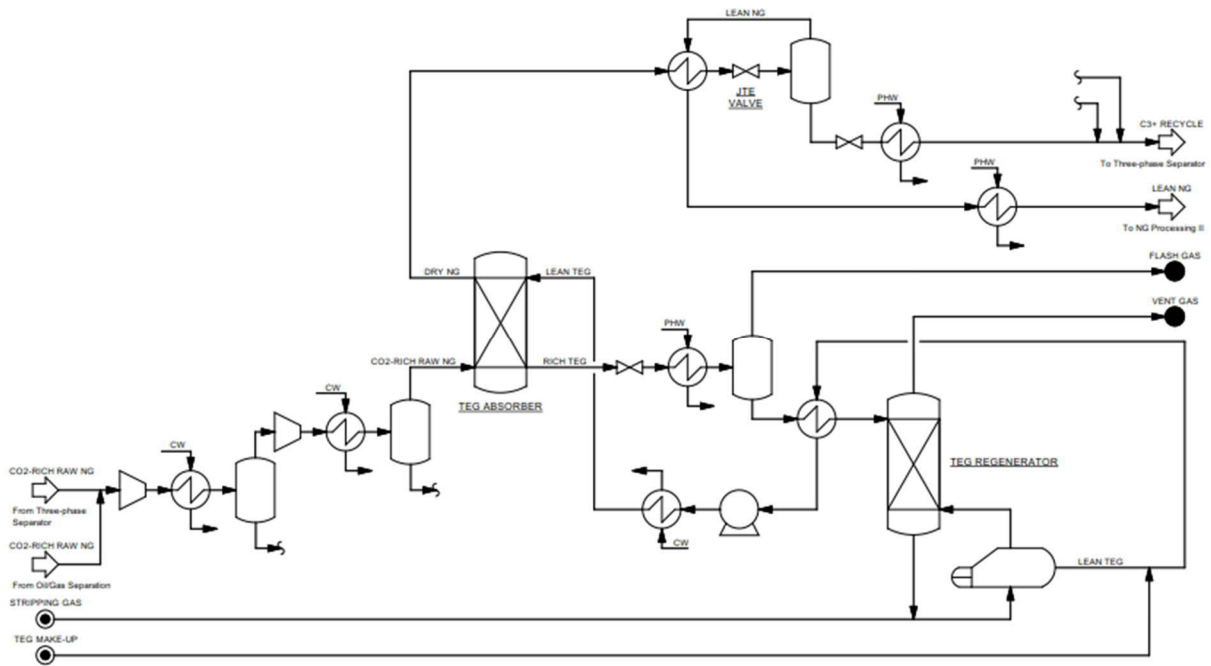


Figure 10. Conventional-Route NG processing (part I): compression, TEG absorption WDPA, TEG regeneration and JTE HCDPA.

In the SS-Route, gas processing (Figure 11) starts with only one compression after-cooled stage (2.525 compression-ratio), since the water-saturated CO_2 -rich raw NG feeds SS at $P=50\text{ bar}$ and $T=40^{\circ}\text{C}$. Therefore, SS is fed with raw gas at lower pressure relatively to the Conventional-Route and accomplishes WDPA+HCDPA simultaneously, with better power allocation than the Conventional-Route, which requires $P=90\text{ bar}$ for JTE expansion. Lean NG leaves SS at $T=42.8^{\circ}\text{C}$, $P=46.9\text{ bar}$ already attaining specifications of three output variables $PS_3=WDP^{NG}=-53.5^{\circ}\text{C}@1\text{atm}$ ($\text{PPM}_{\text{Water}}=40.2\text{ppm}$), $PS_8=HCDP^{MP\text{-Feed}}=-19^{\circ}\text{C}@45\text{bar}$ and $PS_9=PPCO_2^{MP\text{-Feed}}=PPCO_2=20.8\text{ bar}$. In the SS-Route, SS must operate linked to LTX, the anti-hydrate separator. The cold SS two-phase water- C_3+ condensate leaves SS at $T=2.4^{\circ}\text{C}$,

$P=46.9$ bar and feeds the LTX top. The LTX is bottom-heated to prevent gas-hydrates producing a bottom water-C3+ stream at $T=20^{\circ}\text{C}$ and a top slip-gas, which is added to SS lean gas. At LTX top, cold water-C3+ condensate directly contacts warm vapors from LTX bottom, resulting in a small (or null) flow rate of slip-gas with insignificant impact on lean gas specifications (Figure 11). The two-phase water-C3+ stream from LTX bottom returns to the three-phase oil-gas-water separator. LTX was implemented according to Arinelli et al. (2017) as two cascaded flashes: a bottom *Flash(P,T)* double-connected to a top *Flash(P,H)* for adiabatic direct-contact of cold two-phase condensate with warm bottom vapor. Gas-hydrate formation inside SS is not a problem thanks to short SS residence time of milliseconds, typically not sufficient for gas-hydrate nucleation given its slow kinetics (Twister, 2010). On the other hand, hydrates could appear downstream in the cold high-pressure water-C3+ condensate. Thus, sending the water-C3+ condensate to LTX eliminates this problem in SS dehydration operations. The simulation SS model is the customized HYSYS unit operation extension, SS-UOE from Arinelli et al (2017), which runs coupled to another extension, PEC-UOE, for phase-equilibrium sound speed determination from de Medeiros et al. (2017). SS design and performance in the SS-Route Base-Case are detailed in Sec. 3.4.1.1.

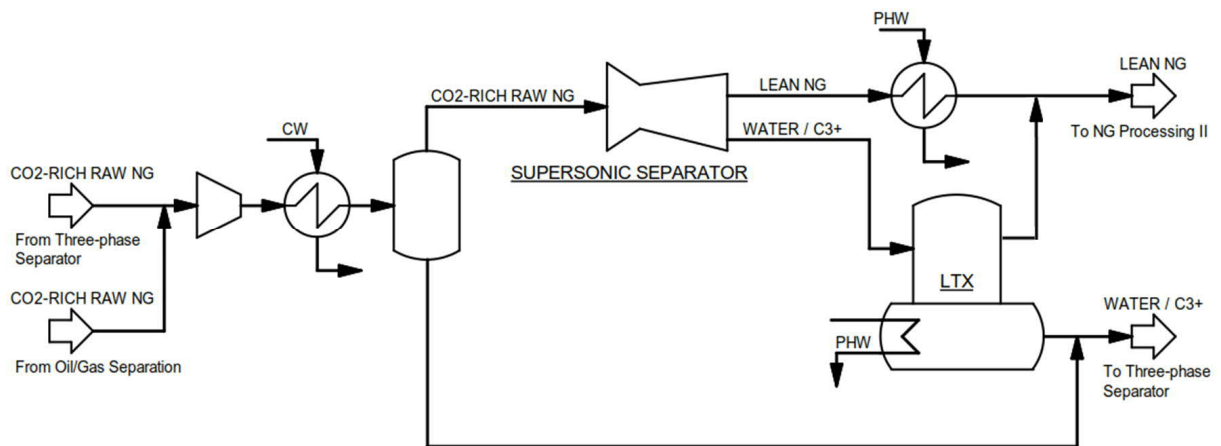


Figure 11. SS-Route NG processing (part I): compression and WDPA+HCDPA via SS.

After WDPA+HCDPA, lean gas – at $P=45$ bar, $T=50^{\circ}\text{C}$ in the Conventional-Route and at $P=46.4$ bar, $T=50^{\circ}\text{C}$ in SS-Route – goes to two-staged Membrane-Permeation (MP) for CO_2 abatement to 3%mol or less (Figure 12). MP stages are designed in the

Conventional-Route Base-Case with areas of 12700 m^2 and 6350 m^2 , while areas of 12300 m^2 and 6150 m^2 are chosen in the SS-Route Base-Case. Each MP stage operates with retentate head-loss of $\Delta P=2\text{ bar}$ and permeate at $P=4\text{ bar}$.

The lean and decarbonated NG at $P=41\text{ bar}$, $T=30.5^\circ\text{C}$ (Conventional-Route) or at $P=42.4\text{ bar}$, $T=29.8^\circ\text{C}$ (SS-Route) is compressed (Figure 12) in two intercooled compressor stages (2.15 stage compression-ratio) to $P=187.9\text{ bar}$, $T=35^\circ\text{C}$ (Conventional-Route), or to $P=194.3\text{ bar}$, $T=35^\circ\text{C}$ (SS-Route), for exportation via subsea pipeline (Figure 14). CO_2 permeate leaves MP at $P=4\text{ bar}$, $T=31.7^\circ\text{C}$ (Conventional-Route) or at $P=4\text{ bar}$, $T=31.2^\circ\text{C}$ (SS-Route), and is compressed (Figure 12) through three intercooled compressor stages (3.82 stage compression-ratio) and one pump to $P=300\text{ bar}$, $T=53.8^\circ\text{C}$ (Conventional-Route) or to $P=300\text{ bar}$, $T=52.8^\circ\text{C}$ (SS-Route), becoming the EOR-Fluid injected in the reservoir via EOR pipeline (Figure 14). The MP model for simulation of MP stages is another customized HYSYS unit operation extension, MP-UOE, developed by Arinelli et al. (2017). MP-UOE models trans-membrane fluxes with driving forces given by logarithmic mean of retentate-permeate differences of partial pressures of all species using calibrated permeances from real MP data of offshore rigs. MP-UOE can handle counter-current or parallel contacts and spiral-wound or hollow-fiber cellulose-acetate membranes. In this work, MP stages are configured as counter-current with spiral-wound membrane.

In the Conventional-Route Base-Case, the following output variables of final NG and EOR-Fluid achieve specifications: $PS_1=y_{\text{CO}_2}=0.0295$, $PS_2=y_{\text{CH}_4}=0.8520$, $PS_3=WDP^{\text{NG}}=-114.2^\circ\text{C}@1\text{atm}$ ($\text{PPM}_{\text{Water}}=0.90\text{ppm}$), $PS_4=HCDP^{\text{NG}}=-3.4^\circ\text{C}@45\text{bar}$ and $PS_6=WDP^{\text{EOR-Fluid}}=-59.1^\circ\text{C}@1\text{atm}$. The value of $PS_4=HCDP^{\text{NG}}$ increases from $PS_8=HCDP^{\text{MP-Feed}}$ thanks to increase of C3+ content in MP retentate due to the transfer of light species CO_2/CH_4 to the permeate. Analogously, the fall of $PS_3=WDP^{\text{NG}}$ after the MP unit is due to water transfer to the permeate thanks to high H_2O permeance (Arinelli et al., 2017). In the SS-Route Base-Case, the following output variables of final NG and EOR-Fluid achieve specifications: $PS_1=y_{\text{CO}_2}=0.0291$, $PS_2=y_{\text{CH}_4}=0.8515$, $PS_3=WDP^{\text{NG}}=-76.4^\circ\text{C}@1\text{atm}$ ($\text{PPM}_{\text{Water}}=2.62\text{ppm}$), $PS_4=HCDP^{\text{NG}}=-6.3^\circ\text{C}@45\text{bar}$ and $PS_6=WDP^{\text{EOR-Fluid}}=-48^\circ\text{C}@1\text{atm}$.

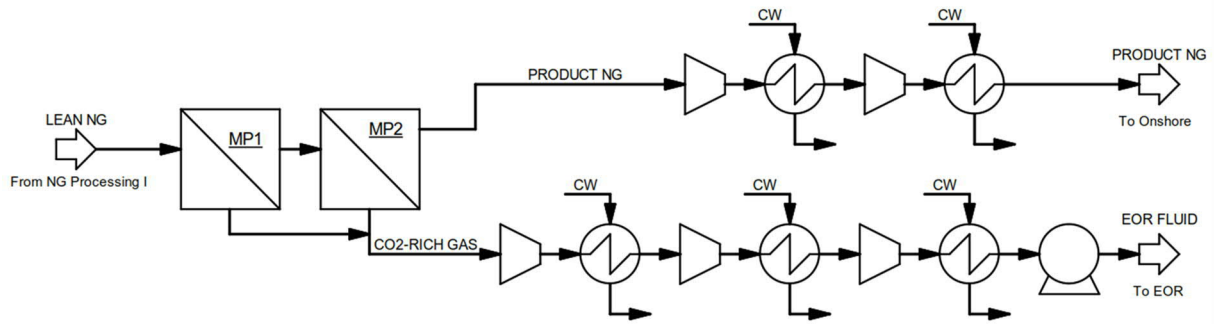
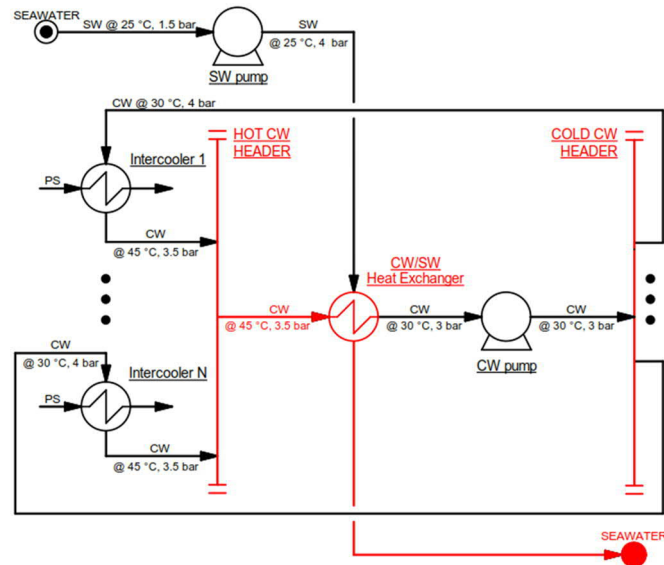


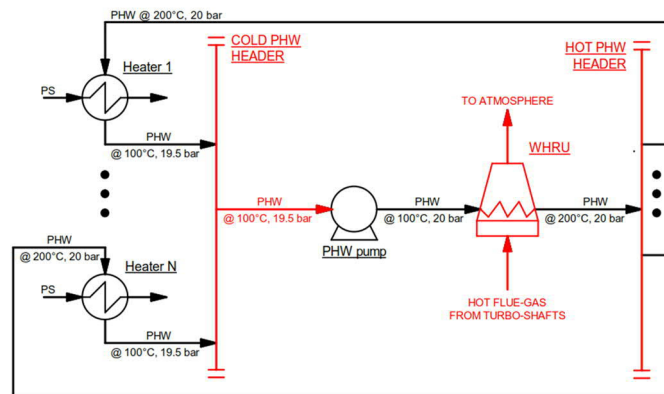
Figure 12. Conventional-Route and SS-Route NG processing (part II): MP CO₂ removal, NG compression and EOR-Fluid compression.

Cooling-Water (CW), Pressurized-Hot-Water (PHW) and seawater (SW) systems are designed according to the requirements of CW, PHW and SW of each route. From CW, PHW and SW flow rates the respective pumping powers are calculated and included in the total power-consumption of Conventional-Route and SS-Route. CW loop is cooled by seawater (SW), whose flow rate is 50% higher than CW flow rate. PHW loop is heated in Waste-Heat Recovery Units (WHRU) with hot flue-gas from power generation turbo-shafts. CW and PHW heat exchangers are shell-and-tube, while SW exchanger is a plate-exchanger with same head-losses. Figure 13 sketches CW, SW and PHW systems. The remaining assumptions for design of Base-Cases comprise: (i) compression stages with same compression ratio; (ii) exchanger head-losses: $\Delta P^{Tubes} = \Delta P^{Shell} = 0.5 \text{ bar}$; (iii) compressor-stage and EOR pump 75% adiabatically efficient; (iv) CW/PHW/SW pumps 40% adiabatically efficient; (v) SW intake: $T = 25^\circ\text{C}$ (superficial water of tropical sea) pumped from $P = 1.5 \text{ bar}$ to $P = 4 \text{ bar}$; (vi) CW thermal range $[30^\circ\text{C}, 45^\circ\text{C}]$ pumped from $P = 3 \text{ bar}$ to $P = 4 \text{ bar}$; (vii) PHW thermal range $[200^\circ\text{C}, 100^\circ\text{C}]$ pumped from $P = 19.5 \text{ bar}$ to $P = 20 \text{ bar}$.

The power-consumption output variable $[PS_{10}]$ attained specification in the Conventional-Route Base-Case with $PS_{10} = \text{Power} = 52 \text{ MW}$ and in the SS-Route Base-Case with $PS_{10} = \text{Power} = 45 \text{ MW}$.



(a)



(b)

Figure 13. Thermal utility systems: (a) CW/SW; and (b) PHW (Conventional-Route and SS-Route).

NG and EOR-Fluid subsea pipelines are also designed in Base-Cases of Conventional-Route and SS-Route to comply with respective specifications of delivery pressures (Table 4). Figure 14 sketches elevation profiles of NG and EOR-Fluid pipelines for both routes, while Table 6 shows the internal diameters, materials and external temperatures of each straight segment of both pipelines. For pipeline design, it is considered operation on a deep-water oil field 200 km from the coast at tropical latitudes and at 2200 m of sea depth with pipeline modeling via HYSYS Beggs-Brill correlation. Pipeline output variables of both routes attained specifications (Table 4) in the respective Base-Cases: for Conventional-Route $PS_5 = P^{NG-Delivery} = 127.2 \text{ bar}$ and $PS_7 = P^{EOR-Delivery} = 651.9 \text{ bar}$; while for SS-Route

$PS_5 = P^{NG-Delivery} = 133.1 \text{ bar}$ and $PS_7 = P^{EOR-Delivery} = 651.9 \text{ bar}$. Consequently, the designs of Conventional-Route and SS-Route Base-Cases are feasible attaining specifications of output variables $[PS_1]$ to $[PS_{10}]$ (Table 4).

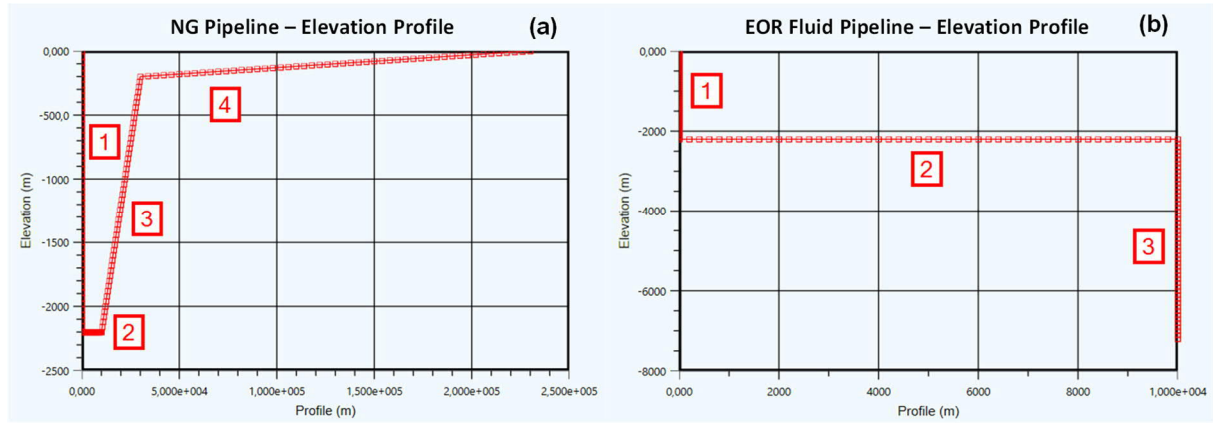


Figure 14. Elevation profiles with sea-level datum: (a) NG pipeline; (b) EOR-Fluid pipeline (Conventional-Route and SS-Route).

Table 6. Straight segments of pipelines (Conventional-Route and SS-Route).

NG Pipeline					EOR-Fluid Pipeline		
Segment	1	2	3	4	1	2	3
$D^{INTERNAL}$	8"	12"	12"	12"	6"	8"	6"
Material	Composite	Steel	Steel	Steel	Composite	Composite	Concrete
$T^{EXTERNAL}$	25°C→5°C	5°C	5°C→15°C	15°C→25°C	25°C→5°C	5°C	5°C→45°C

3.4.1.1. Supersonic Separator Design: SS-Route Base-Case

The SS unit of SS-Route Base-Case is designed with three SS nozzles in parallel and one LTX vessel. Figure 11 depicts SS feed and products lean gas and two-phase water-C3+ condensate. SS feed is calculated via simulation using the Base-Case multiphase feed from expected values in Table 5. Nozzles are specified with $D_I=0.10\text{ m}$, $D_O=0.08\text{ m}$, $\alpha=12.67^\circ$, $\beta=2.66^\circ$, $\eta^{EXP\%}=\eta^{CMP\%}=100\%$ and $Ma^{Shock}=1.4$. The geometry of nozzles demands some explanation. Actually, there are an infinity of possible choices of angles (α,β) , which are normally chosen small (like above) to avoid too short and abrupt nozzles (e.g., for $\alpha=\beta=2.66^\circ$, a longer, more elegant, nozzle results with same throat diameter D_T and same diverging section). In the same way, there are an infinity of nozzle designs with same (α,β) and D_I/D_O working with same Ma^{Shock} and same performance. For example, if D_I and D_O are doubled for fixed (α,β) and Ma^{Shock} , the same D_T and same cooling/condensation performances are obtained with a longer and wider (and more expensive) nozzle. Table 7 reports SS specifications and design/performance variables. The throat diameter, converging length (throat position) and total length are calculated respectively as $D_T=0.0554\text{ m}$, $L_C=0.09889\text{ m}$ and $L=0.3623\text{ m}$. Some impressive aspects in Table 7 encompass the SS condensate molar fraction of 0.86% sufficient for removing 98.27% of water and $18.58\%mol$ of C3+ from raw NG. Minimum SS temperature and pressure of $T_{BS}=-29.49^\circ\text{C}$ and $P_{BS}=16.82\text{ bar}$ are attained at $x=L^{Shock}=0.1357\text{ m}$ (Figure 3), where Ma reaches its maximum specified value $Ma^{Shock}=1.4$. After condensate withdrawal, Ma decreases from Ma^{Shock} to $Ma_{BS}=1.367$, a still supersonic value sufficient to trigger a normal shock. The shock transition recompresses the flow also boosted by sub-sonic compression through the ending diffuser leading the final lean gas to be discharged at $P^{Discharge}=46.88\text{ bar}$, meaning an excellent head-loss $\Delta P^{SS}=4.118\text{ bar}$ or 93.76% of pressure recovery.

Table 7. SS-Route Base-Case: SS specifications, design, feed and performance.

Specified Items	Values	Calculated by SS-UOE	Values
No.of SS	3	$D_T(m)$	0.0555
$D_I(m)$	0.10	$L_C(m)$	0.0989
$D_O(m)$	0.12	$L_D(m)$	0.2634
$\alpha(^{\circ})$	12.67	$L(m)$	0.3623
$\beta(^{\circ})$	2.66	$L^{Shock}(m)$	0.1357
Ma^{Shock}	1.4	$L^{Diff}(m)$	0.2266
$\eta^{EXP}\%$	100	$P_{BS}(bar)$	16.82
$\eta^{CMP}\%$	100	$T_{BS}(^{\circ}C)$	-29.49
$P^{Feed}(bar)$	50	Ma_{BS}	1.367*
$T^{Feed}(^{\circ}C)$	40	$P_{Outlet}(bar)$	46.88
$MMsm^3/d$	6.14	$T_{Outlet}(^{\circ}C)$	42.78
%mol C3 ^{+Feed}	2.14%	%P Recovery	93.76%
ppmH ₂ O ^{Feed}	2298	%mol Condensed [#]	0.86%
%mol CO ₂ ^{Feed}	44.58%	REC% H ₂ O	98.27%
		REC%mol C3+	18.58%
		REC% CO ₂	0.38%

*After condensate withdrawal. #Total Condensate (54%molHC+26%molH₂O+20%molCO₂).

Figure 15 shows SS profiles versus SS axial position x . Figure 15a depicts the SS silhouette and molar vapor-fraction (ψ) versus x showing a typical SS signature $d\psi/dx=-\infty$ at the sonic throat ($Ma \rightarrow 1^-$). SS signatures are $\pm\infty$ singularities of dT/dx , dP/dx , dMa/dx , dc/dx and $d\psi/x$ that occur at sonic throat ($Ma \rightarrow 1^-$) whenever $(dA/dx)^{Throat} \neq 0$ where $A(x)$ represents the flow section area (de Medeiros et al., 2019; de Medeiros et al., 2017). This is the case of SS with linear dia meter profiles (Figure 3) selected for the SS-Route Base-Case. In Figure 15a the fall of ψ corresponds to condensation of C3+/water which is maximum at $x=L^{Shock}=0.1357$ m, where condensate is collected (ψ suddenly returns to $\psi=1$).

Figure 15b depicts SS profiles of P and Ma also with SS signatures $dP/dx=-\infty$, $dMa/dx=+\infty$ at the throat ($x=L_C=0.09889$ m). The minimum $P=P_{BS}=16.82$ bar occurs with the maximum $Ma=Ma^{Shock}=1.4$ at the point of liquid withdrawal. The immediately subsequent sudden rise of P and fall of Ma corresponds to the normal shock transition. After the shock, the monotonous Ma decrease and P increase correspond to the sub-sonic compressing flow through the ending diffuser.

Figure 15c depicts SS profiles of T and c also with SS throat signatures $dT/dx=-\infty$, $dc/dx=-\infty$ ($x=L_c=0.09889\text{ m}$). The minimum $T=T_{BS}=-29.49^\circ\text{C}$ occurs with the maximum $Ma=Ma^{Shock}=1.4$ at the point of liquid withdrawal. It must be noticed that condensate withdrawal occurs at constant $T=T_{BS}$ and $P=P_{BS}$, but with some fall of Ma to $Ma_{BS}=1.367$. The sudden increase of T and c at $x=L^{Shock}=0.1357\text{ m}$ followed by respective monotonous increases are also fingerprints of normal shock and ending diffuser compression. Figure 15c also reveals that the multiphase sound speed c continuously falls due to temperature decrease and condensation (Figure 15a) in the pre-shock section. After the shock, the fluid is superheated vapor and c reaches typical gas sound speed around 310 m/s . Figure 15d depicts %mol condensed of water, CO_2 and hydrocarbons versus x on the SS pre-shock section. It shows that water is almost entirely condensed (98.27%) at $x=L^{Shock}=0.1357\text{ m}$, while $0.924\%\text{mol}$ and $0.38\%\text{mol}$ of hydrocarbons and CO_2 have condensed respectively (hydrocarbon condensation includes condensation of C3+).

Figure 15e represents the behaviors of Ma_{BS} , molar vapor-fraction at $x=L^{Shock}$ and CO_2 mole fraction in the final gas as functions of Ma^{Shock} . It is shown that Ma_{BS} (Ma after condensate withdrawal and just before shock) linearly rises with Ma^{Shock} , while the falls of vapor-fraction and y_{CO_2} with Ma^{Shock} are almost imperceptible. Figure 15e also shows that Ma^{Shock} specification should not surpass 1.85 otherwise T_{BS} would fall deeper reaching about -60°C where CO_2 freeze-out starts, potentially clogging SS. Thus, with $Ma^{Shock}=1.4$ there is no chance of CO_2 freeze-out in this SS unit. Figure 15f shows the SS path on plane $P \times T$ also depicting feed VLE locus, feed WDP locus, lean gas VLE locus (slenderer) and the solid-vapor-liquid equilibrium (SVLE) CO_2 freeze-out boundary of the feed. SS feed is on its WDP locus, meaning that water starts condensing at SS inlet, while hydrocarbons and CO_2 start condensing when SS path crosses the dew-point boundary of the feed VLE envelope. When Ma^{Shock} is attained, the SS path is deeply inside the feed VLE locus and touches the dew-point boundary of the lean gas VLE envelope. At this point liquids are collected and the SS flow is now saturated lean gas. The CO_2 SVLE freeze-out boundary is far beneath the deepest point ($P=P_{BS}=16.82\text{ bar}$, $T=T_{BS}=-29.49^\circ\text{C}$) of SS path, ruling out the possibility of dry-ice precipitation, a common issue in cold processes with CO_2 -rich NG (de Medeiros et al., 2019). From this point, the shock transition appears as a

rectilinear jump back to higher (P,T) , followed by a slightly arched path of sub-sonic compression through the ending diffuser.

Figure 16a/b depict the SS path on plane $Tx\bar{S}$, where the latter is a magnification of the former. Plane $Tx\bar{S}$ analysis is important to prove that the 2nd Law of Thermodynamics is being satisfied; i.e. by showing that entropy is not destroyed in an isolated transition like the expansion section of SS. Figure 16a/b also show the feed WDP locus, the VLE loci of feed and lean gas product and the feed SVLE freeze-out boundary. SS path starts at point A ($x=0$) on the feed WDP curve and penetrates the feed VLE envelope through its HCDP boundary following a vertical isentropic expansion and cooling through the Laval until point B ($x=L^{Shock}=0.1357\text{ m}$) slightly below the HCDP $Tx\bar{S}$ locus of lean gas product. As the feed SVLE freeze-out $Tx\bar{S}$ boundary lies far beneath point B, there is no possibility of CO₂ freeze-out on A→B. From point B, low-entropy condensate is withdrawn isothermally, so that SS path moves horizontally increasing \bar{S} towards point C of saturated vapor on lean gas HCDP locus. As any adiabatic irreversible transition, the shock is represented by the inclined segment C→D towards greater \bar{S} and T . From D, the SS path follows the vertical isentropic compression D→E through the ending diffuser until point E at SS discharge ($x=L=0.3623\text{ m}$).

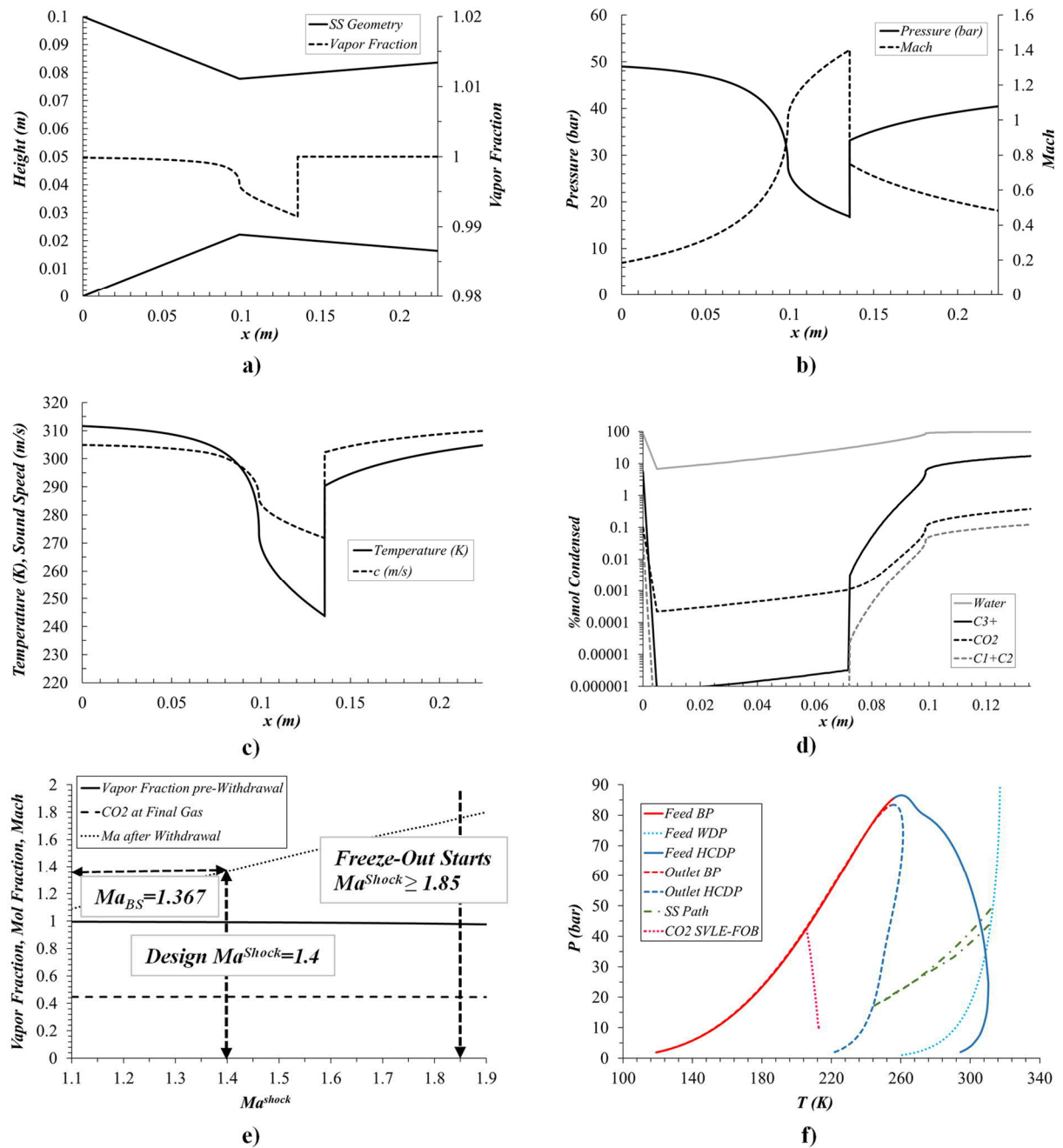


Figure 15. SS axial profiles in SS-Route Base-Case: (a) SS silhouette and vapor-fraction vs $x(m)$; (b) $P(\text{bar})$ and Ma vs $x(m)$; (c) $T(K)$ and $c(m/s)$ vs $x(m)$; (d) species %mol condensation vs $x(m)$; (e) Ma_{BS} , final CO_2 molar fraction and pre-shock vapor-fraction vs Ma^{Shock} for CO_2 freeze-out design check; and (f) plane $P \times T$ with SS path, feed WDP locus, feed VLE envelope, product VLE envelope and feed CO_2 freeze-out SVLE border.

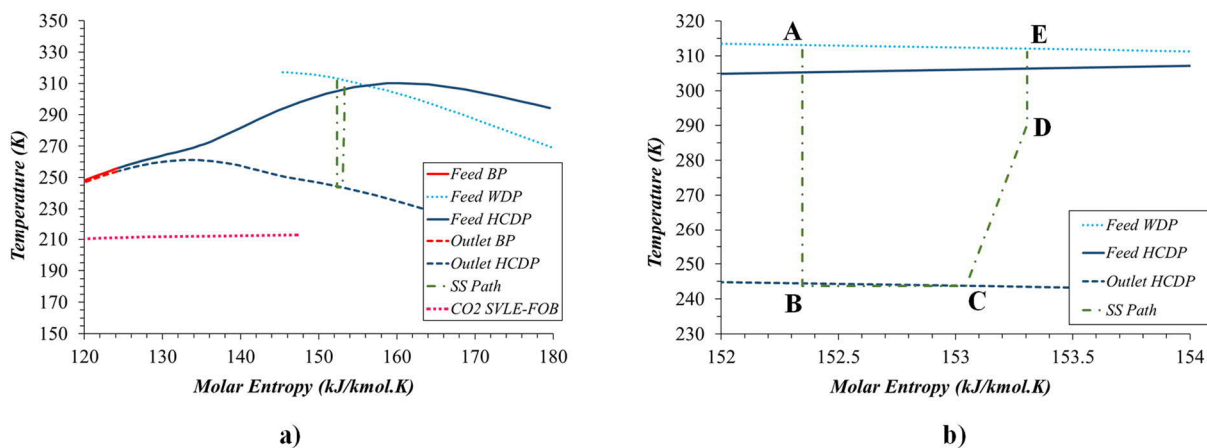


Figure 16. SS-Route Base-Case: (a) plane $T \times \bar{S}$ with SS path, feed and product VLE envelopes, feed WDP locus and feed CO₂ SVLE freeze-out boundary; and (b) magnification of (a).

3.4.2. Conventional-Route (Plant 3) Base-Cases

This section describes the process design of Base-Case for the “light” Conventional-Route – Plant 3 – starting start with the gas leaving the three-phase oil-water-gas separator (Figure 7c).

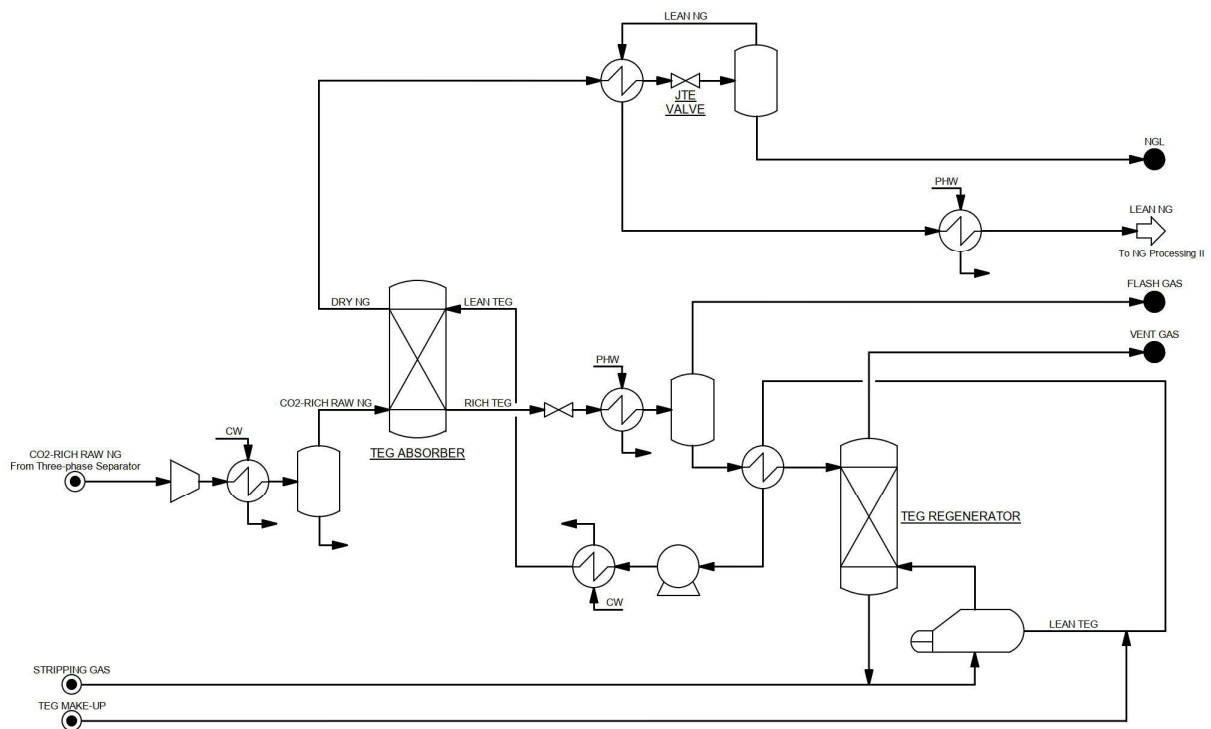
To stipulate values of $[PU_1]$ CO₂-rich NG flow rate and $[PU_2]$ CO₂ mole fraction in CO₂-rich NG and $[PU_3]$ GOR for designing the Base-Cases, mean values μ_{U1} , μ_{U2_1} and μ_{U2_2} (Table 3) define the raw CO₂-rich NG conditions for Plant 3. Table 8 shows compositions and flow rate of dry CO₂-rich NG, dry oil and water for reconstitution of the multiphase feed for designing Base-Cases of Conventional-Route of both CO₂ content scenarios.

Base-Case for $\mu_{U2_1} = 20\%mol$ CO₂ starts with raw NG processing (Table 8). Part I of gas processing (Figure 17) is the same as the process described for the Conventional-Route – Plant 1 – from Sec. 3.4.1, except for the following conditions: (i) one-staged intercooled compression (3.525 compression-ratio) for TEG dehydration in a six-staged absorption column at $P=70$ bar and $T=25^\circ C$; (ii) JTE brings NG to $T=-26.2^\circ C$; (iii) liquid NGL stream leaving JTE as final product; (iv) eight-staged TEG regeneration column.

Table 8. Constituents of raw NG feed for Base-Cases considering two CO₂ content scenarios.

Raw NG	Case 20%mol CO ₂	Case 50%mol CO ₂
Flow Rate	6 MMsm ³ /d *	6 MMsm ³ /d *
Molar Fractions		
CO ₂	0.20000*	0.50000*
CH ₄	0.77882	0.48676
C ₂ H ₆	0.01199	0.00749
C ₃ H ₈	0.00355	0.00222
iC ₄ H ₁₀	0.00090	0.00056
nC ₄ H ₁₀	0.00079	0.00049
iC ₅ H ₁₂	0.00039	0.00024
nC ₅ H ₁₂	0.00021	0.00013
C ₆ H ₁₄	0.00024	0.00016
C ₇ H ₁₆	0.00037	0.00023
C ₈ H ₁₈	0.00024	0.00016
C ₉ H ₂₀	0.00002	0.00001
N ₂	0.00248	0.00155
H ₂ O	-	-

*Mean values from Table 3.

**Figure 17.** Base-Case for $\mu_{U2_1} = 20\% \text{mol CO}_2$: NG processing (part I): compression, TEG absorption WDPA, TEG regeneration and JTE HCDPA.

After WDPA+HCDPA, lean gas goes to two-staged Membrane-Permeation (MP) for CO₂ abatement (Figure 18) at $P=39 \text{ bar}$, $T=35^\circ\text{C}$. MP stages are designed in the

Conventional-Route Base-Case with areas of 34000 m^2 and 17000 m^2 . Each MP stage operates with retentate head-loss of $\Delta P=1 \text{ bar}$ and permeate at $P=1 \text{ bar}$.

The lean and decarbonated NG is compressed (Figure 18) in two intercooled compressor stages (2.650 stage compression-ratio) to $P=258 \text{ bar}$, $T=35^\circ\text{C}$ for exportation via subsea pipeline. CO_2 permeate leaves MP at $P=1 \text{ bar}$, $T=25.8^\circ\text{C}$, and is compressed (Figure 18) through five intercooled compressor stages (3.20 stage compression-ratio) to $P=260 \text{ bar}$, $T=35^\circ\text{C}$, becoming the EOR-Fluid injected in the reservoir via EOR pipeline. The MP model for simulation of MP stages is the same used for Plants 1 and 2, and MP stages are also configured as counter-current with spiral-wound membrane. Modeling of subsea pipelines is not included in Plant 3 design. Modeling of Cooling-Water (CW), Pressurized-Hot-Water (PHW) and seawater (SW) systems are also not included in Plant 3 design. The remaining assumptions are the same for the routes described in Sec 3.4.1.

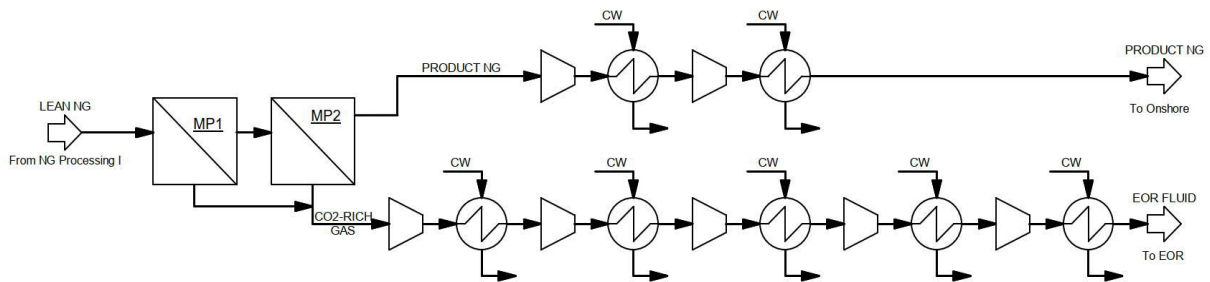


Figure 18. Base-Case for $\mu_{U2_1} = 20\% \text{mol CO}_2$: NG processing (part II): MP CO_2 removal, NG compression and EOR-Fluid.

The same unit designed for Base-Case for $\mu_{U2_1} = 20\% \text{mol CO}_2$ is capable to accommodate Base-Case for $\mu_{U2_2} = 50\% \text{mol CO}_2$. However, it is not possible to recover NGL product stream due to the elevated CO_2 content, hence a small design modification is made to cool C3+ stream from JTE and send its gas phase to EOR and its liquid phase to flare (Figures 19 and 20). This modification generates an extra flare stream as output waste, hindering environmental performance of the process. In addition, MP area shall be increased in 10% to attain specifications and accommodate higher CO_2 content, showing the advantage of MP modularity for process design under uncertain scenarios. Design modification and increase in MP area brings additional costs to economic performance.

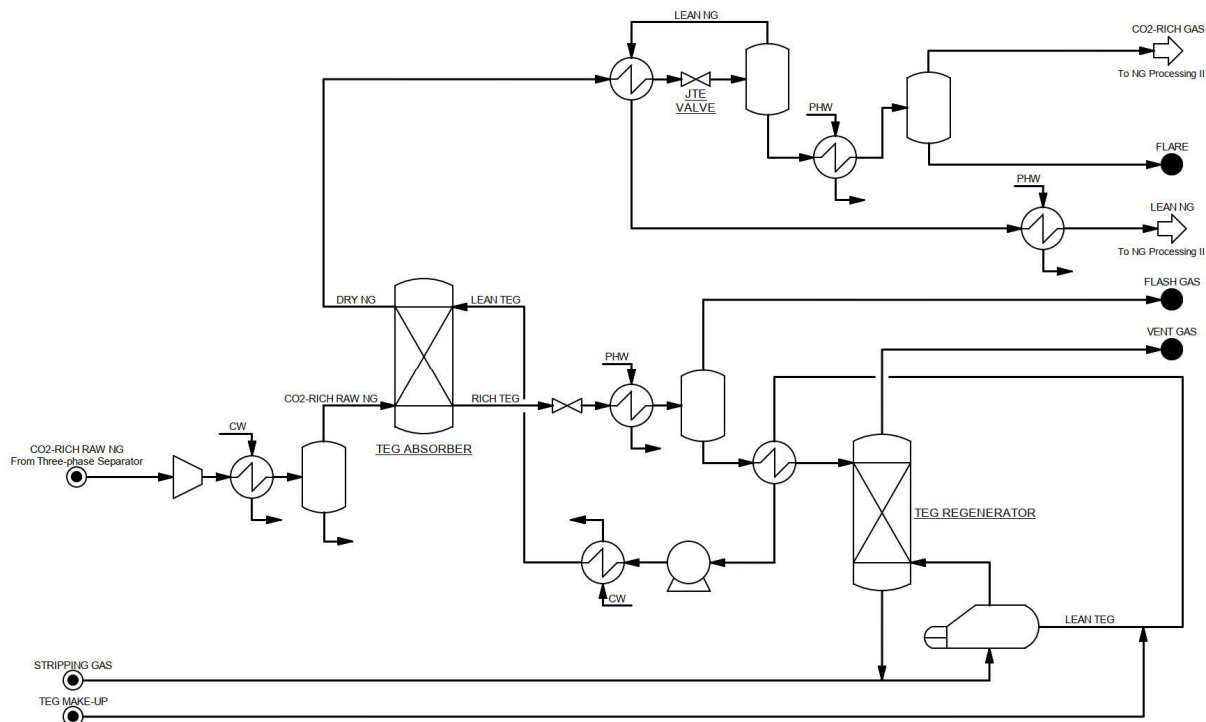


Figure 19. Base-Case for $\mu_{U2,2} = 50\% \text{mol CO}_2$: NG processing (part I): compression, TEG absorption WDPA, TEG regeneration and JTE HCDPA.

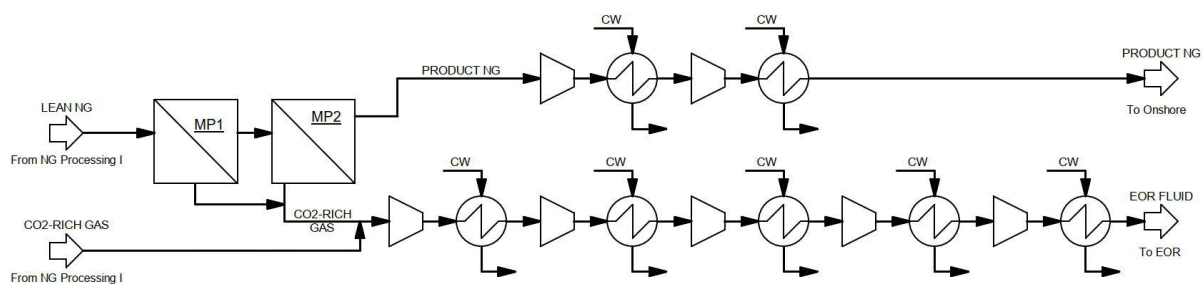


Figure 20. Base-Case for $\mu_{U2,2} = 50\% \text{mol CO}_2$: NG processing (part II): MP CO₂ removal, NG compression and EOR-Fluid.

3.5. ENVIRONMENTAL AND ECONOMIC PREMISES

The environmental assessment in this work is based on the following premises: (i) output PEIs for each individual category originated of offshore processing of CO₂-rich NG are used as environmental performance indicators; (ii) impacts from product streams are not considered in PEIs calculations; and (iii) PCA is used to identify the most relevant output PEIs to environmental performance.

Table 9 lists the premises considered for the economic assessment and Table 10 shows the selected output variables and their respective specifications.

Considering the premises listed in Table 9, (i) C_{OL} is constant; (ii) C_{RM} is constant; (iii) C_{WT} is negligible; (iv) C_{UT} is negligible; (v) R can still be influenced by uncertainties on both process and economic input variables, as products flow, price and demand, power consumption, and carbon tax; (vi) FCI can be influenced by uncertainties on economic input variables, as equipment prices. Therefore, COM is influenced only by uncertainties on FCI (uncertainties on economic input variables).

Based on Table 9, it is important to highlight that the revenue is R consists of the revenue obtained from products (NG sale and EOR-Fluid re-injection) minus the cost of NG used for power generation due to power consumption (this cost is not considered as C_{UT} for COM) minus the cost of the penalty fee to be paid as Carbon tax.

Table 9. Premises for economic assessment.

Assumptions	Prices	Parameters
(i) <i>Uncertainties in FCI shall be considered.</i> [EU1] <i>FCI:</i> $\mu = FCI_{Base-Case}$ (<i>FCI calculated for Base-Cases</i>); $\sigma = 10\% FCI_{Base-Case}$	[EU2] <i>NG price</i> ^(b) : $\mu = 3 \text{ USD/million BTU}$; $\sigma = 0.3 \text{ USD/million BTU}$	<i>Plant availability:</i> 350 days per year of operation
(ii) <i>Revenue consists of NG sale and EOR-fluid re-injection; oil sale is not considered.</i>	[EU3] <i>Oil price</i> ^(b) : $\mu = 60 \text{ USD/bbl}$; $\sigma = 3 \text{ USD/bbl}$	<i>Plant lifetime:</i> 20 years
(iii) <i>NG produced in the plant is used to fuel the turbines. Electricity cost is zero and the NG used for powering the plant is deducted from revenue R.</i>	<i>TEG price</i> ^(c) : 1500 USD/t	<i>CEPCI</i> ^(f) : 567,5 (2017)
(iv) <i>Raw NG is costless, since it is associated to oil production.</i>	<i>Membrane price</i> ^(d) : 50 USD/m ²	<i>Working time:</i> 8 h/d
(v) <i>EOR recovery factor = 1.5 bbl oil / t EOR-fluid re-injected</i> ^(a) .	<i>Membrane maintenance price</i> ^(d) : 6.25 USD/(m ² .y)	<i>Working labor:</i> 15 USD/h
(vi) <i>Carbon tax accounts CO₂ emissions from power generation and from outlet waste streams, and it is deducted from revenue R.</i>	<i>SS price</i> ^(e) : 3 430 000 USD	<i>Depreciation:</i> MACRS
(vii) <i>Membrane maintenance cost is added to COM.</i>	<i>LTX price</i> ^(e) : 1 430 000 USD	<i>Capacity adjustment</i> ^(g) : Six-Tenth rule
(viii) <i>C_{UT} and C_{WT} are negligible in offshore context. SS-Route: C_{RM} = 0 ; Conventional-Route: C_{RM} consists of make-up TEG.</i>	-	[EU4] <i>Carbon pricing</i> ^(h) : $\mu = 50 \text{ USD/t CO}_2$; $\sigma = 10 \text{ USD/t CO}_2$
(iv) <i>I₀ = FCI, consumed in the first year of plant operation.</i>	-	-
(x) <i>NGL price = oil price.</i>	-	-

(a) (Godec, 2012); (b) Distributions based on the statistics of 2014-2019, available at www.indexmundi.com/; (c) https://www.alibaba.com/product-detail/Factory-price-Triethylene-glycol-Cas-12_60839173275.html?spm=a2700.7724857.normalList.2.2f896e0fcLW3fu&s=p; (d) (Peters et al., 2011); (e) (Machado et al., 2012); (f) Calculated *FCI* is corrected in time with CEPCI, available at <http://www.chemengonline.com/economic-indicators-cepci>; (g) Six-Tenth rule is used to adjust equipment capacity when calculating C_{BM} ; (h) Distribution based on statistics of *State and Trends of Carbon Pricing 2019* (2019), considering average and standard deviation from exiting carbon policies worldwide.

Table 10. Selected economic responses for MC analysis and their specifications.

Output Variable	Description	Specification	Comment
[ES ₁]	<i>FCI</i>	-	<i>Fixed cost evaluation</i>
[ES ₂]	<i>COM</i>	-	<i>Operation cost evaluation</i>
[ES ₃]	<i>Power consumption cost</i>	-	<i>Power consumption impact on plant cost (deduction from revenue)</i>
[ES ₄]	<i>Carbon tax per power consumption</i>	-	<i>Power consumption impact on plant CO₂ emissions</i>
[ES ₅]	<i>Carbon tax per outlet waste streams</i>	-	<i>Outlet waste impact on plant CO₂ emissions</i>
[ES ₆]	<i>Carbon tax</i>	-	<i>CO₂ emission impact on the plant cost (deduction from revenue)</i>
[ES ₇]	<i>Revenue from NG</i>	-	<i>Impact of NG production on revenue</i>
[ES ₈]	<i>Revenue from EOR-Fluid</i>	-	<i>Impact of EOR on revenue</i>
[ES ₉]	<i>Revenue</i>	-	<i>Revenue evaluation</i>
[ES ₁₀]	<i>NPV</i>	<i>NPV > 0</i>	<i>Economic viability</i>

3.6. INVERSE TRANSFORM MONTE-CARLO SAMPLING

The Inverse-Transform method uses random numbers in $[0,1]$ and the cumulative distribution function (*CDF*) of a random variable to generate samples obeying its *PDF*. The *CDF* is numerically inverted to generate its inverse function *iCDF*. Eq. (19) gives the relationship between a sample X_I , the *CDF* and a random number $rnd_I \in [0,1]$. Eq. (19) is inverted as Eq. (20) giving X_I via the *iCDF*. That is, the *iCDF* maps a set of random numbers in $[0,1]$ onto a set of values of a random variable obeying a given *PDF*.

$$\int_{-\infty}^{X_I} PDF(X) dX = CDF(X_I) = rnd_I \in [0,1] \quad (19)$$

$$X_I = iCDF(rnd_I) \quad (20)$$

For sampling a population of normal *PDF* $N(\mu, \sigma^2)$ with parameters (μ, σ^2) , the procedure uses the numeric approximant of the *iCDF* of the standard normal *PDF* $N(0,1)$ ($\mu=0, \sigma=1$) (Abramowitz and Stegun, 1965). Such approximant converts a population of random numbers $P \in [0,1]$ into a population approximately following the standard normal *PDF* $N(0,1)$ as stated in Eq. (21). The central term of Eq. (21) approximates the standard normal *iCDF* with absolute error $\varepsilon \leq 4.5 * 10^{-4}$, where $c_0 = 2.515517$, $c_1 = 0.8202853$, $c_2 = 0.010328$, $d_1 = 1.432788$, $d_2 = 0.189269$, $d_3 = 0.001308$. Eq. (21) considers the *PDF* symmetry being valid for $0 < P \leq 0.5$. For $0.5 \leq P < 1$, Eq. (21) is used with $1-P$ switching the signal of the standard abscissa Z . While Z values approximately follow the standard normal *PDF* $N(0,1)$, X values approximately follow the normal *PDF* $N(\mu, \sigma^2)$ with parameters (μ, σ^2) . Figure 21 illustrates the generation of normal *PDF* samples from random numbers $P \in [0,1]$ via normal *iCDF* and *CDF*.

$$t = \sqrt{-2 \ln P} \rightarrow z = t - \frac{c_0 + c_1 t + c_2 t^2}{1 + d_1 t + d_2 t^2 + d_3 t^3} \rightarrow X = \mu + z \cdot \sigma \quad (21)$$

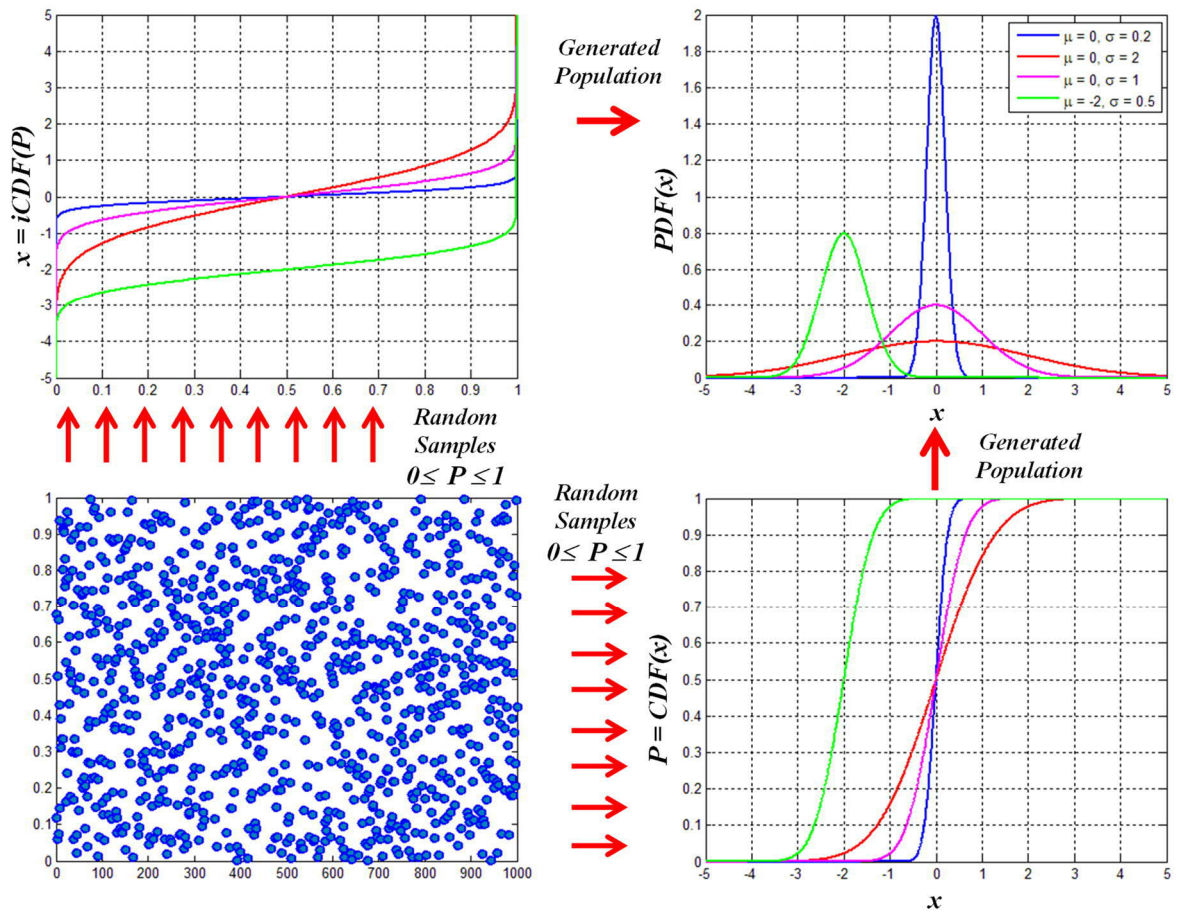


Figure 21. Random $0 \leq P \leq 1$ samples generating normal PDF samples via CDF and $iCDF$.

3.7. MONTE-CARLO ANALYSIS WORKFLOW

The proposed MC analysis workflow (Gonzaga et al., 2019b), depicted in Figure 22, configures a new strategy for design under uncertainties and can lead to more sustainable plant designs by avoiding oversizing, excessive gas-firing and/or unachieved specifications, pollutants emissions and investment costs.

Process design is the first step in the workflow: (i) independent stochastic process inputs following normal *PDFs* are selected and MC sampling is generated via Inverse-Transform method; (ii) Base-Case process simulations are designed using average values of process inputs; (iii) process simulations are performed in batch considering process inputs of MC sampling; (iv) process outputs of interest are collected; (v) MC analysis evaluates statistic scores of goal-attainment of process design targets (typically product specifications and operational constraints) for the assessed base-case; (vi) if all design targets are accomplished in at least 75% of the sampled cases, process design is approved; and, (vii) if not, process design must be re-designed for debottlenecking of unit operations compromising design targets and new MC analyses shall be performed until success is reached. Process re-design shall be made by the designer based on his knowledge of the process, changing fixed design parameters to increase the efficiency of unachieved specifications. More details of the results of MC analysis are given in Sec. 4, where designs of offshore units for CO₂-rich NG processing are assessed.

Environmental performance is assessed via the WAR algorithm (Young et al., 2000) for obtaining statistics PEIs, and economic performance is performed via the methodology proposed by Turton et al. (2009) for onshore facilities. Only process uncertainties are considered for environmental assessment. Economic input variables following normal *PFDs* are considered for calculating *FCI*, *COM*, and *NPV* in addition to process inputs. MC analysis workflow for environmental and economic assessments is the same as described for process design. When all three steps are successfully assessed, a sustainable plant design covering process and economic stochastic scenarios is complete. Plant designs can also be assessed as non-sustainable if they are not capable of attaining all targeted design, environmental and economic targets in at least 75% of the sampled cases.

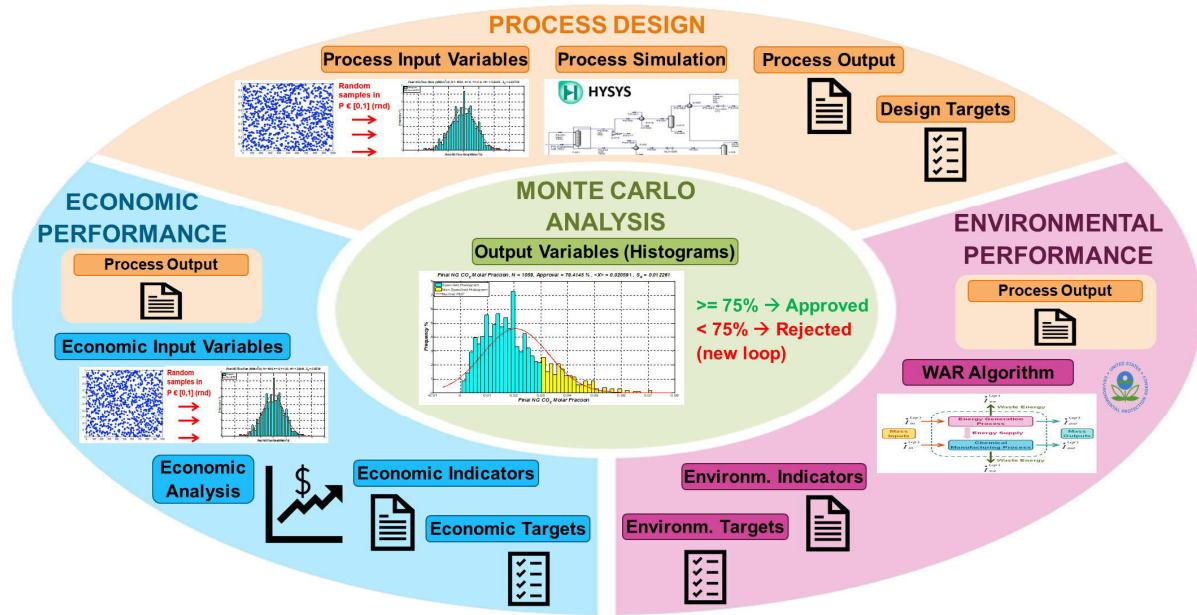


Figure 22. MC analysis workflow.

The Monte-Carlo methodology proposed by this work considers the approval criteria of minimum attainment of specifications in at least 75% of the sampled cases to be representative as sufficiency for a project design to be accepted. Numbers lower than 75% would probably lead to undersized designs, while numbers much higher than 75% would probably only approve oversized designs close to designs based on worst-case scenario. Assuming that the response to be evaluated follows a normal distribution pattern, process design by average values ensures specifications attainment in only 50% of the cases, while process design by worst-case assumptions ensures specifications attainment in 100% of the cases, however, leading to infinite design, which can be interpreted as elevated investments, footprint and weight; conditions not affordable at offshore rigs. Designing a plant to achieve all specification in at least 75% of cases will eventually lead to non-specified products as such design is not immune to all possible scenarios. Considering this reasonable limitation, typical protection conditions at offshore rigs can and shall be used, as flaring or re-injecting non-specified NG, for example, depending on the not accomplished specifications. The goal with the selected percentage of 75% is to achieve a reasonable process design to be more efficient than undersized designs simply made based on average values and oversized designs made on worst-case assumptions, as both often lead to designs with high environmental and economic losses.

3.8. CAE TOOL *MCAnalysis*-HUB

In order to handle complex models, research has focused on developing computational tools for data exchange and interoperability among software (Bolliger et al., 2009; Batres et al., 1999). This is the outline of *MCAnalysis*-HUB (Gonzaga et al., 2019e), designed in a modular architecture for dissociating technology models from analysis modules, since this type of arrangement enables assemblage of different software in a superstructure (HUB) for subsequent larger and more complete analysis (Laurence and Maréchal, 2012). *MCAnalysis*-HUB is developed in Visual Basic.NET (VB.net) framework due to its good operability with the Application Programming Interface (API) of process simulator Aspen HYSYS (Gonzaga, 2014).

MCAnalysis-HUB automatically executes MC analysis on complex process flowsheets by integrating the following steps via eXtensible Markup Language (XML), known as key language to exchange multiple varieties of data in the web and in applications: (i) generation of normal random samples of process input variables with uncertainties using Eq. (21); (ii) management of HYSYS to provide samples of process output variables to the samples of process input variables; (iii) assessment of environmental performance to the samples of process input variables with WAR algorithm; (iv) assessment of environmental performance to the samples of process input variables combined with samples of economic input variables also generated via step (i); and (v) processing and handling of MC results statistically and graphically with MATLAB (Gonzaga et al., 2019b).

MCAnalysis (Gonzaga et al., 2017b), depicted on Figure 23, is the first version of *MCAnalysis*-HUB, depicted on Figure 24, including modules “Generate Batch Data” and “MCM Analysis”. It was designed to be further expanded with new modules to a HUB structure (Gonzaga et al., 2019c). *MCAnalysis*-HUB coupled two new modules, “Environmental Indicators” and “Economic Analysis”, being “MCM Analysis” the central module of the HUB to execute design, environmental and economic assessments via MC analysis. Both *MCAnalysis* and *MCAnalysis*-HUB were developed for HYSYS 8.8 (34.0.0.8909) and MATLAB R2012b (8.0.0.783). They are also compatible with other versions of HYSYS and MATLAB.

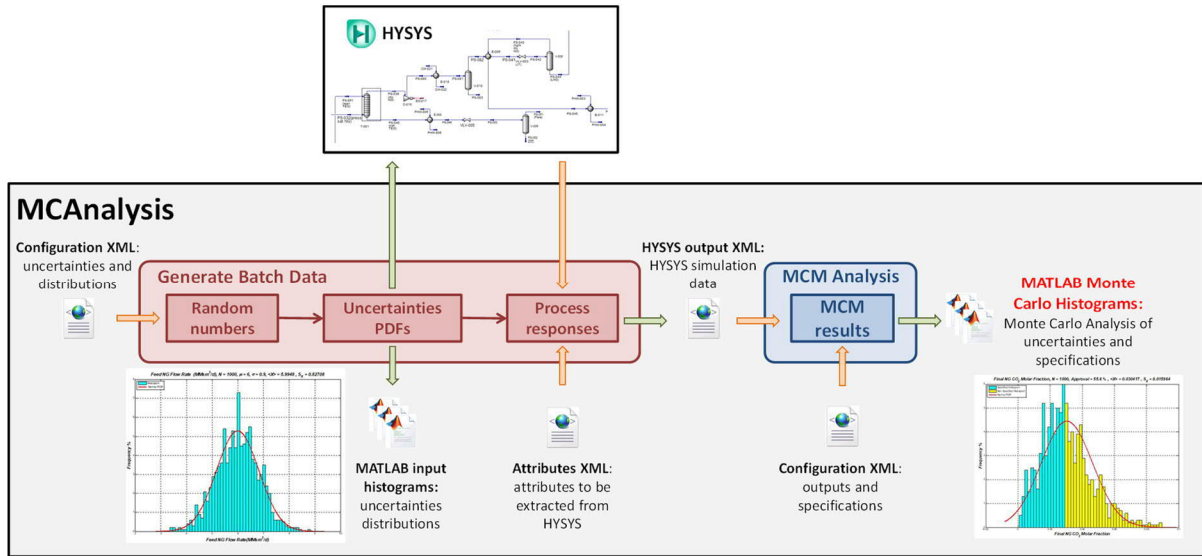


Figure 23. *MCAnalysis* modular architecture.

The modular architecture of *MCAnalysis*-HUB (Figures 23 and 24) starts with module “Generate Batch Data”, which: (i) processes a configurable XML file (Simulation Configuration XML) containing definition of the MCM non-deterministic independent input variables, their respective *PDFs* and their identification within HYSYS; (ii) randomly generates samples of the inputs (uncertainties); (iii) graphically processes input samples in MATLAB, generating histograms and *PDFs*; and (iv) executes HYSYS simulation of process flowsheet in batch mode for each sample of input variables, storing the relevant attributes for MC analysis (process output variables), listed in a configuration XML file (Attributes XML), in an output XML file (HYSYS output XML).

For assessing environmental performance (Figure 24), HYSYS Output XML is processed by module “Environmental Indicators” together with a configurable XML (WAR Configuration XML), extracted from HYSYS, containing a list of components, input and output streams (process and energy) data, where process output streams are classified by the user as product or outlet waste. This module uses WAR algorithm data (Barrett et al., 2011) to generate an XML file (WAR output) containing statistics PEIs responses to process input variables in MC sampling.

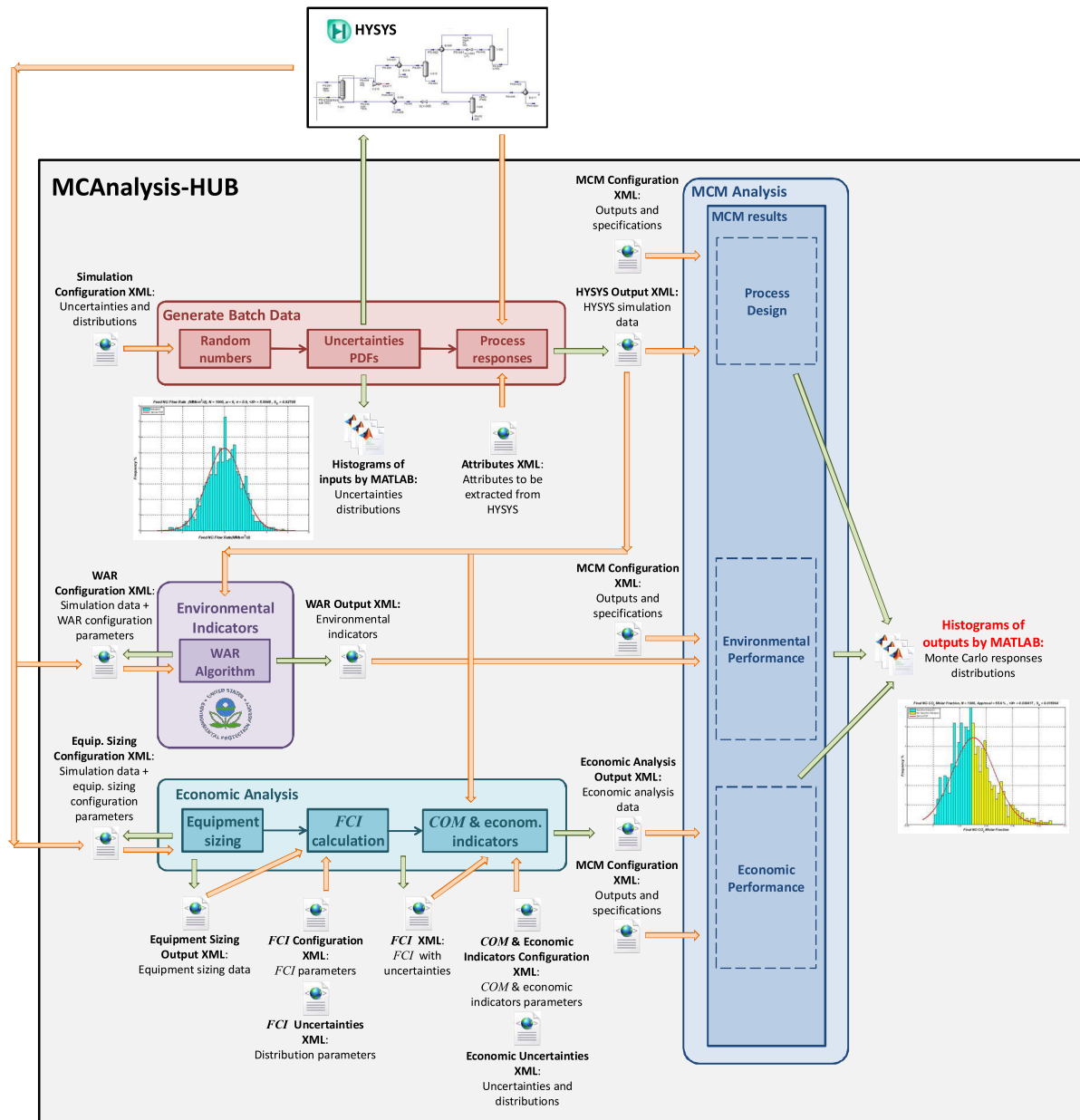


Figure 24. MCAAnalysis-HUB modular architecture.

Assessment of economic performance (Figure 24) starts with equipment sizing in module “Economic Analysis”, which (i) processes a configurable XML file (Equip. Sizing Configuration XML), extracted from HYSYS, containing equipment data from base-case; and (ii) executes equipment sizing and generates an output XML file with results (Equipment Sizing Output XML). No process input variables with uncertainties are considered at this stage. Next step (iv) uses this output XML file together with two configurable XML files (*FCI* Configuration XML and *FCI* Uncertainties XML) for (v) calculating *FCI* considering uncertainties (*FCI* XML). Last step of this module is (vi) to calculate *COM* and economic indicators and store results in an XML file (Economic

Analysis Output XML) by (iv) processing *FCI* XML file and two configurable XML files (*COM* & Economic Indicator Configuration XML and Economic Uncertainties XML). This step considers economic input variables with uncertainties on raw material, products, energy, and waste treatment prices to cover market fluctuations. Carbon tax is also considered as a pertinent economic variable with high level of uncertainty, as discussions on how to best predict such costs are a global topic. The same engine for handling input variables with uncertainties used in module “Generate Batch Data” (steps ii and iii) is also used in this module.

Finally, module “MCM Analysis” (Figures 23 and 24) performs MC analysis itself, and this single module covers process design, environmental and economic assessments. Such setup is feasible due to the interoperability architecture of *MCAnalysis-HUB*; as output files from all the three modules are produced with the same node structure. This module (i) processes the output XML file containing the batch process response data (process design, environmental or economic results) with a configurable XML (MCM Configuration XML) containing the output variables relevant for MC analysis as well as their maximum/minimum specifications; and (ii) generates graphical Monte-Carlo analysis in MATLAB as simple/cumulative frequency histograms, *PDF* and *CDF* curves and percentage of specification-attainment achieved by sampled cases.

4. RESULTS AND DISCUSSIONS: MONTE-CARLO ANALYSIS AND DESIGN OF CO₂-RICH NG PROCESSING ROUTES

This chapter is structured to detail the assessments of process design, environmental and economic performances. Each assessment is composed by two sub-chapters (in parallel): one to compare the novel SS-Route – Plant 2 (Figure 7b) – with the Conventional-Route– Plant 1 (Figure 7a), as the first application proposed in this work; and a second to assess the effects of the CO₂ content increase in NG via conventional processing – Plant 3 (Figure 7), as the second application proposed in this work. It is important to highlight that Plant 3 is a simplified conventional offshore NG processing compared to Plant 1, as it does not include oil processing nor NG and EOR-fluid pipelines, and fewer process specifications are considered for design.

4.1.PROCESS DESIGN ASSESSMENT: CONVENTIONAL-ROUTE versus SS-ROUTE

The Base-Cases of offshore processing of CO₂-rich NG via Conventional-Route – Plant 1 (Figure 7a) – and SS-Route – Plant 2 (Figure 7b) – designed in Sec. 3.4.1 are assessed via Monte-Carlo analysis considering non-deterministic input variables [*PU*₁] raw NG flow rate (*MMsm*³/*d*), [*PU*₂] raw NG CO₂ molar fraction and [*PU*₃] feed GOR (*sm*³/*m*³) following normal *PDFs* (Table 2). Monte-Carlo analysis generated 1000 samples of sets of input variables. Stochastic design approval criterion corresponds to accomplishing all specifications in at least 75% of sampled cases. Histograms and normal *PDFs* of input variables [*PU*₁] to [*PU*₃] are shown in Figure 25 with headers informing number of samples, *PDF* parameters (μ, σ), sample average $\langle X \rangle$ and sample standard deviation S_X in Eq. (22). An important precaution to graphically harmonize simple-frequency histograms with *PDF*'s is to scale up the *PDF* integral to the histogram area.

Eq. (22) defines sample statistics $\langle X \rangle$, S_X^2 , S_X , respectively, sample average, sample variance and sample standard deviation. It is straightforward to show (Himmelblau, 1970) that the expectancies and variances of $\langle X \rangle$ and S_X^2 are respectively given in Eqs. (23) and (24), where Eq. (23) is valid for any *PDF* and Eq. (24) is valid for normal *PDF* $N(\mu, \sigma^2)$. Additionally, for normal *PDF* it can be shown that

(Himmelblau, 1970): (i) $\langle X \rangle$ and S_X^2 are uncorrelated; (ii) $\langle X \rangle$ follows a normal $PDF N(\mu, \sigma^2/N)$ such that $(\langle X \rangle - \mu)/(\sigma/\sqrt{N})$ follows the standard normal $PDF N(0,1)$ in Eq. (25); (iii) $(N-1)S_X^2/\sigma^2$ follows the χ^2 PDF with $N-1$ degrees of freedom in Eq. (25); (iv) both variables in Eq. (25) are uncorrelated as consequence of (i), which allows to use the t -Student Theorem and the F -Fisher Theorem leading to the two behaviors in Eq. (26), where $t_{v=N-1}$ and $F(1, N-1)$, respectively, represent the t -Student PDF with $N-1$ degrees of freedom and the Fisher PDF with 1 and $N-1$ degrees of freedom; and (v) Eq. (26) allows constructing confidence intervals with $(1-\alpha)*100\%$ probability for both variables in Eq. (27), where $t_{1-\alpha/2, N-1}$ and $\phi_{1-\alpha, 1, N-1}$, respectively, represent t -Student abscissa for $N-1$ degrees of freedom and $(1-\alpha/2)*100\%$ probability, and F -Fisher abscissa for $(1, N-1)$ degrees of freedom and $(1-\alpha)*100\%$ probability (with $\alpha=0.05$, for 95% confidence intervals).

$$\langle X \rangle = \frac{\sum_{i=1}^N X_i}{N} \quad , \quad S_X^2 = \frac{\sum_{i=1}^N (X_i - \langle X \rangle)^2}{N-1} \quad , \quad S_X = \sqrt{\frac{\sum_{i=1}^N (X_i - \langle X \rangle)^2}{N-1}} \quad (22)$$

$$E(\langle X \rangle) = \mu \quad , \quad E(S_X^2) = \sigma^2 \quad , \quad VAR(\langle X \rangle) = \sigma^2 / N \quad (23)$$

$$VAR(S_X^2) = \frac{2\sigma^4}{N-1} \quad (24)$$

$$\frac{\langle X \rangle - \mu}{\sigma / \sqrt{N}} \rightarrow N(0,1) \quad , \quad \frac{(N-1)S_X^2}{\sigma^2} \rightarrow \chi_{v=N-1}^2 \quad \{uncorrelated\} \quad (25)$$

$$\frac{\langle X \rangle - \mu}{S_X / \sqrt{N}} \rightarrow t_{v=N-1} \quad , \quad \frac{(\langle X \rangle - \mu)^2}{S_X^2 / N} \rightarrow F(1, N-1) \quad (26)$$

$$-t_{1-\alpha/2, N-1} \leq \frac{\langle X \rangle - \mu}{S_X / \sqrt{N}} \leq t_{1-\alpha/2, N-1} \quad , \quad \frac{(\langle X \rangle - \mu)^2}{S_X^2 / N} \leq \phi_{1-\alpha, 1, N-1} \quad \{(1-\alpha)*100\% \text{ Prob.}\} \quad (27)$$

Table 11 lists sample statistics $\langle X \rangle$, S_X^2 , S_X of input variables $[PU_1]$ to $[PU_3]$, respective *PDF* parameters μ, σ^2, σ and several related statistical entities such as statistics expectancies, standard deviations (*SD*'s) and widths/semi-widths of 95% confidence intervals. For $N=1000$ samples, Table 11 shows $\langle X \rangle$, S_X^2 , S_X close to μ , σ^2 , σ , with low *SD*'s and perfectly inside the respective confidence intervals. The convergence $\langle X \rangle \rightarrow \mu$ is faster ($\langle X \rangle$'s are ≈ 1 *SD* or less from μ 's) compared with $S_X^2 \rightarrow \sigma^2$ and $S_X \rightarrow \sigma$, despite S_X^2 being the best, unbiased and coherent estimator of σ^2 , the S_X^2 's are 3-4 *SD*'s from σ^2 's. The proximity of statistics and parameters, and the convergence of histograms to *PDF*'s curves in Figure 25, show that the populations of input variables $[PU_1]$ to $[PU_3]$ are reasonably normal; i.e., the sampling with $N=1000$ individuals is sufficient in terms of ergodicity.

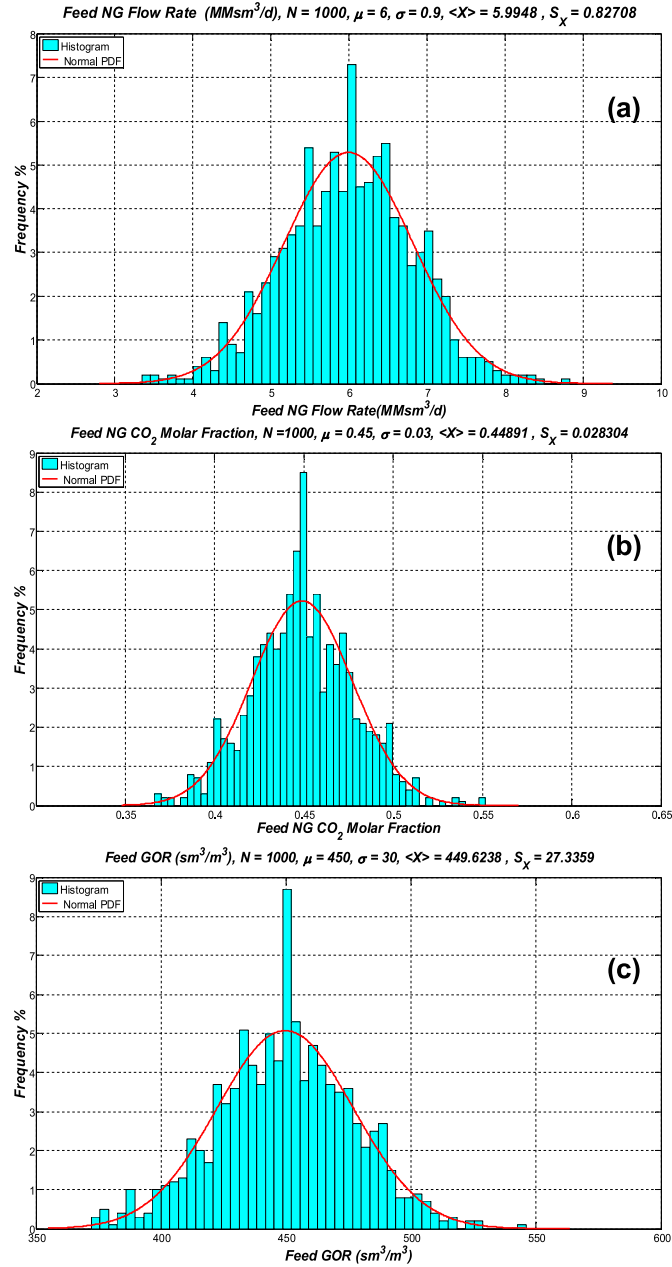


Figure 25. Simple-frequency histograms and normal *PDFs* of input variables: (a) [PU₁] raw NG flow rate(MMsm³/d); (b) [PU₂] raw NG CO₂ molar fraction; and (c) [PU₃] multiphase-feed GOR(sm³/m³).

Table 11. Sample statistics $\langle X \rangle, S_X, S_X^2$, parameters μ, σ^2 , statistics standard deviations (SD), statistics standardizations and 95% confidence intervals: $N=1000$ samples of inputs $[PU_1], [PU_2], [PU_3]$ ($\alpha=0.05$).

Statistics & Parameters	Stochastic Input Variable		
	$[PU_1]$ Raw NG flow rate (MMsm ³ /d)	$[PU_2]$ Raw NG CO ₂ molar fraction	$[PU_3]$ Multiphase- Feed GOR (sm ³ /m ³)
$\langle X \rangle$	5.9948	0.44891	449.624
μ	6	0.45	450
$(\langle X \rangle - \mu) * 100 / \mu$	-0.09%	-0.24%	-0.08%
$SD_{\langle X \rangle} = \sigma / \sqrt{N}$	0.02846	0.0009487	0.9487
$\frac{\langle X \rangle - \mu}{\sigma / \sqrt{N}}$	-0.18271	-1.1490	-0.39634
S_X	0.82708	0.028304	27.336
σ	0.9	0.03	30
$(S_X - \sigma) * 100 / \sigma$	-8.10%	-5.65%	-8.88%
S_X^2	0.68406	0.0008011	747.25
σ^2	0.81	0.0009	900
$SD_{S_X^2} = \sqrt{2\sigma^2} / \sqrt{N-1}$	0.036242	0.00004027	40.269
$(N-1)S_X^2 / \sigma^2$	843.67	889.22	829.45
$\frac{\langle X \rangle - \mu}{S_X / \sqrt{N}}$	-0.19882	-1.2178	-0.43496
$\pm t_{1-\alpha/2, N-1}$	± 1.9623	± 1.9623	± 1.9623
$\frac{(\langle X \rangle - \mu)^2}{S_X^2 / N}$	0.039529	1.48304	0.18919
$\phi_{1-\alpha, 1, N-1}$	3.8508	3.8508	3.8508

Module “Generate Batch Data” also obtains responses of Base-Cases from HYSYS for the populations of input variables. The generated populations of process output variables $[PS_1]$ to $[PS_{10}]$ (Table 4) of Base-Cases are assessed by module “MCM Analysis” in terms of matched specifications. “MCM Analysis” renders graphics consisting of: (i) population simple-frequency histograms of output variables with plots of normal *PDF*’s using the respective sample average ($\langle X \rangle$) and sample standard deviation (S_X) as *PDF* parameters; and (ii) population cumulative-frequency histograms of output variables with plots of normal *CDF*’s again using $\langle X \rangle$ and S_X^2 as *CDF* parameters. This graphic comparison aims at identifying similarity of the output behavior with normal patterns, because, given the non-linear character of

such processes, in general output variables present statistical behaviors discrepant from normal patterns.

4.1.1. Conventional-Route Base-Case

MC analysis of the Base-Case of Conventional-Route is depicted in Figures 26 and 27. Results for the responses of interest can be expressed as simple-frequency, as well as cumulative-frequency histograms with superposed normal *PDF* or *CDF* plots using statistics $\langle X \rangle$ and S_X^2 as parameters to test suitability of normal behavior. Figure 26 depicts simple-frequency histograms and normal *PDF*s of output variables $[PS_1]$ to $[PS_5]$, $[PS_7]$ and $[PS_8]$, and cumulative-frequency histogram and normal *CDF* of $[PS_6]$, while Figure 27 depicts the simple-frequency histogram and normal *PDF* of $[PS_9]$ and the cumulative-frequency histogram and normal *CDF* of $[PS_{10}]$. The title bar of the graphics informs number of samples, percentage of samples attaining/exceeding specifications, and statistics ($\langle X \rangle, S_X$). In all histograms, blue color indicates the population bars reaching/exceeding the respective specification, while yellow marks the extracts not achieving it. This is seen in Figure 26a for the MC analysis of response $[PS_1]$ NG CO₂ molar fraction (y_{CO_2}), with specification $y_{CO_2} \leq 0.03$ (Table 4), showing only 55.6% of specified samples. On the other hand, response $[PS_2]$, NG CH₄ molar fraction (y_{CH_4}) with specification $y_{CH_4} \geq 0.85$, attains 90.2% of specified samples. In Figure 26f, the cumulative-frequency histogram of response $[PS_6]$ $WDP^{EOR-Fluid}$ – specification $WDP^{EOR-Fluid} \leq -45^\circ\text{C}@1\text{atm}$ – shows 100% of specified samples.

Regarding the manifestation of normal behavior, $[PS_1]$ NG y_{CO_2} (Figure 26a) and $[PS_4]$ $HCDP^{NG}$ (Figure 26d) histograms are relatively close to the respective normal *PDF*'s despite some right-skewness. $[PS_2]$ NG y_{CH_4} (Figure 26b) exhibits a discrepant behavior from the normal *PDF* despite its frank unimodality, while $[PS_3]$ WDP^{NG} (Figure 26c), $[PS_6]$ $WDP^{EOR-Fluid}$ (Figure 26f), $[PS_9]$ $PPCO_2^{MP-Feed}$ (Figure 27a) and $[PS_{10}]$ power-consumption (Figure 27b) histograms are all well-balanced and close to the respective normal *PDF*'s. $[PS_5]$ $P^{NG-Delivery}$ (Figure 26e) and $[PS_7]$ $P^{EOR-Delivery}$ (Figure 26g) presented left-skewed behaviors relatively to respective

normal *PDF*'s, while $[PS_8]$ $HCDP^{MP-Feed}$ histogram (Figure 26h), despite apparently resembling a normal *PDF*, subtly departs from a true normal because it is thinner in the middle.

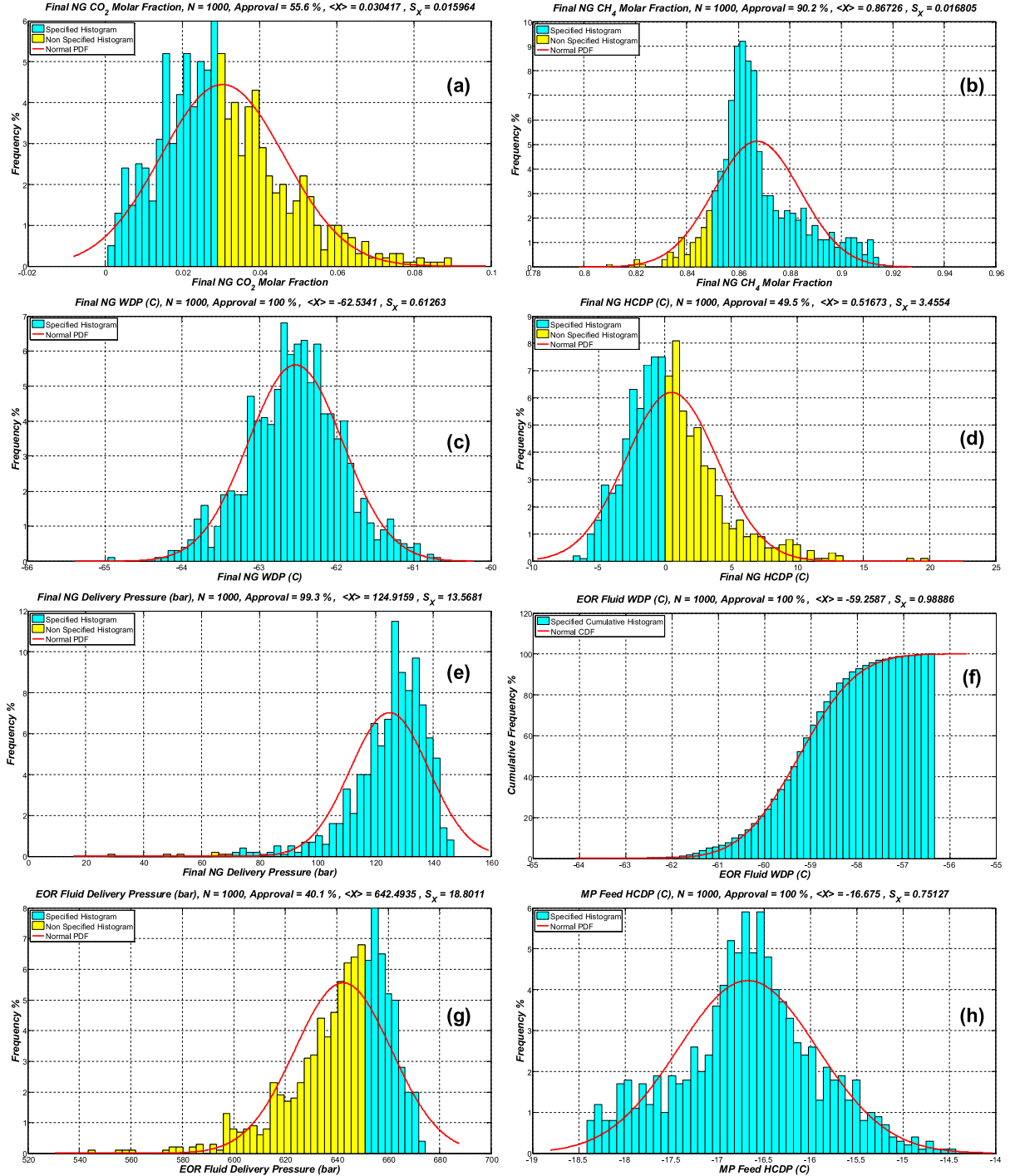


Figure 26. Conventional-Route Base-Case: simple-frequency histograms and normal *PDF*s ($\langle X \rangle$, S_X^2): (a) $[PS_1]$ NG y_{CO_2} ; (b) $[PS_2]$ NG y_{CH_4} ; (c) $[PS_3]$ $WDP^{NG} (^{\circ}C)$; (d) $[PS_4]$ $HCDP^{NG} (^{\circ}C)$; (e) $[PS_5]$ $P^{NG-Delivery} (bar)$; (g) $[PS_7]$ $P^{EOR-Delivery} (bar)$;

(h) $[PS_8]$ $HCDP^{MP-Feed} (^{\circ}C)$; and (f) cumulative-frequency histogram and normal $CDF(<X>, S_X^2)$ of $[PS_6]$ $WDP^{EOR-Fluid} (^{\circ}C)$.

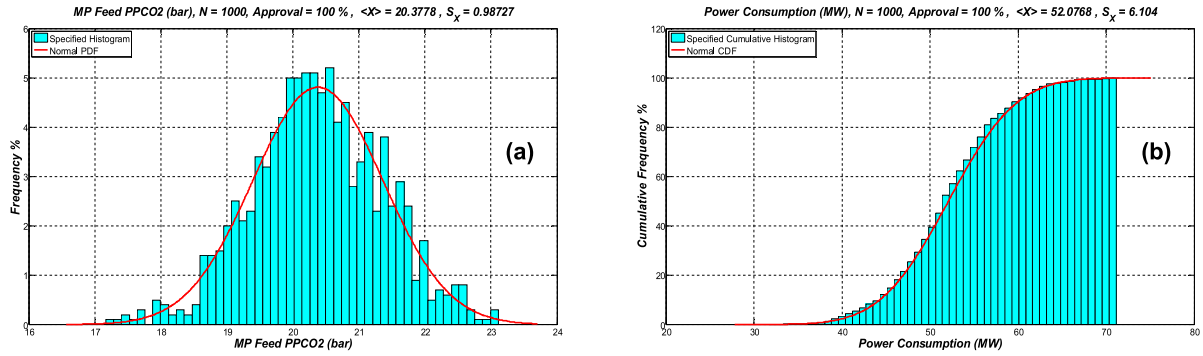


Figure 27. Conventional-Route Base-Case: (a) simple-frequency histogram and normal $PDF(<X>, S_X^2)$ of $[PS_9]$ $PPCO_2^{MP-Feed}$; and (b) cumulative-frequency histogram and normal $CDF(<X>, S_X^2)$ of $[PS_{10}]$ power-consumption.

These results plainly exemplify the non-linearity of offshore processing of CO_2 -rich NG via the Conventional-Route and justify using MC analysis for design assessment. Table 12 lists percentages of approval, statistics ($<X>, S_X$) and simple/cumulative frequency histograms compared to the respective normal $PDFs/CDFs(<X>, S_X^2)$ for the populations ($N=1000$) of responses $[PS_1]$ to $[PS_{10}]$.

Table 12. MC analysis ($N=1000$) of responses $[PS_1]$ to $[PS_{10}]$ of Conventional-Route Base-Case: approval percentages, statistics ($<X>, S_X$) and comparison of simple/cumulative frequency histograms versus normal $PDF/CDF(<X>, S_X^2)$.

Response	Approval	$<X>$	S_X	Histogram vs normal $PDF/CDF (<X>, S_X^2)$
$[PS_1]$ NG y_{CO_2}	55.6%	0.030417	0.0145964	Close, right-skewed
$[PS_2]$ NG y_{CH_4}	90.2%	0.86726	0.016805	Thinner
$[PS_3]$ $WDP^{NG} (^{\circ}C)$	100 %	-62.5341	0.61263	Close
$[PS_4]$ $HCDP^{NG} (^{\circ}C)$	49.5%	0.51673	3.4554	Close, right-skewed
$[PS_5]$ $P^{NG-Delivery} (bar)$	99.3%	124.9159	13.5681	Dislocated, left-skewed
$[PS_6]$ $WDP^{EOR-Fluid} (^{\circ}C)$	100 %	-59.2587	0.98886	Close
$[PS_7]$ $P^{EOR-Delivery} (bar)$	40.1%	642.4935	18.8011	Dislocated, left-skewed
$[PS_8]$ $HCDP^{MP-Feed} (^{\circ}C)$	100 %	-16.675	0.75127	Close
$[PS_9]$ $PPCO_2^{MP-Feed} (bar)$	100 %	20.3778	0.98727	Close
$[PS_{10}]$ Power-Consumption(MW)	100 %	52.0768	6.104	Close

Figure 26a, d and g show that the Conventional-Route Base-Case did not attain specifications in 75% of the sampled cases for three output variables: $[PS_1]$ NG y_{CO_2} , $[PS_4]$ $HCDP^{NG}$ and $[PS_7]$ $P^{EOR-Delivery}$, respectively, with 55.6%, 49.5% and 40.1% of specified samples. Therefore, Conventional-Route must be re-designed and re-tested with MC analysis.

4.1.1.1. Re-designed Conventional-Route

Conventional-Route is re-designed to increase performance of three underachieved responses by means of following debottlenecking measures: to increase 10% of MP area ($13970+6985 \text{ m}^2$) (Figure 12) to lower $[PS_1]$; to decrease JTE feed temperature from $T=12^\circ\text{C}$ to $T=7.5^\circ\text{C}$, increasing exchanger area and C3+ liquefaction (Figure 10) and lowering $[PS_4]$; and to increase the diameter of segment 3 (injection bore) of EOR pipeline from 6" to 8" (Figure 14), simultaneously decreasing the discharge pressure of EOR-Fluid pump (Figure 12) from $P=300 \text{ bar}$ to $P=245 \text{ bar}$ to increase $[PS_7]$. Another alternative to correct $[PS_7]$ would be to increase EOR pump pressure alone; however, this would require a significant pressure increase, drastically increasing power-consumption $[PS_{10}]$, and making the enlargement of EOR injection bore preferable. The process adjustments proposed above result of multiple loops of Monte-Carlo analysis to achieve a viable process design, based on the knowledge of which fixed design parameters can improve the performances of each unachieved response.

MC analysis of the debottlenecked Conventional-Route is shown in Figures 28 and 29. Figure 28 depicts simple-frequency histograms and normal $PDF(<X>, S_x^2)$ of responses $[PS_1]$ to $[PS_5]$, $[PS_7]$ and $[PS_8]$, and cumulative-frequency histogram and normal $CDF(<X>, S_x^2)$ of $[PS_6]$. Figure 29 depicts simple-frequency histogram and normal $PDF(<X>, S_x^2)$ for $[PS_9]$ and the cumulative-frequency histogram and normal $CDF(<X>, S_x^2)$ for $[PS_{10}]$. Table 13 presents percentages of approval, statistics $(<X>, S_x)$ and comparisons of simple/cumulative frequency histograms with normal $PDFs/CDFs$ for responses $[PS_1]$ to $[PS_{10}]$.

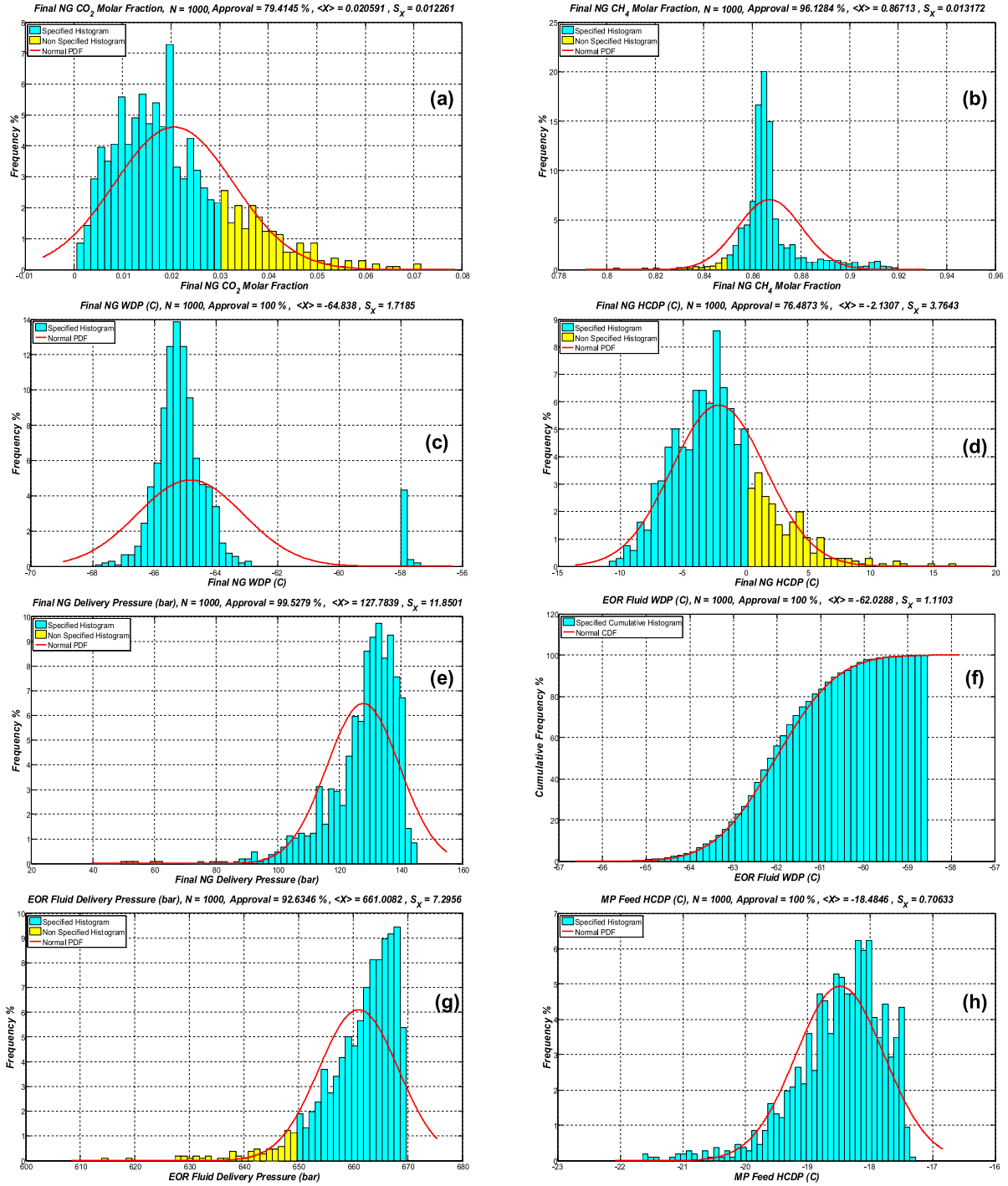


Figure 28. Re-designed Conventional-Route Base-Case: simple-frequency histograms and normal $PDFs(\langle X \rangle, S_x^2)$: (a) [PS₁] NG y_{CO_2} ; (b) [PS₂] NG y_{CH_4} ; (c) [PS₃] $HCDP^{NG} (^{\circ}C)$; (e) [PS₅] $P^{NG-Delivery} (bar)$; (g) [PS₇] $P^{EOR-Delivery} (bar)$; (h) [PS₈] $HCDP^{MP-Feed} (^{\circ}C)$; and (f) cumulative-frequency histogram and normal $CDF(\langle X \rangle, S_x^2)$ of [PS₆] $WDP^{EOR-Fluid} (^{\circ}C)$.

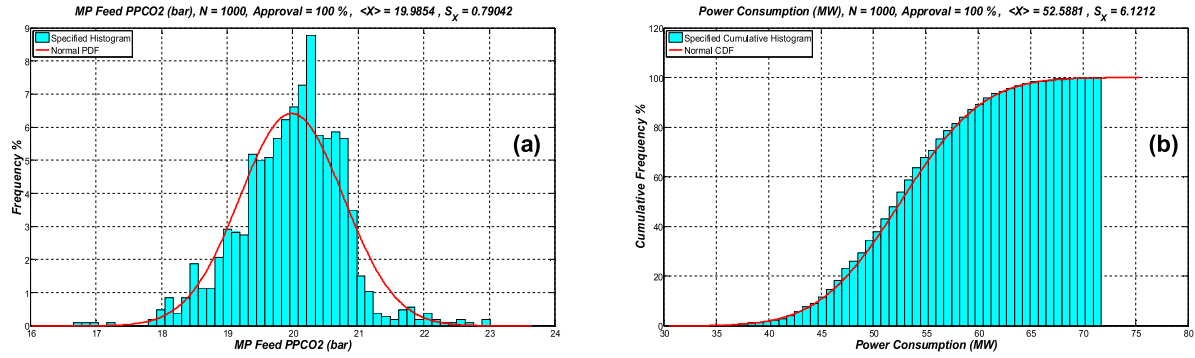


Figure 29. Re-designed Conventional-Route Base-Case: (a) simple-frequency histogram and normal $PDF(<X>, S_x^2)$ of $[PS_9]$ $PPCO_2^{MP-Feed}$, and (b) cumulative-frequency histogram and normal $CDF(<X>, S_x^2)$ of $[PS_{10}]$ power-consumption.

Table 13. MC analysis ($N=1000$) of responses $[PS_1]$ to $[PS_{10}]$ of re-designed Conventional-Route Base-Case: approval percentages, statistics ($<X>$, S_x) and comparison of simple/cumulative frequency histograms versus normal $PDF/CDF(<X>, S_x^2)$.

Response	Approval	$<X>$	S_x	Histogram vs normal $PDF/CDF(<X>, S_x^2)$
$[PS_1]$ NG y_{CO_2}	79.4%	0.020591	0.012261	Close
$[PS_2]$ NG y_{CH_4}	96.1%	0.86713	0.013172	Thinner
$[PS_3]$ $WDP^{NG} (^{\circ}C)$	100 %	-64.838	1.7185	Bimodal, thinner
$[PS_4]$ $HCDP^{NG} (^{\circ}C)$	76.5%	-2.1307	3.7643	Close
$[PS_5]$ $P^{NG-Delivery} (bar)$	99.5%	127.7839	11.8501	Dislocated
$[PS_6]$ $WDP^{EOR-Fluid} (^{\circ}C)$	100 %	-62.0288	1.1103	Close
$[PS_7]$ $P^{EOR-Delivery} (bar)$	92.6%	661.0082	7.2956	Left-skewed
$[PS_8]$ $HCDP^{MP-Feed} (^{\circ}C)$	100 %	-18.4846	0.70633	Left-skewed
$[PS_9]$ $PPCO_2^{MP-Feed} (bar)$	100 %	19.9854	0.7942	Close
$[PS_{10}]$ Power-Consumption(MW)	100 %	52.5881	6.1212	Close

Figures 28-29 and Table 13 show that the re-designed Conventional-Route accomplished specifications for all responses $[PS_1]$ to $[PS_{10}]$ for at least 75% of samples. Table 14 summarizes variations of approval percentages and of statistics ($<X>$, S_x), and changes of histograms of $[PS_1]$ to $[PS_{10}]$ from the original Base-Case to the debottlenecked Conventional-Route.

The approval percentages listed in Table 13 may indicate that the Conventional-Route is oversized, as multiple percentages are not close to 75%. However, this is not the case, therefore, it is important to clarify that many specifications are already

achieved in 100% of the sampled cases in the original Base-Case, and also that some specifications may be limiting to process design, as it is the case of $[PS_1]$ NG y_{CO_2} and $[PS_4]$ $HCDP^{NG}$, which present approval percentage very close to 75%. This consideration is valid to all process re-designs achieved via the proposed Monte-Carlo analysis.

Table 14. Original versus re-designed Conventional-Route: changes of approval percentages, statistics ($\langle X \rangle$, S_X) and histograms of responses $[PS_1]$ to $[PS_{10}]$ in MC analysis.

Response	Approval Difference	$\langle X \rangle$ Difference	S_X Difference	Changes of Histograms
$[PS_1]$ NG y_{CO_2}	43%	-32%	-16%	Similar histograms
$[PS_2]$ NG y_{CH_4}	7%	0%	-22%	Similar, but thinner
$[PS_3]$ $WDP^{NG} (^{\circ}C)$	0%	-4%	181%	From close to bimodal
$[PS_4]$ $HCDP^{NG} (^{\circ}C)$	55%	-512%	9%	Similar histograms
$[PS_5]$ $P^{NG-Delivery} (bar)$	0%	2%	-13%	Similar histograms
$[PS_6]$ $WDP^{EOR-Fluid} (^{\circ}C)$	0%	-5%	12%	Similar histograms
$[PS_7]$ $P^{EOR-Delivery} (bar)$	131%	3%	-61%	Similar histograms
$[PS_8]$ $HCDP^{MP-Feed} (^{\circ}C)$	0%	-11%	-6%	From close to left-skewed
$[PS_9]$ $PPCO_2^{MP-Feed} (bar)$	0%	-2%	-20%	Similar histograms
$[PS_{10}]$ Power-Consumption(MW)	0%	1%	0%	Similar histograms

Figs. 28-29 and Table 14 show that the most relevant changes from re-designing the original Conventional-Route Base-Case are: (i) 43% increase of approval percentage of $[PS_1]$ NG y_{CO_2} by decreasing $\langle X \rangle$ by 32% and S_X by 16%, while keeping the shape of the simple-frequency histogram relatively close; (ii) 7% increase of approval percentage of $[PS_2]$ NG y_{CH_4} by decreasing S_X by 22%, keeping the histogram shape but making it thinner in the middle; (iii) keeping the approval percentage of $[PS_3]$ WDP^{NG} , decreasing $\langle X \rangle$ by 4%, increasing S_X by 181%, and changing the shape of the simple-frequency histogram from very close to normal PDF to a bimodal pattern; (iv) 55% increase of approval percentage of $[PS_4]$ $HCDP^{NG}$ by decreasing $\langle X \rangle$ by 512% and keeping histogram shape; (v) 131% increase of approval percentage of

[PS₇] $P^{EOR-Delivery}$ by decreasing S_X by 61% and accentuating the left-skewness of the simple-frequency histogram; (vi) 11% decrease of $\langle X \rangle$ and 6% decrease of S_X of [PS₈] $HCDP^{MP-Feed}$, changing the shape of the simple-frequency histogram from relatively close to normal PDF to left-skewed; and (vii) 2% decrease of $\langle X \rangle$ and 20% decrease of S_X of [PS₉] $PPCO_2^{MP-Feed}$, keeping the shape of the simple-frequency histogram very close to normal PDF .

The results of the re-designed Conventional-Route vis-à-vis the original Base-Case confirm the non-linearity of offshore processing of CO₂-rich NG and the utility of MC analysis for debottlenecking and re-design so that all selected output variables could attain specifications in 75% of sampled cases.

4.1.2. SS-Route Base-Case

An important aspect of MC analysis of SS-Route is that, as the raw NG feed flow rate changes (input variable $[PU_1]$, Table 2) in the sampling process, the SS design, which is strongly dependent of the raw gas flow rate and is expressed in terms of throat diameter, converging, diverging and total lengths (D_T , L_C , L_D , L , Figure 3), also changes from the Base-Case SS design values in Table 7. Only the inlet/outlet diameters, the wall angles, the number of SS nozzles and the chosen Ma^{Shock} and efficiencies are kept constant. Also the performance plots in Figures 15 and 16 – built for the SS-Route Base-Case with average values of inputs (Table 2) – are different for each sample of input variables in the ensemble. In other words, MC analysis of SS-Route also produces histograms of SS throat diameter (D_T), SS converging length (L_C), SS diverging length (L_D) and SS length (L). This is a critical difference from MC analysis of Conventional-Route, whose equipment designs are constant throughout the MC sampling.

Results of MC analysis of SS-Route Base-Case are shown in Figures 30 and 31. Figure 30 depicts simple-frequency histograms and normal $PDFs(\langle X \rangle, S_X^2)$ for responses [PS₁] to [PS₈], while Figure 31 depicts cumulative-frequency histograms and normal $CDFs(\langle X \rangle, S_X^2)$ for [PS₉] and [PS₁₀].

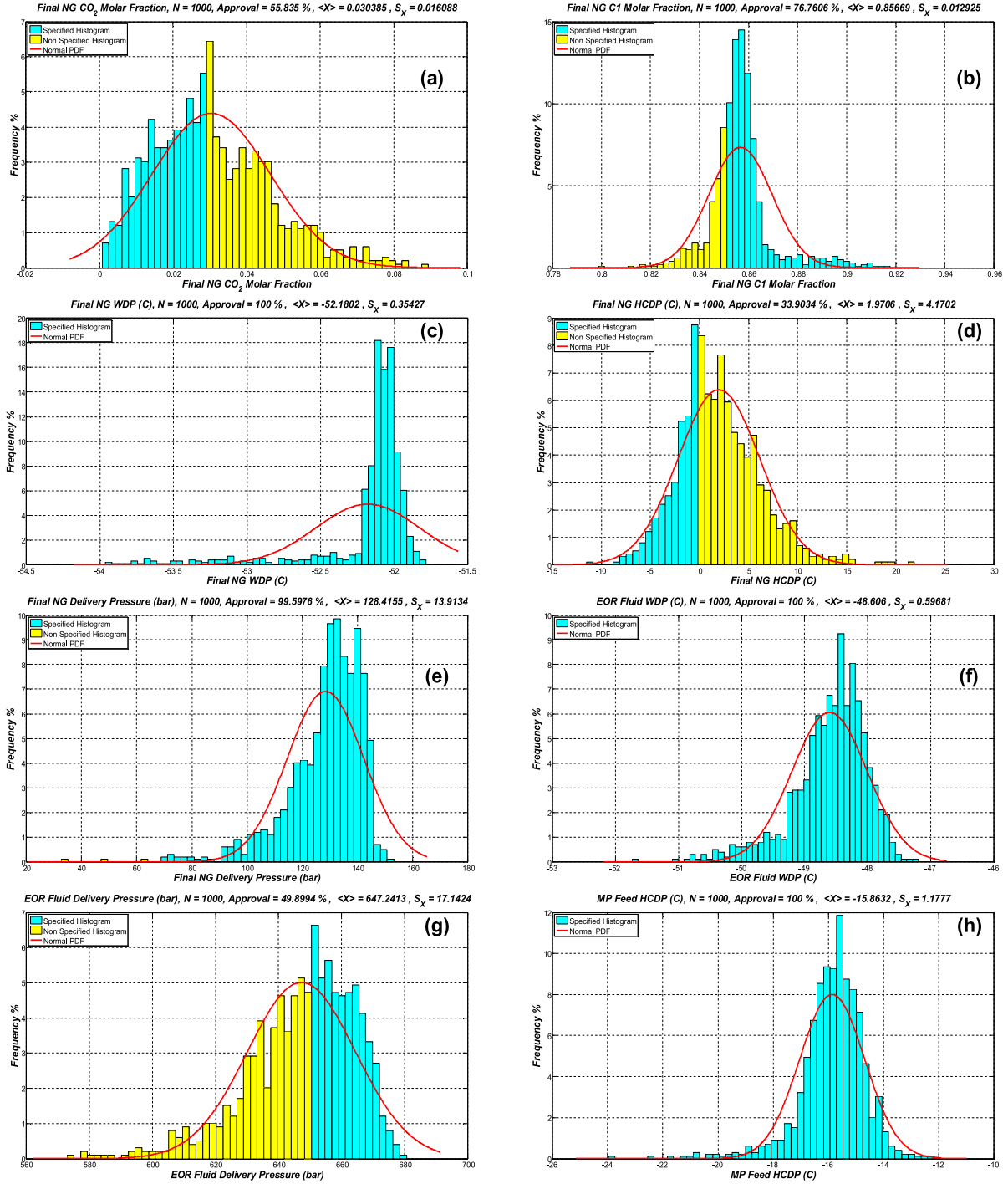


Figure 30. SS-Route Base-Case: simple-frequency histograms and normal PDFs($\langle X \rangle$, S_x^2): (a) [PS₁] NG y_{CO_2} ; (b) [PS₂] NG y_{CH_4} ; (c) [PS₃] WDP^{NG} ; (d) [PS₄] $HCDP^{NG}$; (e) [PS₅] $P^{NG-Delivery}$; (f) [PS₆] $WDP^{EOR-Fluid}$; (g) [PS₇] $P^{EOR-Delivery}$; and (h) [PS₈] $HCDP^{MP-Feed}$.

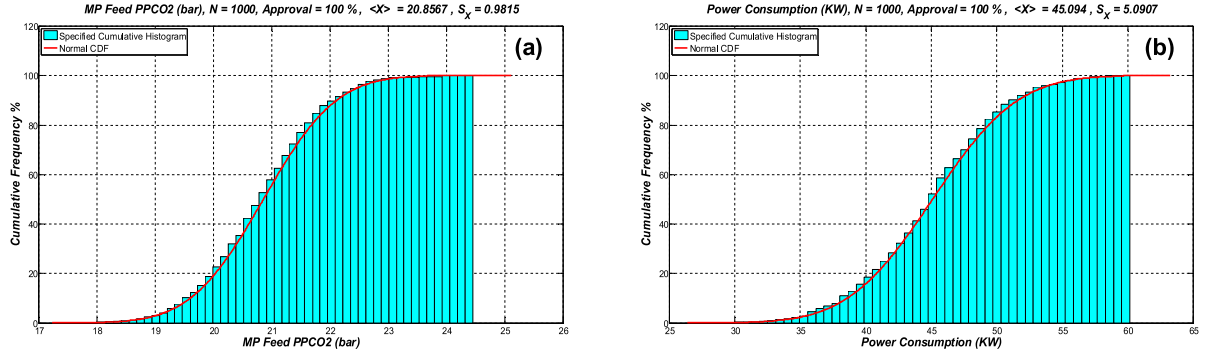


Figure 31. SS-Route Base-Case cumulative-frequency histograms and normal CDFs($\langle X \rangle$, S_X^2): (a) $[PS_9]$ $PPCO_2^{MP-Feed}$; and (b) $[PS_{10}]$ power-consumption.

Table 15 lists percentages of specification attainment, statistics ($\langle X \rangle$, S_X), and simple/cumulative frequency histograms compared to respective normal PDFs/CDFs($\langle X \rangle$, S_X^2) for responses $[PS_1]$ to $[PS_{10}]$.

Table 15 shows that three responses did not attain 75% of specified samples: $[PS_1]$ NG_{yCO_2} , $[PS_4]$ $HCDP^{NG}$ and $[PS_7]$ $p^{EOR-Delivery}$, respectively, with 55.8%, 33.9% and 49.9% of specified samples (also confirmed in Figure 30 a, d and g). Therefore, the SS-Route Base-Case must also be re-designed for debottlenecking and re-testing with MC analysis.

Table 15. MC analysis ($N=1000$) of responses $[PS_1]$ to $[PS_{10}]$ of SS-Route Base-Case: approval percentages, statistics ($\langle X \rangle$, S_x) and comparison of simple/cumulative frequency histograms versus normal $PDF/CDF(\langle X \rangle, S_x^2)$.

Response	Approval	$\langle X \rangle$	S_x	Histogram vs normal $PDF/CDF(\langle X \rangle, S_x^2)$
$[PS_1]$ NG y_{CO_2}	55.8%	0.030385	0.016088	Close, right-skewed
$[PS_2]$ NG y_{CH_4}	76.8%	0.85669	0.012925	Thinner
$[PS_3]$ $WDP^{NG} (^{\circ}C)$	100 %	-52.1802	0.35427	Thinner, left-skewed
$[PS_4]$ $HCDP^{NG} (^{\circ}C)$	33.9%	1.9706	4.1702	Close, right-skewed
$[PS_5]$ $P^{NG-Delivery} (bar)$	99.6%	128.4155	13.9134	Left-skewed, long-tail
$[PS_6]$ $WDP^{EOR-Fluid} (^{\circ}C)$	100 %	-48.606	0.59681	Left-skewed, long-tail
$[PS_7]$ $P^{EOR-Delivery} (bar)$	49.9%	647.2413	17.1424	Left-skewed, long-tail
$[PS_8]$ $HCDP^{MP-Feed} (^{\circ}C)$	100 %	-15.8632	1.1777	Close, thinner
$[PS_9]$ $PPCO_2^{MP-Feed} (bar)$	100 %	20.8567	0.9815	Close
$[PS_{10}]$ Power-Consumption(MW)	100 %	45.094	5.0907	Close

4.1.2.1. Re-designed SS-Route

SS-Route is re-designed to increase performance of the three underachieved responses by means of three design modifications: to increase 14% of MP area ($14020+7010 \text{ m}^2$) (Figure 12) to lower $[PS_1]$; to increase SS (Figure 11) severity by rising $Ma^{Shock}=1.4$ to $Ma^{Shock}=1.52$ (Table 7) to increase SS C3+ removal (Figure 15d), lowering $[PS_4]$; and to increase the diameter of segment 3 (injection bore) of EOR pipeline from 6" to 8" (Fig. 9) simultaneously decreasing EOR pump discharge pressure (Figure 12) from $P=300 \text{ bar}$ to $P=240 \text{ bar}$ to increase $[PS_7]$. The process adjustments proposed above also result of multiple loops of Monte-Carlo analysis to achieve a viable process design, as described in the re-designed Conventional-Route (Sec. 4.1.1.1).

MC analysis of the resized SS-Route is shown in Figs. 32 and 33. Figure 32 depicts simple-frequency histograms and normal $PDFs(\langle X \rangle, S_x^2)$ of responses $[PS_1]$ to $[PS_8]$, while Figure 33 shows cumulative-frequency histograms and normal $CDFs(\langle X \rangle, S_x^2)$ for $[PS_9]$ and $[PS_{10}]$. Table 16 presents percentages of approval, statistics ($\langle X \rangle$, S_x) and comparisons of simple/cumulative frequency histograms with normal $PDFs/CDFs(\langle X \rangle, S_x^2)$ for $[PS_1]$ to $[PS_{10}]$.

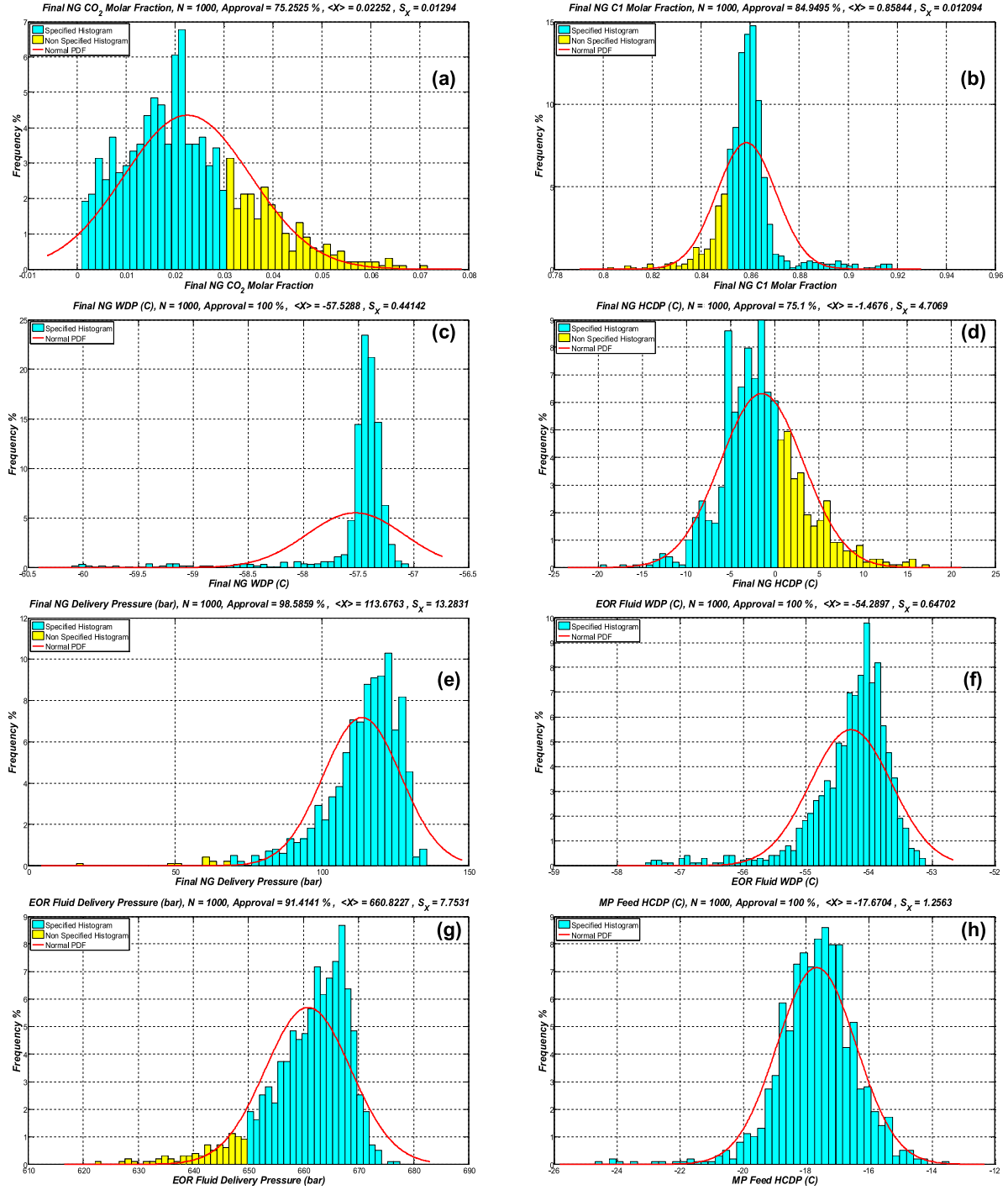


Figure 32. Re-designed SS-Route Base-Case: simple-frequency histograms and normal $PDFs(\langle X \rangle, S_x^2)$: (a) [PS₁] NG y_{CO_2} ; (b) [PS₂] NG y_{CH_4} ; (c) [PS₃] WDP^{NG} ; (d) [PS₄] $HCDP^{NG}$; (e) [PS₅] $P^{NG-Delivery}$; (f) [PS₆] $WDP^{EOR-Fluid}$; (g) [PS₇] $P^{EOR-Delivery}$; and (h) [PS₈] $HCDP^{MP-Feed}$.

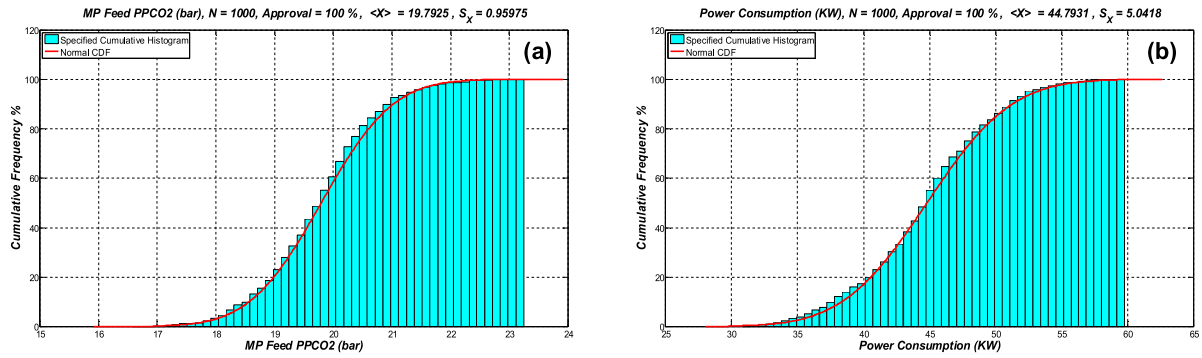


Figure 33. Re-designed SS-Route Base-Case cumulative-frequency histograms and normal $CDFs(\langle X \rangle, S_X^2)$: (a) $[PS_9]$ $PPCO2^{MP-Feed}$; and (b) $[PS_{10}]$ power-consumption.

Table 16. MC analysis ($N=1000$) of responses $[PS_1]$ to $[PS_{10}]$ of re-designed SS-Route Base-Case: approval percentages, statistics ($\langle X \rangle, S_X$) and comparison of simple/cumulative frequency histograms versus normal $PDF/CDF(\langle X \rangle, S_X^2)$.

Response	Approval	$\langle X \rangle$	S_X	Histogram vs normal $PDF/CDF(\langle X \rangle, S_X^2)$
$[PS_1]$ NG y_{CO2}	75.3%	0.02252	0.01294	Close, right-skewed
$[PS_2]$ NG y_{CH4}	84.9%	0.849495	0.012094	Thinner
$[PS_3]$ $WDP^{NG} (^{\circ}C)$	100 %	-57.5288	0.44142	Left-skewed, long tail
$[PS_4]$ $HCDP^{NG} (^{\circ}C)$	75.1%	-1.4676	4.7069	Close
$[PS_5]$ $P^{NG-Delivery} (bar)$	98.6%	113.6763	13.2831	Left-skewed, long tail
$[PS_6]$ $WDP^{EOR-Fluid} (^{\circ}C)$	100 %	-54.2897	0.64702	Left-skewed, long tail
$[PS_7]$ $P^{EOR-Delivery} (bar)$	91.4%	660.8227	7.7531	Left-skewed, long tail
$[PS_8]$ $HCDP^{MP-Feed} (^{\circ}C)$	100 %	-17.6704	1.2563	Close, thinner
$[PS_9]$ $PPCO2^{MP-Feed} (bar)$	100 %	19.7925	0.95975	Close
$[PS_{10}]$ Power-Consumption(MW)	100 %	44.7931	5.0418	Close

Figs. 32-33, and Table 16 show that the re-designed SS-Route accomplished at least 75% of specified samples for all responses $[PS_1]$ to $[PS_{10}]$. Table 17 summarizes variations of approval percentages and of statistics ($\langle X \rangle, S_X$), and changes of histograms of $[PS_1]$ to $[PS_{10}]$ from the original Base-Case to the debottlenecked SS-Route.

Table 17. Original versus re-designed SS-Route: changes of approval percentages, statistics ($\langle X \rangle$, S_X) and histograms of responses [PS1] to [PS10] in MC analysis.

Response	Approval Difference	$\langle X \rangle$ Difference	S_X Difference	Changes of Histograms
[PS ₁] NG y_{CO_2}	35%	-26%	-20%	Similar histograms
[PS ₂] NG y_{CH_4}	10%	-1%	-6%	Similar histograms
[PS ₃] WDP ^{NG} (°C)	0%	-10%	25%	Similar histograms
[PS ₄] HCDP ^{NG} (°C)	122%	-174%	13%	Similar histograms
[PS ₅] P ^{NG-Delivery} (bar)	-1%	-11%	-5%	Similar histograms
[PS ₆] WDP ^{EOR-Fluid} (°C)	0%	-12%	8%	Similar histograms
[PS ₇] P ^{EOR-Delivery} (bar)	83%	2%	-55%	Similar histograms
[PS ₈] HCDP ^{MP-Feed} (°C)	0%	-11%	7%	Similar histograms
[PS ₉] PPCO ₂ ^{MP-Feed} (bar)	0%	-5%	-2%	Similar histograms
[PS ₁₀] Power-Consumption(MW)	0%	-1%	-1%	Similar histograms

Figs. 32-33 and Table 17 show that re-designing the original SS-Route Base-Case practically kept the departure of all histograms relatively to the respective PDF/CDF($\langle X \rangle$, S_X^2) with the following main effects: (i) 35% increase of the percentage of specification attainment of [PS₁] NG y_{CO_2} by decreasing $\langle X \rangle$ by 26% and S_X by 20%; (ii) 122% increase of the approval percentage of [PS₄] HCDP^{NG} by decreasing $\langle X \rangle$ by 174%; (iii) 83% increase of the approval percentage of [PS₇] P^{EOR-Delivery} by decreasing S_X by 55% and accentuating the left-skewness of the simple-frequency histogram; and (iv) 11% decrease of $\langle X \rangle$ and 6% increase of S_X of [PS₈] HCDP^{MP-Feed}.

As in the Conventional-Route, results of the re-designed SS-Route confirm the utility of MC analysis in adjusting the SS-Route design so that all selected output variables attain specifications in 75% of sampled cases. In consonance with the previous mention that MC analysis of SS-Route generates histograms of items of SS design, Fig. 34 shows a conjoint simple-frequency histogram of SS length (L) versus throat diameter (D_T) for the re-designed SS-Route. The diagonal distribution in Figure 34 evidences an inverse correlation between D_T and L under constant SS inlet-outlet diameters (D_L, D_O), angles (α, β) and Ma^{Shock} , which translates the following SS characteristic: for low feed flow rates (low Ma^{Inlet}), L_C 's are longer, D_T 's are narrower

and L 's are longer, whereas for high flow rates (high Ma^{Inlet}), L_C 's are shorter, D_T 's are wider and L 's are shorter.

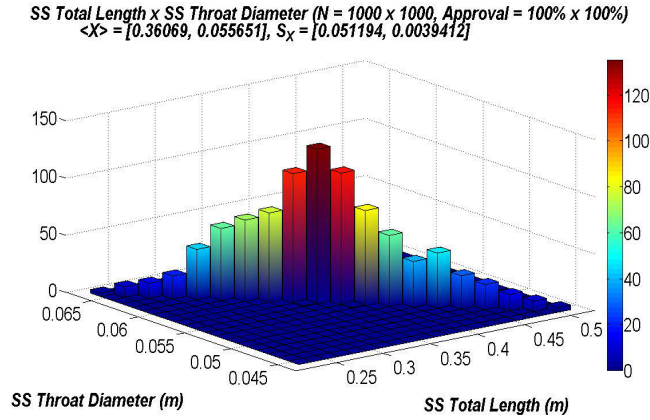


Figure 34. Re-Designed SS-Route: Conjoint histogram of SS length (L) vs SS throat diameter (D_T).

The result depicted on Figure 34 may imply that it is not fair to compare the the SS-Route design with the Conventional-Route design, as the design of the SS changes with the sampling of process input values. However, other types of equipment besides the SS present flexible design according to the sampling in both routes, as highlighted in Sec. 3.4.

4.1.3. Conventional-Route versus SS-Route

MC assessment of CO_2 -rich NG offshore processing via Conventional-Route and SS-Route under non-deterministic input variables, unveils certain differences between the routes. Firstly, comparing the changes of simple-frequency histograms of $[PS_1]$ to $[PS_{10}]$ from the original Base-Cases to the re-designed Conventional-Route and re-designed SS-Route, the responses of the Conventional-Route present greater sensitivity to design modifications, changing inclusive the shape of histograms and their departures from the respective normal $PDF/CDF(<X>, S_x^2)$. For the Conventional-Route this chiefly occurred for responses $[PS_1]$ NG y_{CO_2} , $[PS_2]$ NG y_{CH_4} , $[PS_3]$ WDP^{NG} and $[S_8]$ $HCDP^{MP-Feed}$, while the majority (only exception is $[PS_7]$ $P^{EOR-Delivery}$) of SS-Route responses kept the shape of histograms and departures from $PDF/CDF(<X>, S_x^2)$ after debottlenecking (compare Tables 14 and

17). Secondly, Table 18 shows $\langle X \rangle$ of response $[PS_{10}]$ power-consumption for the re-designed SS-Route 15% lower than the counterpart of the re-designed Conventional-Route. This statistically makes the SS-Route more attractive on economic and environmental grounds, and reflects a well-known SS aspect (Arinelli et al., 2017): other things constant, SS is always less power demanding than conventional technologies for WDPA/HCDPA of natural gas.

Table 18. Debottlenecked Conventional-Route minus debottlenecked SS-Route: differences for responses $[PS_1]$ to $[PS_{10}]$ in terms of: specified samples and statistics ($\langle X \rangle, S_x$).

Response	Specified Samples Difference	$\langle X \rangle$ Difference	S_x Difference
$[PS_1]$ NG y_{CO_2}	-5%	9%	6%
$[PS_2]$ NG y_{CH_4}	-12%	-2%	-8%
$[PS_3]$ $WDP^{NG} (^{\circ}C)$	0%	11%	-74%
$[PS_4]$ $HCDP^{NG} (^{\circ}C)$	-2%	31%	25%
$[PS_5]$ $P^{NG-Delivery} (bar)$	-1%	-11%	12%
$[PS_6]$ $WDP^{EOR-Fluid} (^{\circ}C)$	0%	12%	-42%
$[PS_7]$ $P^{EOR-Delivery} (bar)$	-1%	0%	6%
$[PS_8]$ $HCDP^{MP-Feed} (^{\circ}C)$	0%	4%	78%
$[PS_9]$ $PPCO_2^{MP-Feed} (bar)$	0%	-1%	21%
$[PS_{10}]$ Power-Consumption(MW)	0%	-15%	-18%

Figure 35 presents simple-frequency histograms for main streams of the re-designed Conventional-Route, while Figure 36 presents the respective counterparts for re-designed SS-Route. Firstly, one immediately recognizes that such simple-frequency histograms match reasonably with the respective normal $PDF(\langle X \rangle, S_x^2)$ translating the fact that y_{CO_2} of C3+ condensate and the flow rates of C3+ condensate, EOR-Fluid, NG product, MP-Feed and oil product approximately follow normal behaviors for both Conventional-Route and SS-Route. Secondly, both routes have similar distributions of flow rates of NG, oil and EOR-Fluid (all revenues), with a little superiority of the Conventional-Route in terms of average oil production (Figures 35f/36f), a consequence of the huge average flow rate of C3+ condensate from the JTE of the Conventional-Route (Figure 35a, $\langle X \rangle = 1536.46 \text{ kmol/h}$), which is recycled to the primary oil-water-gas separator positively impacting oil production. Such huge C3+ flow rate from Conventional-Route JTE results from a chosen high

pressure of $P=90$ bar upstream the JTE which operates at $P=45.5$ bar, thus producing huge condensation at $T \approx -19^\circ\text{C}$ and attaining $[PS_8]=HCDP^{MP-Feed} \leq -10^\circ\text{C}@45\text{bar}$ (Table 4) in at least 75% of samples. As usual in JTE, the selectivity for C3+ is poor in such condensate as seen in Figure 35b, which shows an average CO_2 molar fraction of 0.6139. Meanwhile, the average flow rate of water-C3+ condensate from SS unit in SS-Route is only 160.03 kmol/h (Figure 36a) with $\langle y_{\text{CO}_2} \rangle = 0.234$ (Figure 36b). In other words, SS-Route generates a much better C3+ condensate with more than 76%mol of hydrocarbons and a compatible low flow rate, perfectly sufficient for $[PS_8]=HCDP^{MP-Feed} \leq -10^\circ\text{C}@45\text{bar}$ in at least 75% of samples.

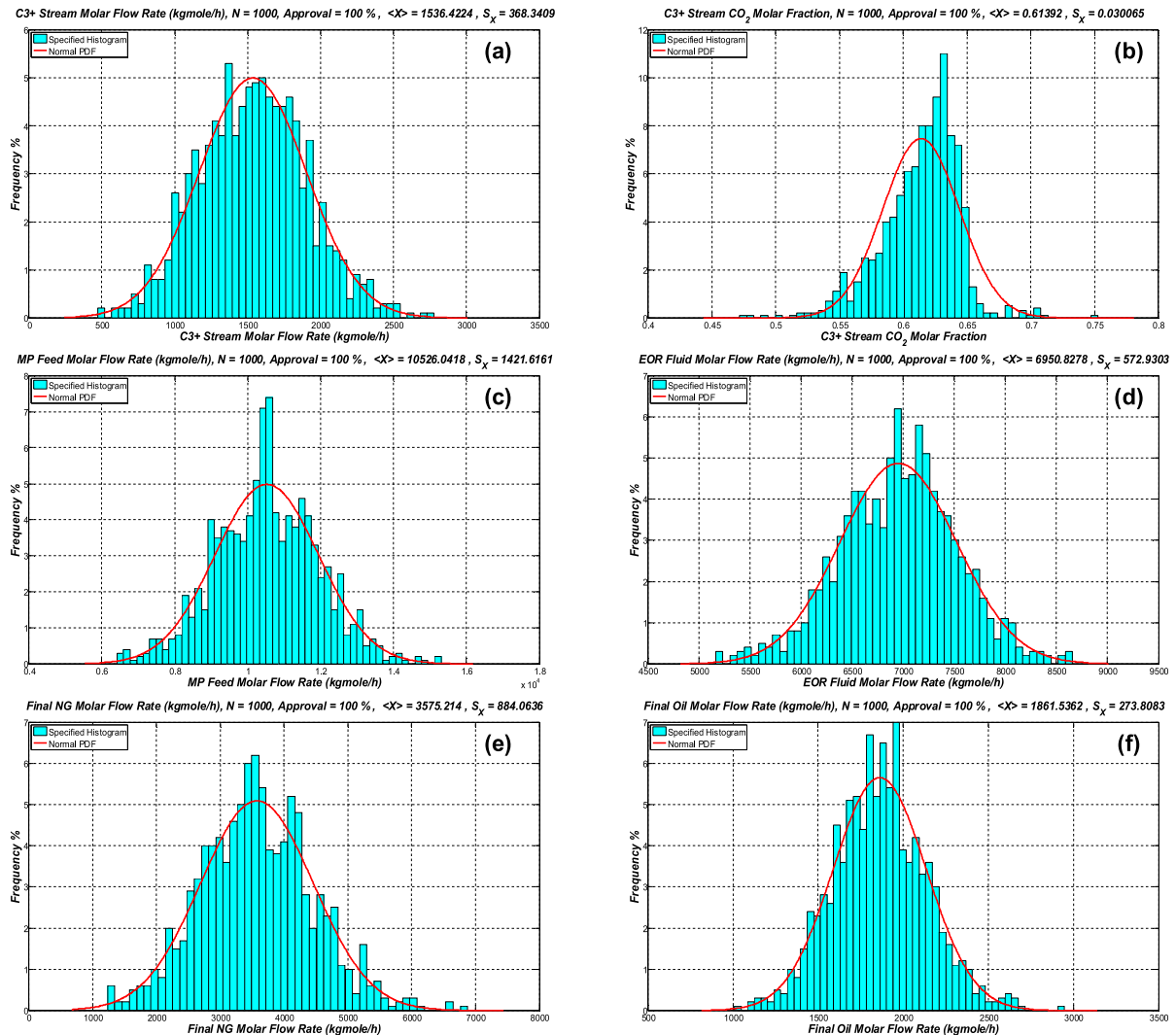


Figure 35. Re-designed Conventional-Route: simple-frequency histograms of main streams and normal $PDFs$: (a) C3+ (kgmole/h); and (b) y_{CO_2} of C3+; (c) MP-Feed (kgmole/h); (d) EOR-Fluid (kgmole/h); (e) NG (kgmole/h); (f) oil (kgmole/h).

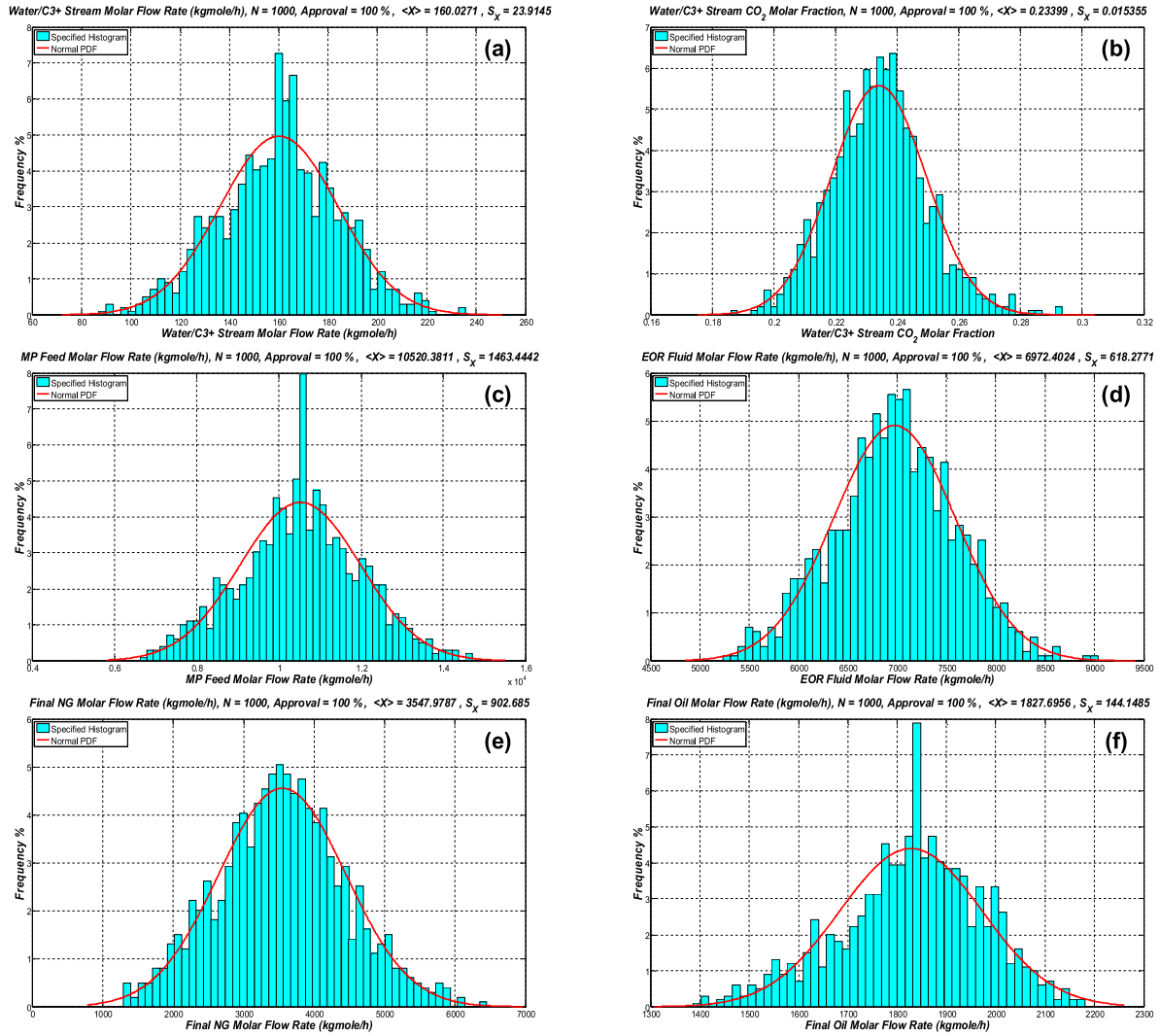


Figure 36. Re-designed SS-Route simple-frequency histograms of main streams and normal *PDFs*: (a) C3+ (kgmole/h); and (b) y_{CO_2} of C3+; (c) MP-Feed (kgmole/h); (d) EOR-Fluid (kgmole/h); (e) NG (kgmole/h); (f) oil (kgmole/h).

4.2. PROCESS DESIGN ASSESSMENT: CO₂ CONTENT INCREASE IN NG - CONVENTIONAL-ROUTE

The Base-Cases of offshore processing of CO₂-rich NG via Conventional-Route Route – Plant 3 (Figure 7c) – (Sec. 3.4.2) are assessed via Monte-Carlo analysis considering non-deterministic process input variables $[PU_1]$ raw NG flow rate ($MMsm^3/d$), $[PU_2]$ raw NG CO₂ molar fraction (2 scenarios) following normal *PDFs* (Table 3). Monte-Carlo analysis generated 1000 samples of sets of input variables. Stochastic design approval criterion corresponds to accomplishing all specifications in at least 75% of sampled cases. Histograms and normal *PDFs* of input variables $[PU_1]$ and $[PU_2]$ are shown in Figure 37.

This Section shows the assessment of the Base-Cases already designed via MC analysis, as the full assessment of Case 20%mol CO₂ was demonstrated in Gonzaga (2014) and a similar design via MC analysis is detailed in Sec. 4.1. MC analysis of Base-Cases of Case 20%mol CO₂ and Case 50%mol CO₂ attaining process output variables $[PS_1]$ to $[PS_4]$ (Table 4) in at least 75% of the sampled cases is depicted in Figs. 38 to 41. In order for accomplishing specification $[PS_1]$ NG y_{CO_2} , MP area was increased in 10% for Case 20%mol CO₂ and in 30% for Case 50%mol CO₂. This corroborates the flexibility of using MP modularity in designs under non-deterministic scenarios.

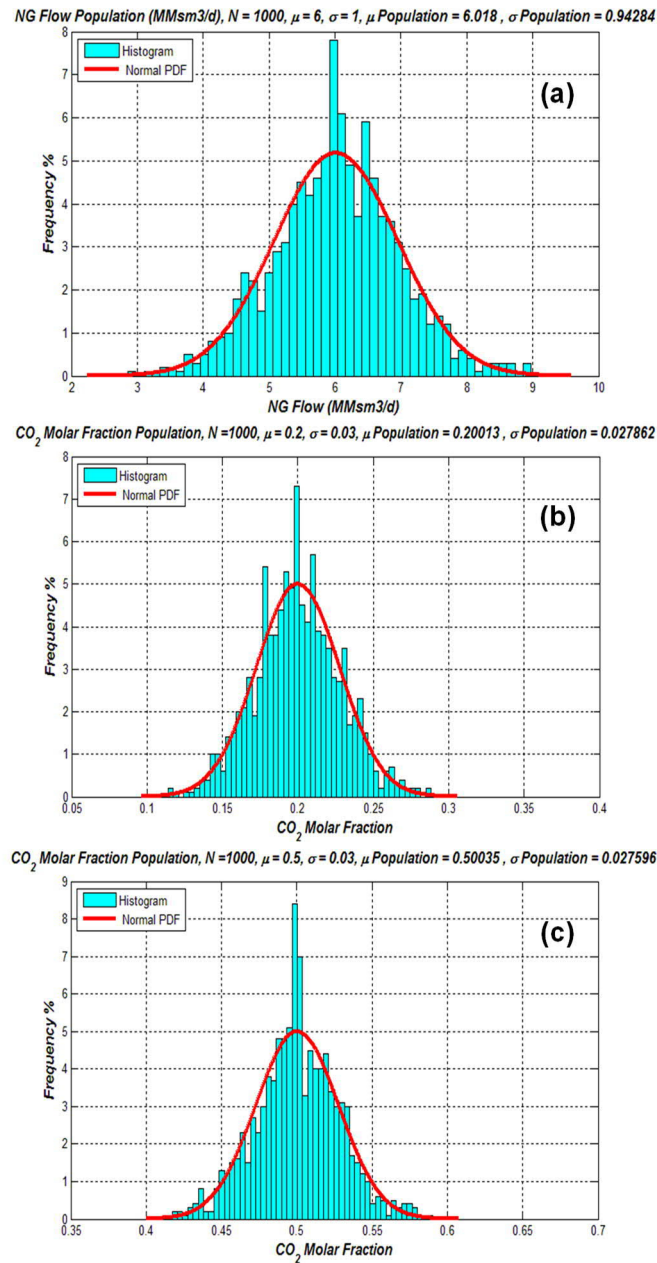


Figure 37. Simple-frequency histograms and normal *PDFs* of input variables: (a) [PU₁] raw NG flow rate(MMsm³/d); (b) [PU₂]₁ raw NG CO₂ molar fraction (Case 20%mol CO₂) ; and (c) [PU₂]₂ raw NG CO₂ molar fraction (Case 50%mol CO₂).

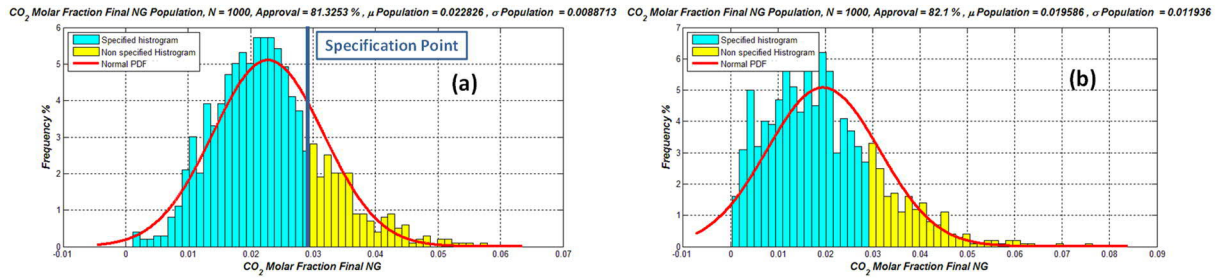


Figure 38. Simple-frequency histograms and normal $PDFs$ of $[PS_1]$ NG y_{CO_2} for (a) Case 20%mol CO_2 ; and (b) Case 50%mol CO_2 .

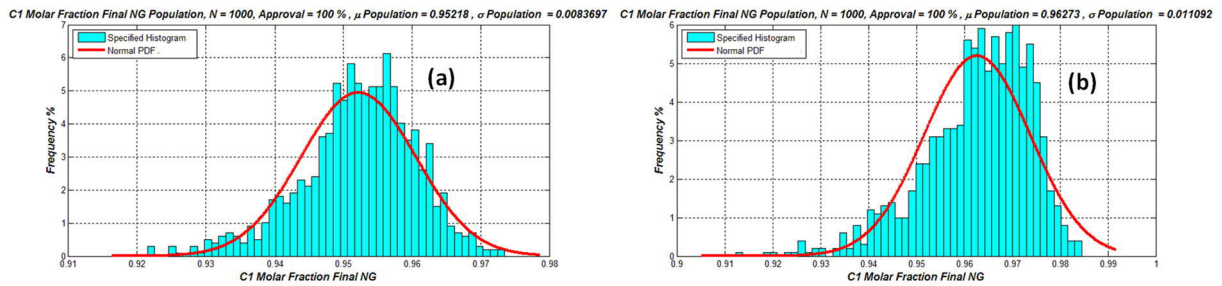


Figure 39. Simple-frequency histograms and normal $PDFs$ of $[PS_2]$ NG y_{CH_4} for (a) Case 20%mol CO_2 ; and (b) Case 50%mol CO_2 .

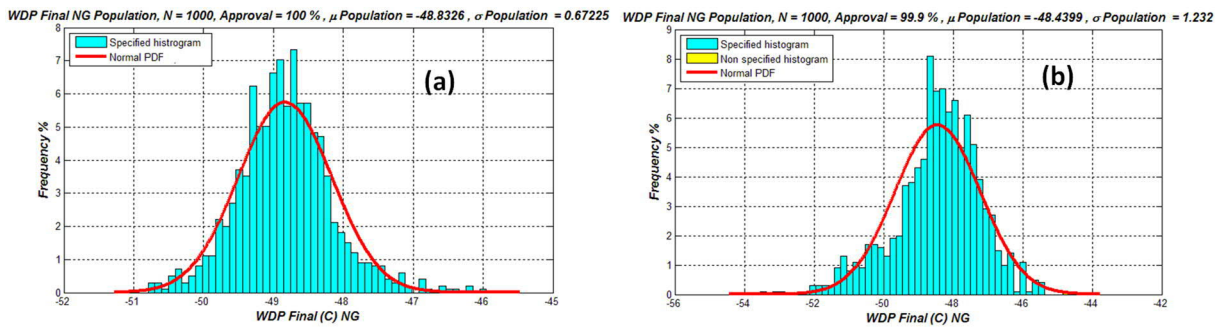


Figure 40. Simple-frequency histograms and normal $PDFs$ of $[PS_3]$ WDP^{NG} ($^{\circ}C$) for (a) Case 20%mol CO_2 ; and (b) Case 50%mol CO_2 .

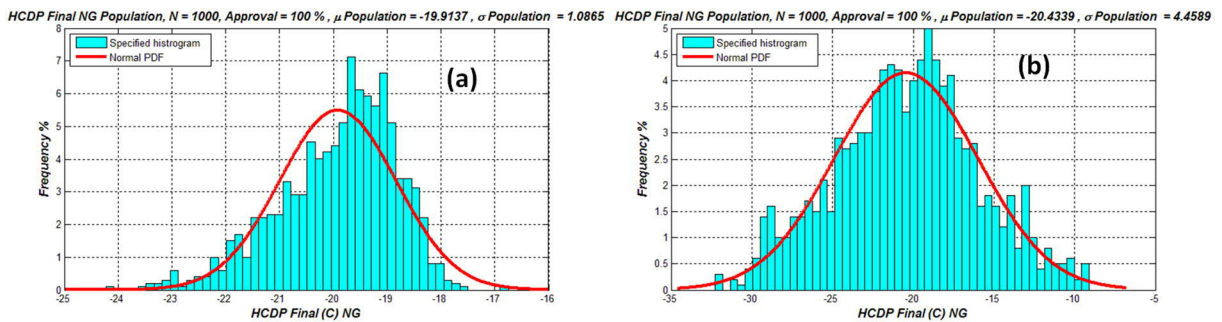


Figure 41. Simple-frequency histograms and normal $PDFs$ of $[PS_4]$ $HCDP^{NG}$ ($^{\circ}C$) for (a) Case 20%mol CO_2 ; and (b) Case 50%mol CO_2 .

Regarding the manifestation of normal behavior, none of the histograms depicted in Figs. 38 to 41, are very close to the respective normal *PDF*'s, except for $[PS_4]$ $HCDP^{NG}$ of Case 50%mol CO₂ (Figure 41b).

These results also exemplify the non-linearity of offshore processing of CO₂-rich NG via Conventional-Route and justify the use of MC analysis for design assessment under non-deterministic scenarios. Table 19 lists percentages of approval, statistics ($\langle X \rangle, S_X$) and simple-frequency histograms compared to the respective normal *PDFs* ($\langle X \rangle, S_X^2$) for the populations ($N=1000$) of responses $[PS_1]$ to $[PS_{10}]$ for Case 20%mol CO₂. Table 20 lists the same results for Case 50%mol CO₂.

Tables 19 and 20 shows that the responses of the Conventional-Route present greater sensitivity to changes in the CO₂ content of raw NG, given that the shape of all histograms are different when comparing Case 20%mol CO₂ and Case 50%mol CO₂. As the process design was slightly modified to accommodate higher content of CO₂ in raw NG, the Conventional-Route also present high sensitivity to design modifications, which is also corroborated by the results presented in Sec. 4.1.1.

Table 19. MC analysis ($N=1000$) of responses $[PS_1]$ to $[PS_4]$ of Case 20%mol CO₂: approval percentages, statistics ($\langle X \rangle, S_X$) and comparison of simple-frequency histograms versus normal *PDF* ($\langle X \rangle, S_X^2$).

Response	Approval	$\langle X \rangle$	S_X	Histogram vs normal <i>PDF</i> ($\langle X \rangle, S_X^2$)
$[PS_1]$ NG y_{CO_2}	81.3%	0.022826	0.0088713	Close, right-skewed
$[PS_2]$ NG y_{CH_4}	100%	0.95218	0.00083697	Close, left- skewed
$[PS_3]$ WDP^{NG} (°C)	100 %	-62.5341	0.61263	Close, thinner, right-skewed
$[PS_4]$ $HCDP^{NG}$ (°C)	100%	-19.9137	1.0865	Left-skewed

Table 20. MC analysis ($N=1000$) of responses $[PS_1]$ to $[PS_4]$ of Case 50%mol CO₂: approval percentages, statistics ($\langle X \rangle$, S_X) and comparison of simple-frequency histograms versus normal $PDF(\langle X \rangle, S_X^2)$.

Response	Approval	$\langle X \rangle$	S_X	Histogram vs normal $PDF(\langle X \rangle, S_X^2)$
$[PS_1]$ NG y_{CO_2}	82.1%	0.019586	0.011936	Right-skewed
$[PS_2]$ NG y_{CH_4}	100%	0.95218	0.00083697	Left-skewed
$[PS_3]$ $WDP^{NG}(^{\circ}C)$	100 %	-62.5341	0.61263	Close, thinner, left-skewed
$[PS_4]$ $HCDP^{NG}(^{\circ}C)$	100%	-19.9137	1.0865	Very-close

4.3. ENVIRONMENTAL ASSESSMENT: CONVENTIONAL-ROUTE versus SS-ROUTE

After achieving successful process design under uncertainties in process inputs (Sec. 4.1), the debottlenecked Base-Cases of offshore processing of CO₂-rich NG via Conventional-Route Route – Plant 1 (Figure 7a) – and SS-Route designed Route – Plant 2 (Figure 7b) – in Sec. 3.4.1 are also assessed via Monte-Carlo analysis for environmental performance via the module “Environmental Indicators” of *MCA*nalysis-HUB. No environmental specifications are imposed to the designs.

Environmental assessment of both routes, depicted in Figures 42 and 43, is performed via the evaluation of total output PEIs – absolute and per product mass – not considering impacts of product streams.

Table 21 lists simple-frequency histograms compared to the respective normal *PDFs* for total output PEI and total output PEI of debottlenecked Conventional-Route and debottlenecked SS-Route, and debottlenecked Conventional-Route minus debottlenecked SS-Route differences for responses total output PEI and total output PEI in terms of statistics ($\langle X \rangle, S_X$).

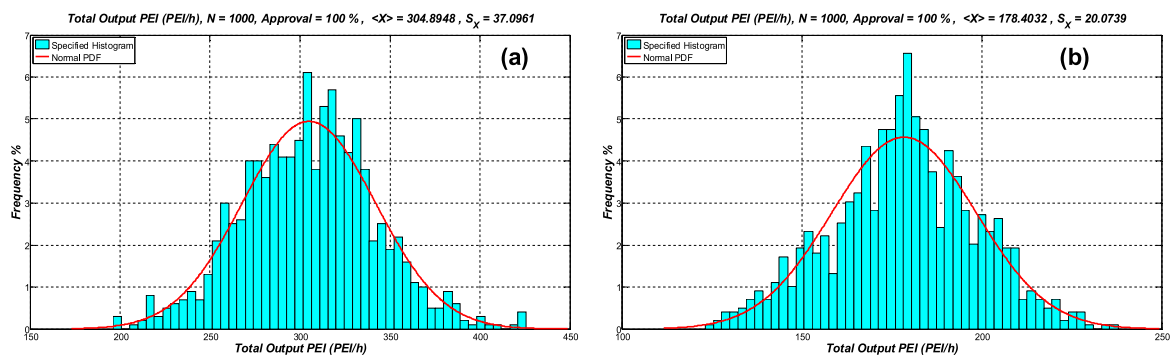


Figure 42. Simple-frequency histograms and normal *PDFs* ($\langle X \rangle, S_X^2$) of total output PEI (PEI/h) of (a) Conventional-Route; and (b) SS-Route.

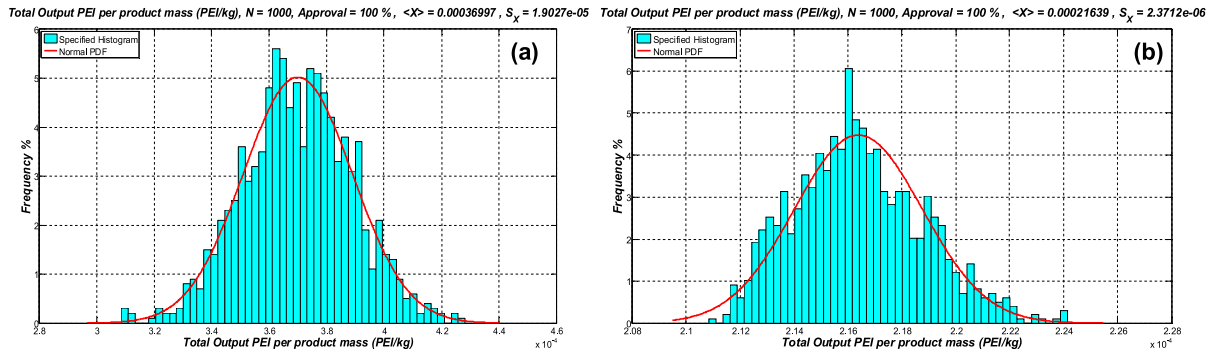


Figure 43. Simple-frequency histograms and normal $PDFs(\langle X \rangle, S_X^2)$ of total output PEI per product mass (PEI/kg) of (a) Conventional-Route; and (b) SS-Route.

Table 21. Environmental responses: simple-frequency histograms versus normal $PDF(\langle X \rangle, S_X^2)$, and debottlenecked Conventional-Route minus debottlenecked SS-Route differences for environmental responses in terms of and statistics ($\langle X \rangle, S_X$).

Response	Conventional-Route: Histogram vs normal PDF	SS-Route: Histogram vs normal PDF	$\langle X \rangle$ Difference	S_X Difference
Total output PEI	Very-close	Very-close	-41%	-46%
Total output PEI per product mass	Very-close	Close, right-skewed	-42%	-82%

Table 21 shows that the SS-Route achieves superior environmental performance over the Conventional-Route (lower $\langle X \rangle$ and S_X), which is expected, as SS-Route presents lower power consumption and lower output waste generation compared to Conventional-Route. In addition, all frequency histograms present very close behavior to their respective normal PDF (Figures 42-43), except total output PEI per product mass for SS-Route, which is slightly right-skewed.

4.4. ENVIRONMENTAL ASSESSMENT: CO₂ CONTENT INCREASE IN NG – CONVENTIONAL-ROUTE

After designed under uncertainties with Monte-Carlo analysis, the Base-Cases adequate to Case 20%mol CO₂ and Case 50%mol CO₂ Route – Plant 3 (Figure 7c) – are also submitted to environmental assessment with MC analysis. The intent is to disclose the behavior of the environmental indicators in Table 1 when increasing CO₂ content in an offshore rig processing CO₂-rich NG via Conventional-Route operating under stochastic process inputs. The results are shown in Figs. 44 to 50, which depict histograms and normal *PDFs* for populations of output PEIs from the eight environmental impact categories considered in WAR algorithm (Table 1).

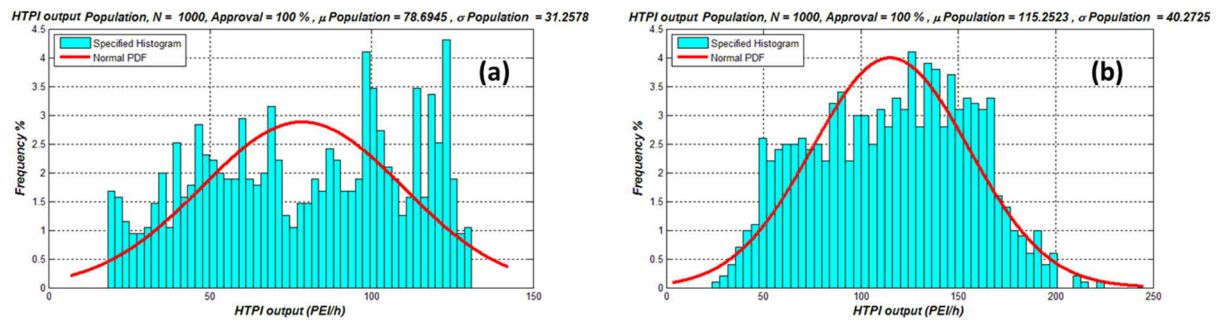


Figure 44. Simple-frequency histograms and normal *PDFs* ($\langle X \rangle$, S_X^2) of output HTPI (PEI/h) of (a) Case 20%mol CO₂; and (b) Case 50%mol CO₂.

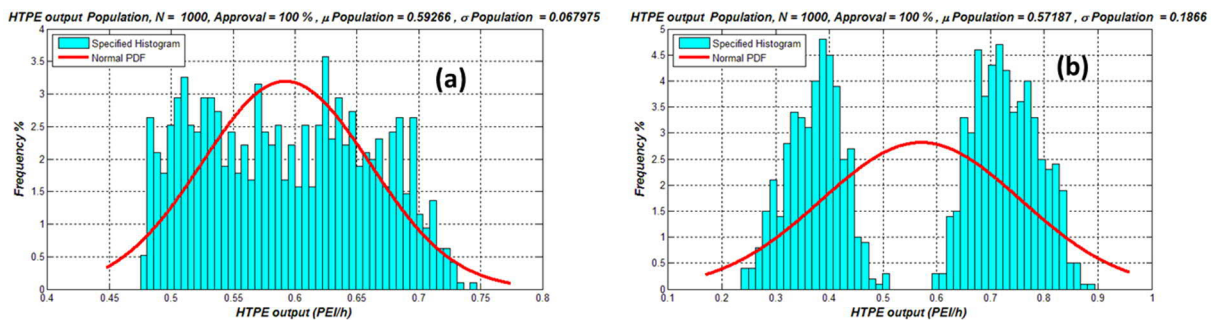


Figure 45. Simple-frequency histograms and normal *PDFs* ($\langle X \rangle$, S_X^2) of output HTPE (PEI/h) of (a) Case 20%mol CO₂; and (b) Case 50%mol CO₂.

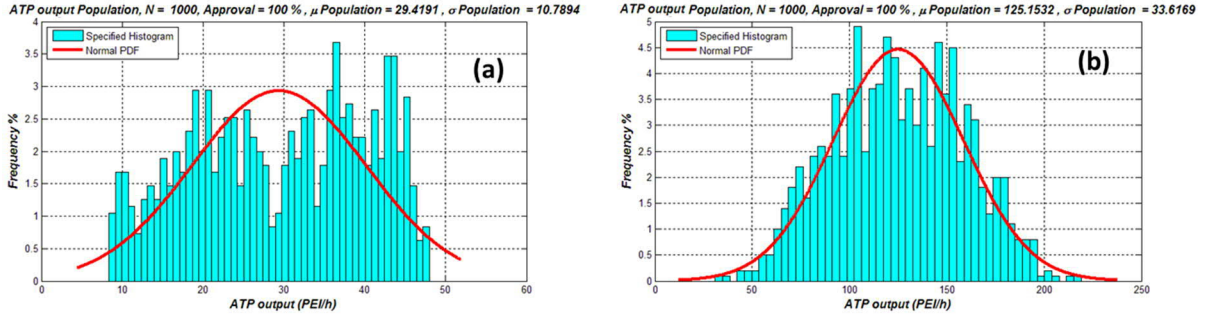


Figure 46. Simple-frequency histograms and normal $PDFs(\langle X \rangle, S_X^2)$ of output ATP (PEI/h) of (a) Case 20%mol CO₂; and (b) Case 50%mol CO₂.

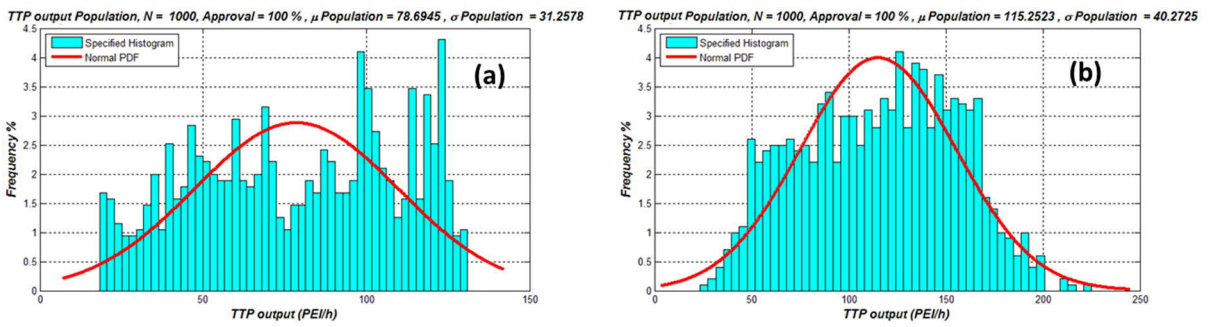


Figure 47. Simple-frequency histograms and normal $PDFs(\langle X \rangle, S_X^2)$ of output TTP (PEI/h) of (a) Case 20%mol CO₂; and (b) Case 50%mol CO₂.

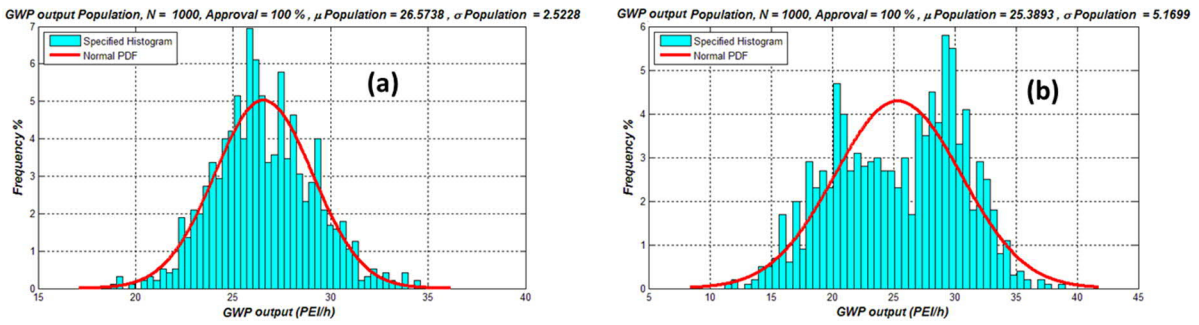


Figure 48. Simple-frequency histograms and normal $PDFs(\langle X \rangle, S_X^2)$ of output GWP (PEI/h) of (a) Case 20%mol CO₂; and (b) Case 50%mol CO₂.

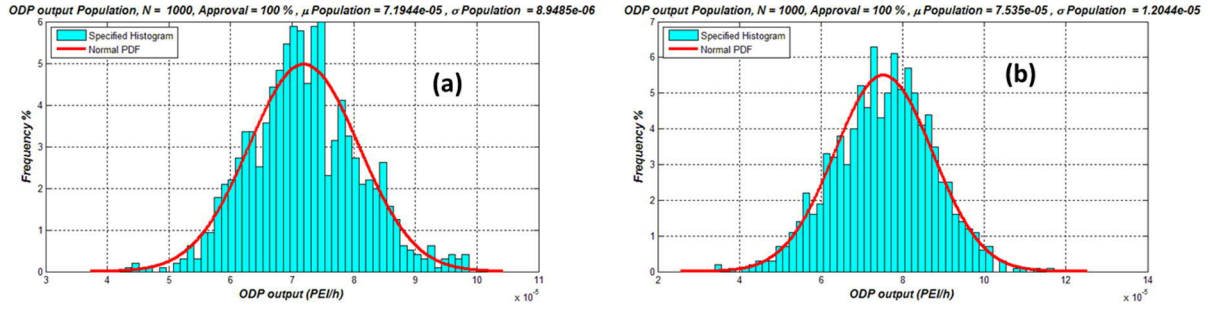


Figure 49. Simple-frequency histograms and normal $PDFs(\langle X \rangle, S_X^2)$ of output ODP (PEI/h) of (a) Case 20%mol CO₂; and (b) Case 50%mol CO₂.

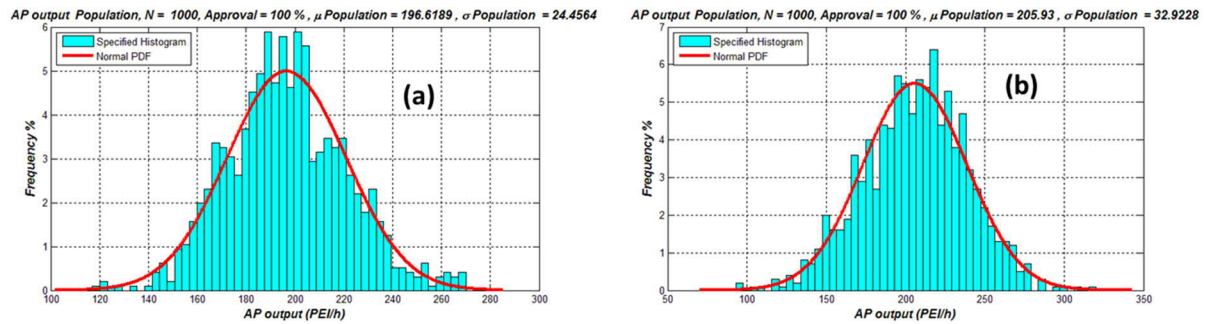


Figure 50. Simple-frequency histograms and normal $PDFs(\langle X \rangle, S_X^2)$ of output AP (PEI/h) of (a) Case 20%mol CO₂; and (b) Case 50%mol CO₂.

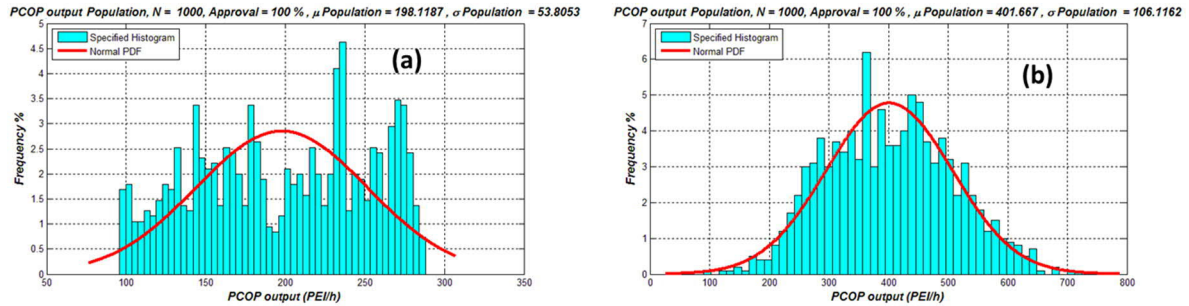


Figure 51. Simple-frequency histograms and normal $PDFs(\langle X \rangle, S_X^2)$ of output PCOP (PEI/h) of (a) Case 20%mol CO₂; and (b) Case 50%mol CO₂.

When considering the uncertainties of both process inputs [PU_1] raw NG flow rate ($MMsm^3/d$), [PU_2] raw NG CO₂ molar fraction, the histograms of HTPI, HTPE, TTP for both cases, ATP and PCOP for Case 20%mol CO₂, and GWP for Case 50%mol CO₂ presented behavior completely different from normal PDF , which shows that the process responds to uncertainties in a highly non-linear way regarding environmental performance. In each one of these instances, the impertinence of normal behavior can be visualized by means of the discrepancy between the statistical behavior of the

histogram and the respective normal *PDF* built with sample mean and sample standard deviation from the histogram. The remaining PEIs presented behavior relatively close to normal patterns. In addition, the histograms of HTPI, HTPE, ATP, TTP, GWP and PCOP exhibit some difference of patterns for the 20%mol and 50%mol CO₂ content cases. This means that the process responds non-linearly to changes in the CO₂ content of raw NG regarding most of the environmental indicators. Table 22 summarizes the percent differences between $\langle X \rangle$ and S_x between the populations for the two CO₂ content cases relative to the values of Case 20%mol CO₂.

Table 22. Summary of output PEI categories, $\langle X \rangle$ and S_x for Cases 20%mol CO₂ and 50%mol CO₂.

Output PEI category	$\langle X \rangle$ (PEI/h) Case 20%mol CO ₂	S_x (PEI/h) Case 50%mol CO ₂	Difference (%)	$\langle X \rangle$ (PEI/h) Case 20%mol CO ₂	S_x (PEI/h) Case 50%mol CO ₂	Difference (%)
HTPI	78.6954	115.2523	46	31.2578	40.2725	29
HTPE	0.5927	0.5719	-4	0.0680	0.1866	175
ATP	29.4191	125.1532	325	10.7894	33.6199	212
TTP	78.6945	115.2523	46	31.2578	40.2725	29
GWP	26.5738	25.3893	-4	2.5228	5.1699	105
ODP	7.19E-05	7.54E-05	5	8.95E-06	1.20E-06	-87
AP	196.6189	205.9300	5	24.4564	32.9228	35
PCOP	198.1187	401.6670	103	53.8053	106.1162	97

By assigning equal weights to each environmental category, total output PEI is depicted in Figure 52 for both cases, showing that Case 50%mol CO₂ has a sample mean 62% higher than Case 20%mol CO₂, and sample standard deviation 74% higher. Therefore, the long-term increase of CO₂ content in raw NG caused by CO₂ reinjection due to EOR will deteriorate the environmental performance of the process.

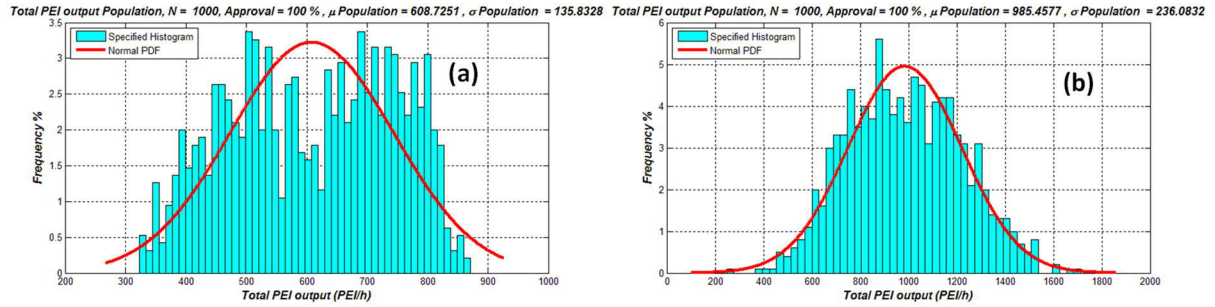


Figure 52. Simple-frequency histograms and normal $PDFs(\langle X \rangle, S_X^2)$ of total output PEI (PEI/h) of (a) Case 20%mol CO₂; and (b) Case 50%mol CO₂.

In addition, the most relevant environmental impact categories were identified with PCA. Table 23 shows the eigenvalues (λ_i), the variances (v_i) and the cumulative variances for Case 20%mol CO₂ and Case 50%mol CO₂. It can be concluded that the first two principal components PC(1) and PC(2) are the only relevant components for explaining the environmental performance of the process, corresponding to, respectively, 81.2% and 18.8% of the variance of Case 20%mol CO₂ and to 92.6 % and 6.5% of Case 50%mol CO₂. For identifying the dominant environmental impact categories corresponding to PC(1) and PC(2), the components of vectors \underline{P}_i with higher absolute values listed in Table 24 for Case 20% CO₂ and Case 50% CO₂, correspond to the most relevant categories.

Table 24 shows that the environmental impact categories GWP (global atmospheric impacts), AP and PCOP (regional atmospheric impacts) are the most significant to PC(1), having high relevance to the process for both cases. When PC(2) is also included, the environmental impact category TTP (ecological toxicity) can be considered as medium relevance to the process for both cases.

Table 23. Eigenvalues λ_i and variance v_i for each principal component for Case 20%mol CO₂ and Case 50%mol CO₂.

Case 20%mol CO₂								
Principal Component	PC(1)	PC(2)	PC(3)	PC(4)	PC(5)	PC(6)	PC(7)	PC(8)
λ_i	4994.8	574.7718	0.3601	0.0364	0.0024	0	0	0
$v_i(\%)$	89.6738	10.3191	0.0065	0.0007	0	0	0	0
Cumulative variance (%)	89.6738	99.9928	99.9993	100	100	100	100	100
Case 50%mol CO₂								
Principal Component	PC(1)	PC(2)	PC(3)	PC(4)	PC(5)	PC(6)	PC(7)	PC(8)
λ_i	11551	1083.3	145.4925	6.7193	0.0199	0	0	0
$v_i(\%)$	92.6247	6.4694	0.08689	0.0369	0.0001	0	0	0
Cumulative variance (%)	92.6247	99.0941	99.963	99.9999	100	100	100	100

Table 24. \underline{P}_i vector of each principal component: Case 20%mol CO₂ and Case 50%mol CO₂.

Case 20%mol CO₂								
\underline{P}_i	PC(1)	PC(2)	PC(3)	PC(4)	PC(5)	PC(6)	PC(7)	PC(8)
<i>HTPI</i>	0.0158	0.0940	0.2728	-0.4001	0.8689	-0.0373	-0.0000	-0.0000
<i>HTPE</i>	0.1526	0.0022	-0.4869	0.7134	0.4795	0.0285	-0.0000	-0.0000
<i>ATP</i>	0.0009	-0.0000	0.0247	-0.3557	0.0186	0.9989	0.0000	-0.0000
<i>TTP</i>	0.0806	0.9920	-0.0290	0.0205	-0.0901	0.0031	-0.0000	-0.0000
<i>GWP</i>	0.4420	-0.0441	-0.4182	-0.3557	-0.0358	-0.0021	0.0000	-0.7071
<i>ODP</i>	0.00000	0.0000	-0.0000	-0.0000	0.0000	-0.0000	10.000	0.0000
<i>AP</i>	0.4420	-0.0441	-0.4182	-0.3557	-0.0358	-0.0021	0.0000	0.7071
<i>PCOP</i>	0.7611	-0.0563	0.5808	0.2763	-0.0631	-0.0040	0.0000	-0.0000
Case 50%mol CO₂								
\underline{P}_i	PC(1)	PC(2)	PC(3)	PC(4)	PC(5)	PC(6)	PC(7)	PC(8)
<i>HTPI</i>	0.0138	0.0940	0.2728	-0.4001	0.8689	-0.0373	-0.0000	-0.0000
<i>HTPE</i>	0.2608	0.0022	-0.4869	0.7134	0.4795	0.0285	-0.0000	-0.0000
<i>ATP</i>	0.0005	-0.0000	0.0247	-0.3557	0.0186	0.9989	0.0000	-0.0000
<i>TTP</i>	0.0806	0.9920	-0.0290	0.0205	-0.0901	0.0031	-0.0000	-0.0000
<i>GWP</i>	0.3133	-0.0441	-0.4182	-0.3557	-0.0358	-0.0021	0.0000	-0.7071
<i>ODP</i>	0.0000	0.0000	-0.0000	-0.0000	0.0000	-0.0000	1.0000	0.0000
<i>AP</i>	0.3133	-0.0441	-0.4182	-0.3557	-0.0358	-0.0021	0.0000	0.7071
<i>PCOP</i>	0.7611	-0.0563	0.5808	0.2763	-0.0631	-0.0040	0.0000	-0.0000

4.5. ECONOMIC ASSESSMENT: CONVENTIONAL-ROUTE versus SS-ROUTE

After achieving successful process design under uncertainties in process inputs (Sec. 4.1), the debottlenecked Base-Cases of offshore processing of CO₂-rich NG via Conventional-Route Route – Plant 1 (Figure 7a) – and SS-Route Route – Plant 2 (Figure 7b) – designed in Sec. 3.4.1 are also assessed via Monte-Carlo analysis for economic performance via the module “Economic analysis” of *MCAnalysis-HUB* to attain profitability via economic specification [ES_{10}] *NPV* (Table 10). Such assessment combines uncertainties in process input variables (Table 2) and in economic variables (Table 9). Economic responses [ES_1] to [ES_9] (Table 10) are also evaluated.

Simple-frequency histograms and normal *PDFs* of input variables [EU_2] to [EU_4] are shown in Figure 53. Simple-frequency histogram and normal *PDF* of input variable [EU_1] = [ES_1] *FCI* are depicted later with other economic parameters in Figure 54.

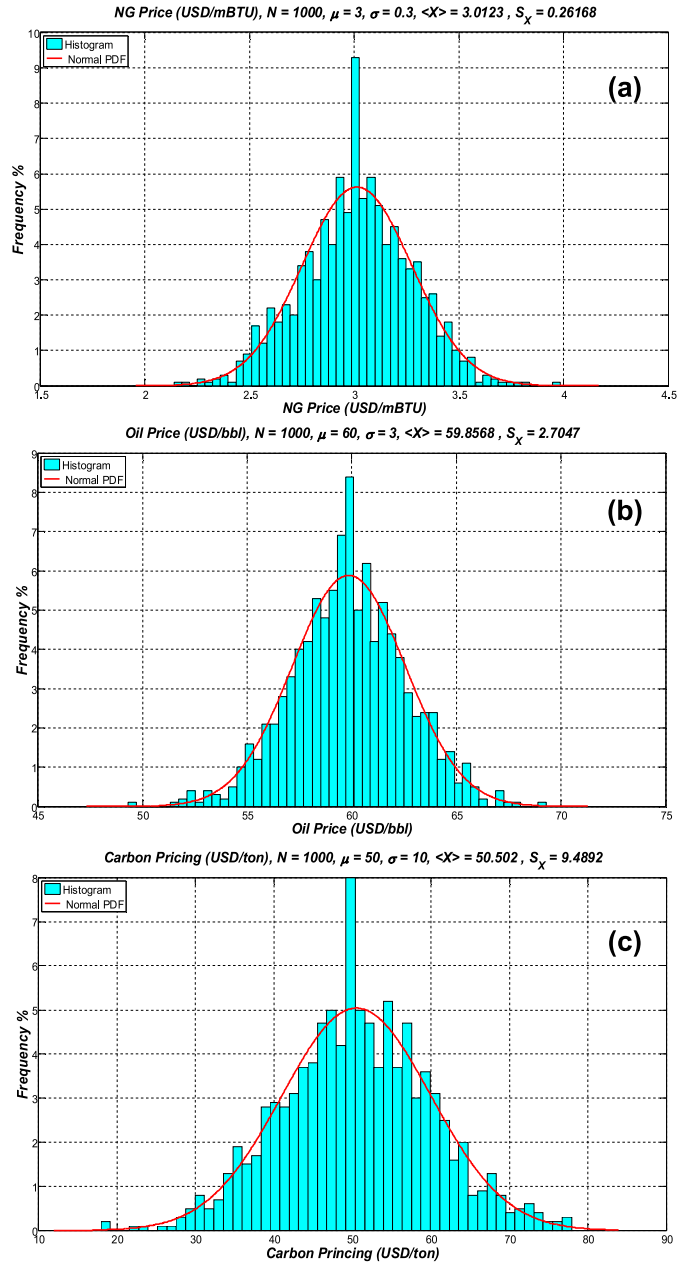


Figure 53. Simple-frequency histograms and normal $PDFs$ of input variables: (a) $[EU_1]$ NG price; (b) $[EU_2]$ oil price; and (c) $[EU_3]$ carbon pricing.

4.5.1. Conventional-Route

Figure 54 depicts simple-frequency histograms and normal $PDFs$ of output variables $[PS_1]$ to $[PS_8]$, and Figure 55 depicts simple-frequency histograms and normal $PDFs$ of output variables $[PS_9]$ to $[PS_{10}]$.

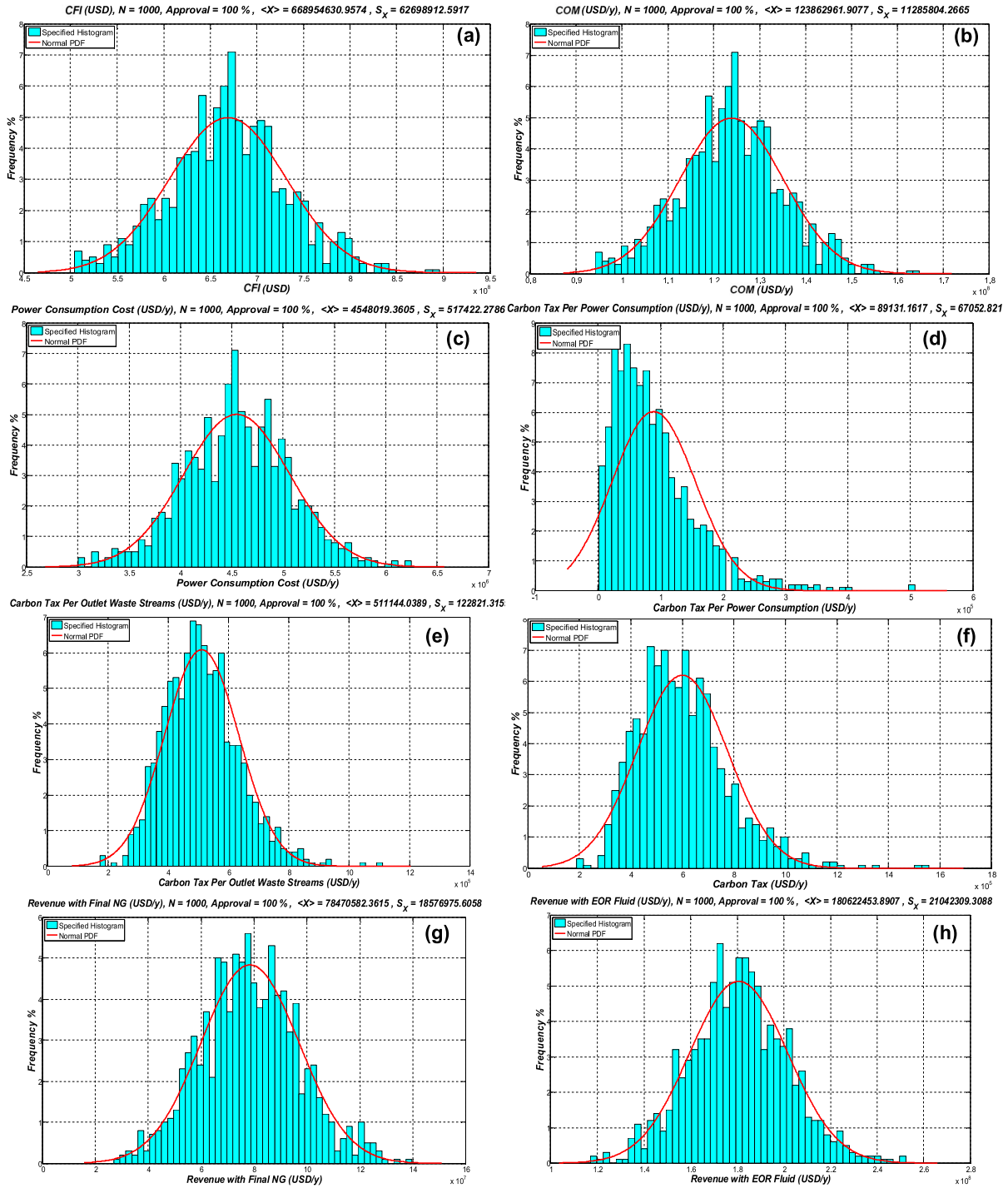


Figure 54. Conventional-Route Base-Case: simple-frequency histograms and normal PDFs($\langle X \rangle$, S_x^2): (a) [ES₁] FCI; (b) [ES₂] COM; (c) [ES₃] Power consumption cost; (d) [ES₄] Carbon tax per power consumption; (e) [ES₅] Carbon tax per outlet waste streams; (f) [ES₆] Carbon tax; (g) [ES₇] Revenue from NG; and (h) [ES₈] Revenue from EOR-Fluid.

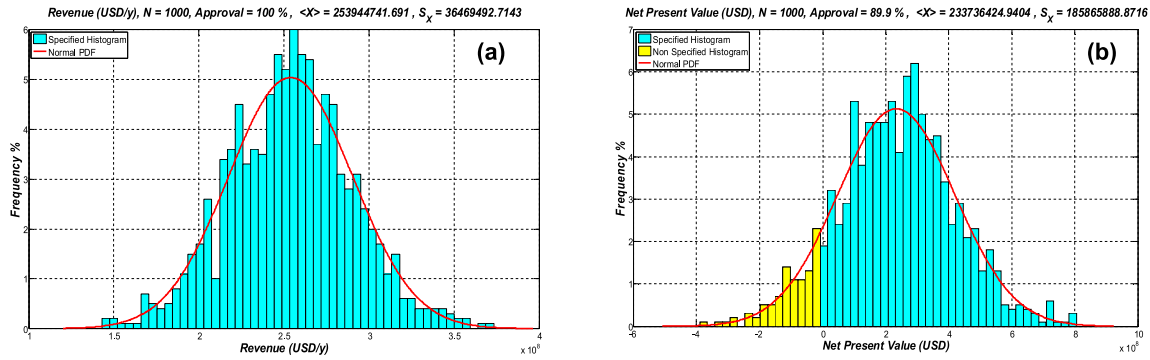


Figure 55. Conventional-Route Base-Case: simple-frequency histograms and normal $PDFs(\langle X \rangle, S_X^2)$: (a) $[ES_9]$ Revenue; and (b) $[ES_{10}]$ NPV.

Table 25 summarizes the economic assessment by listing percentages of approval, statistics ($\langle X \rangle, S_X$) and simple/cumulative frequency histograms compared to the respective normal $PDFs(\langle X \rangle, S_X^2)$ for the populations ($N=1000$) of responses $[ES_1]$ to $[ES_{10}]$, and a brief analysis of the results.

$[ES_1]$ FCI histogram is very close to the normal PDF as it is the economic input variables with uncertainties $[EU_1]$; $[ES_2]$ COM has similar behavior as $[EU_1] = [ES_1]$ FCI, since $[EU_1]$ FCI is the only input variable with uncertainties affecting COM; $[ES_3]$ Power consumption cost has low influence in this assessment as it only corresponds to 1.8% of the revenue coming from products; the left-skewed behavior of $[ES_4]$ Carbon tax per power consumption slightly accentuated the left-skewed behavior – and close – of $[ES_5]$ Carbon tax per outlet waste streams to compose of $[ES_6]$ Carbon tax, as it only corresponds to 15% of contribution for the total CO₂ emissions; effects of $[ES_6]$ Carbon tax are negligible in this assessment as it only corresponds to 0.2% of the revenue coming from products; $[ES_7]$ Revenue from NG corresponds to 30% of revenue from products, while $[ES_8]$ Revenue from EOR-Fluid corresponds to 70%; and $[ES_{10}]$ NPV is positive in 89.9% of sampled cases, meaning that the Base-Case design is economically viable in over 75% of the cases, achieving a successful design in terms of economic basis.

Table 25. MC analysis ($N=1000$) of responses $[ES_1]$ to $[ES_{10}]$ of Conventional-Route Base-Case: approval percentages, statistics ($\langle X \rangle$, S_X), comparison of simple-frequency histograms versus normal $PDF(\langle X \rangle, S_X^2)$, and brief analysis.

Response	$\langle X \rangle$	S_X	Histogram vs normal PDF ($\langle X \rangle$, S_X^2)	Analysis
$[ES_1]$ FCI (USD/y)	668 950 000	62 699 000	Very-close	-
$[ES_2]$ COM (USD/y)	123 860 000	11 286 000	Very-close	48.8% Revenue
$[ES_3]$ Power consumption cost (USD/y)	4 548 000	517 420	Very-close	1.8% Revenue from products: low influence
$[ES_4]$ Carbon tax per power consumption (USD/y)	89 131	67 053	Left-skewed	15% Carbon tax
$[ES_5]$ Carbon tax per outlet waste streams (USD/y)	511 140	122 820	Very-close, left-skewed	85% Carbon tax
$[ES_6]$ Carbon tax(USD/y)	600 280	176 080	Close, left- skewed	0.2% Revenue from products: negligible
$[ES_7]$ Revenue from NG (USD/y)	78 471 000	18 577 000	Very-close	30% Revenue from products
$[ES_8]$ Revenue from EOR-Fluid (USD/y)	180 620 000	21 042 000	Very-close	70% Revenue from products
$[ES_9]$ Revenue (USD/y)	253 940 000	36 469 000	Very-close	98% Revenue from products
$[ES_{10}]$ NPV(USD)	233 740 000	185 870 000	Very-close	Economically viable in 89.9% of sampled cases

4.5.2. SS-Route

Figure 56 depicts simple-frequency histograms and normal PDF s of output variables $[PS_1]$ to $[PS_8]$, and Figure 57 depicts simple-frequency histograms and normal PDF s of output variables $[PS_9]$ to $[PS_{10}]$.

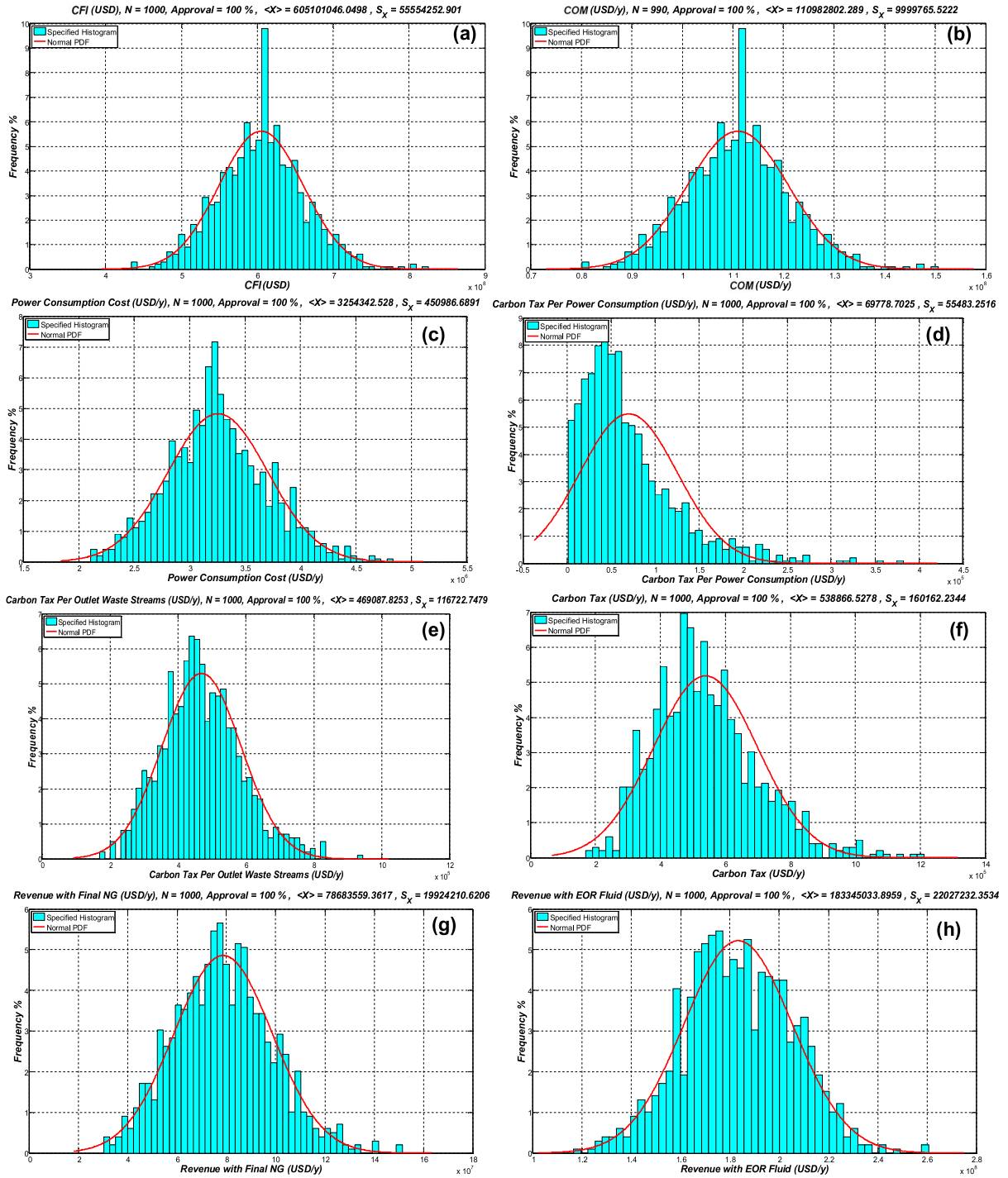


Figure 56. SS-Route Base-Case: simple-frequency histograms and normal PDFs($\langle X \rangle$, S_x^2): (a) [ES₁] FCI; (b) [ES₂] COM; (c) [ES₃] Power consumption cost; (d) [ES₄] Carbon tax per power consumption; (e) [ES₅] Carbon tax per outlet waste streams; (f) [ES₆] Carbon tax; (g) [ES₇] Revenue from NG; and (h) [ES₈] Revenue from EOR-Fluid.

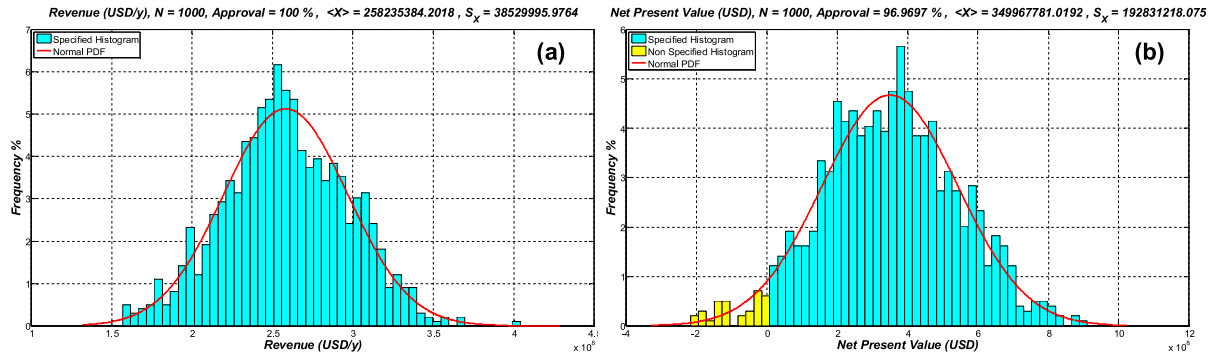


Figure 57. SS-Route Base-Case: simple-frequency histograms and normal $PDFs(<X>, S_x^2)$: (a) [ES₉] Revenue; and (b) [ES₁₀] NPV.

Table 26 summarizes the economic assessment by listing percentages of approval, statistics ($<X>, S_x$) and simple-frequency histograms compared to the respective normal $PDFs(<X>, S_x^2)$ for the populations ($N=1000$) of responses [ES₁] to [ES₁₀], and a brief analysis of the results.

Table 26. MC analysis ($N=1000$) of responses $[ES_1]$ to $[ES_{10}]$ of SS-Route Base-Case: approval percentages, statistics ($\langle X \rangle$, S_x), comparison of simple-frequency histograms versus normal $PDF(\langle X \rangle, S_x^2)$, and brief analysis.

Response	$\langle X \rangle$	S_x	Histogram vs normal PDF ($\langle X \rangle$, S_x^2)	Analysis
$[ES_1]$ FCI (USD/y)	605 100 000	55 554 000	Very-close	-
$[ES_2]$ COM (USD/y)	110 980 000	9 999 800	Very-close	31.7% Revenue
$[ES_3]$ Power consumption cost (USD/y)	3 254 300	450 990	Very-close	1.2% Revenue from products: low influence
$[ES_4]$ Carbon tax per power consumption (USD/y)	69 779	55 483	Left-skewed	13% Carbon tax
$[ES_5]$ Carbon tax per outlet waste streams (USD/y)	469 090	116 720	Very-close, left-skewed	87% Carbon tax
$[ES_6]$ Carbon tax(USD/y)	538 870	160 160	Close, left-skewed	0.2% Revenue from products: negligible
$[ES_7]$ Revenue from NG (USD/y)	78 684 000	19 924 000	Very-close	30% Revenue from products
$[ES_8]$ Revenue from EOR-Fluid (USD/y)	183 350 000	22 027 000	Very-close	70% Revenue from products
$[ES_9]$ Revenue (USD/y)	258 240 000	38 530 000	Very-close	98.6% Revenue from products
$[ES_{10}]$ NPV(USD)	349 970 000 (USD)	192 830 000 (USD)	Very-close	Economically viable in 97% of sampled cases

4.5.3. Conventional-Route versus SS-Route

Histogram behaviors of economic responses $[ES_1]$ to $[ES_{10}]$ to stochastic input process and economic variables are very similar when comparing Conventional-Route and SS-Route.

When comparing the performance of the SS-Route to the Conventional-Route via Table 27, the SS-Route achieves (i) $\langle X \rangle$ of $[ES_1]$ *FCI* and $[ES_2]$ *COM* 10% lower; (ii) $\langle X \rangle$ of $[ES_3]$ Power consumption cost 28% lower; (iii) $\langle X \rangle$ of $[ES_6]$ Carbon tax 10% lower (expected, as the SS-Route presented superior environmental performance over the Conventional-Route in Sec. 4.3); and (vi) $\langle X \rangle$ of $[ES_{10}]$ *NPV* 50% higher and percentage of specified samples 8% higher, meaning that the SS-Route presents economic performance superior over the Conventional-Route.

Table 27. Debottlenecked Conventional-Route minus debottlenecked SS-Route: differences for responses $[ES_1]$ to $[ES_{10}]$ in terms of: specified samples and statistics ($\langle X \rangle, S_x$).

Response	Specified Samples Difference	$\langle X \rangle$ Difference	S_x Difference
$[ES_1]$ <i>FCI</i> (USD/y)	-	-10 %	-11 %
$[ES_2]$ <i>COM</i> (USD/y)	-	-10 %	-11 %
$[ES_3]$ Power consumption cost (USD/y)	-	-28 %	-13 %
$[ES_4]$ Carbon tax per power consumption (USD/y)	-	-22 %	-17 %
$[ES_5]$ Carbon tax per outlet waste streams (USD/y)	-	-8 %	-5 %
$[ES_6]$ Carbon tax(USD/y)	-	-10 %	-9 %
$[ES_7]$ Revenue from NG (USD/y)	-	0 %	7 %
$[ES_8]$ Revenue from EOR-Fluid (USD/y)	-	2 %	5 %
$[ES_9]$ Revenue (USD/y)	-	2 %	6 %
$[ES_{10}]$ <i>NPV</i> (USD)	8 %	50 %	4 %

In addition, $[ES_3]$ Power consumption cost of the SS-Route is 28% lower compared to the Conventional-Route (Table 27) while $[PS_{10}]$ Power-Consumption in only 15%

lower (Table 18), and both histograms present behavior very-close to the normal *PDF*. This difference can be explained by comparing the mass lower heat value of product NG ($MLHV^{NG}$), depicted in Figure 58 as NG price is proportional to this value. Both histograms present left-skewed behavior compared to the respective *PDFs*, however, the SS-Route presents S_X 11% higher than the Conventional-Route, despite its 0.5% lower $\langle X \rangle$.

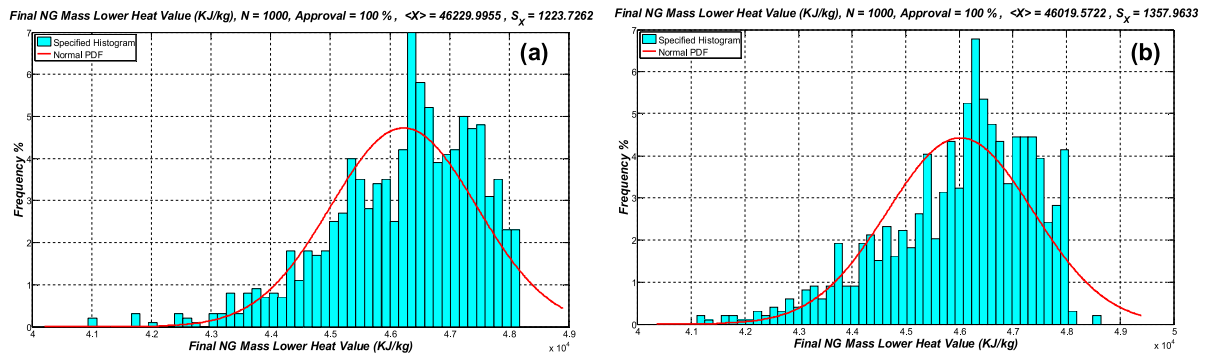


Figure 58. Simple-frequency histograms and normal *PDFs* ($\langle X \rangle$, S_X^2) of $MLHV^{NG}$ of (a) Conventional-Route; and (b) SS-Route.

Another interesting assessment is to remove the uncertainties in economic inputs and evaluate the performance of both routes only under uncertainties in process inputs. $[ES_{10}]$ NPV for both routes are depicted in Figure 59.

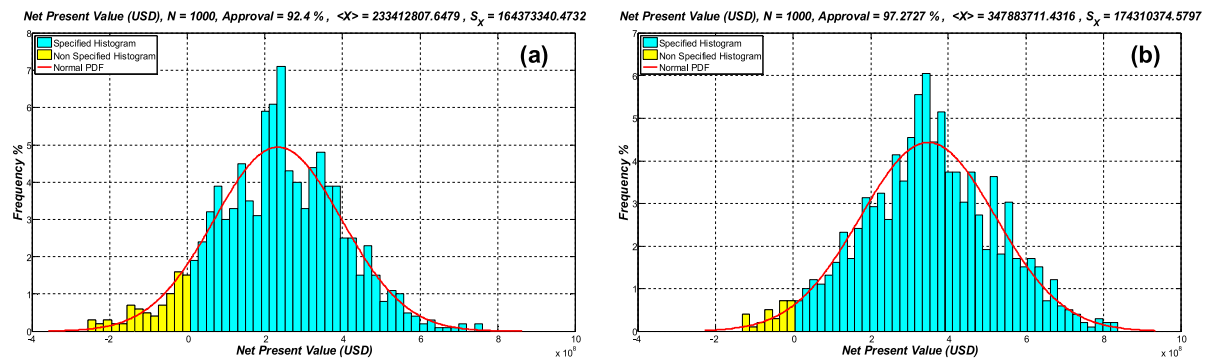


Figure 59. Simple-frequency histograms and normal *PDFs* ($\langle X \rangle$, S_X^2) of NVP without uncertainties in economic inputs of (a) Conventional-Route; and (b) SS-Route.

$[ES_{10}]$ NPV histograms of both routes present behavior very-close to the normal *PDFs*, keeping the same behavior when the economic stochastic scenario was considered (Figure 55b and Figure 57b). The SS-Route presents slightly higher

resilience to economic inputs than the Conventional-Route, as there is very low difference in specified samples attained for economic viability via $[ES_{10}]$ NPV. Conventional-Route has also good resilience to economic inputs.

Table 28. Process and economic stochastic scenarios minus process economic scenario for Conventional-Route and SS-Route: differences for response $[ES_{10}]$ in terms of: specified samples and statistics ($\langle X \rangle$, S_X).

Response	Specified Samples Difference	$\langle X \rangle$ Difference	S_X Difference
<i>$[ES_{10}]$ NPV: Conventional-Route</i>	2.8 %	-11 %	0 %
<i>$[ES_{10}]$ NPV: SS-Route</i>	0.3 %	-10 %	-1 %

4.6. ECONOMIC ASSESSMENT: CO₂ CONTENT INCREASE IN NG – CONVENTIONAL-ROUTE

The debottlenecked Base-Cases of offshore processing of CO₂-rich NG via Conventional-Route for Cases 20%mol CO₂ and 50%mol CO₂ Route – Plant 3 (Figure 7c) – (Sec. 3.4.2) are assessed via Monte-Carlo analysis for economic performance via the module “Economic analysis” of *MCAnalysis-HUB* to attain profitability via economic specification [*ES*₁₀] *NPV* (Table 10). Such assessment combines uncertainties in process input variables (Table 3) and in economic variables (Table 9). Economic responses [*ES*₁] to [*ES*₉] (Table 10) are also evaluated.

4.6.1. Case 20%mol CO₂

Figure 60 depicts simple-frequency histograms and normal *PDFs* of output variables [*PS*₁] to [*PS*₈], and Figure 61 depicts simple-frequency histograms and normal *PDFs* of output variables [*PS*₉] to [*PS*₁₀].

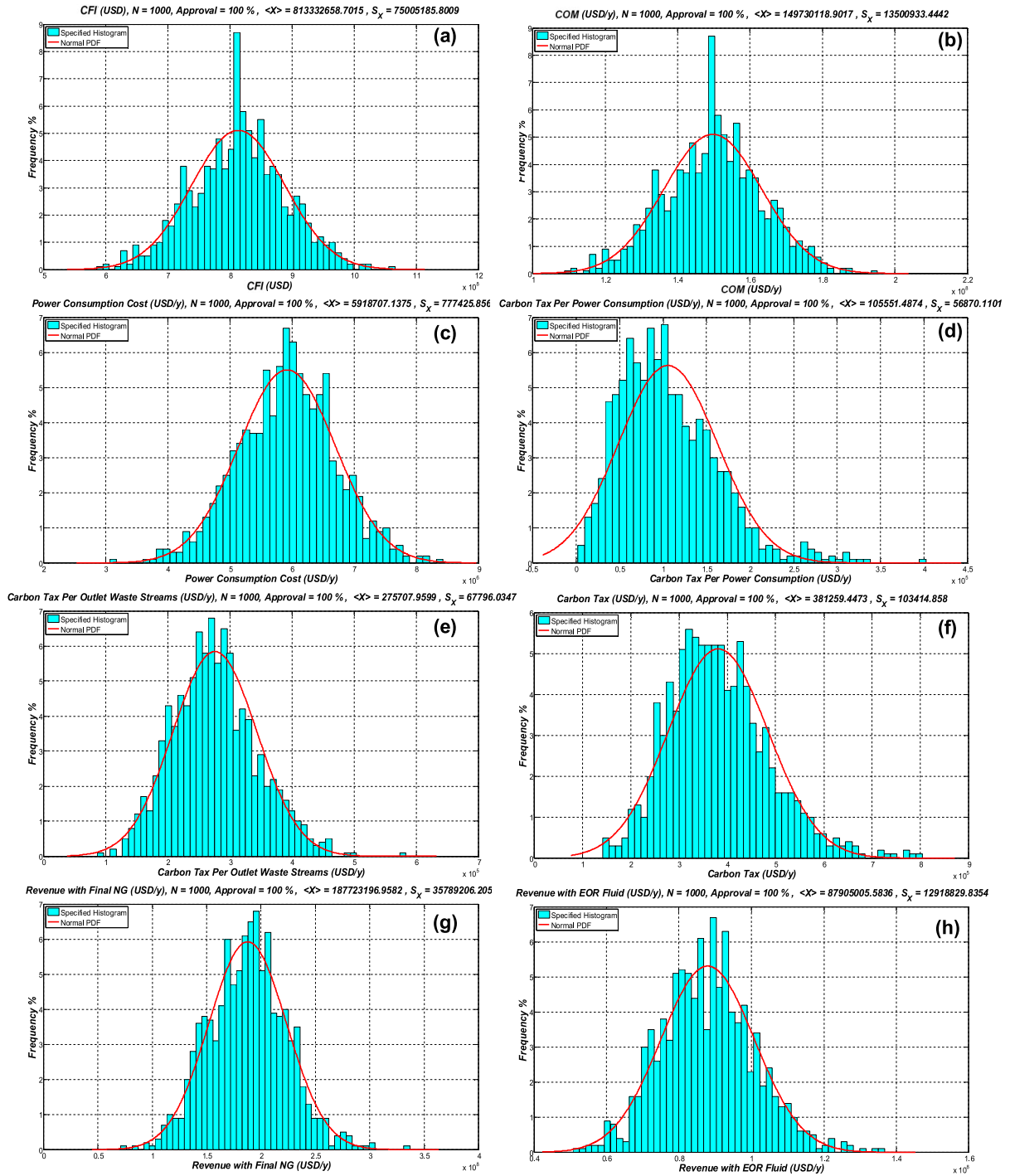


Figure 60. Case 20%mol CO₂: simple-frequency histograms and normal PDFs($\langle X \rangle$, S_x^2): (a) [ES₁] FCI; (b) [ES₂] COM; (c) [ES₃] Power consumption cost; (d) [ES₄] Carbon tax per power consumption; (e) [ES₅] Carbon tax per outlet waste streams; (f) [ES₆] Carbon tax; (g) [ES₇] Revenue from NG; and (h) [ES₈] Revenue from EOR-Fluid.

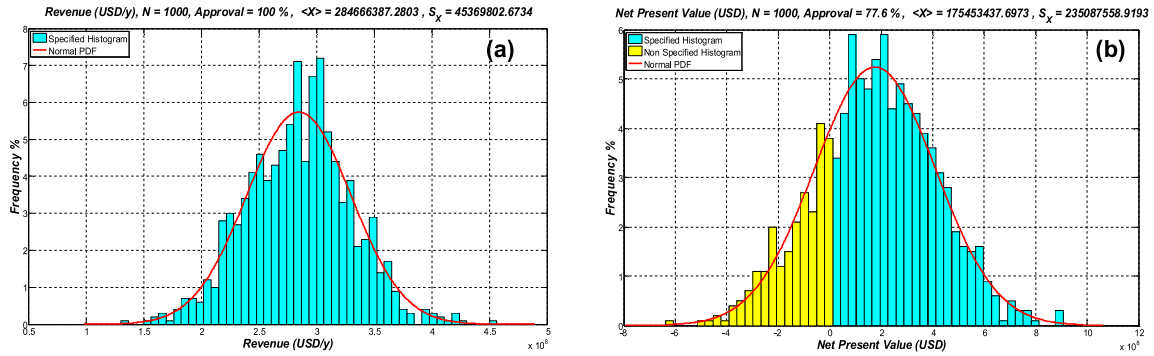


Figure 61. Case 20%mol CO₂: simple-frequency histograms and normal $PDFs(<X>, S_x^2)$: (a) [ES₉] Revenue; and (b) [ES₁₀] NPV.

Table 29 summarizes the economic assessment by listing percentages of approval, statistics ($<X>, S_x$) and simple-frequency histograms compared to the respective normal $PDFs(<X>, S_x^2)$ for the populations ($N=1000$) of responses [ES₁] to [ES₁₀], and a brief analysis of the results. The analysis of the results from Table 29 is similar to the Conventional-Route assessed in Sec. 4.5.1. Table 29 also shows that the Base-Case designed for Case 20%mol CO₂ is economically viable in the proposed economic scenario (Table 9) by attaining positive [ES₁₀] NPV in 77.6% of the sampled cases.

In addition, the missing 5% to account for 100% of revenue from products correspond to NGL revenue, illustrated in Figure 62.

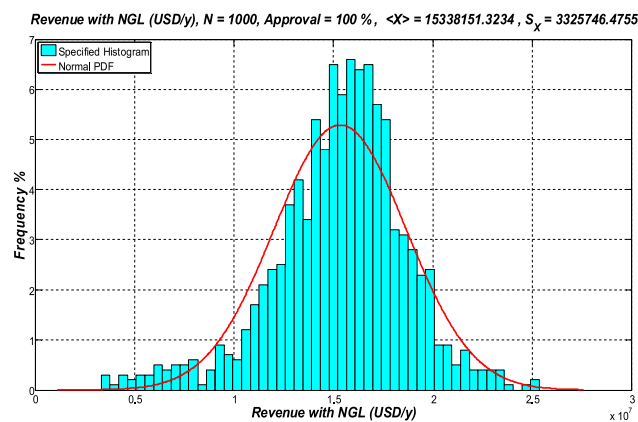


Figure 62. Case 20%mol CO₂: simple-frequency histogram and normal $PDF(<X>, S_x^2)$ of Revenue from NGL.

Table 29. MC analysis ($N=1000$) of responses $[ES_1]$ to $[ES_{10}]$ of Case 20%mol CO₂: approval percentages, statistics ($\langle X \rangle$, S_x), comparison of simple-frequency histograms versus normal $PDF(\langle X \rangle, S_x^2)$, and brief analysis.

Response	$\langle X \rangle$	S_x	Histogram vs normal PDF ($\langle X \rangle$, S_x^2)	Analysis
$[ES_1]$ FCI (USD/y)	813 330 000	75 005 000	Very-close	-
$[ES_2]$ COM (USD/y)	149 730 000	13 501 000	Very-close	53% of Revenue
$[ES_3]$ Power consumption cost (USD/y)	5 918 700	777 430	Very-close	2% revenue from products: low influence
$[ES_4]$ Carbon tax per power consumption (USD/y)	105 550	56 870	Left-skewed	28% carbon tax
$[ES_5]$ Carbon tax per outlet waste streams (USD/y)	275 710	67 796	Very-close	72% carbon tax
$[ES_6]$ Carbon tax(USD/y)	381 260	103 410	Close, left- skewed	0.1% revenue from products: negligible
$[ES_7]$ Revenue from NG (USD/y)	187 720 000	35 789 000	Very-close	65% revenue from products
$[ES_8]$ Revenue from EOR-Fluid (USD/y)	87 905 000	12 919 000	Very-close	30% revenue from products
$[ES_9]$ Revenue (USD/y)	284 670 000	45 370 000	Very-close	98% revenue from products
$[ES_{10}]$ NPV(USD)	175 450 000	235 090 000	Very-close	Economically viable in 77.6% of sampled cases

4.6.2. Case 50%mol CO₂

Figure 63 depicts simple-frequency histograms and normal PDF s of output variables $[PS_1]$ to $[PS_8]$, and Figure 64 depicts simple-frequency histograms and normal PDF s of output variables $[PS_9]$ to $[PS_{10}]$.

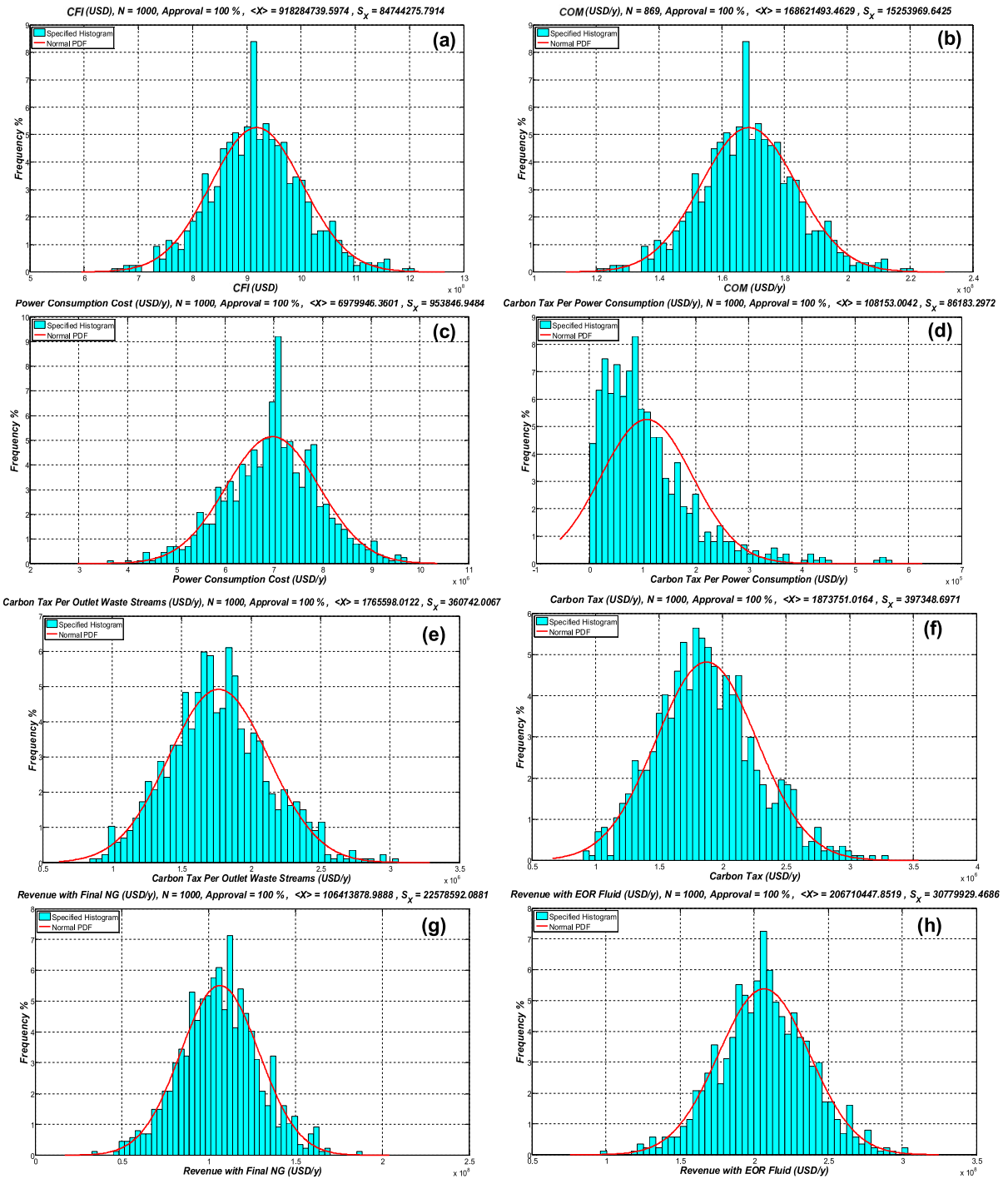


Figure 63. Case 50%mol CO₂: simple-frequency histograms and normal PDFs($\langle X \rangle$, S_x^2): (a) [ES₁] FCI; (b) [ES₂] COM; (c) [ES₃] Power consumption cost; (d) [ES₄] Carbon tax per power consumption; (e) [ES₅] Carbon tax per outlet waste streams; (f) [ES₆] Carbon tax; (g) [ES₇] Revenue from NG; and (h) [ES₈] Revenue from EOR-Fluid.

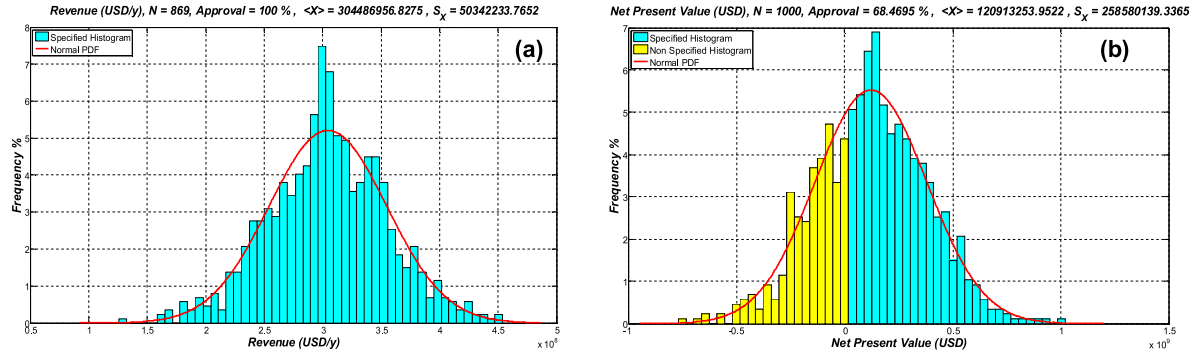


Figure 64. Case 50%mol CO₂: simple-frequency histograms and normal $PDFs(<X>, S_X^2)$: (a) [ES₉] Revenue; and (b) [ES₁₀] NPV.

Table 30 summarizes the economic assessment by listing percentages of approval, statistics ($<X>, S_X$) and simple-frequency histograms compared to the respective normal $PDFs(<X>, S_X^2)$ for the populations ($N=1000$) of responses [ES₁] to [ES₁₀], and a brief analysis of the results. Table 30 shows that the Base-Case designed for Case 50%mol CO₂ is not economically viable in the proposed economic scenario (Table 9) as [ES₁₀] NPV is only positive in 68.5% of the sampled cases, not attaining minimum success percentage of 75%

Table 30. MC analysis ($N=1000$) of responses $[ES_1]$ to $[ES_{10}]$ of Case 50%mol CO₂: approval percentages, statistics ($\langle X \rangle$, S_x), comparison of simple-frequency histograms versus normal $PDF(\langle X \rangle, S_x^2)$, and brief analysis.

Response	$\langle X \rangle$	S_x	Histogram vs normal PDF ($\langle X \rangle$, S_x^2)	Analysis
$[ES_1]$ FCI (USD/y)	918 280 000	84 744 000	Very-close	-
$[ES_2]$ COM (USD/y)	168 620 000	15 254 000	Very-close	139% of Revenue
$[ES_3]$ Power consumption cost (USD/y)	6 979 900	953 850	Very-close	2% revenue from products: low influence
$[ES_4]$ Carbon tax per power consumption (USD/y)	108 150	86 183	Left-skewed	6% carbon tax
$[ES_5]$ Carbon tax per outlet waste streams (USD/y)	1 765 600	360 740	Very-close	94% carbon tax
$[ES_6]$ Carbon tax(USD/y)	1 873 800	397 350	Close, left- skewed	0.6% revenue from products: negligible
$[ES_7]$ Revenue from NG (USD/y)	106 410 000	22 579 000	Very-close	34% revenue from products
$[ES_8]$ Revenue from EOR-Fluid (USD/y)	206 710 000	30 780 000	Very-close	66% revenue from products
$[ES_9]$ Revenue (USD/y)	304 490 000	50 342 000	Very-close	97.2% revenue from products
$[ES_{10}]$ NPV(USD)	120 910 000	258 580 000	Very-close	Economically viable in 68.5% of sampled cases

4.6.3. CO₂ content increase in NG effects

The increase of CO₂ content in NG from 20%mol average to 50%mol average did not change histogram behaviors of economic responses $[ES_1]$ to $[ES_{10}]$, except accentuating left-skewed behavior of $[ES_4]$ Carbon tax per power consumption.

The results of CO₂ content increase in NG, summarized in Table 31, are: (i) $\langle X \rangle$ of $[ES_1]$ FCI and $[ES_2]$ COM 13% higher; (ii) $\langle X \rangle$ of $[ES_3]$ Power consumption cost 18% higher; (iii) $\langle X \rangle$ of $[ES_6]$ Carbon tax 540% higher due to $[ES_5]$ Carbon tax per

outlet waste streams 540% higher (expected, as Case 50%mol CO₂ presented inferior environmental performance over Case 20%mol CO₂ in Sec. 4.4); (vi) [ES₇] Revenue from NG 43% lower and [ES₈] Revenue from EOR-Fluid lower as expected; (v) [ES₉] Revenue 7% higher ; and (vi) $\langle X \rangle$ of [ES₁₀] NPV 31% lower and percentage of specified samples 12% lower, meaning that the CO₂ increase in the raw NG hindered the economic performance of the Conventional-Route considering the proposed economic scenario in Table 9. Even though [ES₉] Revenue increased with CO₂ content increase, it was not high enough to balance increases in [ES₁] FCI, [ES₂] COM and [ES₆] Carbon tax.

Table 31. Debottlenecked Case 20%mol CO₂ minus debottlenecked Case 50%mol CO₂ differences for responses [ES₁] to [ES₁₀] in terms of: specified samples and statistics ($\langle X \rangle$, S_x).

Response	Specified Samples Difference	$\langle X \rangle$ Difference	S_x Difference
[ES ₁] FCI (USD/y)	-	13 %	13 %
[ES ₂] COM (USD/y)	-	13 %	13 %
[ES ₃] Power consumption cost (USD/y)	-	18 %	23 %
[ES ₄] Carbon tax per power consumption (USD/y)	-	2 %	52 %
[ES ₅] Carbon tax per outlet waste streams (USD/y)	-	540 %	432 %
[ES ₆] Carbon tax(USD/y)	-	391 %	284 %
[ES ₇] Revenue from NG (USD/y)	-	-43 %	-37 %
[ES ₈] Revenue from EOR-Fluid (USD/y)	-	135 %	138 %
[ES ₉] Revenue (USD/y)	-	7 %	11 %
[ES ₁₀] NPV(USD)	-12	-31 %	10 %

However, this assessment is highly sensitive to the proposed economic scenario, as the increase of CO₂ in NG may increase [ES₉] Revenue if EOR recovery factor and oil prices increase, and if NG price decreases.

By increasing EOR recovery factor = 1.5 bbl oil / t EOR-fluid re-injected (premise (iv) of Table 9) to 2 bbl oil / t EOR-fluid re-injected, value still feasible according to Godec

(2012), CO₂ content increase in NG improves economic performance of the Conventional-Route (Table 32) by achieving (i) [ES₈] Revenue from EOR-Fluid 135% higher; (ii) [ES₉] Revenue 12% higher; (iii) [ES₁₀] NPV 10% higher and; (iv) similar percentage of specified samples. Similar results can be achieved by increasing oil price or decreasing NG price. In this new scenario, both Cases 20%mol CO₂ and 50%mol CO₂ are economically viable by attaining positive [ES₁₀] NPV over 75% of the sampled cases.

Figures 65 and 66 depict simple-frequency histograms and normal *PDFs* of output variables [PS₈] to [PS₁₀] to Cases 20%mol CO₂ and 50%mol CO₂, respectively.

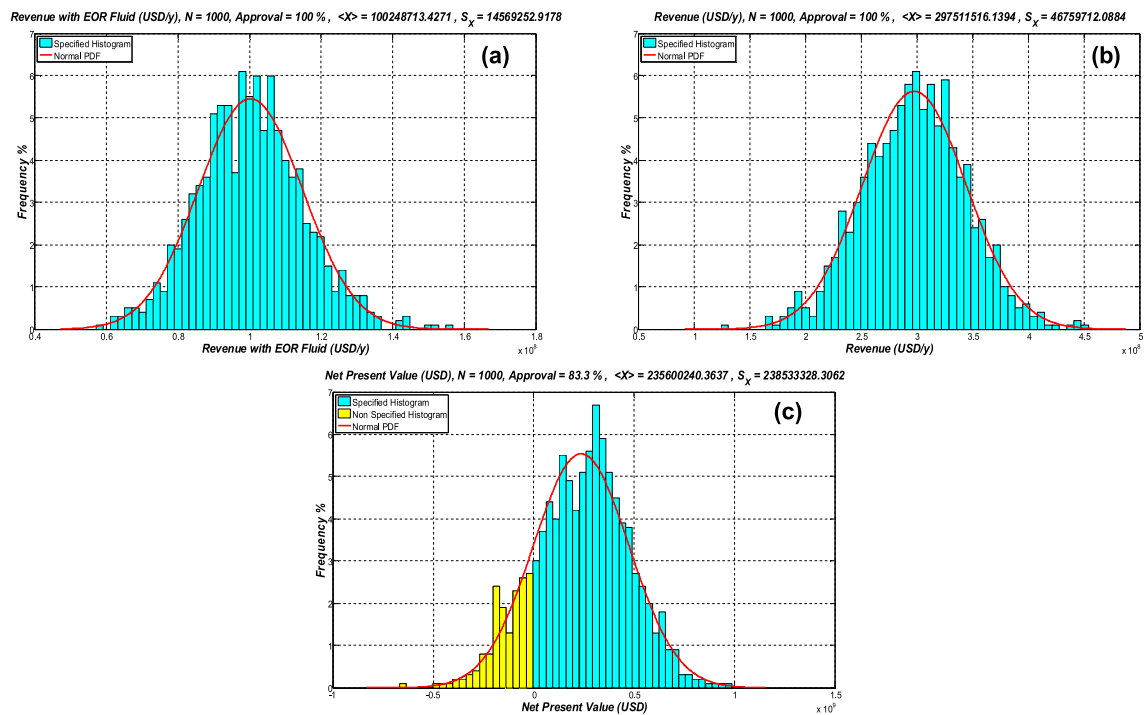


Figure 65. Case 20%mol CO₂: simple-frequency histograms and normal *PDFs* ($\langle X \rangle$, S_x^2): (a) [ES₈] Revenue from EOR-Fluid; (b) [ES₉] Revenue; and (c) [ES₁₀] NPV.

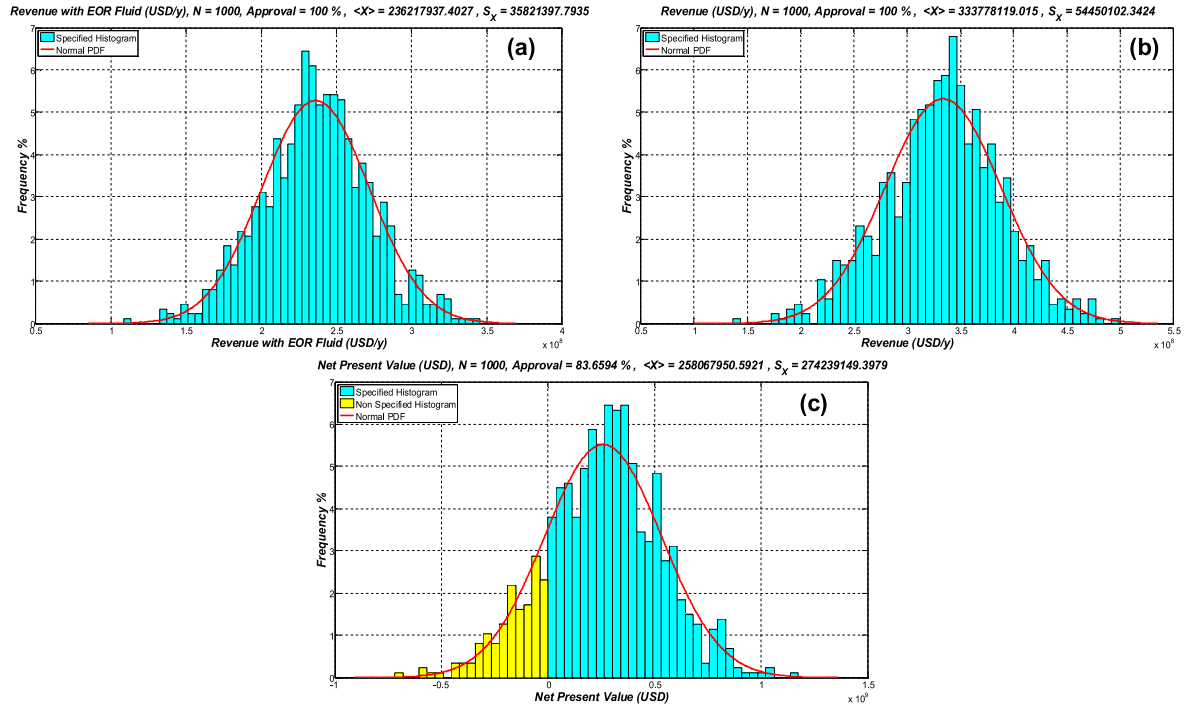


Figure 66. Case 50%mol CO₂: simple-frequency histograms and normal PDFs($\langle X \rangle$, S_x^2): (a) [ES₈] Revenue from EOR-Fluid; (b) [ES₉] Revenue; and (c) [ES₁₀] NPV.

Table 32. Debottlenecked Case 20%mol CO₂ minus debottlenecked Case 50%mol CO₂ differences for responses [ES₈] to [ES₁₀] in terms of: specified samples and statistics ($\langle X \rangle$, S_x).

Response	Specified Samples Difference	$\langle X \rangle$ Difference	S_x Difference
[ES ₈] Revenue from EOR-Fluid (USD/y)	-	136 %	146 %
[ES ₉] Revenue (USD/y)	-	12 %	16 %
[ES ₁₀] NPV(USD)	0.5%	10 %	15 %

The performance of [ES₁] FCI, [ES₂] COM, [ES₃] Power consumption cost, and [ES₆] Carbon tax decreases with CO₂ content increase in NG regardless of the proposed economic scenario. [ES₉] Revenue and [ES₁₀] NPV are highly sensitive to oil and gas prices, and EOR recovery factor.

5. CONCLUSIONS

Conventional-Route versus SS-Route

Designs of offshore processing of CO₂-rich NG via Conventional-Route Route – Plant 1 (Figure 7a) – and via SS-Route Route – Plant 2 (Figure 7b) –were submitted to Monte-Carlo analysis considering non-deterministic feed variables NG flow rate, NG molar fraction of CO₂ and GOR. Monte-Carlo analysis was based on the statistical behavior of chosen output variables [PS_1] to [PS_{10}] (Table 4) with minimum/maximum threshold values for commercial specification and/or process constraint attainment. To begin with, processes were originally sized considering average values of the three stochastic input variables. Subsequently, the 1st Monte-Carlo round was executed and both original designs of the Conventional-Route and SS-Route were considered insufficient as three out of ten output variables – NG y_{CO_2} , $HCDP^{NG}$, $P^{EOR-Delivery}$ – did not attain at least 75% of approved samples in both routes. Both routes were then re-designed with appropriate increases of Membrane-Permeation area, EOR well diameter, Ma^{Shock} of SS nozzles and decrease of inlet temperature of JTE unit (by increasing exchanger area). A 2nd round of Monte-Carlo analysis then approved both debottlenecked Conventional-Route and SS-Route designs based on at least 75% of samples accomplishing specifications for all [PS_1] to [PS_{10}] output variables. This demonstration illustrates the importance of Monte-Carlo analysis for testing and correcting designs of offshore CO₂-rich NG processing under uncertainties. Both Monte-Carlo analyses were executed with the new *MCAnalysis-HUB* CAE software.

In all instances of Conventional-Route and SS-Route, Monte-Carlo analysis also unveiled several process responses not following normal pattern and also changes in stochastic behaviors of some responses after the re-design, indicating highly non-linear causality relationships for these responses (e.g., $HCDP^{NG}$). This confirms the importance of Monte-Carlo assessment in design decisions under uncertainties for offshore processing of CO₂-rich NG and *MCAnalysis-HUB* was proven to be adequate for such scenario.

Additionally, the comparison of Monte-Carlo assessment of designs for Conventional-Route and SS-Route, showed that the latter presented less sensitivity of the stochastic behavior of responses regarding debottlenecking. In other words, SS-Route was re-designed with tighter margins of debottlenecking in order to achieve all specifications in at least 75% of the sampled cases. This can be understood as a greater resilience or elasticity of SS-Route, which translates a simpler, more straightforward and safer process. To accept this fact, one just has to compare the simplicity of SS unit operating at $P=50$ bar (Figure 11) with cumbersome TEG dehydration and JTE plants operating at $P=90$ bar (Figure 10).

Lastly, Monte-Carlo analysis also signifies to submit designs to a great variety of conditions and to assess the resilience and coherency of their responses. In this regard, the SS-Route for CO₂-rich NG processing showed higher resilience than the Conventional-Route, as its design can be retrofitted with smaller adjustments. Moreover, SS-Route consistently showed inferior power-consumption and compressor investment, requiring, in average, 15% less power-consumption and extracting water/C3+ condensate for HCDPA more selectively in terms of CO₂ (i.e. $\approx 23\%mol$ CO₂ versus $\approx 61\%mol$ in Conventional-Route); i.e., SS-Route is statistically better on economic and environmental grounds.

In addition to process design assessment under non-deterministic process scenario, designs of offshore processing of CO₂-rich NG via Conventional-Route and via SS-Route were also assessed for environmental and economic performances via Monte-Carlo analysis combining stochastic process and economic scenarios. Uncertainties on oil and gas prices, and carbon tax were considered, and positive *NPV* was selected as criteria for economic viability. Both routes were economically viable, and SS-route presented superior environmental and economic performances over Conventional-Route, and it was slightly more resilient to uncertainties in economic inputs than Conventional-Route.

Even though most of environmental – total output PEI and total output PEI per product mass – and economic – $[PS_1]$ to $[PS_{10}]$ – responses presented behavior close to normal pattern, such result does not mean that Monte-Carlo analysis is not needed for design assessment under uncertainties. The histograms of power

consumption and power consumption cost presented behaviors very-close to their normal *PDFs*, however, their relationship is not linear, as power consumption cost of the SS-Route is 28% lower compared to the Conventional-Route, while power consumption is only 15% lower.

CO₂ content increase in raw NG

Designs of offshore processing of CO₂-rich NG via Conventional-Route Route – Plant 3 (Figure 7c) – were submitted to Monte-Carlo analysis considering non-deterministic feed variables NG flow rate and NG molar fraction of CO₂. Two scenarios considering averages of 20%mol and 50%mol with 3%mol SD were evaluated. Monte-Carlo analysis was based on the statistical behavior of chosen output variables [*PS*₁] to [*PS*₄] (Table 4) with minimum/maximum threshold values for NG commercial specification. The same unit designed via Monte-Carlo analysis for Case 20%mol CO₂ could be adjusted to accommodate Case 50%mol CO₂ with increase of 30% in MP area, plus the burden of not generating NGL product stream, adding then an extra vessel and an extra flare stream as output waste, hindering both environmental and economic performances.

Considering the debottlenecked designs for both CO₂ content cases, Monte-Carlo analysis also unveiled several process responses not following normal patterns, and also changes of stochastic behaviors of some responses after the re-design to accommodate higher CO₂ content, indicating highly non-linear causality relationships for these responses. This corroborates the importance of Monte-Carlo assessment in design decisions under uncertainties for offshore processing of CO₂-rich NG via *MCA*Analysis-HUB.

Monte-Carlo analysis was also successfully applied for environmental assessment of both debottlenecked designs. Processing NG with higher CO₂ content carries a higher potential environmental impact, as expected, since CO₂ is the main emission from the plant, due to the power demand of compressors for NG exportation and CO₂ injection for EOR. The extra outlet waste stream due to the unviability to recover NGL also contributes to such decrease of environmental performance. This result raises an alert

for the impact of the CO₂ injection in the reservoir for EOR, which will increase the CO₂ content in the NG in the long-term.

The statistical behaviors of the PEIs corresponding to each environmental potential category evidence highly non-linear responses of the process. Such results also validates the recommendation to adopt decision making under influence of stochastic factors as Monte-Carlo analysis, again proving the value of CAE tool *MCAnalysis-HUB* for conducting design under uncertainties.

The categories GWP (global atmospheric impacts), AP and PCOP (regional atmospheric impacts) were identified by PCA as very relevant to process environmental performance under uncertainties, while the category TTP (ecological toxicity) exhibited medium relevance, independently of the CO₂ content of raw NG, because TTP is also related to emissions of unburnt hydrocarbons in the atmosphere due to leakages and incomplete burning. These aspects have reflexes on offshore rig design decision-making and can influence environmental policies of regulating agencies in connection with CO₂ rich NG exploration and production by offshore platforms.

Lastly, an economic assessment combining uncertainties in process inputs with economic uncertainties in oil and gas prices, and carbon tax was also conducted via Monte-Carlo analysis. The assessment showed that CO₂ increase in NG can influence economic performance not only negatively, as it is the case for fixed costs *FCI*, operational costs *COM*, power consumption cost, and carbon tax, but positively, as it is the case for revenue and *NPV*, highly depending on the premises adopted to the economic input variables (oil and gas prices, and carbon tax), and to EOR recovery factor.

General considerations

The new design concept via Monte-Carlo analysis for offshore processing of CO₂-rich NG under process and economic stochastic scenarios was successfully applied to process design, environmental and economic performances by automating simulations of complex flowsheets to compare conventional technologies with break-

through SS technology, and to evaluate impacts of the increase of CO₂ content in raw NG, which is a big concern in the long-term.

The importance of the proposed Monte-Carlo analysis approach has been corroborated by the assessments conducted in this D.Sc. Thesis. Such assessments were realized via CAE tool *MCAnalysis-HUB*, which proved its value by conducting sustainability assessment under uncertainties, combining process and economic non-deterministic scenarios.

Carbon tax presented low influence in economic performance of all the assessed Base-Cases. However, it presented left-skewed behavior when compared to its *PDF* in all Base-Cases and could influence designs with higher CO₂ emissions and/or lower cash flows.

Proposal for future work

Several improvements can be implemented in Monte-Carlo analysis methodology proposed in this work, and constitute proposal for future work: (i) implement a more efficient sampling method as an alternative to Monte-Carlo, as for example Quasi-Monte-Carlo; (ii) consider sensitivity analysis on results using approval criteria with other percentages besides 75%; (iii) consider process flowsheets with only fixed design equipment (SS, compressors, heat exchangers, pumping systems,...), which demand control loops to ensure the fixed design; (iv) include new features in the module “Economic Analysis” of *MCAnalysis-HUB* to calculate, in addition to *NPV*, the internal rate of return (IRR) to estimate the plant potential investment to achieve *NPV=0*, and also distributions of products price to achieve *NPV=0* (minimum selling price).

REFERENCES

- Abramowitz, M., Stegun, I.A., 1965. **Handbook of Mathematical Functions With Formulas, Graphs and Mathematical Tables**. Dover.
<https://doi.org/10.1115/1.3625776>
- Albrecht, J., 2013. **Estimating reaction model parameter uncertainty with Markov Chain Monte Carlo**. *Comput. Chem. Eng.* 48, 14–28.
<https://doi.org/10.1016/j.compchemeng.2012.07.011>
- Andronov, A., 2005. **Monte-Carlo approximation for probability distribution of monotone Boolean function**. *J. Stat. Plan. Inference* 132, 21–31.
<https://doi.org/10.1016/j.jspi.2004.06.013>
- Araújo, O.Q.F., de Medeiros, J.L., Yokoyama, L., Morgado, C.R.V., 2015. **Metrics for sustainability analysis of post-combustion abatement of CO₂ emissions: Microalgae mediated routes and CCS (carbon capture and storage)**. *Energy* 92, 556–568. <https://doi.org/10.1016/j.energy.2015.03.116>
- Araújo, O.Q.F., Reis, A. de C., de Medeiros, J.L., Nascimento, J.F., Grava, W.M., Musse, A.P.S., 2017. **Comparative analysis of separation technologies for processing carbon dioxide rich natural gas in ultra-deepwater oil fields**. *J. Clean. Prod.* 155, 12–22. <https://doi.org/10.1016/j.jclepro.2016.06.073>
- Arellano-Garcia, H., Wozny, G., 2009. **Chance constrained optimization of process systems under uncertainty: I. Strict monotonicity**. *Comput. Chem. Eng.* 33, 1568–1583. <https://doi.org/10.1016/j.compchemeng.2009.01.022>
- Arinelli, L.O., Trotta, T.A.F., Teixeira, A.M., de Medeiros, J.L., Araújo, O.Q.F., 2017. **Offshore processing of CO₂ rich natural gas with supersonic separator versus conventional routes**. *J. Nat. Gas Sci. Eng.* 46, 199–221.
<https://doi.org/10.1016/j.jngse.2017.07.010>
- Arinelli, L.O., de Medeiros, J.L., de Melo, D.C., Teixeira, A.M., Brigadão, G.V., Passarelli, F.M., Grava, W.M., Araújo, O.Q.F., 2019. **Carbon capture and high-capacity supercritical fluid processing with supersonic separator: Natural gas with ultra-high CO₂ content**. *J. Nat. Gas Sci. Eng.* 66, 265–283.
<https://doi.org/10.1016/j.jngse.2019.04.004>
- Arunraj, N.S., Mandal, S., Maiti, J., 2013. **Modeling uncertainty in risk assessment: An integrated approach with fuzzy set theory and Monte Carlo simulation**. *Accid. Anal. Prev.* 55, 242–255.
<https://doi.org/10.1016/j.aap.2013.03.007>
- Bahadori, A., Vuthaluru, H.B., 2009. **Rapid estimation of equilibrium water dew point of natural gas in TEG dehydration systems**. *J. Nat. Gas Sci. Eng.* 1, 68–71.
<https://doi.org/10.1016/j.jngse.2009.08.001>
- Baker, R.W., Lokhandwala, K., 2008. **Natural Gas Processing with Membranes: An Overview**. *Ind. Eng. Chem. Res.* 47, 2109–2121.

<https://doi.org/10.1021/ie071083w>

Bakshi, B.R., 2003. **The Quest for Sustainability: Challenges for Process Systems Engineering**. AIChE J. 49, 1350–1358.

Barrett, W.M., van Baten, J., Martin, T., 2011. **Implementation of the waste reduction (WAR) algorithm utilizing flowsheet monitoring**. Comput. Chem. Eng. 35, 2680–2686. <https://doi.org/10.1016/j.compchemeng.2011.02.004>

Batres, R., Asprey, S.P., Fuchino, T., Naka, Y., 1999. A KQML multi-agent environment for concurrent process engineering. Comput. Chem. Eng. 23. [https://doi.org/10.1016/S0098-1354\(99\)80160-4](https://doi.org/10.1016/S0098-1354(99)80160-4)

Bolliger, R., Becker, H., Maréchal, F., 2009. **New Generic Approach for the Analysis of Energy Conversion System Models**. 10th Int. Symp. Process Syst. Eng. Part A. [https://doi.org/10.1016/S1570-7946\(09\)70261-5](https://doi.org/10.1016/S1570-7946(09)70261-5)

BP, 2019a. **BP Statistical Review of World Energy**.

BP, 2019b. **BP Energy Outlook**.

Brigadão, G.V., Arinelli, L.O., de Medeiros, J.L., Araújo, O.Q.F., 2019. **A new concept of air pre-purification unit for cryogenic separation: Low- pressure supersonic separator coupled to finishing adsorption**. Sep. Purif. Technol. 215, 173–189. <https://doi.org/10.1016/j.seppur.2019.01.015>

Cabezas, H., Bare, J.C., Mallick, S.K., 1999. **Pollution prevention with chemical process simulators: The generalized waste reduction (WAR) algorithm - Full version**. Comput. Chem. Eng. 23, 623–634. [https://doi.org/10.1016/S0098-1354\(98\)00298-1](https://doi.org/10.1016/S0098-1354(98)00298-1)

Caflich, R.E., 1998. **Monte Carlo and quasi-Monte Carlo methods**. Acta Numer. 7, 1–49. <https://doi.org/https://doi.proxy.ufrj.br/10.1017/S0962492900002804>

Clift, R., 2006. **Sustainable development and its implications for chemical engineering**. Chem. Eng. Sci. 61, 4179–4187. <https://doi.org/10.1016/j.ces.2005.10.017>

de Medeiros, J.L., Arinelli, L.O., Araújo, O.Q.F., 2017. **Speed of sound of multiphase and multi-reactive equilibrium streams: A numerical approach for natural gas applications**. J. Nat. Gas Sci. Eng. <https://doi.org/10.1016/j.jngse.2017.08.006>

de Medeiros, J.L., Arinelli, L.O., Teixeira, A.M., Araújo, O.Q.F., 2019. **Offshore Processing of CO₂-Rich Natural Gas with Supersonic Separator: Multiphase Sound Speed, CO₂ Freeze-Out and HYSYS Implementation**. Springer, Cham, Switzerland. <https://doi.org/https://doi.org/10.1007/978-3-030-04006-2>

Dehghani, M., Asghari, M., Mohammadi, A.H., Mokhtari, M., 2017. **Molecular simulation and Monte Carlo study of structural-transport-properties of PEBA-MFI zeolite mixed matrix membranes for CO₂, CH₄ and N₂ separation.** Comput. Chem. Eng. 103, 12–22. <https://doi.org/10.1016/j.compchemeng.2017.03.002>

Diaz, S., Brignole, E.A., Bandoni, A., 2002. **Flexibility study on a dual mode natural gas plant in operation.** Chem. Eng. Commun. 189, 37–41. <https://doi.org/10.1080/00986440211744>

Duong, P.L.T., Ali, W., Kwok, E., Lee, M., 2016. **Uncertainty quantification and global sensitivity analysis of complex chemical process using a generalized polynomial chaos approach.** Comput. Chem. Eng. 90, 23–30. <https://doi.org/10.1016/j.compchemeng.2016.03.020>

Dzobo, O., Gaunt, C.T., Herman, R., 2012. **Investigating the use of probability distribution functions in reliability-worth analysis of electric power systems.** Int. J. Electr. Power Energy Syst. 37, 110–116. <https://doi.org/10.1016/j.ijepes.2011.12.013>

Eckstein, J., Chen, J.-Y., Chou, C.-P., Janicka, J., 2000. **Modeling of turbulent mixing in opposed jet configuration: one-dimensional Monte Carlo probability density function simulation.** Proc. Combust. Inst. 28, 141–148. [https://doi.org/https://doi.org/10.1016/S0082-0784\(00\)80205-2](https://doi.org/https://doi.org/10.1016/S0082-0784(00)80205-2)

Fleshman, J., Alderton, P., Bahnassi, E., Khouri, A.R., 2005. **Achieving product specifications for ethane through to pentane plus from NGL fractionation plants**, in: AIChE Annual Meeting. Cincinnati.

Getu, M., Mahadzir, S., Samyudia, Y., Khan, M.S., Bahadori, A., Lee, M., 2015. **Risk-based optimization for representative natural gas liquid (NGL) recovery processes by considering uncertainty from the plant inlet.** J. Nat. Gas Sci. Eng. 27, 42–54. <https://doi.org/10.1016/j.jngse.2015.01.028>

Godec, M.L., 2012. From CO₂-EOR to CCS: ‘**Prospects and Challenges of Combining CO₂-EOR with Storage**’, in: IEA – OPEC CO₂-EOR Kuwait Workshop. Kuwait City.

Gonzaga, C.S.B., 2014. **Uma metodologia Monte Carlo para projeto de processamento offshore de gás natural.** MSc. Thesis. Federal University of Rio de Janeiro.

Gonzaga, C.S.B., Araújo, O.Q.F., de Medeiros, J.L., 2017a. **Offshore Processing of CO₂ Rich Natural Gas : A Monte Carlo Methodology Applied to Assessment of Environmental Performance**, in: 12th SDEWES - Conference on Sustainable Development of Energy, Water and Environment Systems. Faculty of Mechanical Engineering and Naval Architecture, Dubrovnik, pp. 1–22.

Gonzaga, C.S.B., Araújo, O.Q.F., de Medeiros, J.L., 2019a. **A Monte Carlo Methodology for Environmental Assessment Applied to Offshore Processing of**

Natural Gas with High Carbon Dioxide Content. J. Sustain. Dev. Energy, Water Environ. Syst. 1–21. <https://doi.org/https://doi.org/10.13044/j.sdewes.d6.0240>

Gonzaga, C.S.B., Araújo, O.Q.F., de Medeiros, J.L., 2019b. **A Novel Tool for Computer-Aided Sustainability Assessment Under Uncertainty: A Design Case of Natural Gas Offshore Processing.** Comput. Aided Chem. Eng. 47, 305–310. <https://doi.org/10.1016/B978-0-12-818597-1.50048-5>

Gonzaga, C.S.B., Arinelli, L.O., de Medeiros, J.L., Araújo, O.Q.F., 2019c. **Automatized Monte-Carlo analysis of offshore processing of CO₂-rich natural gas: Conventional versus supersonic separator routes.** J. Nat. Gas Sci. Eng. 69. <https://doi.org/10.1016/j.jngse.2019.102943>

Gonzaga, C.S.B., de Medeiros, J.L., Araújo, O.Q.F., 2017b. **MCANALYSIS (APP-VB-XML-HYSYS-MATLAB).** BR 51 2016 000909-8. INPI - Instituto Nacional da Propriedade Industrial.

Gonzaga, C.S.B., de Medeiros, J.L., Araújo, O.Q.F., 2019d. **Conventional Versus Supersonic Separator Routes for Offshore Processing of CO₂-Rich Natural Gas : Sustainability Assessment under Uncertainties via Monte Carlo Analysis,** in: The 5th International Conference on Sustainable Chemical Product and Process Engineering. Tianjin University, Tianjin, p. 196.

Gonzaga, C.S.B., de Medeiros, J.L., Araújo, O.Q.F., 2019e. **MCAnalysis-HUB (HUB for Monte Carlo Analysis based on Process Simulations).** BR 51 20190 00249-0. INPI - Instituto Nacional da Propriedade Industrial.

Gozalpour, F., Ren, S.R., Tohidi, B., 2005. **CO₂ EOR and Storage in Oil Reservoir.** Oil Gas Sci. Technol. 60, 537–546. <https://doi.org/10.2516/ogst:2005036>

Grossmann, I.E., 2004. **Challenges in the new millennium: product discovery and design, enterprise and supply chain optimization, global life cycle assessment.** Comput. Chem. Eng. 29, 29–39. <https://doi.org/10.1016/j.compchemeng.2004.07.016>

Grossmann, I.E., Apap, R.M., Calfa, B.A., Garcia-Herreros, P., Zhang, Q., 2015. **Recent Advances in Mathematical Programming Techniques for the Optimization of Process Systems under Uncertainty.** Comput. Aided Chem. Eng. 37, 1–14. <https://doi.org/10.1016/B978-0-444-63578-5.50001-3>

Guimarães, C. da C., Moralles, M., Martinelli, J.R., 2014. **Monte Carlo simulation of liver cancer treatment with 166Ho-loaded glass microspheres.** Radiat. Phys. Chem. 95, 185–187. <https://doi.org/10.1016/j.radphyschem.2012.12.050>

Habib, A.S., Shutt, A.L., Regan, P.H., Matthews, M.C., Alsulaiti, H., Bradley, D.A., 2014. **Characterization of naturally occurring radioactive materials in Libyan oil pipe scale using a germanium detector and Monte Carlo simulation.** Radiat. Phys. Chem. 95, 352–355. <https://doi.org/10.1016/j.radphyschem.2013.01.028>

Hao, J., Rice, P.A., Stern, S.A., 2008. **Upgrading low-quality natural gas with H₂S- and CO₂-selective polymer membranes. Part II. Process design, economics, and sensitivity study of membrane stages with recycle streams.** J. Memb. Sci. 320, 108–122. <https://doi.org/10.1016/j.memsci.2008.03.040>

Hastings, W.K., 1970. **Monte Carlo sampling methods using Markov chains and their applications.** Biometrika 57, 97. <https://doi.org/10.1093/biomet/57.1.97>

Himmelblau, D.M., 1970. **Process analysis by statistical methods.** John Wiley & Sons.

Jacques, S., 1998. **Monte Carlo sampling of probability distributions: How to make the computer roll dice.** Oregon Med. Laser Cent. <https://omlc.org/news/sep98/montecarlosampling/index.html> (accessed 2 April 2018).

Jain, S., Acharya, M., Gupta, S., Bhaskarwar, A.N., 2003. **Monte Carlo simulation of flow of fluids through porous media.** Comput. Chem. Eng. 27, 385–400. [https://doi.org/10.1016/S0098-1354\(02\)00211-9](https://doi.org/10.1016/S0098-1354(02)00211-9)

Jiménez-González, C., Kim, S., Overcash, M.R., 2000. **Methodology for developing gate-to-gate Life Cycle Inventory information.** Int. J. Life Cycle Assess. 5, 153–159. <https://doi.org/10.1007/BF02978615>

Kamal, M.S., Hussein, I.A., Sultan, A.S., Von Solms, N., 2016. **Application of various water soluble polymers in gas hydrate inhibition.** Renew. Sustain. Energy Rev. 60, 206–225. <https://doi.org/10.1016/j.rser.2016.01.092>

Lagache, M.H., Ungerer, P., Boutin, A., 2004. **Prediction of thermodynamic derivative properties of natural condensate gases at high pressure by Monte Carlo simulation.** Fluid Phase Equilib. 220, 211–223. <https://doi.org/10.1016/j.fluid.2004.03.015>

Laurence, T., Maréchal, F., 2012. **Platform development for studying integrated energy conversion processes: Application to a power plant process with CO₂ capture.** Comput. Aided Chem. Eng. 31, 1015–1019. <https://doi.org/https://doi.org/10.1016/B978-0-444-59506-5.50034-1>

Lemieux, C., 2009. **Monte Carlo and Quasi-Monte Carlo Sampling.** Springer, New York. <https://doi.org/10.1007/978-0-387-78165-5>

Li, P., Wendt, M., Wozny, G., 2004. **Optimal Production Planning for Chemical Processes under Uncertain Market Conditions.** Chem. Eng. Technol. 27, 641–651. <https://doi.org/10.1002/ceat.200400048>

Lonati, G., Zanoni, F., 2013. **Monte-Carlo human health risk assessment of mercury emissions from a MSW gasification plant.** Waste Manag. 33, 347–355. <https://doi.org/10.1016/j.wasman.2012.10.015>

Machado, P.B., Monteiro, J.G.M., Medeiros, J.L., Epsom, H.D., Araújo, O.Q.F., 2012. **Supersonic separation in onshore natural gas dew point plant.** J. Nat. Gas Sci. Eng. 6, 43–49. <https://doi.org/10.1016/j.jngse.2012.03.001>

Mesfin, G., Shuhaimi, M., 2010. **A chance constrained approach for a gas processing plant with uncertain feed conditions.** Comput. Chem. Eng. 34, 1256–1267. <https://doi.org/10.1016/j.compchemeng.2010.03.009>

Netusil, M., Dittl, P., 2011. Comparison of three methods for natural gas dehydration. J. Nat. Gas Chem. 20, 471–476. [https://doi.org/10.1016/S1003-9953\(10\)60218-6](https://doi.org/10.1016/S1003-9953(10)60218-6)

Nguyen, T.-V., de Oliveira Júnior, S., 2018. System evaluation of offshore platforms with gas liquefaction processes. Energy 144, 594–606. <https://doi.org/http://dx.doi.org/10.1016/B978-008044910-4.00476-4>

Olaru, M., Șandru, M., Pirnea, I.C., 2014. **Monte Carlo Method Application for Environmental Risks Impact Assessment in Investment Projects.** Procedia - Soc. Behav. Sci. 109, 940–943. <https://doi.org/10.1016/j.sbspro.2013.12.568>

Perez, F., Devegowda, D., 2017. **Estimation of adsorbed-phase density of methane in realistic overmature kerogen models using molecular simulations for accurate gas in place calculations.** J. Nat. Gas Sci. Eng. 46, 865–872. <https://doi.org/10.1016/j.jngse.2017.08.008>

Peters, L., Hussain, A., Follmann, M., Melin, T., Hägg, M.B., 2011. **CO₂ removal from natural gas by employing amine absorption and membrane technology-A technical and economical analysis.** Chem. Eng. J. 172, 952–960. <https://doi.org/10.1016/j.cej.2011.07.007>

Ratick, S., Schwarz, G., 2009. **Monte Carlo Simulation.** Int. Encycl. Hum. Geogr. 175–184. <https://doi.org/https://doi.org/10.1016/B978-008044910-4.00476-4>

Reis, A.C., de Medeiros, J.L., Nunes, G.C., Araújo, O.Q.F., 2017. **Upgrading of natural gas ultra-rich in carbon dioxide: Optimal arrangement of membrane skids and polishing with chemical absorption.** J. Clean. Prod. 165, 1013–1024. <https://doi.org/10.1016/j.jclepro.2017.07.198>

Roffel, B., Betlem, B., 2006. **Process Dynamics and Control: Modeling for Control and Prediction.** John Wiley & Sons, Inc., New Jersey.

Rostamian, H., Lotfollahi, M.N., 2019. **A New Correlation Method for Estimating Thermal Conductivity of Carbon Dioxide in Liquid, Vapor and Supercritical Phases.** Period. Polytech. Chem. Eng. 60, 93–97. <https://doi.org/10.3311/ppch.12754>

Sant'Anna, A.A., de Medeiros, J.L., Araújo, O.Q.F., 2005. **Simulação de processamento de gás natural em plataforma off-shore**, in: 3º Congresso Brasileiro de P&D Em Petróleo e Gás. Salvador.

Sepiacci, P., Depetri, V., Manca, D., 2017. **A systematic approach to the optimal design of chemical plants with waste reduction and market uncertainty.** Comput. Chem. Eng. 102, 96–109.

<https://doi.org/10.1016/j.compchemeng.2016.11.032>

Shahid, S., Nijmeijer, K., 2014. **Performance and plasticization behavior of polymer-MOF membranes for gas separation at elevated pressures.** J. Memb. Sci. 470, 166–177. <https://doi.org/10.1016/j.memsci.2014.07.034>

Sikdar, S.K., 2003. **Sustainability Metrics.** AIChE J. 49, 1928–1932.

Sikdar, S.K., Sengupta, D., Mukherjee, R., 2016. **Measuring Progress Towards Sustainability.** Springer, Cham. <https://doi.org/10.1007/978-3-319-42719-5>

State and Trends of Carbon Pricing 2019, 2019. World Bank, Washington, DC. <https://doi.org/10.1596/978-1-4648-1435-8>

Tan, R.R., Aviso, K.B., Foo, D.C.Y., 2017. **P-graph and Monte Carlo simulation approach to planning carbon management networks.** Comput. Chem. Eng. 106, 872–882. <https://doi.org/10.1016/j.compchemeng.2017.01.047>

Tang, Y., Zou, Z., Jing, J., Zhang, Z., Xie, C., 2015. **A framework for making maintenance decisions for oil and gas drilling and production equipment.** J. Nat. Gas Sci. Eng. 26, 1050–1058. <https://doi.org/10.1016/j.jngse.2015.07.038>

Taut, C., Correa, C., Deutschmann, O., Warnatz, J., Einecke, S., Schulz, C., Wolfrum, J., 2000. **3D-modeling with Monte-Carlo-PDF methods and laser diagnostics of the combustion in a two-stroke engine.** Proc. Combust. Inst. 28, 1153–1159. [https://doi.org/https://doi.org/10.1016/S0082-0784\(00\)80325-2](https://doi.org/https://doi.org/10.1016/S0082-0784(00)80325-2)

Teixeira, A.M., Arinelli, L.O., de Medeiros, J.L., Araújo, O.Q.F., 2018. **Recovery of thermodynamic hydrate inhibitors methanol, ethanol and MEG with supersonic separators in offshore natural gas processing.** J. Nat. Gas Sci. Eng. 52, 166–186. <https://doi.org/10.1016/j.jngse.2018.01.038>

Tula, A.K., Babi, D.K., Bottlaender, J., Eden, M.R., Gani, R., 2017. **A computer-aided software-tool for sustainable process synthesis-intensification.** Comput. Chem. Eng. 105, 74–95. <https://doi.org/10.1016/j.compchemeng.2017.01.001>

Turton, R., Bailie, R.C., Whiting, W.B., Shaeiwitz, J.A., 2009. **Analysis, Synthesis, and Design of Chemical Processes**, Third Edit. ed. Prentice Hall.

Twister, B.V., 2010. SS twister site.pdf, <http://www.twisterbv.com/twister-supersonic/> (accessed 11 November 2018).

Wan Ahmad, W.N.K., Rezaei, J., de Brito, M.P., Tavasszy, L.A., 2016. **The influence of external factors on supply chain sustainability goals of the oil and gas industry.** Resour. Policy 49, 302–314. <https://doi.org/10.1016/j.resourpol.2016.06.006>

- Wen, C., Cao, X., Yang, Y., Li, W., 2012. **Numerical simulation of natural gas flows in diffusers for supersonic separators.** Energy 37, 195–200. <https://doi.org/10.1016/j.energy.2011.11.047>
- Yang, Y., Wen, C., Wang, S., Feng, Y., 2014. **Theoretical and numerical analysis on pressure recovery of supersonic separators for natural gas dehydration.** Appl. Energy 132, 248–253. <https://doi.org/10.1016/j.apenergy.2014.07.018>
- Yeh, C.Y., Lee, C.C., Chao, T.C., Lin, M.H., Lai, P.A., Liu, F.H., Tung, C.J., 2014. **Application of the measurement-based Monte Carlo method in nasopharyngeal cancer patients for intensity modulated radiation therapy.** Radiat. Phys. Chem. 95, 240–242. <https://doi.org/10.1016/j.radphyschem.2013.01.024>
- Yeo, Z.Y., Chew, T.L., Zhu, P.W., Mohamed, A.R., Chai, S., 2012. **Conventional processes and membrane technology for carbon dioxide removal from natural gas : A review.** J. Nat. Gas Chem. 21, 282–298. [https://doi.org/10.1016/S1003-9953\(11\)60366-6](https://doi.org/10.1016/S1003-9953(11)60366-6)
- Young, D., Scharp, R., Cabezas, H., 2000. **The waste reduction (WAR) algorithm: Environmental impacts, energy consumption, and engineering economics.** Waste Manag. 20, 605–615. [https://doi.org/10.1016/S0956-053X\(00\)00047-7](https://doi.org/10.1016/S0956-053X(00)00047-7)
- Young, D.M., Cabezas, H., 1999. **Designing sustainable processes with simulation: The waste reduction (WAR) algorithm.** Comput. Chem. Eng. 23, 1477–1491. [https://doi.org/10.1016/S0098-1354\(99\)00306-3](https://doi.org/10.1016/S0098-1354(99)00306-3)
- Yu, W., Gong, J., Song, S., Huang, W., Li, Y., Zhang, J., 2019. **Gas supply reliability analysis of a natural gas pipeline system considering the effects of underground gas storages.** Appl. Energy 252, 113418. <https://doi.org/10.1016/j.apenergy.2019.113418>
- Yu, W., Song, S., Li, Y., Min, Y., Huang, W., Wen, K., 2018. **Gas supply reliability assessment of natural gas transmission pipeline systems.** Energy 162, 853–870. <https://doi.org/10.1016/j.energy.2018.08.039>
- Zhang, B., Kang, J., Kang, T., 2018. **Monte Carlo simulations of methane adsorption on kaolinite as a function of pore size.** J. Nat. Gas Sci. Eng. 49, 410–416. <https://doi.org/10.1016/j.jngse.2017.11.026>
- Zhang, H., Liang, Y., Liao, Q., Chen, J., Zhang, W., Long, Y., Qian, C., 2019. **Optimal design and operation for supply chain system of multi-state natural gas under uncertainties of demand and purchase price.** Comput. Ind. Eng. 131, 115–130. <https://doi.org/10.1016/j.cie.2019.03.041>

APPENDIX A – Products of this Thesis: Publications and Registered Software

This section lists the products of this D.Sc. thesis including the respective front pages.

Article in Scientific Journals:

1. GONZAGA, CRISTIANE SÃO BENTO; ARINELLI, LARA DE OLIVEIRA ; DE MEDEIROS, JOSÉ LUIZ ; ARAÚJO, OFÉLIA DE QUEIROZ F. . Automatized Monte-Carlo analysis of offshore processing of CO₂-rich natural gas: Conventional versus supersonic separator routes. *Journal of Natural Gas Science and Engineering*, v. 69, p. 102943, 2019.
2. GONZAGA, CRISTIANE SÃO BENTO; DE MEDEIROS, JOSÉ LUIZ ; ARAÚJO, OFÉLIA DE QUEIROZ F. . A Monte Carlo Methodology for Environmental Assessment Applied to Offshore Processing of Natural Gas with High Carbon Dioxide Content. *Journal of Sustainable Development of Energy, Water and Environment Systems*, v. -, p. -, 2019.

Book Chapter Published

1. GONZAGA, CRISTIANE SÃO BENTO; ARAÚJO, OFÉLIA DE QUEIROZ F. ; DE MEDEIROS, JOSÉ LUIZ . A NOVEL TOOL FOR COMPUTER-AIDED SUSTAINABILITY ASSESSMENT UNDER UNCERTAINTY: A DESIGN CASE OF NATURAL GAS OFFSHORE PROCESSING. In: Salvador Munoz; Carl Laird; Matthew Realff. (Org.). FOCAPD-19/Proceedings of the 9th International Conference on Foundations of Computer-Aided Process Design, July 14 - 18, 2019. 1ed.Amsterdam: ELSEVIER, 2019, v. 47, p. 305-310.

Complete work published in proceedings of conferences

1. GONZAGA, CRISTIANE SÃO BENTO; ARAÚJO, OFÉLIA DE QUEIROZ F. ; DE MEDEIROS, JOSÉ LUIZ . A NOVEL TOOL FOR COMPUTER-AIDED SUSTAINABILITY ASSESSMENT UNDER UNCERTAINTY: A DESIGN CASE OF NATURAL GAS OFFSHORE PROCESSING. In: 9TH INTERNATIONAL CONFERENCE ON FOUNDATIONS OF COMPUTER-AIDED PROCESS DESIGN, 2019, Copper Mountain. PROCEEDINGS OF THE 9TH INTERNATIONAL CONFERENCE ON FOUNDATIONS OF COMPUTER-AIDED PROCESS DESIGN. Amsterdam: ELSEVIER, 2019. v. 1. p. 305-310.
2. GONZAGA, CRISTIANE SÃO BENTO; ARAÚJO, OFÉLIA DE QUEIROZ F. ; DE MEDEIROS, JOSÉ LUIZ . Offshore Processing of CO₂ Rich Natural Gas: A Monte Carlo Methodology Applied to Assessment of Environmental Performance. In: 12th SDEWES - Conference on Sustainable Development of Energy, Water and Environment Systems, 2017, Dubrovnik. 12th SDEWES - Conference on Sustainable Development of Energy, Water and Environment Systems. Zagreb: Faculty of Mechanical Engineering and Naval Architecture, 2017. v. 1. p. 1-22.

Abstracts published in proceedings of conferences

1. GONZAGA, CRISTIANE SÃO BENTO; DE MEDEIROS, JOSÉ LUIZ ; ARAÚJO, OFÉLIA DE QUEIROZ F. . Conventional versus Supersonic Separator Routes for Offshore Processing of CO₂-Rich Natural Gas: Sustainability Assessment under Uncertainties via Monte Carlo Analysis. In: The 5th International Conference on Sustainable Chemical Product and Process Engineering, 2019, Tianjin. SCPPE-2019 Abstracts. Tianjin: Tianjin University, 2019. v. 1. p. 196-196.

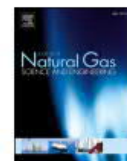
Registered software:

1. GONZAGA, CRISTIANE SÃO BENTO; DE MEDEIROS, JOSÉ LUIZ ; ARAÚJO, OFÉLIA DE QUEIROZ F. . MCANALYSIS (APP-VB-XML-HYSYS-MATLAB). 2017. Register number: BR512016000909-8, Date of register: 30/05/2017, Title: "MCANALYSIS (APP-VB-XML-HYSYS-MATLAB)", Title: INPI - Instituto Nacional da Propriedade Industrial.
2. GONZAGA, CRISTIANE SÃO BENTO; DE MEDEIROS, JOSÉ LUIZ ; ARAÚJO, OFÉLIA DE QUEIROZ F. . MCAnalysis-HUB (HUB for Monte Carlo Analysis based on Process Simulations). 2019. Register number: BR512019000249-0, Date of register: 15/02/2019, Title: "MCAnalysis-HUB (HUB for Monte Carlo Analysis based on Process Simulations)", Title: INPI - Instituto Nacional da Propriedade Industrial.



Contents lists available at ScienceDirect

Journal of Natural Gas Science and Engineering

journal homepage: www.elsevier.com/locate/jngse

Automatized Monte-Carlo analysis of offshore processing of CO₂-rich natural gas: Conventional versus supersonic separator routes

Cristiane São Bento Gonzaga, Lara de Oliveira Arinelli, José Luiz de Medeiros*,
Ofélia de Queiroz F. Araújo

Escola de Química, Federal University of Rio de Janeiro, CT, E, Ilha do Fundão, Rio de Janeiro, RJ, 21941-909, Brazil



ARTICLE INFO

Keywords:

CO₂-Rich natural gas conditioning
Supersonic separator
Membrane permeation
Monte-Carlo analysis
Computer-aided engineering
Interoperability

ABSTRACT

Offshore oil/gas production with high %CO₂ and gas-to-oil ratio impose processing large volumes of CO₂-rich gas. This requires first-of-a-kind designs and creates design uncertainties besides offshore operation uncertainties. Therefore, the design of offshore units under influence of stochastic factors is recommended to avoid oversized worst-case designs or underachieved specifications implying economic/environmental losses. This work presents a novel Computer-Aided Engineering tool, *MCAnalysis*, a VB.NET/XML interoperability framework between HYSYS and MATLAB to statistically assess design performance via Monte-Carlo analysis. Designs of offshore processing of CO₂-rich gas via Conventional-Route and a novel Supersonic-Separator-Route were tested submitting stochastic populations of gas flow rate, %CO₂ and gas-to-oil ratio. Supersonic-Separator-Route presented higher resilience to input overshoots and less necessity of design changes to accomplish specifications in at least 75% of sampled cases compared to Conventional-Route. Supersonic-Separator-Route also showed 15% less average power consumption and hydrocarbons dew-point adjustment with lower %CO₂ in the condensate.

1. Introduction

Offshore processing of natural gas (NG) is susceptible to many severe uncertainties, such as load conditions (Fleshman et al., 2005), sales-gas price and consumer market, equipment and utilities costs (Arellano-Garcia and Wozny, 2009), meteorological events, and even operational risks of submarine devices and oversea processes. Feed composition and flow rate, temperature and pipeline pressure (Diaz et al., 2002; Mesfin and Shuhaimi, 2010) are critical load conditions as their variation effects propagate throughout the plant, disturbing operating conditions and also compromising the attainment of product specifications (Getu et al., 2015).

Some deepwater oil-gas fields as in Brazilian Pre-Salt present additional technology challenges due to elevated gas-oil ratio (GOR) and high CO₂ content, as huge gas flow rates cannot simply be flared (as commonly and freely done 40 years ago) for environmental reasons. In

other words, such CO₂-rich raw NG at high flow rates must be processed and exported, and the huge CO₂ inventory adequately separated and handled.

Large-scale processing of CO₂-rich NG on the topside of offshore rigs aims at increasing NG heating value (Peters et al., 2011), avoiding occupying gas pipeline capacity with inert (e.g., CO₂) and providing a safe destination of CO₂ separated from NG as re-injection fluid for Enhanced Oil Recovery (EOR). Such gas processing must ensure water dew-point adjustment (WDPA) via dehydration, hydrocarbon dew-point adjustment (HCDPA) via removal of propane and heavier hydrocarbons (C₃+), efficient CO₂ removal and huge machinery for dispatching treated gas through pipeline to onshore facilities and for dispatching high-pressure CO₂ to EOR (Araújo et al., 2017). Hence offshore CO₂-rich NG processing requires innovative topside technologies usually with first-of-a-kind designs, which brings uncertainties into discussion derived from the lack of previous similar commercial-scale

Abbreviations: C₃+, Propane and Heavier Alkanes; BSW, Basic-Sediment and Water; CAE, Computer-Aided Engineering; CW, Cooling-Water; EOR, Enhanced Oil Recovery; GOR, Gas-Oil Ratio; HCDP, Hydrocarbon Dew-Point; HCDPA, Hydrocarbon Dew-Point Adjustment; JTE, Joule-Thomson Expansion; LTX, Anti-Hydrate Separator; MC, Monte-Carlo; MMsm³/d, Millions of Standard Cubic Meters per Day; MP, Membrane-Permeation; NG, Natural Gas; PHW, Pressurized-Hot-Water; PR-EOS, Peng-Robinson Equation-of-State; SS, Supersonic Separator; SVLE, Solid-Vapor-Liquid Equilibrium; SW, Seawater; TEG, Triethylene Glycol; VLWE, Vapor-Liquid-Water Equilibrium; VLE, Vapor-Liquid Equilibrium; WDP, Water Dew-Point; WDPA, Water Dew-Point Adjustment; WHRU, Waste-Heat Recovery Unit; XML, eXtensible Markup Language

* Corresponding author.

E-mail addresses: crissbg@gmail.com (C.S.B. Gonzaga), lara.arinelli@gmail.com (L.O. Arinelli), jlm@eq.ufrj.br (J.L. de Medeiros), ofelia@eq.ufrj.br (O.d.Q.F. Araújo).

<https://doi.org/10.1016/j.jngse.2019.102943>

Received 31 March 2019; Received in revised form 2 July 2019; Accepted 14 July 2019

Available online 18 July 2019

1875-5100/ © 2019 Elsevier B.V. All rights reserved.



A Monte Carlo Methodology for Environmental Assessment Applied to Offshore Processing of Natural Gas with High Carbon Dioxide Content

Cristiane S. B. Gonzaga^{*1}, Ofélia de Q. F. Araújo², José L. de Medeiros³

¹School of Chemistry, Federal University of Rio de Janeiro, CT, E, Ilha do Fundão, Rio de Janeiro, RJ, 21941-909, Brazil

e-mail: crissbg@gmail.com

²School of Chemistry, Federal University of Rio de Janeiro, CT, E, Ilha do Fundão, Rio de Janeiro, RJ, 21941-909, Brazil

e-mail: ofelia@eq.ufrj.br

³School of Chemistry, Federal University of Rio de Janeiro, CT, E, Ilha do Fundão, Rio de Janeiro, RJ, 21941-909, Brazil

e-mail: jlmed@eq.ufrj.br

Cite as: Gonzaga, C. S. B., Araújo, O. de Q. F., de Medeiros, J. L., A Monte Carlo Methodology for Environmental Assessment Applied to Offshore Processing of Natural Gas with High Carbon Dioxide Content, J. sustain. dev. energy water environ. syst., DOI: <https://doi.org/10.13044/j.sdewes.d6.0240>

ABSTRACT

Offshore production of oil and natural gas with high carbon dioxide content and high gas-to-oil ratio entail stringent processing conditions that require innovations and first-of-a-kind designs, which bear uncertainties derived from the scarcity of commercial-scale projects, hindering to move along technology learning curves. Consequently, unpredicted scenarios and unachieved specifications cause economic and environmental losses. Such uncertainties force offshore plants to be designed under stochastic factors seeking best statistical performance. The Monte Carlo Method is suitable to such finality. This work proposes a computer-aided engineering framework 'MCAnalysis' automatically applying a probabilistic environmental assessment of offshore gas processing. 'MCAnalysis' integrates HYSYS simulator with 'Waste Reduction Algorithm' to assess potential environmental impacts, whose most relevant categories were identified via Principal Component Analysis. An offshore plant processing natural gas with high carbon dioxide content was submitted to probabilistic raw gas flow rate under two scenarios of carbon dioxide content. The higher carbon dioxide content scenario presented the highest probabilistic potential environmental impacts, being the atmospheric category the most relevant.

KEYWORDS

Environmental assessment, Monte Carlo, Waste reduction algorithm, Principal component analysis, Offshore gas processing, Carbon dioxide rich natural gas.

INTRODUCTION

Offshore Natural Gas (NG) production has been experiencing continuous increase, especially in Brazil, where it is over 36.6 MM Nm³/d [1] as a result of recent discovery of huge oil and gas reserves in deep-water Pre-Salt fields with high Gas-Oil Ratio (GOR) from 250 to 500 Nm³/m³ and high Carbon dioxide (CO₂) content in the associated NG.

^{*} Corresponding author

Salvador Garcia Muñoz, Carl Laird, Matthew Realf (Eds.)

Proceedings of the 9th International Conference on Foundations of Computer-Aided Process Design

July 14th to 18th, 2019, Copper Mountain, Colorado, USA. © 2019 Elsevier B.V. All rights reserved.

<http://dx.doi.org/10.1016/B978-0-12-818597-1.50048-5>

A NOVEL TOOL FOR COMPUTER-AIDED SUSTAINABILITY ASSESSMENT UNDER UNCERTAINTY: A DESIGN CASE OF NATURAL GAS OFFSHORE PROCESSING

Cristiane São Bento Gonzaga*, Ofélia de Queiroz Fernandes Araújo, José Luiz de Medeiros
Federal University of Rio de Janeiro – Brazil
Rio de Janeiro, RJ 21941-909

Abstract

Sustainability assessment under design uncertainties is widely approached through linear sensitivity analysis considering best, average and worst-case scenarios. However, multi-process systems are submitted to varying feedstock conditions, and uncertain environmental and economic scenarios, exhibiting highly non-linear responses when a design is submitted to unpredicted scenarios. Underestimating the influence of uncertainties on critical design responses often leads to economic and environmental performance losses. Therefore, plants subjected to severe uncertainties should be designed under stochastic factors being Monte Carlo Method (MCM) a powerful approach for this purpose. This work presents a novel computer-aided design tool, *MCAnalysis-HUB*, a VB.NET/XML interoperability framework between process simulator Aspen HYSYS and MATLAB, to statistically assess the sustainability performance of process design under uncertainty using MCM. The design of an offshore unit for processing CO₂-rich natural gas (NG) submitted to probabilistic process and economic uncertainties with known Probability Distribution Functions (PDFs) is successfully assessed via MCM analysis to meet all specifications in at least 75% of the sampled cases while reporting sustainability indicators.

Keywords

Monte Carlo Method, Natural gas processing, Sustainability analysis, Computer-Aided Design, Interoperability framework

Introduction

Currently, the process industry is moving towards the design of innovative and more sustainable processes that show improvements in both economic and environmental factors (Tula et al., 2017). Corporations worldwide are realizing that sustainability makes good business sense and is fundamental to their survival and growth (Bakshi, 2003).

For designing more sustainable processes, besides multiple metrics (Sikdar, 2003), multi-criteria analysis (Araújo et al., 2015) and tools to quantify sustainability,

statistical algorithms have been developed to evaluate performance metrics and support decision making (Sikdar et al., 2016). For achieving superior environmental performance, several alternative process flowsheets are generated by combining multiple unit operations, rendering performance assessment of alternatives cumbersome. Therefore, it is beneficial the use of computer-aided design (CAD) methods to evaluate all possible alternatives for defining the most sustainable option (Tula et al., 2017).

* To whom all correspondence should be addressed

0122-1

Offshore Processing of CO₂ Rich Natural Gas: A Monte Carlo Methodology Applied to Assessment of Environmental Performance

Gonzaga, Cristiane São Bento*

Federal University of Rio de Janeiro, Rio de Janeiro, Brazil
e-mail: crissbg@gmail.com

Araújo, Ofélia de Queiroz Fernandes

Federal University of Rio de Janeiro, Rio de Janeiro, Brazil
e-mail: ofelia@eq.ufrj.br

de Medeiros, José Luiz

Federal University of Rio de Janeiro, Rio de Janeiro, Brazil
e-mail: jlm@eq.ufrj.br

ABSTRACT

The consumption of natural gas (NG), considered to be the cleanest fossil fuel, has been continuously increasing worldwide over the recent years, particularly in Brazil due to recent discoveries of huge oil reserves in the ultra-deep water fields of the Pre-Salt Pole, possessing high gas to oil ratio (GOR, from 250 to 500 m³ gas / m³ oil) and high CO₂ content in the associated gas, processed in Floating Production Storage and Offloading units, FPSOs. The stringent conditions are intensified by the initiative of avoiding gas flaring to reduce emissions in oil & gas offshore platforms in Brazil, which lead to a record of processing over 96% of produced gas. This scenario requires innovative topside processes on FPSO – large scale conditioning of CO₂ rich gas in ultra-deep waters, resulting in first of a kind (FOAK) design conceptions. FOAK technologies bear large uncertainties derived from the absence of previous commercial scale projects that promote moving along the technology learning curve. Consequently, worst case scenarios or unachieved product specifications may occur, resulting in economic and environmental losses. Such huge uncertainties demand that the design of NG processing plants located on the topside of the Pre-Salt FPSOs adopts decision techniques under influence of stochastic factors. A classic technique for decision under non-deterministic scenarios is the Monte Carlo Method (MCM). By using techniques from computer-aided engineering (CAE), this work applies MCM for designing offshore NG processing, focusing on assessing the environmental performance of the designed plant. This is accomplished via the development of a computational tool (*MCAnalysis*) that integrates a process simulator (Aspen HYSYS) to a software of environmental impact analysis (WAR, Waste Reduction algorithm) for generation and analysis of process responses under stochastic scenarios, followed by statistical analysis. The proposed MCM is applied to an offshore CO₂ rich NG processing plant, with design submitted to probabilistic feed flow rates, under two scenarios of CO₂ concentration, adopting normal distributions. Deterministic process responses under stochastic inputs were used to assess environmental performance, in association with Principal Component Analysis (PCA) to identify the most relevant indicators to support design decisions. The plant was successfully designed with MCM for both scenarios of CO₂ concentration and the environmental assessment showed that the scenario with higher CO₂ content has higher environmental impact potential with more relevance regarding atmospheric impacts.

O9-7: Conventional Versus Supersonic Separator Routes for Offshore Processing of CO₂-Rich Natural Gas: Sustainability Assessment under Uncertainties via Monte Carlo Analysis

**Cristiana São Bento Gonzaga, José Luiz de Medeiros,
Ofélia de Queiroz F. Araújo**

Escola de Química, Federal University of Rio de Janeiro, CT, Bl. E, Ilha do Fundão, Rio de Janeiro, RJ, 21941-909, Brazil.

Offshore production of oil and CO₂-rich gas with high gas-to-oil ratio requires innovative and first-of-a-kind topside designs. This scenario brings severe uncertainties in the process design, production rate and performance (environmental and economic). Plants submitted to unpredicted scenarios can exhibit highly non-linear responses. Therefore, assessing sustainability considering a best scenario, and average and worst-case scenarios often leads to economic and environmental losses. A sustainability analysis with focus on environmental and economic performance is presented for two offshore plant designs processing CO₂-rich gas. One plant employs conventional gas processing technology (Plant 1), and another uses an innovative supersonic separator (Plant 2), and both are designed under stochastic factors via Monte Carlo analysis. This assessment uses the computer-aided engineering tool MCAAnalysis-HUB, a powerful VB.NET/XML interoperability framework between process simulator Aspen HYSYS and MATLAB, developed by the authors. The plant designs are submitted to stochastic populations influencing process performance – gas flow rate, CO₂ content, and gas-to-oil ratio – and economic scenario – gas and oil prices, and carbon tax. Plant 2 shows superior environmental and economic performance when compared to Plant 1. Both routes were sustainably viable.

**INPI**INSTITUTO
NACIONAL
DA PROPRIEDADE
INDUSTRIAL**INPI**
Assinado
Digitalmente

REPÚBLICA FEDERATIVA DO BRASIL
MINISTÉRIO DA INDÚSTRIA, COMÉRCIO EXTERIOR E SERVIÇOS
INSTITUTO NACIONAL DA PROPRIEDADE INDUSTRIAL
DIRETORIA DE PATENTES, PROGRAMAS DE COMPUTADOR E TOPOGRAFIA DE CIRCUITOS INTEGRADOS

**CERTIFICADO DE REGISTRO
DE PROGRAMA DE COMPUTADOR**

Processo: BR 51 2016 000909-8

O INSTITUTO NACIONAL DA PROPRIEDADE INDUSTRIAL expede o presente Certificado de Registro de Programa de Computador, **válido por 50 anos** a partir de 1º de janeiro subsequente à data de criação indicada, em conformidade com o parágrafo 2º, artigo 2º da Lei Nº 9.609, de 19 de Fevereiro de 1998, e arts. 1º e 2º do Decreto 2.556 de 20 de Abril de 1998.

Título: **MCANALYSIS (APP-VB-XML-HYSYS-MATLAB)**
Criação: 30 de junho de 2014
Titular(es): UNIVERSIDADE FEDERAL DO RIO DE JANEIRO (33.663.683/0001-16)
Autor(es): CRISTIANE SÃO BENTO GONZAGA (111.785.007-21)
JOSÉ LUIZ DE MEDEIROS (495.399.577-53)
OFÉLIA DE QUEIROZ FERNANDES ARAUJO (728.121.337-91)
Linguagem: MATLAB, VISUAL BASIC.NET, XML
Aplicação: EN-03, EN-04
Tipo Prog.: SM-01

DOCUMENTAÇÃO TÉCNICA EM DEPÓSITO SOB SIGILO ATÉ 16/07/2026.

Os Direitos Patrimoniais relativos ao programa de computador objeto do presente registro foram cedidos dos Criadores para o Titular, na data de 09 de setembro de 2014, conforme documentação

A exclusividade de comercialização deste programa de computador não tem a abrangência relativa à exclusividade de fornecimento estatuida pelo art.25, I, da Lei nº8.666, de 21 de Junho de 1993, para fins de inexigibilidade de licitação para compras pelo poder público.
Expedido em 30 de maio de 2017

Assinado digitalmente por:

Julio Cesar Castelo Branco Reis Moreira
Diretor de Patentes, Programas de Computador e Topografia de Circuitos Integrados



15/02/2019 870190015518
11:40

29409191810596670

Pedido de Registro de Programa de Computador - RPC

Número do Processo: 512019000249-0

Dados do Titular

Titular 1 de 1

Nome ou Razão Social: UNIVERSIDADE FEDERAL DO RIO DE JANEIRO

Tipo de Pessoa: Pessoa Jurídica

CPF/CNPJ: 33663683000116

Nacionalidade: Brasileira

Qualificação Jurídica: Instituição de Ensino e Pesquisa

Endereço: Av. Pedro Calmon, 550 - Cidade Universitária

Cidade: Rio de Janeiro

Estado: RJ

CEP: 21941901

País: Brasil

Telefone: (21)37331793

Fax:

Email: agenciadeinovacao@inovacao.ufrj.br

Dados do Programa

Data de Publicação: 01/10/2018

Data de Criação: 01/10/2018

- § 2º do art. 2º da Lei 9.609/98: "Fica assegurada a tutela dos direitos relativos a programa de computador pelo prazo de cinquenta anos contados a partir de 1º de janeiro do ano subsequente ao da sua publicação ou, na ausência desta, da sua criação"

Título: MCAAnalysis-HUB (HUB for Monte Carlo Analysis based on Process Simulations)

**PETICIONAMENTO
ELETRÔNICO**

Esta solicitação foi enviada pelo sistema Petição Eletrônica em 15/02/2019 às 11:40, Petição 870190015518

APPENDIX B – CAE tool *MCAnalysis*-HUB User Manual

This session show a preliminary version the User Manual in development for the CAE tool *MCAnalysis*- HUB. The session to describe the configuration of the module “Economic Performance” is under development.”

MCAnalysis-HUB (version 1.0.0) – User Manual

Table of Contents

1.	Introduction	149
2.	Scope of Document	149
3.	Abbreviations	149
4.	<i>MCAnalysis</i> -HUB Architecture Overview.....	149
5.	<i>MCAnalysis</i> -HUB Initialization.....	152
6.	Module “Generate Batch Data”	153
6.1.	XML Configuration Parameters File.....	154
6.2.	XML Read Library File.....	159
6.3.	XML Output File	161
6.4.	MATLAB histograms files of input variables	163
7.	Module “Environmental Performance”	164
7.1.	XML Configuration Parameters file.....	165
8.	Module “Economic Performance”	169
8.1.	Configuration XMLs.....	170
9.	Module “Monte Carlo Analysis”	171
9.1.	XML MC Parameters.....	171
9.2.	MATLAB histograms files of output variables	174

0	02-Sep-2019	Initial Revision	São Bento Gonzaga, Cristiane
Rev.	Date	Description	Author

1. Introduction

MCAnalysis-HUB is a Computer-Aided Engineering (CAE) tool to perform process design, environmental and economic assessments under process and economic uncertainties via automatized Monte Carlo analysis based on process simulations.

The current version of *MCAnalysis*-HUB supports process simulations developed in Aspen HYSYS from AspenTech.

2. Scope of Document

This document describes the usage and of *MCAnalysis*-HUB version 1.0.0.

3. Abbreviations

API – Application Programming Interface
 CAE – Computer-Aided Engineering
 CAPEX – Capital Expenditures
 CAS – Chemical Abstracts Service
 CDF – Cumulative Distribution Function
 GUI – Graphical User Interface
 OPEX – Operational Expenditures
 PDF – Probabilistic Distribution Function
 VB.net – Visual Basic.NET
 WAR – Waste Reduction
 XML – eXtensible Markup Language

4. *MCAnalysis*-HUB Architecture Overview

In order to handle complex models, research has focused on developing computational tools for data exchange and interoperability among software. This is the outline of CAE tool *MCAnalysis*-HUB, designed in a modular architecture for dissociating technology models from analysis modules, since this type of arrangement enables assemblage of different software in a superstructure (HUB) for subsequent larger and more complete analysis (Laurence and Maréchal, 2012). *MCAnalysis*-HUB is developed in Visual Basic.NET (VB.net) framework due to its good operability with the Application Programming Interface (API) of process simulator Aspen HYSYS.

MCAnalysis-HUB automatically executes MC analysis on complex process flowsheets by integrating the following steps via eXtensible Markup Language (XML), known as key language to exchange multiple varieties of data in the web and in applications: (i) generation of normal random samples of process input variables with uncertainties using Eq. (21); (ii) management of HYSYS to provide samples of process output variables to the samples of process input variables; (iii) assessment of environmental performance to the samples of process input variables with Waste Reduction (WAR) algorithm; (iv) assessment of environmental performance to the samples of process input variables combined with samples of economic

input variables also generated via step (i); and (v) processing and handling of MC results statistically and graphically with MATLAB.

The modular architecture of *MCAnalysis-HUB* (Figure 1) starts with module “Generate Batch Data”, which: (i) processes a configurable XML file (Simulation Configuration XML) containing definition of the MCM non-deterministic independent input variables, their respective PDFs and their identification within HYSYS; (ii) randomly generates samples of the inputs (uncertainties); (iii) graphically processes input samples in MATLAB, generating histograms and PDFs; and (iv) executes HYSYS simulation of process flowsheet in batch mode for each sample of input variables, storing the relevant attributes for MC analysis (process output variables), listed in a configuration XML file (Attributes XML), in an output XML file (HYSYS output XML).

For assessing environmental performance, HYSYS Output XML is processed by module “Environmental Indicators” together with a configurable XML (WAR Configuration XML), extracted from HYSYS, containing a list of components, input and output streams (process and energy) data, where process output streams are classified by the user as product or outlet waste. This module uses WAR algorithm data to generate an XML file (WAR output) containing statistics PEIs responses to process input variables in MC sampling.

Assessment of economic performance starts with equipment sizing in module “Economic Analysis”, which (i) processes a configurable XML file (Equip. Sizing Configuration XML), extracted from HYSYS, containing equipment data from base-case; and (ii) executes equipment sizing and generates an output XML file with results (Equipment Sizing Output XML). No process input variables with uncertainties are considered at this stage. Next step (iv) uses this output XML file together with two configurable XML files (CAPEX Configuration XML and CAPEX Uncertainties XML) for (v) calculating CAPEX considering uncertainties (CAPEX XML). Last step of this module is (vi) to calculate OPEX and economic indicators and store results in an XML file (Economic Analysis Output XML) by (iv) processing CAPEX XML file and two configurable XML files (OPEX & Economic Indicator Configuration XML and Economic Uncertainties XML). This step considers economic input variables with uncertainties on raw material, products, energy, and waste treatment prices to cover market fluctuations. Carbon tax is also considered as a pertinent economic variable with high level of uncertainty, as discussions on how to best predict such costs are a global topic. The same engine for handling input variables with uncertainties used in module “Generate Batch Data” (steps ii and iii) is also used in this module.

Finally, module “MCM Analysis – Monte Carlo Analysis” performs MC analysis itself, and this single module covers process design, environmental and economic assessments. Such setup is feasible due to the interoperability architecture of *MCAnalysis-HUB*; as output files from all the three modules are produced with the same node structure. This module (i) processes the output XML file containing the batch process response data (process design, environmental or economic results) with a configurable XML (MCM Configuration XML) containing the output variables relevant for MC analysis as well as their maximum/minimum specifications; and (ii) generates graphical Monte Carlo analysis in MATLAB as simple/cumulative frequency histograms, PDF and CDF curves and percentage of specification-attainment achieved by sampled cases.

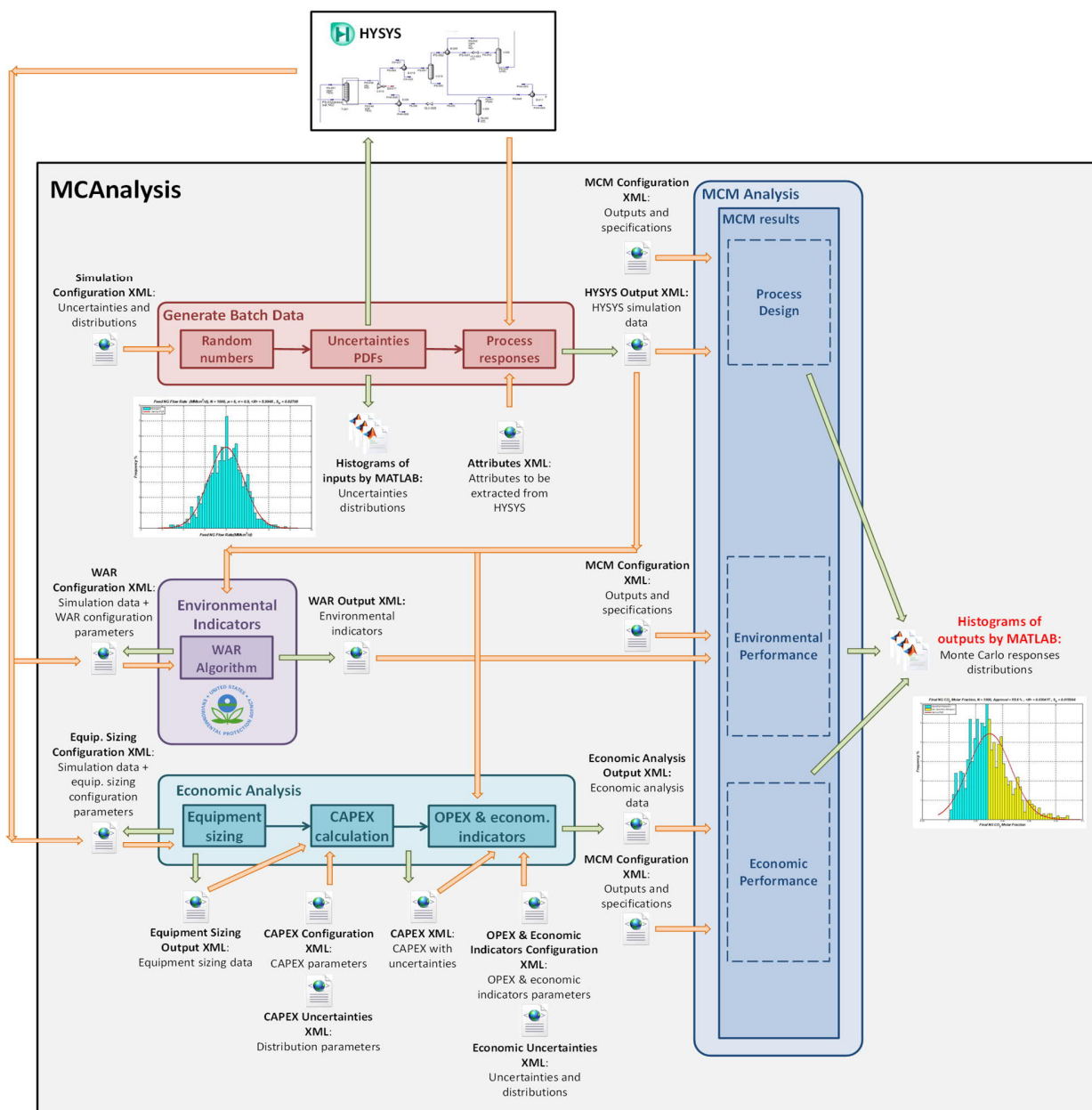


Figure 1. MCAAnalysis-HUB modular architecture.

5. *MCAnalysis*-HUB Initialization

MCAnalysis-HUB starts with language settings (Figure 2). Language selection defines the language of *MCAnalysis*-HUB graphical user interface (GUI) and of output graphical files in MATLAB. The following languages are available:

- English;
- Portuguese.

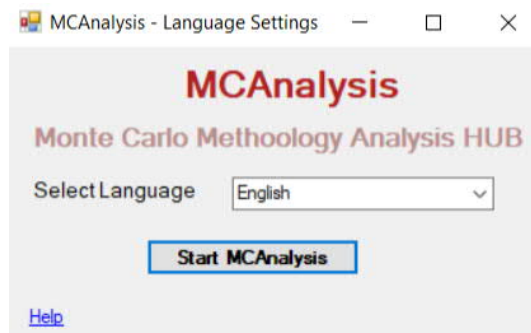


Figure 2. *MCAnalysis*-HUB – Selection of language GUI.

Next step is selection of the desired module of *MCAnalysis*-HUB (Figure 3).

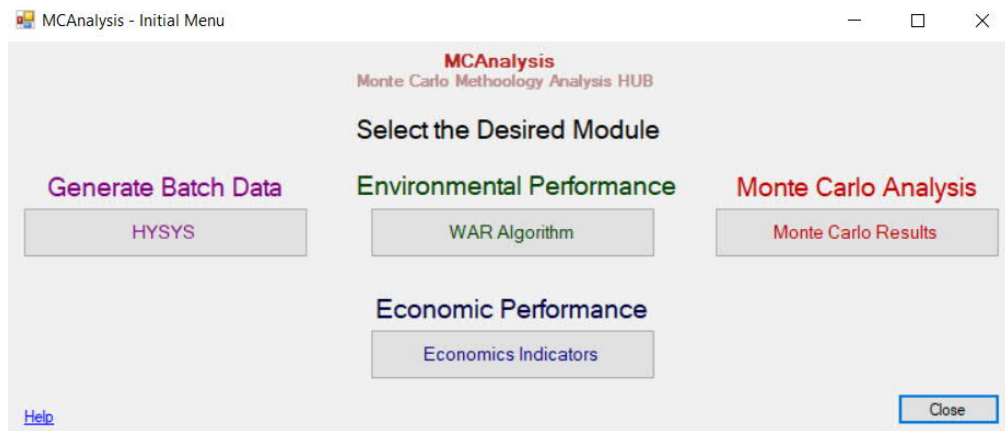


Figure 3. *MCAnalysis*-HUB – Selection of module GUI.

6. Module “Generate Batch Data”

Module “Generate Batch Data” (Figure 4) is responsible for generating batch data from process simulation under process uncertainties.

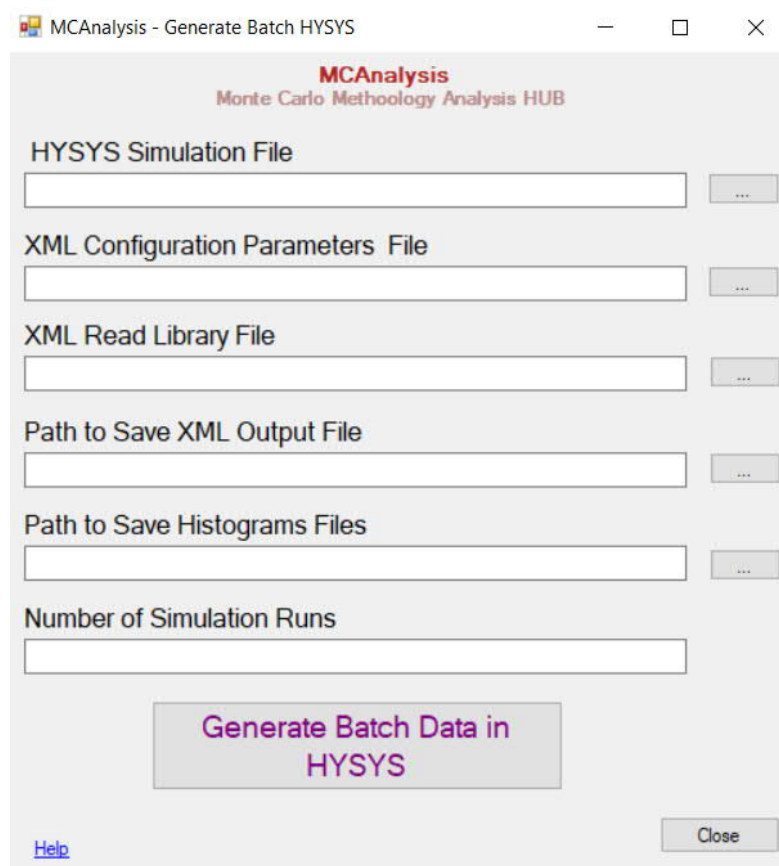


Figure 4. Module “Generate Batch Data” GUI.

This module requires the following inputs from the user:

- **HYSYS Simulation File:** File containing the process simulation in software Aspen HYSYS. This file has an “.hsc” extension and contains the target process simulation for executing automatized Monte Carlo analysis under uncertainties.
- **XML Configuration Parameters File:** XML file containing the configuration parameters for the uncertainties in process inputs and how they are connected to the process simulation. The content of this XML file and how to configure it is detailed in Sec. 6.1.
- **XML Read Library File:** XML file containing the relevant attributes to be extracted from the process simulation and stored for Monte Carlo analysis. It is important to consider that attributes relevant for process design and for environmental and economic assessments shall be included in this file. The content of this XML file and how to configure it are detailed in Sec. 6.2.
- **Path to Save Output XML file:** Path to save the Output XML file containing the results from the process simulation considering uncertainties in process inputs. This file lists all

the output variables from the process simulation necessary for the subsequent Monte Carlo Analysis (process design, environmental and economic assessments). The content of this XML file is detailed in Sec. 6.3.

- **Path to Save Histograms files:** Path to save the histograms of input variables in MATLAB format. Such histograms are detailed in Sec. 6.4
- **Number of Simulation runs:** Amount of process simulations runs to be considered for the Monte Carlo analysis. This number corresponds to the amount of independent pseudo-random number shall be generated to each process input variable influenced by uncertainties.

6.1. XML Configuration Parameters File

The Configuration XML file is structured to provide process uncertainties (input variables) and how they relate to process simulation objects. The input variables are defined as below:

- **Monte Carlo:** Stochastic process uncertainties variables targeted for Monte Carlo analysis. These variables are random, independent from each other and follow a probabilistic distribution function (PDF):
 - **Direct:** These variables correspond to editable attributes of simulation objects, which can be written directly in the simulation;
 - **Indirect:** These variables do not correspond to editable attributes of simulation objects and shall be written in the simulation through auxiliary variables, which can be written directly in the simulation;
- **Expression:** These variables correspond to editable attributes of simulation objects. However, they are not carrying any process uncertainties themselves. They are influenced by Monte Carlo variables, and they can either be influenced by one or multiple Monte Carlo Direct and Indirect variables, or they can be used as auxiliary variables to input Monte Carlo Indirect variables in the simulation.

This version (v1.0.0) supports only input variables following Normal PDFs. Therefore, the structures of the XML node described in this section consider parameters applicable for defining Normal PDFs.

The node structure of the Configuration XML file depends on the type of input variable and the XML starts with the main node <Variables>, which is composed by the nodes <Variable>, corresponding to each input variable of the Monte Carlo Analysis.

Numeric values must always use decimal separators as defined in the language settings of the computer executing *MCA*alysis-HUB.

Monte Carlo Direct Variables:

The node structure for **Monte Carlo Direct** variables is shown in Figure 5 and an example of the node <Variable> of the XML file is depicted in Figure 6.

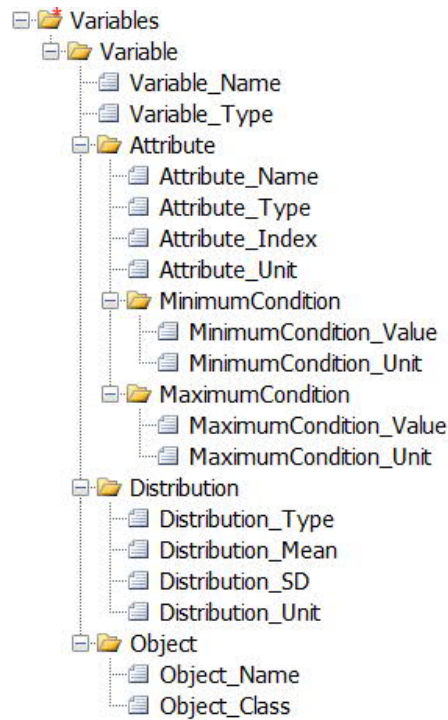


Figure 5. Node structure of XML Configuration Parameters for Monte Carlo Direct Variables.

```

<Variable>
  <Variable_Name>CO_2 Molar Fraction</Variable_Name>
  <Variable_Type>Monte_Carlo_Direct</Variable_Type>
  <Attribute>
    <Attribute_Name>ComponentMolarFraction</Attribute_Name>
    <Attribute_Type>RealFlexVariable</Attribute_Type>
    <Attribute_Index>3</Attribute_Index>
    <Attribute_Unit>NA</Attribute_Unit>
    <MinimumCondition>
      <MinimumCondition_Value>0,35</MinimumCondition_Value>
      <MinimumCondition_Unit>NA</MinimumCondition_Unit>
    </MinimumCondition>
    <MaximumCondition>
      <MaximumCondition_Value>0,55</MaximumCondition_Value>
      <MaximumCondition_Unit>NA</MaximumCondition_Unit>
    </MaximumCondition>
  </Attribute>
  <Distribution>
    <Distribution_Type>Normal</Distribution_Type>
    <Distribution_Mean>0,45</Distribution_Mean>
    <Distribution_SD>0,03</Distribution_SD>
    <Distribution_Unit>NA</Distribution_Unit>
  </Distribution>
  <Object>
    <Object_Name>PS-001 (dry inlet NG)</Object_Name>
    <Object_Class>MaterialStreams</Object_Class>
  </Object>
</Variable>
  
```

Figure 6. Example of node <Variable> of XML Configuration Parameters for Monte Carlo Direct Variables.

The values to be filled in for each node are described below:

- **Variable_Name:** Name of the variable defined by the user;
- **Variable_Type:** Defines which type of variable. The value “Monte_Carlo_Direct” shall be selected;
- **Attribute:** Collection of information relevant to the mapping of the attribute of the process simulation:
 - **Attribute_Name:** Name of the attribute to be written in the simulation as defined by the process simulator API (application programming interface);
 - **Attribute_Type:** Type of the attribute as defined by the process simulator API. The most relevant types are:
 - “RealVariable”: The attribute contains a value and a unit of measurement (when applicable);
 - “RealFlexVariable”: The attribute contains an array of values and a unit of measurement (when applicable);
 - **Attribute_Index:** Applicable only to attributes type “RealFlexVariable” to indicate the position of the variable in the array (integer number, starting from 0). For attributes type “RealVariable”, this field shall be filled in with the value “NA”.
 - **Attribute_Unit:** Unit of the attribute as string defined by the process simulator API;
- **MinimumCondition:** Collection of information relevant to the minimum conditions of the distribution and is an optional node for information. This node is not processed by *McAnalysis-HUB*:
 - **MinimumCondition_Value:** Minimum value that the variable can achieve;
 - **MinimumCondition_Unit:** Unit of the minimum value that the variable can achieve;
- **MaximumCondition:** Collection of information relevant to the maximum conditions of the distribution and is an optional node for information. This node is not processed by *McAnalysis-HUB*:
 - **MaximumCondition_Value:** Maximum value that the variable can achieve;
 - **MaximumCondition_Unit:** Unit of the maximum value that the variable can achieve;
- **Distribution:** Collection of the information relevant to the distribution of the variable:
 - **Distribution_Type:** Type of the distribution. The value “Normal” shall be used, since this is the only distribution currently available;
 - **Distribution_Mean:** Value of the mean μ of the Normal distribution;
 - **Distribution_SD:** Value of the standard deviation σ of the Normal distribution;
 - **Distribution_Unit:** Unit of both μ and σ of the Normal distribution as string defined by the process simulator API;
- **Object:** Collection of the information relevant to the mapping of the object of the process simulation:
 - **Object_Name:** Name of the object containing the attribute to be written in the simulation as defined in the process simulation;
 - **Object_Class:** Class of the object as defined by the process simulator API;

Monte Carlo Indirect Variables:

The node structure for **Monte Carlo Indirect** variables is shown in Figure 7 and an example of the node <Variable> the XML file in Figure 8.

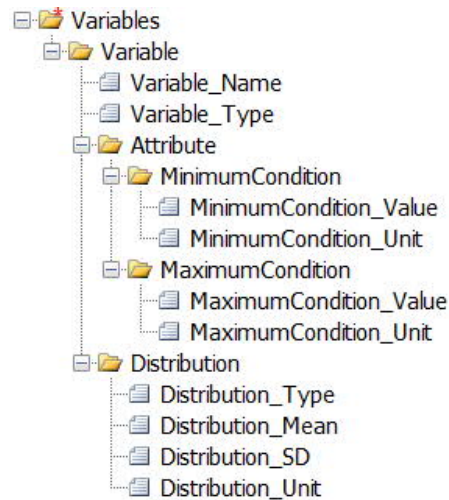


Figure 7. Node structure of XML Configuration Parameters for Monte Carlo Indirect Variables.

```

<Variable>
  <Variable_Name>NG Flow Rate</Variable_Name>
  <Variable_Type>Monte_Carlo_Indirect</Variable_Type>
  <Attribute>
    <MinimumCondition>
      <MinimumCondition_Value>3</MinimumCondition_Value>
      <MinimumCondition_Unit>Mm3/d</MinimumCondition_Unit>
    </MinimumCondition>
    <MaximumCondition>
      <MaximumCondition_Value>9</MaximumCondition_Value>
      <MaximumCondition_Unit>Mm3/d</MaximumCondition_Unit>
    </MaximumCondition>
  </Attribute>
  <Distribution>
    <Distribution_Type>Normal</Distribution_Type>
    <Distribution_Mean>6</Distribution_Mean>
    <Distribution_SD>0,9</Distribution_SD>
    <Distribution_Unit>Mm3/d</Distribution_Unit>
  </Distribution>
</Variable>
  
```

Figure 8. Example of node <Variable> of XML Configuration Parameters for Monte Carlo Indirect Variables.

Monte Carlo Indirect variables contain the same nodes as Monte Carlo Direct variables, except for the nodes to map attribute and object in the process simulation.

The value “Monte_Carlo_Indirect” shall be selected for the node <Variable_Type>.

Expression Variables:

The node structure for **Expression** variables is shown in Figure 9 and an example of the node <Variable> XML file in Figure 10.

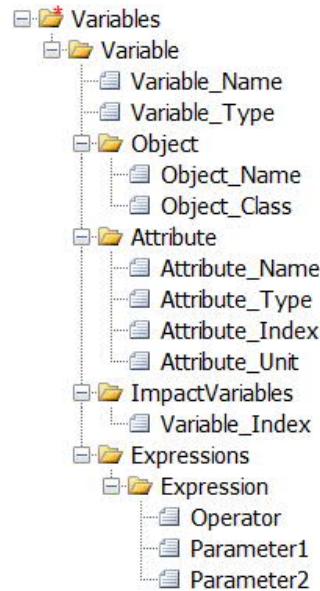


Figure 9. Node structure of XML Configuration Parameters for Expression Variables.

```

<Variable>
  <Variable_Name>NG Std. Volume Flow</Variable_Name>
  <Variable_Type>Expression</Variable_Type>
  <Object>
    <Object_Name>PS-001 (dry inlet NG)</Object_Name>
    <Object_Class>MaterialStreams</Object_Class>
  </Object>
  <Attribute>
    <Attribute_Name>StdLiqVolFlow</Attribute_Name>
    <Attribute_Type>RealVariable</Attribute_Type>
    <Attribute_Index>NA</Attribute_Index>
    <Attribute_Unit>m3/h</Attribute_Unit>
  </Attribute>
  <ImpactVariables>
    <Variable_Index>1</Variable_Index>
  </ImpactVariables>
  <Expressions>
    <Expression>
      <Operator>Multiply</Operator>
      <Parameter1>41666,67</Parameter1>
      <Parameter2>Variable_1</Parameter2>
    </Expression>
  </Expressions>
</Variable>
  
```

Figure 10. Example of node <Variable> of XML Configuration Parameters for Expression Variables.

Expression variables contain the same node structures as the Monte Carlo Direct variables to map attribute and object in the process simulation. However, the nodes related to the distribution are replaced by nodes to indicate which variables in the XML are correlated to the expression variable and to calculate result of the expression variable, as listed below:

- **ImpactVariables:** Collection of variables from the XML which impact the expression variable:
 - **Variable_Index:** Position of the impact variable in the XML (integer number, starting from zero). Multiple nodes of variable indexes can be listed;
- **Expressions:** Collection of expressions to calculate the value of the expression variable:
 - **Expression:** Collection of expression parameters. Multiple nodes of expressions can be listed and Each expression is executed in the sequence presented in the XML: Each expression consists of one operator and two parameters:
 - **Operator:** Operator to be executed between Parameter1 and Parameter2, in this sequence. The following operators can be selected: “Sum”, “Deduct”, “Multiply”, “Divide”;
 - **Parameter1:** First parameter to be executed by the expression calculation. It can be a constant number, an impact variable, or the result of a previous expression. To define an impact variable, the value “Variable_X”, shall be selected. To define the result of an expression, the value “Expression_X” shall be selected. X in an integer number, starting with zero, corresponding to the position of the variable or of the expression in the XML;
 - **Parameter2:** Second parameter to be executed by the expression calculation. The same premises defined for Parameter1 apply.

The value “Expression” shall be selected for the node <Variable_Type>.

6.2. XML Read Library File

This XML files contains the attributes from the process simulation relevant for process design and for environmental and economic assessments.

It is structured in the following classes of attributes:

- Process streams;
- Components of process streams;
- Energy streams;
- Operation (one structure per operation type, since the attributes are specific to operation type).

The node structure of this XML is shown in Figure 11 and an example of the node <Collection> XML file in Figure 12.

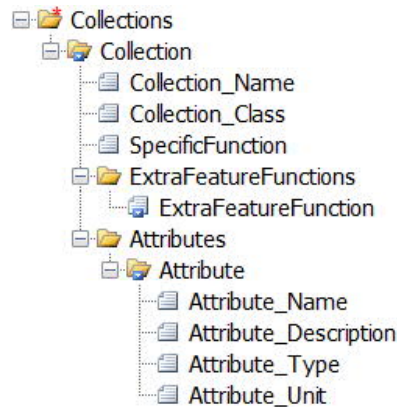


Figure 11. Node structure of XML Read Library.

```

<Collection>
  <Collection_Name>Process Streams</Collection_Name>
  <Collection_Class>MaterialStreams</Collection_Class>
  <SpecificFunction>NA</SpecificFunction>
  <ExtraFeatureFunctions>
    <ExtraFeatureFunction>CalculateWDP</ExtraFeatureFunction>
    <ExtraFeatureFunction>CalculateHCDF</ExtraFeatureFunction>
  </ExtraFeatureFunctions>
  <Attributes>
    <Attribute>
      <Attribute_Name>Temperature</Attribute_Name>
      <Attribute_Description>Temperature</Attribute_Description>
      <Attribute_Type>RealVariable</Attribute_Type>
      <Attribute_Unit>C</Attribute_Unit>
    </Attribute>
    <Attribute>
      <Attribute_Name>Pressure</Attribute_Name>
      <Attribute_Description>Pressure</Attribute_Description>
      <Attribute_Type>RealVariable</Attribute_Type>
      <Attribute_Unit>bar</Attribute_Unit>
    </Attribute>
    <Attribute>
      <Attribute_Name>MassFlow</Attribute_Name>
      <Attribute_Description>Mass Flow</Attribute_Description>
      <Attribute_Type>RealVariable</Attribute_Type>
      <Attribute_Unit>kg/h</Attribute_Unit>
    </Attribute>
    <Attribute>
      <Attribute_Name>MolarFlow</Attribute_Name>
      <Attribute_Description>Molar Flow</Attribute_Description>
      <Attribute_Type>RealVariable</Attribute_Type>
      <Attribute_Unit>kgmole/h</Attribute_Unit>
    </Attribute>
    <Attribute>
      <Attribute_Name>StdLiqVolFlow</Attribute_Name>
      <Attribute_Description>Standard Volume Flow</Attribute_Description>
      <Attribute_Type>RealVariable</Attribute_Type>
      <Attribute_Unit>m3/h</Attribute_Unit>
    </Attribute>
    <Attribute>
      <Attribute_Name>IdealLiquidVolumeFlow</Attribute_Name>
      <Attribute_Description>Volume Flow</Attribute_Description>
      <Attribute_Type>RealVariable</Attribute_Type>
      <Attribute_Unit>m3/h</Attribute_Unit>
    </Attribute>
    <Attribute>
      <Attribute_Name>MassLowerHeatValue</Attribute_Name>
      <Attribute_Description>Mass Lower Heat Value</Attribute_Description>
      <Attribute_Type>RealVariable</Attribute_Type>
      <Attribute_Unit>KJ/kg</Attribute_Unit>
    </Attribute>
  </Attributes>
</Collection>
  
```

Figure 12. Example of node <Collection> of XML Read Library.

The XML starts with the main node “Collections”, which is composed by the nodes “Collection” corresponding to each collection of attributes to be extracted from the process simulation.

The values to be filled in for each node are described below:

- **Collection_Name**: Name of the attributes collection defined by the user;
- **Collection_Class**: Class of the object which the attributes shall be read from, as defined by the process simulator API;
- **SpecificFunction**: Specific function to cover cases that the parameters of the collection cannot be read through a generic reading function. The value of this node must be written as hardcoded in *McAnalysis-HUB*. The following specific functions are currently available: “ReadComponentsData” and “ReadUserVariableData”. This function is used to read all attributes defined in the “Attributes” node.
- **ExtraFeatureFunctions**: Collection of functions to extract data when calculations are needed to provide the target value, once the target value is not a direct data extracted from the process simulation:
 - **ExtraFeatureFunction**: Name of the function as hardcoded in *McAnalysis-HUB*. The following extra feature functions are available: “CalculateWDP” and “CalculateHCDP”. They are used to extract Water Dew Point (WDP) and Hydrocarbons Dew Point (HCDP) from the HYSYS simulation via property correlation of the process stream object.
- **Attributes**: Collection of attributes to be extracted from the process simulation
 - **Attribute**: Collection of information relevant to the mapping of the attribute of the process simulation:
 - **Attribute_Name**: Name of the attribute to be written in the simulation as defined by the process simulator API (application programming interface);
 - **Attribute_Type**: Type of the attribute as defined by the process simulator API. The most relevant types are:
 - “RealVariable”: The attribute contains a value and a unit of measurement (when applicable);
 - “RealFlexVariable”: The attribute contains an array of values and a unit of measurement (when applicable);
 - “UserVariable”: Customized attributes for objects of the simulation;
 - **Attribute_Index**: Applicable only to attributes type “RealFlexVariable” to indicate the position of the variable in the array (integer number, starting from 0). For attributes type “RealVariable”, this field shall be filled in with the value “NA”.
 - **Attribute_Unit**: Unit of the attribute as string defined by the process simulator API.

6.3. XML Output File

This XML file contains the relevant data extracted from the process simulation for process design and for environmental and economic assessments. It is structured to organize the data per run with uncertainties.

This file is the input file to the Monte Carlo analysis performed by the Module “Monte Carlo Analysis” and to the modules “Environmental Performance” and “Economic Performance”, which also produce output XML files with the same node structured of this output XML file to be consumed by the module “Monte Carlo Analysis”.

The node structure of this XML is shown in Figure 13.

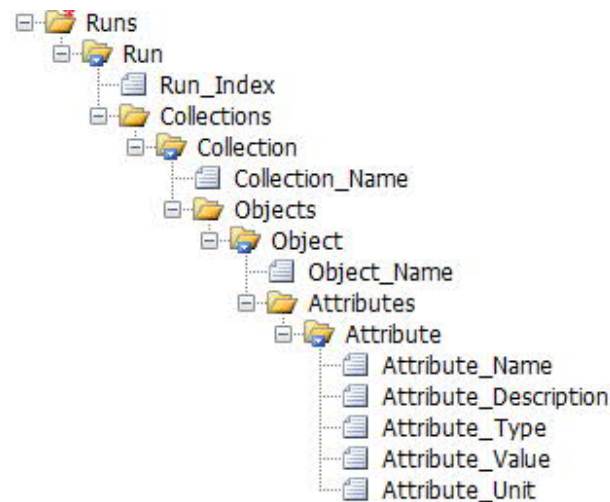


Figure 13. Node structure of XML Output File.

The XML starts with the main node “Runs”, which is composed by the nodes “Run” corresponding to the output data of each run of the process simulation.

The values to be filled in for each node are described below:

- **Run_Index:** Index of the run;
- **Collections:** Collection of the nodes referring to all pertinent collections:
 - **Collection:** Collection of properties of the collection:
 - **Collection_Name:** Name of the collection;
 - **Objects:** Collection of the nodes referring to all pertinent objects of the collection:
 - **Object:** Collection of object properties:
 - **Object_Name:** Name of the object;
 - **Attributes:** Collection of the nodes referring to all pertinent attributes of the object:
 - **Attribute_Name:** Name of the attribute;
 - **Attribute_Description:** Description of the attribute;
 - **Attribute_Type:** Type of the attribute. The most relevant types are:
 - “RealVariable”: The attribute contains a value and a unit of measurement (when applicable);

- “RealFlexVariable”: The attribute contains an array of values and a unit of measurement (when applicable);
- “UserVariable”: Attributes customized by the user for objects of the simulation;
- “String”: The attribute contains a string value.

6.4. MATLAB histograms files of input variables

Simple frequency histograms and PDF curves of the input variables under uncertainties with headers informing number of samples, PDF parameters (μ, σ), sample average $\langle X \rangle$ and sample standard deviation S_X are generated. Figure 14 shows an example.

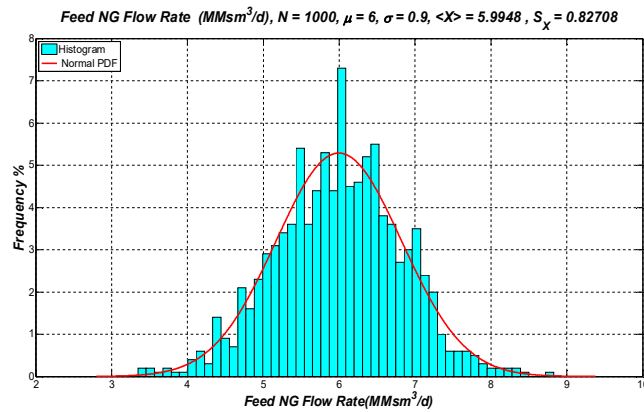


Figure 14. Example of MATLAB Histogram File Monte Carlo analysis input variables.

7. Module “Environmental Performance”

Module “Environmental Performance” (Figure 15) is responsible assessing environmental performance via WAR algorithm based on the process simulation output data considering uncertainties on the process input variables.

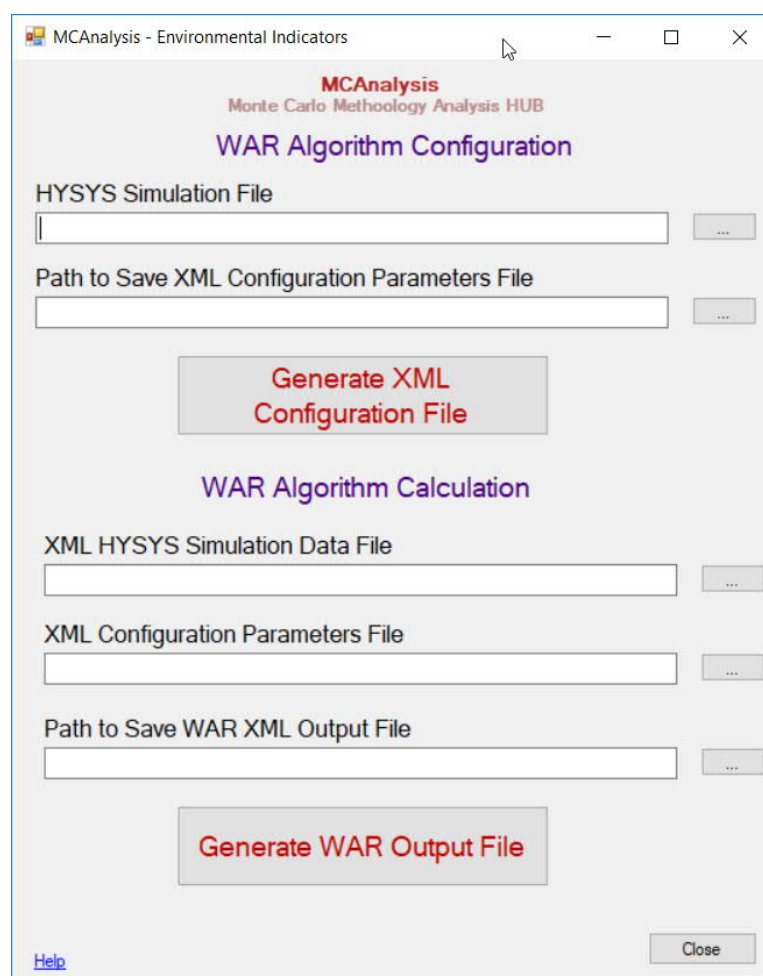


Figure 15. Module “Environmental Performance” GUI.

This module requires the following inputs from the user:

- **HYSYS Simulation File:** File containing the process simulation in software Aspen HYSYS. This file has an “.hsc” extension and contains the target process simulation for Monte Carlo analysis.
- **Path to Save XML Configuration Parameters file:** Path to save the Configuration XML file containing the configuration parameters for the WAR algorithm based on data extracted from the process simulation. The content of this XML file is detailed in Sec.7.1.
- **XML HYSYS Simulation Data File:** Output XML file containing the batch results from the process simulation considering uncertainties in process inputs.

- **Path to Save WAR XML Output file:** Path to save the WAR Output XML file containing the indicators for environmental performance assessment considering uncertainties in process inputs. This XML file has exactly the same node structure of the XML Output file from module “Generate Batch Data” detailed in Sec. 6.3.

7.1. XML Configuration Parameters file

This XML files contains configuration data necessary for the WAR algorithm. The node structure is shown in Figure 16.

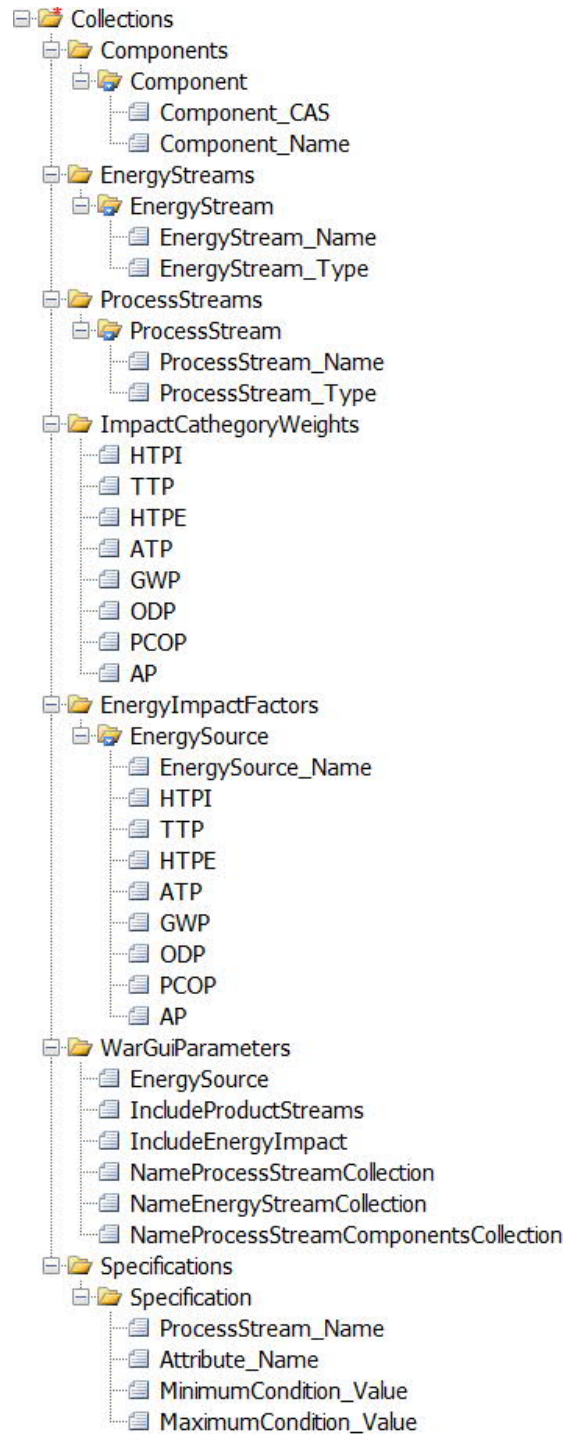


Figure 16. Node structure of XML Configuration Parameters for Environmental Assessment.

The XML starts with the main node “Collections”, corresponding to collection of necessary data for the WAR algorithm.

The values to be filled in for each node are described below:

- **Components:** Collection of components present in the process simulation:
 - **Component:** Collection of information relevant to the component:
 - **Component_CAS:** CAS (Chemical Abstracts Service) number of the component for mapping with WAR algorithm data;
 - **Component_Name:** Component name as defined by the process simulator API;
- **EnergyStreams:** Collection of energy streams present in the process simulation:
 - **EnergyStream:** Collection of information relevant to the energy stream:
 - **EnergyStream_Name:** Energy stream name;
 - **EnergyStream_Type:** Type of energy stream calculated based on the process simulation: "Inlet" or "Outlet".
- **ProcessStreams:** Collection of process streams present in the process simulation:
 - **EnergyStream:** Collection of information relevant to the process stream:
 - **EnergyStream_Name:** Process stream name;
 - **EnergyStream_Type:** Type of process stream calculated based on the process simulation: "Inlet" or "Outlet". "Outlet" streams must be classified by the user among "Product" or "Outlet Waste", as this information is not extracted from the process simulation.
- **ImpactCategoryWeights:** Collection node for impact factors for each potential impact (HTPI, TTP, HTPE, ATP, GWP, OPD, PCOP and AP). The default factor is 1 to select the same weight for all the impacts, and this setting can be changed according to the user's needs;
- **EnergyImpactFactors:** Collection node for energy factors for each potential impact for each type of fuel (coal, gas and oil) according to data from WAR algorithm and it is not recommended to change this setting;
- **WARGuiParameters:** Collection node for information relevant to the WAR algorithm calculation:
 - **EnergySource:** "Coal", "Gas" or "Oil";
 - **IncludeProductsStreams:** "Yes" or "No". Define if the impacts of product streams shall be included to calculate output potential impacts;
 - **IncludeEnergyImpact:** "Yes" or "No". Define if the impacts of energy generation shall be included to calculate output potential impacts;
 - **NameEnergyStreamCollection:** Name of the collection of energy streams as available in the Output XML file containing the batch results from the process simulation;
 - **NameProcessStreamComponentsCollection:** Name of the collection of process streams as available in the Output XML file containing the batch results from the process simulation;
- **Specifications:** This node is used if any product stream shall be considered as outlet waste if specifications are not achieved and corresponds to the collection node for process stream specifications:

- **Specification:** Collection node for information relevant process stream specification:
 - **ProcessStream_Name:** Name of process stream. One stream can be associated to multiple specifications;
 - **Attribute_Name:** Name of the attribute containing the specification according to the process simulator API;
 - **MinimumCondition_Value:** Specification of minimum condition. If not applicable, "NA" shall be used;
 - **MaximumCondition_Value:** Specification of maximum condition. If not applicable, "NA" shall be used.

Nodes <Components>, <EnergyStreams> and <ProcessStreams> are extracted directly from HYSYS.

Nodes < ImpactCategoryWeights>, <EnergyImpactFactors>, < WarGuiParameters> and <Specifications> must be inserted in the XML file extracted from the simulation.

8. Module “Economic Performance”

Module “Economic Performance” is responsible assessing economic performance based on the process simulation output data considering uncertainties on the process input variables combined with uncertainties in economic input variables.

This chapter is under development. The GUIs available for this module are depicted in Figures 17-19.

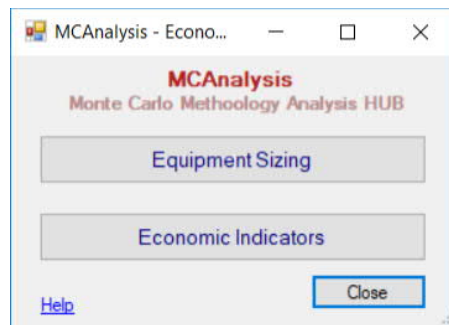


Figure 17. Module “Economic Analysis” GUI: Select “Equipment Sizing” or “Economic Indicators”.

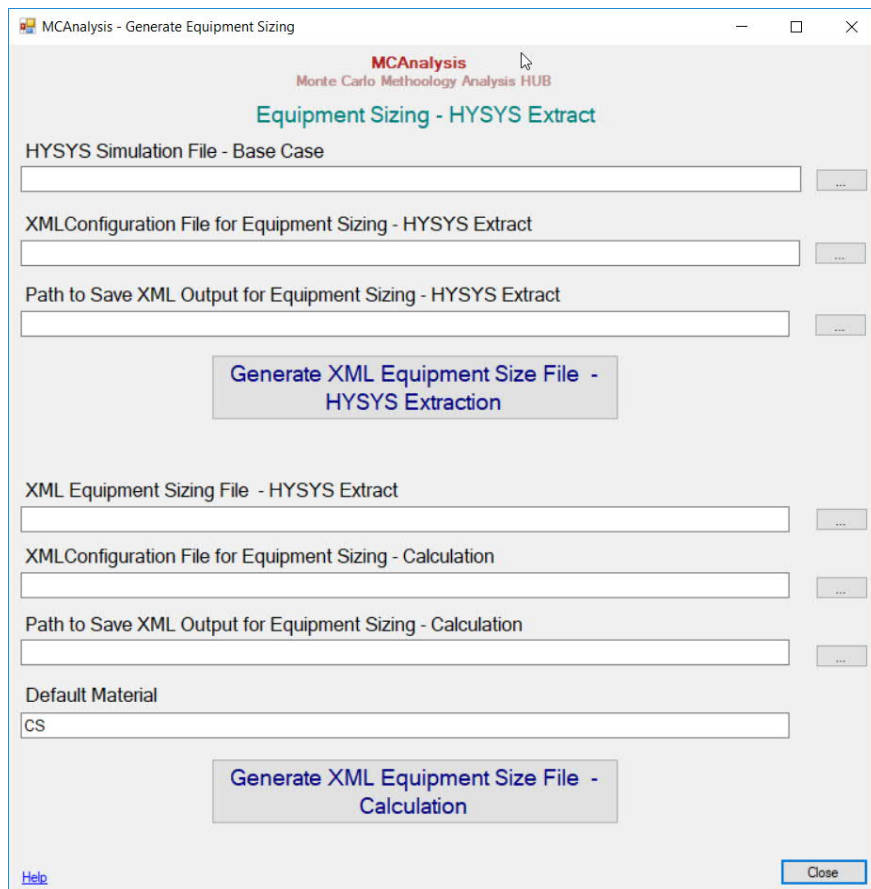


Figure 18. Module “Economic Analysis” GUI “Equipment Sizing”.

MCAnalysis - Generate Economic Indicators

MCAnalysis
Monte Carlo Methodology Analysis HUB

CAPEX Calculation

XML Equipment Sizing File

XML Configuration File for CAPEX Calculation

Path to Save XML Output for CAPEX Calculation

☐ Include Uncertainties

XML Configuration File for CAPEX Uncertainties

Number of Uncertainties

Generate XML CAPEX Calculation

OPEX, Cash Flow and Economic Indicators Calculation

HYSYS Simulation File

Path to Save XML Configuration for HYSYS Simulation

Generate XML Simulation Configuration

XML HYSYS Simulation Data File

XML Configuration File for HYSYS Simulation

XML CAPEX Calculation File

XML Configuration File for OPEX, Cash Flow and Economic Indicators

Path to Save XML Output for OPEX, Cash Flow and Economic Indicators Calculation

Generate XML OPEX, Cash Flow and Economic Indicators Calculation

Help

Close

Figure 19. Module “Economic Analysis” GUI “Economic Indicators”.

8.1. Configuration XMLs

This chapter is under development.

9. Module “Monte Carlo Analysis”

Module “Monte Carlo Analysis” (Figure 20) performs Monte Carlo analysis itself, and this single module covers process design, environmental and economic assessments.

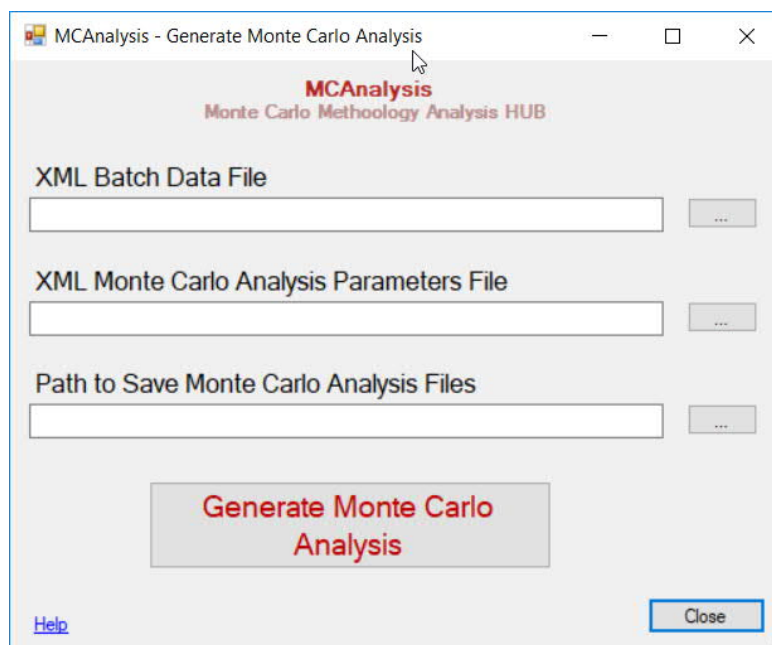


Figure 20. Module “Monte Carlo Analysis” GUI.

This module requires the following inputs from the user:

- **XML Batch Data File:** Output XML file containing the batch results from the process simulation, environmental indicator or economic analysis.
- **XML Monte Carlo Analysis Parameters File:** XML file containing the configuration parameters for output variable for Monte Carlo analysis, as well as their minimum/maximum specifications. The content of this XML file and how to configure it are detailed in Sec. 9.1.
- **Path to Save Monte Carlo Analysis file:** Path to save the histograms of output variables of Monte Carlo analysis in MATLAB format. An output XML file containing the results of Monte Carlo analysis output variables is also generated in addition.

9.1. XML MC Parameters

This XML file contains the attributes from the XML Output Files relevant for process design, environmental and economic assessments via Monte Carlo analysis.

The output variables are defined as below:

- **XML_Direct:** This variable corresponds directly to an attribute available in the Output File XML;

- **Expression:** This variable corresponds to correlations between XML_Direct variables and/or other Expression variables.

The node structure of the MC Parameters XML file depends on the type of output variable and the XML starts with the main node “Variables”, which is composed by the nodes “Variable”, corresponding to each output variable of the Monte Carlo Analysis.

XML Direct Variables:

The node structure for **XML_Direct** variables is shown in Figure 21 and an example of the node “Variable” of the XML file is depicted in Figure 22.

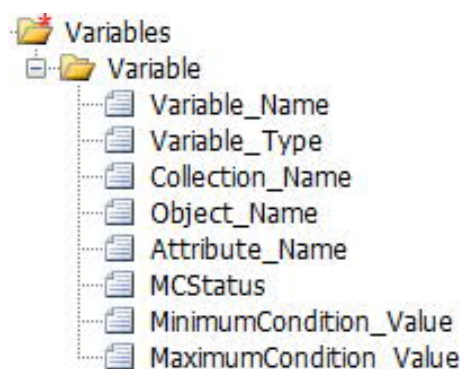


Figure 21. Node structure of XML MC Parameters for XML_Direct Variables.

```
<Variable>
  <Variable_Name>Molar Flow Final NG</Variable_Name>
  <Variable_Type>XML_Direct</Variable_Type>
  <Collection_Name>Process Streams</Collection_Name>
  <Object_Name>PS-070 (comp. final NG)</Object_Name>
  <Attribute_Name>MolarFlow</Attribute_Name>
  <Attribute_Type>RealVariable</Attribute_Type>
  <Attribute_Index>NA</Attribute_Index>
  <MCStatus>Relevant</MCStatus>
  <MinimumCondition_Value>NA</MinimumCondition_Value>
  <MaximumCondition_Value>NA</MaximumCondition_Value>
</Variable>
```

Figure 22. Example of node “Variable” of XML MC Parameters for XML_Direct Variables.

The values to be filled in for each node are described below:

- **Variable_Name:** Name of the variable defined by the user;
- **Variable_Type:** Defines which type of variable. The value “XML_Direct” shall be selected;
- **Collection_Name:** Name of the collection containing the object containing the attribute of interest;
- **Object_Name:** Name of the object containing the attribute of interest;
- **Attribute Name:** Name of the attribute of interest;
- **MCStatus:** Defines if the variables is relevant to Monte Carlo analysis or if it shall be extracted only for the calculation of Expression variables. The values “Relevant” or

“Auxiliar” can be select. It is important to highlight that this node is not available for “Expression” variables, since they shall be always relevant to Monte Carlo analysis.

- **MinimumCondition_Value**: Minimum value of specification;
- **MaximumCondition_Value**: Maximum value of specification.

Expression Variables:

The node structure for Expression variables (Figure 23) has common nodes to XML_Direct variables (<Variable_Name>, <Variable_Type>, <MinimumCondition_Value> and <MaximumCondition_Value>) to Expression Variables described in Sec. 6.1 XML Configuration Parameters File (ImpactVariables and Expressions). The node “Variable_Unit” shall contain the unit of measurement of the value resultant of the expressions.

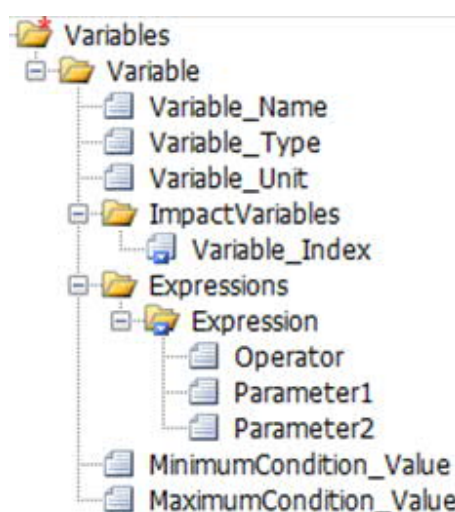


Figure 23. Node structure of XML MC Parameters for Expression Variables.

An example of the node “Variable” of the XML file is depicted in Figure 24.

```
<Variable>
  <Variable_Name>Molar Flow Final NG</Variable_Name>
  <Variable_Type>XML_Direct</Variable_Type>
  <Collection_Name>Process Streams</Collection_Name>
  <Object_Name>PS-070 (comp. final NG)</Object_Name>
  <Attribute_Name>MolarFlow</Attribute_Name>
  <Attribute_Type>RealVariable</Attribute_Type>
  <Attribute_Index>NA</Attribute_Index>
  <MCStatus>Relevant</MCStatus>
  <MinimumCondition_Value>NA</MinimumCondition_Value>
  <MaximumCondition_Value>NA</MaximumCondition_Value>
</Variable>
```

Figure 24. Example of node “Variable” of XML MC Parameters for XML_Direct Variables.

9.2. MATLAB histograms files of output variables

Simple and cumulative frequency histograms, with superposed with normal PDF and CDF curves of the Monte Carlo output variables are generated. Headers inform number of samples, percentage of samples attaining/exceeding specifications, and statistics ($\langle X \rangle$, S_X). Figure 25 shows an example.

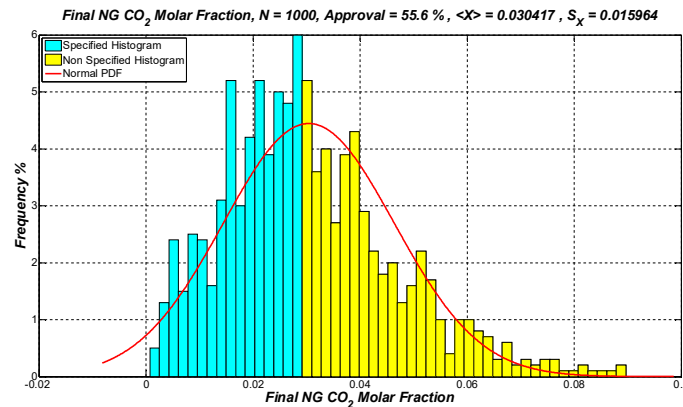


Figure 25. Example of MATLAB Histogram File for Monte Carlo analysis output variables.